

**Phase Behaviour, Thermodynamics and
Kinetics of Clathrate Hydrate Systems
of Carbon Dioxide in Presence of
Tetrahydrofuran and Electrolytes**

Proefschrift

ter verkrijging van de graad van doctor
aan de Technische Universiteit Delft,
op gezag van de Rector Magnificus Prof. dr. ir. J.T. Fokkema,
voorzitter van het College voor Promoties,
in het openbaar te verdedigen
op donderdag 18 juni 2009 om 10.00 uur

door

Khalik BIN MOHAMAD SABIL

Master of Science in Chemical Engineering
Universiti Sains Malaysia, Malaysia
geboren te Sarawak, Malaysia

Dit proefschrift is goedgekeurd door de promotor:

Prof. dr. G.J. Witkamp
Prof. dr. ir. C.J. Peters

Samenstelling promotiecommissie:

Rector Magnificus	Voorzitter
Prof. dr. G.J. Witkamp	Technische Universiteit Delft, promotor
Prof. dr. ir. C.J. Peters	Petroleum Inst. Abu Dhabi, promotor
Prof. dr. ir. G. Ooms	Technische Universiteit Delft
Prof. dr. J.J.C. Geerlings	Technische Universiteit Delft
Prof. dr. P. Englezos	University of British Columbia
Prof. dr. S. Yusup	Universiti Teknologi PETRONAS
Dr. ir. M.M. M.-van den Heuvel	Shell Global Solution (Malaysia)

ISBN: 978-90-9024366-5

Copyright © 2009 by Khalik Bin Mohamad Sabil*
Printed by: CPI Wöhrmann Print Service

All rights reserved. No part of the material protected by this copyright notice may be produced or utilized in any form or by any means, electronic or mechanical, including photocopying, recording or by any information storage and retrieval system, without written permission from the publisher.

* email: halik98@yahoo.com

ACKNOWLEDGEMENTS

"No man is an island, entire of itself; every man is a piece of the continent, a part of the main". - John Donne, Meditation XVII, Devotions upon Emergent Occasions, 1624

Therefore, I am extending my deepest appreciations to all of those who have contributed either directly or indirectly to the completion of this thesis:

- My foremost gratitude goes to my supervisors, Prof. dr. ir. Cor J. Peters and Prof. dr. Geert-Jan Witkamp. Thank you for the opportunity to do a PhD and your relentless supports both scientifically and socially throughout the last four years.

- Louw Florusse, Eugene Straver and John Zevenbergen. Your hands-on guidance, assistance and technical discussions throughout this work are very much appreciated. Special thanks to Michiel Aalbrecht for his assistance during the kinetic measurement.

- Angel Martin and Vicente Roman. Your contributions on the development of the computer programme used in this work are highly acknowledged.

- The management of Universiti Teknologi PETRONAS. Thanks for the given opportunity and financial support throughout the years.

- Ali, Alondra, Bianca, Eliane, Eliff, Ernesto, Helene, Jaap, Ivona, Kamarza, Maaïke, Marta, Laura, Lawien, Lola, Rita, Ryan, Sara, Sona, Selva, Somayeh and Theo. During the time we spent together in PCMT and P&E, I am sure each one of you have contributing some ideas that help to shape the outcome of this thesis and for that, I thank you.

- My dearest mum, siblings, relatives, 'deartje', friends and colleagues,

*You may not have stood beside me
or touched my hand each day
but I knew that you were with me
each step along the way.*

*Your prayers and thoughts and glances
meant more than you will know
'cause I keep them down deep in my heart
and feel the love aglow.*

*It's there for me to rekindle
to light the path I take
It guides me, holds me, rocks me,
each morning I awake. -Debra Sue Dant, USA*

- In memory of my late father. May your soul rest in peace, Amin.

***Khalik M. Sabil
June 2009***

SUMMARY

In view of the possibilities for new development of carbon dioxide hydrate processes, this study focused on experimental measurements to obtain fundamental insight into the phase behaviour and the kinetic of formation of carbon dioxide hydrate forming systems. These data are essential for the development of process design of any carbon dioxide hydrate based processes such as separation of carbon dioxide via hydrate formation and refrigeration processes. In addition, a modelling approach is also being used to predict the phase behaviour of the systems. In this work, special attention is paid to the influence of tetrahydrofuran, a hydrate promoter, and electrolytes on the phase behaviour and the kinetics of formation of these systems and their implications for practical applications.

The phase behaviour has been measured with the Cailletet apparatus. Significant pressure reduction or temperature increment at a specific temperature or pressure has been observed in the presence of tetrahydrofuran, when the equilibria in the ternary system are compared to the corresponding equilibria in the binary system of carbon dioxide and water. A liquid-liquid phase split, which is frequently observed to occur in the ternary system, creates a four-phase equilibrium line of $H-L_W-L_V-V$ in the hydrate forming region. For this equilibrium line, the equilibrium conditions are independent of the composition of tetrahydrofuran in the system. The pseudo-retrograde behaviour, in which the equilibrium temperature is decreasing with an increase of the pressure, is frequently observed for the four-phase equilibrium line. The presence of electrolyte in the mixed hydrate forming system reduces the hydrate stability region. Moreover, the liquid-liquid phase split in the systems is further enhanced by the presence of these electrolytes. The hydrate inhibiting effect of the metal halides (electrolyte) is increasing in the following order: $NaF < KBr < NaCl < NaBr <$

$\text{CaCl}_2 < \text{MgCl}_2$. Among the cations studied, the strength of hydrate inhibition increases in the following order: $\text{K}^+ < \text{Na}^+ < \text{Ca}^{2+} < \text{Mg}^{2+}$. Meanwhile, the strength of hydrate inhibition among the halogen anions studied decreases in the following order: $\text{Br}^- > \text{Cl}^- > \text{F}^-$. Based on the results, it is suggested that the probability of formation and the strength of the ionic-hydrogen bond between an ion and water molecule and the effects of this bond on the surrounding network of water molecules are the major factors that contribute to hydrate inhibition by electrolytes.

The phase behaviour is modelled with the combination of the Van der Waals – Platteeuw model and the Peng-Robinson-Stryjek-Vera Equation of State (PRSV EoS) with Huron-Vidal-Orbey-Sandler (HVOS) mixing rule to describe the clathrate hydrate phase and the fluid phases respectively. In the presence of an electrolyte, the effect of the electrolyte is taken into account by a Debye-Hückel electrostatic term. For the equilibria of the fluid phases ($\text{L}_\text{W}-\text{L}_\text{V}-\text{V} \rightarrow \text{L}_\text{W}-\text{L}_\text{V}$ and $\text{L}_\text{W}-\text{L}_\text{V}-\text{V} \rightarrow \text{L}_\text{W}-\text{V}$), excellent agreement between experimental and modelling data is achieved. On the other hand, for the hydrate equilibria for the ternary and quaternary systems, good agreement is achieved for the three phase $\text{H}-\text{L}_\text{W}-\text{V}$ equilibrium while acceptable agreement is obtained for the $\text{H}-\text{L}_\text{W}-\text{L}_\text{V}-\text{V}$ and $\text{H}-\text{L}_\text{W}-\text{L}_\text{V}$ equilibria.

By taking advantage of the availability of the measured three-phase $\text{H}-\text{L}_\text{W}-\text{V}$ data, the enthalpy of dissociation of simple carbon dioxide and mixed carbon dioxide and tetrahydrofuran hydrates is estimated by using the Clausius-Clapeyron equation. The estimated value is found to be significantly influenced by the compressibility factor of carbon dioxide in the system. Therefore, it is shown that this method can be used for the estimation of the enthalpy of hydrate dissociation in a small range where the compressibility factor is almost constant. Moreover, it is also found that the enthalpy of dissociation of the mixed hydrate is significantly higher than that of simple carbon dioxide hydrate. The presence of electrolyte is observed to

slightly reduce the value of the enthalpy of dissociation of both the simple carbon dioxide and the mixed hydrates.

The kinetics of formation of simple carbon dioxide and mixed carbon dioxide and tetrahydrofuran hydrates are studied in a 150 ml batch reactor with the T-cycle method. The clathrate hydrate formation is divided into two parts, hydrate nucleation and hydrate growth processes. From the measured induction time, it is shown that the hydrate nucleation process is more readily to occur in the mixed hydrate system. The presence of sodium chloride is found to slightly prolong the induction time in the mixed hydrate systems. For the hydrate growth process, the activation energy of mixed carbon dioxide and tetrahydrofuran hydrates is found to be significantly lower than that of simple carbon dioxide hydrate, implying that the mixed system is more susceptible for hydrate growth. The presence of tetrahydrofuran results in a strongly reduced storage potential of carbon dioxide in mixed clathrate hydrates. Furthermore, the presence of sodium chloride is found to slightly reduce the carbon dioxide consumption and increases the activation energy for hydrate formation in the mixed hydrate systems.

The experimental and modelling results provide a better understanding of the phase behaviour and hydrate formation kinetics of simple carbon dioxide and mixed carbon dioxide and tetrahydrofuran in water or aqueous electrolyte solutions. In general, this allows better assessment of practical hydrate applications with tetrahydrofuran. The reduction of the pressure for the hydrate equilibria, the increase of enthalpy of dissociation and the decrease in the induction time achieved with the inclusion of tetrahydrofuran might allow the hydrate process becoming more attractive for applications such as a cooling medium or secondary refrigerant. However, the reduction of storage potential of carbon dioxide in the hydrate formed may cause it to be less attractive for storage

applications. Additionally, the pseudo-retrograde behaviour at which the shift of the equilibrium to lower temperatures is restricting the clathrate hydrate stability region and may hinder the mixed hydrates based process to operate close to ambient temperatures.

INDEX

Acknowledgements	iii
Summary	v
1. Introduction	1
1.1 Clathrate Hydrates	2
1.2 Carbon Dioxide Hydrate	7
1.3 Concerns on Atmospheric Carbon Dioxide	8
1.4 Interests on Carbon Dioxide Hydrate	11
1.4.1 Marine Carbon Dioxide Sequestration	12
1.4.2 Separation Processes	13
1.4.3 Cool Storage Application	15
1.4.4 Others	16
1.5 Electrolytes and Hydrate Promoters	16
1.5.1 Electrolytes	16
1.5.2 Hydrate Promoters	18
1.6 Aims and Outline of the Thesis	20
1.7 References	22
2. Background	27
2.1 Phase Diagrams	28
2.1.1 The Gibbs' Phase Rule	28
2.1.2 Unary System (Water)	29
2.1.3 Binary Systems (Water and One Guest Molecule) in Hydrate Forming Region	30
2.1.4 Ternary and Multicomponent Systems in Hydrate Forming Region	35
2.2 Hydrate Formation and Dissociation	37
2.2.1 Hydrate Formation	37
2.2.1.1 Hydrate nucleation	38

2.2.1.2 Hydrate growth	43
2.2.2 Hydrate Dissociation	46
2.3 References	48
3. Experimental Methodology	51
3.1 Chemicals	52
3.2 Phase Behaviour Measurement	53
3.2.1 Sample Preparation	53
3.2.2 Cailletet Apparatus	55
3.2.3 Phase Behaviour Measurement Procedures	57
3.2.3.1 Hydrate equilibrium points measurement	57
3.2.3.2 Bubble- and dew points measurement	59
3.3 Kinetics of Hydrate Formation Measurement	60
3.3.1 High Pressure Kinetics Measurement Apparatus	60
3.3.2 Kinetics Measurement Procedure	62
3.4 References	63
4. Phase Behaviour of Simple Carbon Dioxide and Mixed Carbon Dioxide and Tetrahydrofuran Hydrates	65
4.1 Introduction	66
4.2 Phase Behaviour of Binary Water and Carbon Dioxide in Hydrate Forming Region	67
4.3 Phase Behaviour of Ternary Water, Tetrahydrofuran and Carbon Dioxide in Hydrate Forming Region	69
4.3.1 Effects of Carbon Dioxide Concentration	73
4.3.2 Effects of Tetrahydrofuran Concentration	78
4.4 References	85
5. Phase Behaviour of Mixed Hydrates in Aqueous Electrolyte Solutions and the Strength of Hydrate Inhibition by Metal Halides	87
5.1 Introduction	88
5.2 Phase Equilibria of Mixed Carbon Dioxide and	

	Tetrahydrofuran in Sodium Chloride Solutions	89
5.3	Competing Effect of Tetrahydrofuran and an Electrolyte and the Strength of Hydrate Inhibition by Metal Halides in Mixed Carbon Dioxide Hydrate Systems	95
5.4	References	105
6.	Enthalpies of Dissociation of Simple and Mixed Carbon Dioxide Clathrate Hydrates	107
6.1	Introduction	108
6.2	Simple Carbon Dioxide Hydrate	110
6.3	Mixed Carbon Dioxide and Tetrahydrofuran Hydrate	116
6.4	Mixed Carbon Dioxide and Tetrahydrofuran Hydrate in Aqueous Electrolyte Solutions	123
6.5	References	126
7.	Modelling the Phase Behaviour of the Hydrate Forming Systems	129
7.1	Principles of Thermodynamics Modelling	130
7.2	Thermodynamics Models of Fluid Phases	132
	7.2.1 The Peng-Robinson-Stryjek-Vera Equation of State	133
	7.2.2 UNIQUAC Model	135
7.3	Thermodynamics Model of Hydrate Phase	138
7.4	Results and Discussion	141
	7.4.1 Modelling Results of the Fluid Phases	142
	7.4.2 Modelling Results of the Hydrate Equilibria in Ternary Water, Carbon Dioxide and Tetrahydrofuran System	150
	7.4.3 Modelling Results of the Hydrate Equilibria of Mixed Carbon Dioxide and Tetrahydrofuran Hydrate in Sodium Chloride Solutions	156
7.5	References	163
8.	Kinetic of Formation of Single and Mixed Carbon Dioxide Hydrates in Water and NaCl Aqueous Solution	165

8.1	Introduction	166
8.2	The Closed Loop (T-Cycle) Method	168
8.3	Nucleation of Simple Carbon Dioxide and Mixed Carbon Dioxide and Tetrahydrofuran Hydrates	171
8.4	Growth of Simple Carbon Dioxide and Mixed Carbon Dioxide and Tetrahydrofuran Hydrates	178
8.5	References	188
9.	Conclusions and Outlook	191
9.1	Conclusions	192
9.2	Outlook	195
	Appendix A	199
	Appendix B	213
	Samenvatting	225
	Curriculum Vitae	229
	Publications	231

1

Introduction

The enticing characteristics of carbon dioxide hydrates initiate numerous research activities around the globe and in a wide variety of fields from carbon dioxide sequestration to cool storage applications. In this chapter, a general introduction to clathrate hydrates and carbon dioxide hydrates in particular, is presented. The motivations behind carbon dioxide hydrate research and the general fields of interest for these compounds are briefly explained. Finally, the aims and the outline of the thesis are also presented.

1.1 CLATHRATE HYDRATES

Gas or clathrate hydrates were discovered almost two centuries ago by Sir Humphrey Davy in 1810. In the early days, interest in gas hydrates was mainly focused on the discovery of new hydrate formers, mainly inorganic chemicals, and the composition of these hydrates [Sloan, 1998]. Only after the discovery of the occurrence of hydrates in oil production pipelines by Hammerschmidt in 1934 [Hammerschmidt, 1934], a shift towards more industrial hydrate research focusing on hydrocarbons based hydrates was carried out to cater for the needs of oil and gas production. Since then, hydrate research has been intensified especially after the discovery of natural gas hydrate deposits in the Siberian permafrost regions by Makogon in 1965 [Makogon, 1981].

Clathrate hydrates or gas hydrates are crystalline solid compounds that are formed in mixtures of water and non- or slightly polar low molecular weight gases or volatile liquids and when subjected to appropriate temperature and pressure conditions. They are formed when hydrogen-bonded water molecules form cage-like structures, known as cavities in the crystalline lattice. These cavities have to be at least partially filled with the hydrate-forming molecules, also known as the 'guest molecules', in order to stabilize the structure. Depending on the type and the size of guest molecule presents, different gas hydrate structures can be formed. The types of cavities that are formed and the distribution of those cavities in a unit cell are used to distinguish the clathrate hydrate structures. Currently, three different structures are known and well studied: structure I (sI), structure II (sII) and structure H (sH) [1]. The types of cavities present in each structure and their coordination number are presented in Figure 1.1.

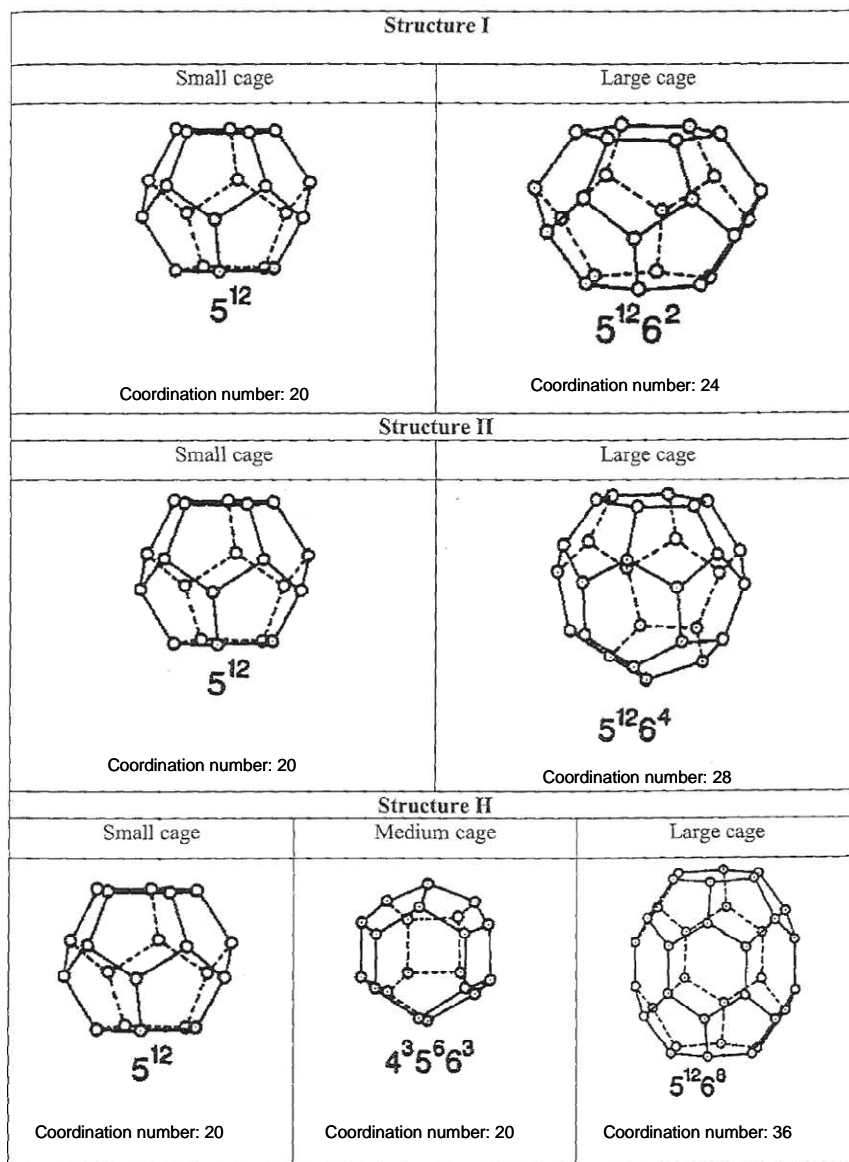


Figure 1.1 Cages and their coordination number in clathrate structures I, II and H [modified from Ripmeester et al., 1994].

The unit cell of each hydrate structure is depicted in Figure 1.2. The unit cell of structure I hydrate consists of 46 water molecules forming two

small cavities and six large cavities. The small cavity has the shape of a pentagonal dodecahedron (5^{12}), while the large cavity has the shape of a tetradecehedron ($5^{12}6^2$). The unit cell of structure II hydrate consists of 136 water molecules forming sixteen small cavities and eight large cavities. Similar to the small cavity of SI, the small cavity of SII also has the shape of a pentagonal dodecahedron (5^{12}) but the large cavity has a shape of a hexadecahedron ($5^{12}6^4$). In structure H, the unit cell consists of three small cavities of 5^{12} , two medium cavities of $4^35^66^3$ and one large cavity of $5^{12}6^8$. The number of water molecules, cages and some geometry of the different hydrate structures are given in Table 1.1.

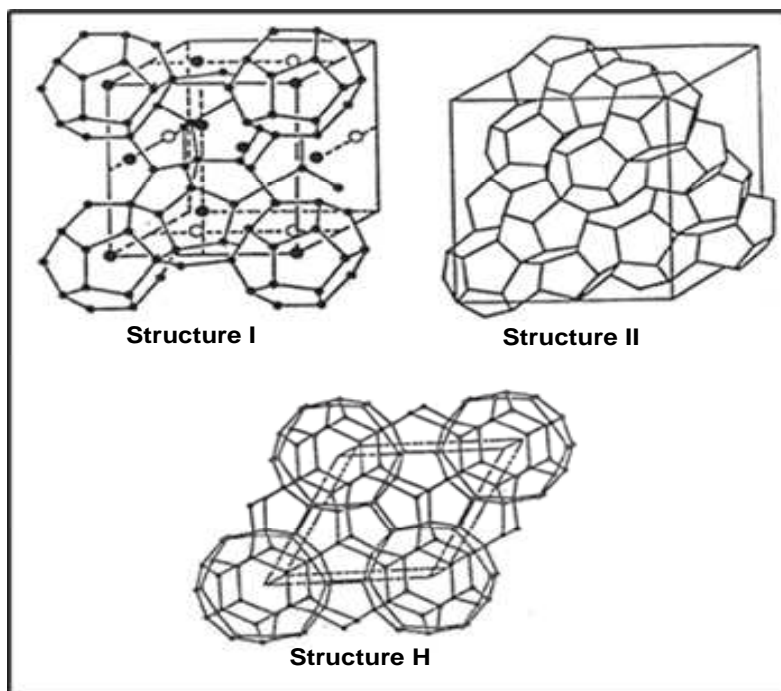


Figure 1.2 The unit cells of the different hydrate structures [modified from Sloan, 1998].

Table 1.1 Geometry of hydrate unit cells and cavities [modified from Sloan and Koh, 2007].

Structure	I		II		H		
Crystal system	Cubic		Cubic		Hexagonal		
Space group	Pm3n		Fd3m		P6/mmm		
Lattice parameter (Å)	a = 12.0		a = 17.3		a = 12.3, c = 10.17		
Number of H ₂ O molecules	46		136		34		
Number of cavities	8		24		6		
Cavity	Small	Large	Small	Large	Small	Medium	Large
Number	2	6	16	8	3	2	1
Description	5 ¹²	5 ¹² 6 ²	5 ¹²	5 ¹² 6 ⁴	5 ¹²	4 ³ 5 ⁶ 6 ³	5 ¹² 6 ⁸
Aver. Cavity radius (Å)	3.95	4.33	3.91	4.73	3.94	4.04	5.79
Variation in radius	3.4	14.4	5.5	1.73	4.0	8.5	15.1
Coordination number	20	24	20	28	20	20	36

In order to form clathrate hydrate, the size of the guest molecules must not be too large or too small compares to the size of the cavities. A ratio of the molecular diameter to the cavity diameter of approximately 0.75 appears to be optimal [Christiansen and Sloan, 1994]. Structures I and II can be formed with a single guest component while structure H requires at least two different guest molecules (large and small). Most components of natural gas (CH₄, C₂H₆, C₃H₈, CO₂, N₂, and H₂S etc.) form hydrates. Table 1.2 presents the diameter ratios of natural gas components and a few other components relative to the diameter of each cavity in structures I and II. In

Table 1.2 size ratios denoted with a superscript “ ζ ” are those occupied by a simple hydrate former. On one hand, if the size ratio is less than 0.76, the molecular attractive forces cannot contribute to cavity stability. On the other hand, above the ratio value of about 1.0, the guest molecule does not fit into a cavity without lattice distortion [Sloan, 1998].

Table 1.2 Ratios of Molecular Diameters to Cavity Diameters^a for Clathrate Hydrate Former [Sloan, 1998].

Cavity Type:		(Molecular Diameter) / (Cavity Diameter)			
		Structure I		Structure II	
		5 ¹²	5 ¹² 6 ²	5 ¹²	5 ¹² 6 ⁴
Type	Dia. (Å)				
H ₂	2.72	0.533	0.464	0.542	0.408
N ₂	4.1	0.804	0.700	0.817 ζ	0.616 ζ
CH ₄	4.36	0.855 ζ	0.744 ζ	0.868	0.655
H ₂ S	4.58	0.898 ζ	0.782 ζ	0.912	0.687
CO ₂	5.12	1.00	0.834 ζ	1.02	0.769
C ₂ H ₆	5.5	1.08	0.939 ζ	1.10	0.826
C ₃ H ₈	6.28	1.23	1.07	1.25	0.943 ζ
i-C ₄ H ₁₀	6.5	1.27	1.11	1.29	0.976 ζ
n-C ₄ H ₁₀	7.1	1.39	1.21	1.41	1.07

a. cavity radii minus 1.4 Å water radii.

1.2 CARBON DIOXIDE HYDRATES

As previously mentioned, carbon dioxide has been known to be among a number of molecules that can form clathrate hydrate. The first evidence for the existence of CO_2 hydrates probably dates back to the year 1882, when Wróblewski [1882] reported the clathrate hydrate formation in a system of carbonic acid and water. The hydrate dissociation curve in the range 267 K to 283 K is first published by Villard in 1897 [Villard, 1897]. Later on, Tamman and Krige [1925] measured the hydrate decomposition curve from 230 K to 250 K. Frost and Deaton [1946] determined the dissociation pressure between 273 K and 283 K. Takenouchi and Kennedy [1965] measured the decomposition curve from 4.5 to 200 MPa. Carbon dioxide hydrate was classified as a structure I clathrate for the first time by von Stackelberg & Muller [1954].

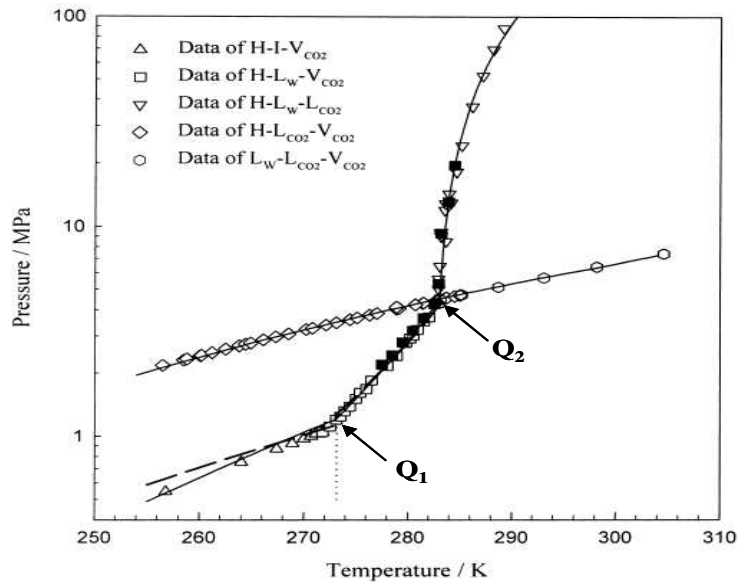


Figure 1.3 Three-phase equilibrium data of simple hydrates of carbon dioxide [adapted from Yang et al., 2000]. The abbreviations are as follows: L - liquid, V - vapour, I - ice, H - hydrate.

As a simple hydrate, carbon dioxide forms structure I hydrate under appropriate pressure and temperature conditions. If all the hydrate cavities are occupied, the chemical formula is $8\text{CO}_2 \cdot 46\text{H}_2\text{O}$ or $\text{CO}_2 \cdot 5.75\text{H}_2\text{O}$. Extended compilations of published hydrate equilibrium conditions of carbon dioxide in pure water can be found in Sloan and Koh [2008]. The phase behaviour of carbon dioxide and water in the hydrate forming region is presented in Figure 1.3. As shown in this figure, the hydrate stability region is bounded by the H-I-V, H-L_W-V and H-L_W-L_{CO2}. As such, at any specified temperature, carbon dioxide hydrate will be stable as long as the pressure of the system is higher or equal to the equilibrium pressure of the system. As shown in this figure, carbon dioxide hydrate has two quadruple points, Q₁ and Q₂. The quadruple point Q₁ is a four-phase equilibrium point of I-L_W-H-V and it is located at 273.1 K and 1.256 MPa. The quadruple point Q₂ is a four-phase equilibrium point of L_W-H-L_V-V and is located at 283.0 K and 4.499 MPa. Carbon dioxide itself has a triple point at $T = 216.58 \text{ K}$ and $P = 0.5185 \text{ MPa}$ and a critical point at $T = 304.2 \text{ K}$ and 7.3858 MPa . In literature, the lowest measured equilibrium pressure for carbon dioxide hydrate is at 0.535 kPa and 151.5 K for I-H-V equilibrium point and its value is reported by Miller and Smythe [1970].

1.3 CONCERNS ON ATMOSPHERIC CARBON DIOXIDE

The increasing demand for energy to supply for the need of industrial developments and the escalating human population has led to accelerated mining and combustion of fossil fuels. These worldwide activities cause a continuing increase of the rates of anthropogenic carbon dioxide emissions, resulting in the increase of the level of atmospheric carbon dioxide. According to Robinson et al. [2007], the atmospheric carbon dioxide level has increased 22% since 1958 and about 30% since 1880. The alarmingly increase of carbon dioxide in the atmosphere is believed to have caused

some significant climate changes. For instance, the worldwide temperature measurements, carefully screened for instrumental and experimental conditions such as effects of urbanization, show an increase in global mean annual surface temperatures of 0.3 to 0.6°C for the last 159 years [Nicholls et al., 1996]. If the temperature continues to increase, devastating effects on world population will be unavoidable. Due to this concern, the increasing quantities of carbon dioxide and other greenhouse gases in the atmosphere has caused widespread global concerns and has attracted international action such as the Kyoto Protocol.

Table 1.3 Annual carbon dioxide emissions from major industrial sources*.

Industry	CO ₂ emission in Mt CO ₂ /yr
Power	10,539
Cement manufacture	932
Iron & steel making	646
Oil refining	798
Petrochemical	379
Oil & natural gas processing	50
Other sources (including biomass)	124

(* source: <http://www.total.com/en/corporate-social-responsibility/special2000l-report/capture/focus-on-carbon-dioxide-capture/>, 5-01-2009)

The main sources of carbon dioxide in the atmosphere are thermal power generation, oil and natural gas refining and processing, cement manufacturing, iron and steel making and petrochemical industries. Table 1.3 lists the annual carbon dioxide emissions from these major industrial sources. As shown in Table 1.3, fossil-fuelled power production combined with oil and gas refining and processing cover more than 87% of the industrial carbon dioxide emissions. A clearer evidence of the direct

correlation between the world's hydrocarbon use and the increase of atmospheric carbon dioxide concentration between the years of 1850 to 2007 is shown in Figure 1.4 [Robinson et al., 2007].

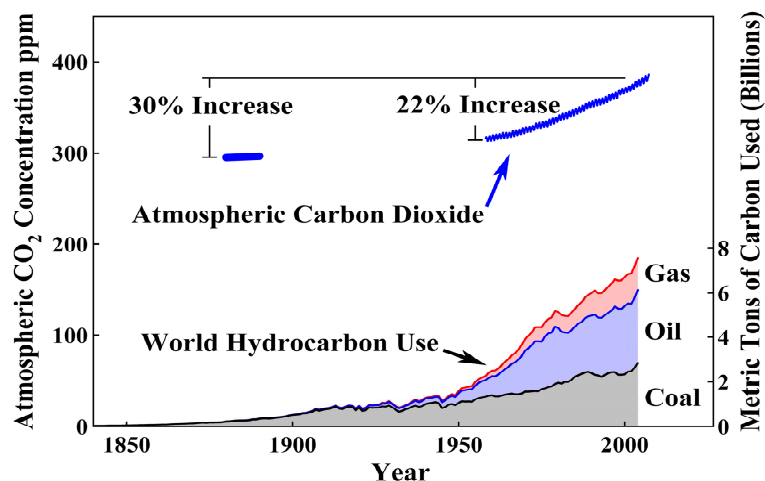


Figure 1.4 Atmospheric CO₂ concentrations in parts per million by volume, ppm, measured at Mauna Loa, Hawaii, between 1958 and 2007. For the period 1880 to 1890, an average literature estimate value of 295 ppm is used [Robinson et al., 2007].

As the world's dependency on oil and gas as the main source of energy is foreseen to continue for years to come, a new approach should be developed in order to reduce the increasing amount of carbon dioxide release as a by-product of energy production. A paradigm shift is required in order to successfully combat this environmental problem and the basis of this paradigm shift is to look at carbon dioxide not just as a polluting greenhouse gas, but also as a valuable raw material. This approach requires the development of separation technologies to separate the carbon dioxide in bulk from the natural gas under different concentrations, techniques to sequester or store the carbon dioxide and processes to convert the bulk

carbon dioxide to different added-value products like chemicals, temperate-farming-agro-products and refrigerants. The benefits from this approach are three-fold. Firstly, for the growth of the hydrocarbon based industries, new technologies suitable to cater for high carbon dioxide concentration have to be developed on a high priority basis. Secondly, from the large quantities of carbon dioxide that is produced, a variety of added-value products could be obtained, thus converting a polluting greenhouse gas into a valuable resource. Thirdly, carbon credit is gained under the Kyoto Protocol for utilizing the carbon dioxide, which can be used to generate additional revenue.

1.4 INTERESTS ON CARBON DIOXIDE HYDRATE

Like other fields of research with a focus on carbon dioxide, the interest of carbon dioxide hydrates is mainly based on the possibilities of using the formation of carbon dioxide hydrates for carbon dioxide separation, capture and storage (CCS). Any technique that prevents or reverses the release of carbon dioxide to the atmosphere and diverts the carbon to a viable carbon sink can be considered carbon capture. Currently, there are a few techniques available for carbon dioxide capture and separation with some degree of success such as chemical solvents, physical absorption, physical adsorption, chemisorptions and chemical bonding through mineralization. However, the main concerns of these techniques are the amount of chemicals use in these processes, the energy penalties and the costs associated with these processes in their present form. These factors make these processes becoming less attractive for large-scale carbon capture [GCEP carbon capture technology assessment, 2005]. The global climate and energy project (GCEP) leads by Stanford University is a major on-going research project with a long-term aim of the development of global energy systems with significantly lower greenhouse gas emissions. In this

retrospect, clathrate hydrate technique offers a couple of advantages. Firstly, the main chemical required for carbon dioxide hydrate formation is water, which provides the process with abundant (cheap) and green raw chemical. Secondly, reduction of energy requirements for hydrate formation can be obtained by including certain organic chemicals in low concentrations, known as hydrate promoter in the hydrate forming system [Mooijer van den Heuvel, 2004]. The inclusion of one of these hydrate promoters will reduce the pressure requirement or increase the temperature at which the clathrate hydrates are stable. This leads to a reduction in the energy required for pressurization or cooling the targeted systems. In bulk, these carbon dioxide hydrates can be transported as slurries in pipelines or in pressurized and chilled vessels from the points of carbon dioxide captured to the points of carbon dioxide sequestered. Moreover, the interest in carbon dioxide hydrates is not limited to carbon capture and sequestration. As mentioned earlier, a paradigm shift is required to look into carbon dioxide also as a material to be used in industrial processes. The various areas of interest of carbon dioxide hydrates in accordance with their respective possibilities to be developed as tools to overcome the ever increasing carbon dioxide concentration in the atmosphere are summarized in the following sections.

1.4.1 Marine Carbon Dioxide Sequestration

Due to the pressures and temperatures at ocean depths which are suitable for carbon dioxide hydrates formation [Aya, 1995; Brewer et al., 1999], sequestration of carbon dioxide as clathrate hydrates has been thoroughly investigated. Between 1000 and 2000 m (deep water), carbon dioxide in the liquid state diffuses and also dissolves in the ocean [Liro et al., 1992]. In addition, carbon dioxide hydrates can appear from 500 to 900 m in CO₂-rich seawater [Kojima et al., 2002]. Due to their densities [Holder et al., 1995], these hydrates sink towards the deep sea bottom where they stabilize

in the long term [Lee et al., 2003; Harrison et al., 1995]. Additionally, it has been proposed to replace the natural gas in naturally occurring hydrate fields with carbon dioxide [Komai et al., 2000]. Currently, marine carbon dioxide sequestration is at an experimental stage implying that on-going research activities on carbon dioxide solubility [Aya et al., 1997; Yang et al., 2000], carbon dioxide hydrate formation and dissociation kinetics [Englezos, 1992; Circone, 2003], carbon dioxide hydrate stability [Harrison and Wendlandt, 1995], hydrodynamics conditions [Yamasaki et al., 2000] and other related fields are required to ensure the success of this sequestration method. However, the possible negative environmental impacts of acidification of seawater [Widdicombe and Spicer, 2008] and elevated carbon dioxide concentration in the ocean [Ishimatsu et al., 2004] to marine life should also be thoroughly investigated.

1.4.2 Separation Processes

In the 1960s and early 1970s, desalination of seawater using gas hydrate formation was thoroughly studied. Knox et al. [1961] proposed a process for the desalination of seawater to produce potable water and to setup a pilot plant to study this process. The feasibility of seawater desalination via hydrates was demonstrated [Colten et al., 1972; Rautenba and Pennigs, 1973], but the process was not developed industrially since it was not economically viable [Englezos, 1993]. However, Javanmardi and Moshfeghian [2003] showed that with the inclusion of a hydrate promoter, the total cost of the hydrate process is comparable with other process such as multistage-flash distillation (MSF), multi-effect distillation (ME) and reverse osmosis (RO) for water desalination.

Extensive studies have been focused on the removal or separation of carbon dioxide from industrial gases through the formation of carbon dioxide

hydrate. Seo et al. [2000] reported the proof-of-concept to carbon dioxide separation from multicomponent gas stream by the formation of carbon dioxide hydrate. Kang and Lee [2000] proposed a hydrate based gas separation (HBGS) for the separation of carbon dioxide from flue gas with tetrahydrofuran as a promoter. According to the authors, the HBGS process makes it possible to recover more than 99 mol% of CO₂ from the flue gas. This process also has several other advantages, such as moderate operational temperatures in the range of 273–283 K and continuous operations, making it possible to treat a large amount of gaseous stream. Rice [2003, 2006] proposed a system for hydrogen production from methane hydrate with sequestering of carbon dioxide hydrate. The author claimed that through this process, the production of hydrogen is made available without the release of carbon dioxide to the atmosphere. In this case, the carbon dioxide is separated from the process stream and injected back in the natural gas hydrates reservoir as clathrate hydrate. Chatti et al. [2005] made a review on the benefits of clathrate hydrate based processes. The post and pre-combustion capture of carbon dioxide by using carbon dioxide formation is extensively studied in University of British Columbia [Kumar et al., 2006; Linga et al., 2007; Linga et al. 2008]. Moreover, the US Department of Energy (DOE) is developing a high pressure process for carbon dioxide separation [Tam et al., 2001]. It focuses on the low temperature SIMTECHE process, where a shifted synthesis gas stream (carbon dioxide, hydrogen and other gases) is combined with pre-cooled nucleated water in a carbon dioxide hydrate slurry reactor. The outlet mixture (carbon dioxide hydrate slurry, hydrogen and other gases) flows into a hydrate slurry gas separator which divides the flow into two streams: carbon dioxide hydrate slurry and hydrogen-rich product gas. Initial economic findings show that in comparison with absorption process with either amine or Selexol, the SIMTECHE process requires less additional capital cost of USD\$ 23.9 millions (USD\$ 56.9 millions for amine and USD\$ 85.1 millions for Selexol) for the integration of carbon capture system (CCS) in an integrated gasification combined cycle

(IGCC) plant [Tam et al., 2001]. Moreover, the authors stated that the cost of carbon dioxide removal for the SIMTECHE process is also found to be the cheapest among the studied processes at USD\$ 8 per ton of CO₂ (USD\$ 21 per ton CO₂ and USD\$ 14 per ton CO₂ for amine and Selexol absorption processes). These initial findings show that carbon dioxide separation process based on hydrate formation may be more economical compared to conventional processes.

1.4.3 Cool Storage Application

Following the discovery of the ozone layer depletion by chlorofluorocarbons (CFCs), which leads to the phasing out of CFCs as working fluid in refrigeration systems, the interest in CO₂ as a working fluid in refrigeration systems has been revived. Large-scale usage of CO₂ based refrigerants will eliminate the need of using conventional refrigerants such as CFC and HFC. One way of using CO₂ in refrigeration process is in the form of clathrate hydrate slurries, as a two-phase (solid-liquid) refrigerant. Due to the latent heat of fusion of the solid, two-phase refrigerants, sometimes also known as phase-change materials, are more energy-efficient than single-phase refrigerants [Darbouret et al., 2005]. CO₂ hydrate slurries are promising systems in the field of cold distribution and storage as phase-change materials due to several factors. Firstly, the melting temperatures of some clathrate hydrates are consistent with the temperature need in applications such as air conditioning [Liang et al., 2001]. Moreover, the heat of dissociation of CO₂ hydrates has been found to be suitable for refrigeration application and it can be generated by direct gas injection into an aqueous solution instead of using mechanical methods, as in the case of ice slurries [Martínez et al., 2008].

1.4.4. Others

A hydrate based process can also be a good alternative to freeze-crystallisation processes to concentrate water-rich streams which require relatively low temperatures [Huang et al., 1966]. Similarly, it might also be a good alternative for processes that use evaporative techniques, which require higher temperature, typically higher than the atmospheric boiling point of water [Gaarder and Englezos, 1995]. Vaessen et al. [2000] have shown the feasibility of using eutectic freeze crystallization with carbon dioxide hydrates for the separation of highly soluble salts from aqueous solutions. In these cases, the development of carbon dioxide hydrate applications is not only relevant to the reduction of energy consumption but also for conservation and transport of temperature-sensitive materials that might be degraded at the conditions applied with freeze crystallisation or evaporative processes such as some vaccines and antibiotics [Zweig, 2006].

1.5 ELECTROLYTES AND HYDRATE PROMOTERS

1.5.1 Electrolytes

Electrolytes such as sodium chloride (NaCl) and magnesium chloride (MgCl_2) are known to inhibit hydrate formation by lowering the activity of water in the coexisting liquid phase, causing hydrates to form at lower temperatures and higher pressures compared to their formation in pure water [Dholabhai et al., 1996; Kang et al., 1998; Duan and Sun, 2006]. In our laboratory, the first striking evidence ofn electrolyte's inhibition effect on clathrate hydrate was shown through the measurement of hydrate equilibrium conditions in the system methane-sodium chloride-water by de Roo et al. [1983]. Due to ionization of salt in aqueous solution, these

electrolyte ions form Coulombic bond with the dipoles of water. This bond is much stronger than either the hydrogen bond or van der Waals forces and its formation causes clustering around the ions by the water molecules. The formation of this bond inhibits the formation of hydrate since water is more attracted to ions than to the hydrate structure [Sloan and Koh, 2007].

Furthermore, Sloan and Koh [2007] stated that a secondary effect of the clustering of the water molecules is a decrease in the solubility of the potential hydrate guest molecules in water, a phenomenon known as 'salting-out'. It is believed that both ion clustering and salting-out cause a substantially more sub-cooling required for formation of the hydrate. Thus, the more ions are present in the solution, the larger hydrate inhibiting effect can be noticed. Although in the past years gas hydrate stability conditions in electrolyte solutions have been intensively studied, the specific role plays by either the cation or the anion in affecting gas hydrate stability in an electrolyte solution is unclear. Through a comparison between the cations of the same acid, Makogon [1981] stated that the salting-out effect of individual ions increases with the ion charge and also depends on the ionic radius. With the decrease in ion size, the bond between the water molecules and the ions becomes stronger. In contrast, the co-ordination number of the ions decreases with the reduction in ion size which will result in a shrink of the size of water coating around the ion. However, the first tendency is stronger and, therefore, the ion's salting-out effect action is usually decreasing with increase of the ion radius. As a result, the author concluded that salt inhibition is approximately a direct function of charge and an inverse function of ion radius implicating that the best inhibitor must have the maximum charge and a minimum radius. However, a study conducted by Lu et al. [2001] showed that cation and anion play different roles in inhibiting hydrate formation in electrolyte solutions. According to these authors, this difference is qualitatively attributed to the difference between cation and anion in

affecting the ambient water networks due to their hydration characteristics in electrolyte solutions. However, due to the limited available data, no conclusive explanation was derived from their study.

1.5.2 Hydrate Promoters

One of the drawbacks for the development of hydrate based processes is due to the high-pressure requirement of such systems, making the processes less feasible and economically less attractive. To overcome this specific problem, additives or promoters are commonly introduced to clathrate hydrate systems in order to dramatically reduce the equilibrium pressure and to make hydrate technology economically more attractive. Cyclic ethers have been generally known to form simple hydrates with water or mixed hydrates with low-molecular weight gases such as CO₂, CH₄ and N₂. Introduction of these additives has been proven to lower the hydrate formation pressure up to about 30 – 80% at a specified temperature. Saito et al. [1996] showed that a large group of water-soluble ethers can stabilize clathrate hydrates when added in low concentration to the aqueous phase. Jager et al. [1999] measured equilibrium data of the hydrate formation in the methane + water +1,4-dioxane system and confirmed that the addition of 1,4-dioxane up to a concentration of 5 mol% drastically reduced the equilibrium pressure of hydrate formation at a specified temperature. Seo et al. [2001] showed that the addition of cyclic ethers such as tetrahydrofuran (THF), propylene oxide, 1,4-dioxane and acetone caused the hydrate equilibrium pressure to be drastically lowered at a specified temperature and equivalently the hydrate equilibrium temperature to be greatly raised at a specified pressure for methane hydrate formation. Also, it was found out that the stabilization effect on hydrate formation was found to be highest for THF and in the order of THF > Propylene oxide > 1, 4-dioxane > acetone as the hydrogen bonding effect of an open chain ether is weaker than that of a

cyclic ether. Kang and Lee [2000] developed and thermodynamically verified a new process for effectively removing and recovering carbon dioxide from large amount of multi-component flue gas. In their study, THF was used as a hydrate stabilizer which greatly reduced the required hydrate formation pressure and moreover promote the corresponding hydrate formation rate. In addition, these stabilizing chemicals might be effectively used for storing gas in solid hydrate state because of their effect on the shift of hydrate-forming equilibrium temperature and pressure to milder ones.

The promoters or additives can be divided into two categories depending on their solubility in water, i.e., water-soluble and water-insoluble additives respectively. THF, propylene oxide, 1,4-dioxane are some examples of water-soluble additives. The introduction of a promoter will result in more complex phase behaviour of the system in the region of hydrate formation since the maximum degree of freedom of the system is increased by one degree ($F_{\max} = 4$). The equilibrium pressure reduction effect by water-soluble compounds differs from the pressure effect of water-insoluble compounds by their concentration dependency [de Duegd et al., 2001]. Insoluble additives like benzene, tetrahydropyran, cyclohexane, cyclopentane and neopentane [Tohidi et al., 1997; Mooijer van den Heuvel, 2004] form an extra liquid phase in the system, which reduces by one the number of degrees of freedom by one according to the Gibbs' phase rule. However, if the solubility limit of the water-soluble compounds is reached, the systems will lose their concentration dependency of the hydrate equilibrium conditions.

1.6 AIMS AND OUTLINE OF THE THESIS

By taking into account the possible benefits of carbon dioxide hydrates for industrial applications, the principal aim of the present study is to get better understanding on the phase behaviour of water and carbon dioxide mixtures in the presence of tetrahydrofuran and/or electrolytes in the hydrate forming region. High-pressure phase equilibrium data of the above mentioned ternary and quaternary clathrate hydrate systems, are still rather scarce. Therefore, it was decided to experimentally determine the hydrate and fluid phase equilibria of such systems and, for that purpose, the phase behaviour has been determined experimentally with the Cailletet apparatus. The investigated region of pressure and temperature ranges from 0.1 to 7.5 MPa and 265 K to 295 K respectively. Another important consideration on the success of carbon dioxide hydrate based processes is the knowledge on the kinetics of such systems. To gain some insight in the kinetics of formation and dissociation of simple and mixed carbon dioxide hydrates, the kinetics of formation and dissociation of these hydrates in water and aqueous sodium chloride solutions are also experimentally determined.

In Chapter 2, the theoretical background of clathrate hydrates is highlighted. The Gibb's phase rule, which is the basis for the construction of phase diagrams, is described. Theory of the phase behaviour is clarified, specifically for binary and ternary hydrate forming systems. Moreover, theories of hydrate formation and dissociation are also presented in this chapter.

In Chapter 3, the experimental apparatus and procedures for the phase equilibria and kinetic measurements of the carbon dioxide hydrate systems are described. The experimental results of the phase behaviour measurements are reported in Chapters 4 and 5. The experimental results of

the binary CO_2 + water and ternary CO_2 + water + THF are presented and discussed in Chapter 4, while the experimental results of mixed CO_2 and THF hydrates in aqueous electrolyte solutions are presented and discussed in Chapter 5. In Chapter 6, the results of the calculated enthalpy of dissociation from phase equilibrium data of simple and mixed carbon dioxide hydrates in water and aqueous electrolyte solutions are presented and discussed.

As an alternative for phase behaviour measurements, which are known to be time-consuming and in certain cases require expensive methods and equipment, the thermodynamic modelling of phase equilibria, including a clathrate hydrate phase, is discussed in Chapter 7. The modelling results of the fluid phases and hydrate phase of mixed carbon dioxide and tetrahydrofuran in water and aqueous sodium chloride solutions are presented and discussed.

In Chapter 8, the experimental results on the kinetics of formation and dissociation of simple and mixed carbon dioxide hydrate with tetrahydrofuran in water and aqueous sodium chloride solutions are presented and discussed. Finally, conclusions of the present work together with recommendations on future directions in clathrate hydrate research are presented in Chapter 9.

1.7 REFERENCES

Anonymous, Carbon dioxide capture & storage. Available from [http://www.total.com/en/corporate-social-responsibility/special-reports / capture/focus-on-carbon-dioxide-capture / CO₂-capture-storage_11360. htm](http://www.total.com/en/corporate-social-responsibility/special-reports/capture/focus-on-carbon-dioxide-capture/CO2-capture-storage_11360.htm) (retrieved on 20th January 2009).

Anonymous, GCEP Technical Report, Geological CO₂ Sequestration Project Results 2003-2004, Stanford University, 2005.

Aya, I., Yamane, K., Nariai, H. Energy, 1997, 22 (2-3), pg. 263-271.

Brewer, P.G., Reiderich, G., Peltzer, E.T., Orr, F. M. Science, 1999, 284 (5416), pg. 943-945.

Chatti, I., Delahaye, A., Fournaison, L., Petitet, J.-P., Energy Conversion and Management, 2005, 46, pg. 1333-1343.

Christiansen, R.L. and Sloan, E.D. Mechanism and kinetics of hydrate formation in "International Conference on Natural Gas Hydrates", Annals of The New York Academy of Sciences 1994, 715, pg. 283-305.

Circone, S., Stern, L.A., Kirby, S.H., Durham, W.B., Chakoumakos, B.C., Rawn, C.J., J Phys Chem B, 2003, 107(23), pg. 5529–5539.

Colten, S.L., Lin, F.-S., Tsao, T.C., Stern, S.A., Barduhn, A.J. Desalination, 1972, 11, pg. 31-59.

Darbouret, M., Cournil, M., Herri, J.-M., Int. J. Refrigeration, 2005, 28, pg. 663-671.

de Deugd, R.M., Jager, M.D., de Swaan Arons, J., AIChE J. 47 (2001), pg. 693-704.

de Roo, J.L., Peters, C.J., Lichtenthaler, R.N., Diepen, G.A.M., AIChE J., 1983, 29, pg. 651-657.

Dholabhai, P.D. Perent, J.S., Bishnoi, P.R., Ind. Eng. Chem. Res., 1996, 35, pg. 819-823.

Duan, Z., Sun, R., American Mineralogist, 2006, 91, pg. 1346-1354.

Englezos P., Ind. Eng. Chem. Res., 1992, 31(9), pg. 2232–2237.

- Englezos P., Ind. Eng. Chem. Res., 1993, 32, pg. 1251-1274.
- Frost, E. M. & Deaton, W. M. Oil and Gas Journal, 1946, 45, pg. 170-178.
- Gaarder, C., Englezos, P., Nordic Pulp and paper Research Journal, 1995, 2, pg. 110-113.
- Hammerschmidt, E.G. Ind. Eng. Chem., 1934, 26, pg. 851-855.
- Harrison, W.J., Wendlandt, R.F, Sloan, E.D. Appl. Geochem., 1995, 10(4), pg. 461-475.
- Holder, G.D., Cugini, A.V., Warzinski, R.P. Environ. Sci. Technol., 1995, 29, pg. 276-278.
- Huang, C.P., Fennema, O., Powrie, W.D., Cryobiology, 1966, 2(5), pg. 240-245.
- Ishinatsu, A., Kikkawa, T., Hayashi, M., Lee, K.S, Kita, J., J. Oceanography, 2004, 60 (4), pg. 731-741.
- Jager, M.D., de Deugd, R.M., Peters, C.J., de Swaan Arons, J., Sloan, E.D., Fluid Phase Equilibr., 1999, 165, pg. 209-223.
- Javanmardi, J. and Moshfeghian, M., Appl. Therm. Eng., 2003, 23, pg. 845-857.
- Kang, S.-P., Chun, M.-K., Lee, H., *Fluid Phase Equilibr.*, 1998, 147, pg. 229-238.
- Kang, S.-P., Lee, H., Environ. Sci. Technol., 2000, 34, pg. 4397-4400.
- Knox, W.G., Hess, M., Jones, G.E., Smith, H.B., Chem. Eng. Prog., 1961, 57(2), pg. 66-71.
- Kojima, R., Yamane, K., Aya, I., Dual nature of CO₂ solubility in hydrate forming region in "Fourth International Conference on Gas Hydrates", 2002, pg. 286-289.
- Komai, T., Yamamo, Y., Ohga, K., Dynamics of reformation and replacement of CO₂ and CH₄ gas hydrates in "Gas Hydrates: Challenges for the Future", Annals of The New York Academy of Sciences 2000, 912, pg. 272-280.
- Kumar, R., Wu, H.-J., Englezos, P., Fluid Phase Equilibr., 2006, 244(2), pg. 167-171.

Lee, S., Liang, L., Riestenberg, D., West, O.R., Tsouris, C. and Adams, E. *Environ. Sci. Technol.*, 2003, 37 (16), pg. 3701-3708.

Liang, D. Guo, K., Wang, R., Fan, S., *Fluid Phase Equilib.*, 2001, 187-188, pg. 61-70.

Liao, S.M., Zhao, T.S., Jakobsen, A., *Applied Therm. Eng.*, 2000, 20(9), pg. 831-841.

Linga, P., Kumar, R., Englezos, P., *Journal Hazardous Materials*, 2007, 149(3), pg. 625-629.

Linga, P., Kumar, R., Englezos, P. *Environ. Sci. Technol.*, 2008, 42(9), pg. 315-320.

Liro, C.R., Adams, E.E., Herzog, H.J. *Energy Convers. Manage.*, 1992, 33(5-8), pg. 667-674.

Lu, H., Matsumoto, R., Tsuji, Y., Oda, H., *Fluid Phase Equilib.*, 2001, 178, pg. 225-232.

Makogon, Y.F. "Hydrates of natural gas", Tulsa, Oklahoma, USA, Penwell Books, 1981.

Martínez, M.C., Dalmazzone, D., Fürst, W., Delahaye, A., Fournaison, L., *AIChE J.*, 2008, 54(2), pg. 1088-1095.

Miller, S.L. and Smythe, W.D., *Science*, 1970, 170, pg. 531.

Mooijer-van den Heuvel, M.M. "Phase Behaviour and Structural Aspects of Ternary Clathrate Hydrate Systems: The Role of Additives". Ph.D thesis, Delft Uni. of Technology, January, 2004.

Nicholls, R.J. and Leatherman, S.P. *Coastal Management*, 1996, 24 (4), pg. 301-324.

Rautenbar, R., Pennigs, P. *Chemie Ingenieur Technik*, 1973, 45 (5), pg. 259-264.

Rice W., J. *Energy Resources Technology – Transaction of the ASME*, 2003, 125(4), pg. 253-257.

Rice W., *International J. Hydrogen Energy*, 2006, 31(14), pg. 1955-1963.

Ripmeester, J. A. and Ratcliffe, C.I., Klug, D.D., Tse, J.S. Molecular perspectives on structure and dynamics in clathrate hydrates in "Natural Gas

Hydrates", Annals of The New York Academy of Sciences 1994, 715, pg. 161-176.

Robinson, A. B., Robinson, N. E, Soon, W. J. American Physicians and Surgeons, 2007, 12, pg. 79-90.

Saito, Y., Kawasaki, T., Okui, T., Kondo, T., Hiraoka, R., Methane storage in hydrate phase with water soluble guests in Proceedings of NGH '96- 2ND International Conference on Natural Gas Hydrates, 1996, pg. 459-465.

Seo, Y.-T., Kang, S.-P., Lee, H., Fluid Phase Equilibr., 2001, 189, pg. 99-110.

Seo., Y.-T, Kang, S.-P., Lee, H., Lee, C.-S., Sung, W.-M. Korean J. Chem. Eng., 2000, 17(6), pg. 659-667.

Sloan Jr., E.D. "Clathrate Hydrates of Natural Gas", 2nd ed., Marcel Dekker, New York, 1998.

Sloan Jr., E.D. and Koh, C.A. "Clathrate Hydrates of Natural Gas", 3rd ed., CRC Press, Florida, 2008.

Takenouchi, S. and Kennedy, G. C. J. Geology, 1965, 73, pg. 383-390.

Tam, S.S., Stanton, M.E., Ghose, S., Deppe, G., Spencer, D.F., Currier, R.P., Young, J.S., Anderson, G.K., Le, L.A., Devlin, D.J., A high pressure process for carbon dioxide separation for IGCC plants. Available from: http://www.netl.doe.gov/publications/proceedings/01/carbon_seq/1b4.pdf (retrieved on 10th July 2008).

Tamman, G. & Krige, G. J., Zeit. Anorg. Und Algem. Chem., 1925, 146, pg. 179-195.

Tohidi, B., Danesh, A., Todd, A.C., Burgass, R.W., Østergaard, K.K., Fluid Phase Equilibr., 1997, 138, pg. 241-250.

Vaessen, R.J.C., vab der Ham, F., Witkamp, G.J., Eutectic freeze cyrtallisation using CO₂ hydrates in "Gas Hydrates: Challenges for the Future", Annals of The New York Academy of Sciences, 2000, 912, pg. 483-495.

Villard, M., P. Ann. Chim. Phys. (7), 1897, 11, pg. 353-360.

Von Stackelberg, M. and Müller, H. R. Z. Electrochem., 1954, 58, pg. 25-39.
Widdicombe, S., Spicer, J.I., J. Experimental Marine Biology and Ecology, 2008, 366 (1-2), pg. 187-197.

Wroblewski, S. Comptes rendus, 1882, 94, pg. 212-213.

Yamasaki, A., Teng, H., Wakatsuki, M. Yanagisawa, Y., Yamada, K. CO₂ hydrate formation in various hydrodynamics conditions in "Gas Hydrates: Challenges for the Future", Annals of The New York Academy of Sciences 2000, 912, pg. 235-245.

Yang, S.O., Yang, I.M., Kim YS, Lee, C.S. Fluid Phase Equilibria, 2000, 175 (1-2), pg. 75-89.

Zweig, S.E., Vaccine, 2006, 24, pg. 5977-5985.

2

Background

The development of carbon dioxide hydrate based processes requires some understanding on the phase behaviour and kinetics of formation and dissociation of simple and mixed carbon dioxide hydrates. To provide some background on the phase behaviour of clathrate hydrate forming systems, the Gibbs' phase rule, the phase behaviour of unary (water), binary, ternary and multi-component systems in hydrate forming regions are presented in Section 2.1. In Section 2.2, some relevant background on clathrate hydrate formation and dissociation is presented. The hydrate nucleation and growth processes are discussed in Sections 2.2.1.1 and 2.2.1.2 respectively. Some related literature background on clathrate hydrate dissociation is presented in Section 2.2.2.

2.1 PHASE DIAGRAMS

2.1.1 The Gibbs' Phase Rule

A system is considered to be in thermodynamic equilibrium when it is in thermal, mechanical, and chemical equilibrium. When these conditions are fulfilled, the chemical potential of a particular component, i , is equal in each phase presents in the system, i.e.:

$$\mu_i^\alpha = \mu_i^\beta = \dots = \mu_i^k \quad (2.1)$$

where μ_i^α is the chemical potential of component i in phase α . This equilibrium equation is valid for each component in the system resulting in $N \cdot (\pi - 1)$ equilibrium equations. Moreover, an equilibrium state of a system with N components can be fully described by $2 + \pi \cdot (N - 1)$ intensive variables namely P , T and the independent composition variables of each phase ($N - 1$), for which normally mole fraction (x_i) is used. The number of degrees of freedom, F , is the difference between the number of variables and the number of equilibrium conditions,

$$F = N - \pi + 2 \quad (2.2)$$

Equation 2.2 is the well-known Gibbs' phase rule de [Smith et al., 2001]. In case of extra relations between the variables occur, these relations are accounted for by the introduction of \emptyset , as shown in Equation 2.3,

$$F = N - \pi + 2 - \emptyset \quad (2.3)$$

These extra relationships occur, for example, in case of a binary azeotrope where $y_i = x_i$, so $\emptyset = 1$. In case of a critical state, a state in a phase diagram where two phases become identical, it can be counted as one phase with $\emptyset = 2$ [de Loos, 1994]. Moreover, since the minimum number of phases, $\Pi = 1$, the maximum value of F is given by $F_{\max} = N + 1$. The value of F_{\max} represents the dimension of space needed to fully represent phase behaviour of an N component system.

2.1.2 Unary System (Water)

For a unary system such as water, the maximum degrees of freedom, F_{\max} , is equal to 2. This means, it is possible to fully represent the phase behaviour of the unary system in a two-dimensional P,T -plane. In Figure 2.1, the phase behaviour of water is schematically presented for a temperature and pressure range of 200 to 700 K and 1 to 100 MPa, respectively. In this region, the various ice (solid) phases, which normally occur at much lower temperatures [Choukroun and Grasset, 2007], are not considered. The example of applying the Gibbs' phase rule for the unary water system is given in Table 2.1. The phases that can occur in a unary water system are solid/ice (I), liquid (L_W) and vapour (V). Each equilibrium line shown in Figure 2.1, represents a phase boundary and gives the conditions at which two phases may coexist in equilibrium. The intersection of these lines represents the triple point, i.e. the conditions where liquid water, gaseous water and ice coexist in equilibrium. Since F is equal to 0 at these conditions, the triple point can only occur at a unique temperature and pressure value, T_{tr} and P_{tr} respectively. A critical point occurs at the end of an equilibrium line where the properties of the two phases become indistinguishable from each other. In the case of the unary water system, the critical point is located at the end of the liquid-vapour line at unique temperature and pressure values of T_c and P_c respectively.

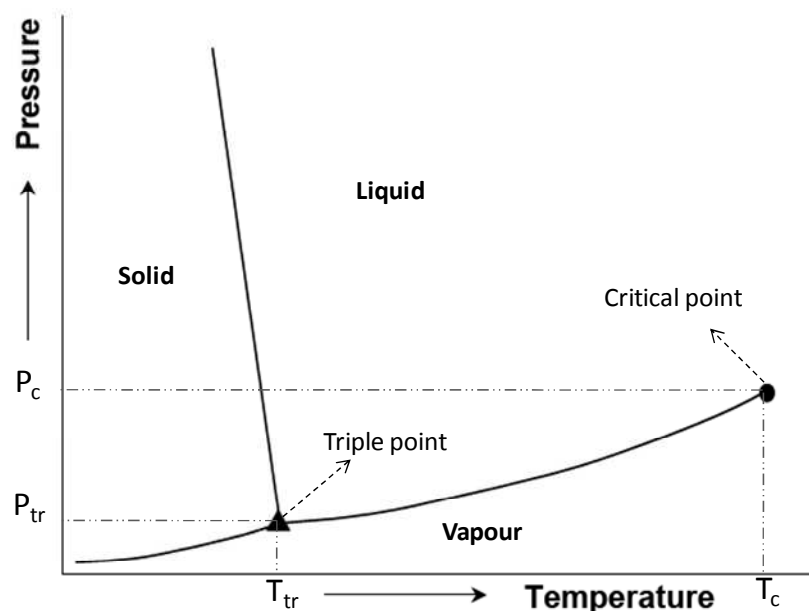


Figure 2.1 Schematic representation of the phase behaviour of water in a P-T diagram [adapted from Mooijer-van den Heuvel, 2004].

Table 2.1 Representation of the various phase(s) in a P-T plane for the unary water system.

π	\emptyset	Example	F	Representation in P-T plane
1	0	I, L, V	2	region, surface
2	0	I-L, I-V, L-V	1	line (curve)
1	2	L=V	0	point
3	0	I-L-V	0	point

2.1.3 Binary Systems (Water and one guest molecule) in the Hydrate Forming Region

In a thermodynamic system with two components ($N=2$), the F_{\max} is equal to 3. This means the full representation of the phase behaviour of the binary system cannot be achieved in just a two-dimensional P-T plane. In

this case, a three-dimensional representation in terms of P, T, x_i is required. However, due to the increased complexity of the phase behaviour in binary systems, the phase behaviour often is presented in a $P-T$ plane in combination with cross-sections at constant temperature ($P-x$) and / or cross-sections at constant pressure ($T-x$). The latter cross-sections cover information on the dependency of the composition of the binary system as a function of pressure and temperature, respectively. For a binary hydrate forming system such as water and a low molecular weight hydrocarbon or a gas, the number of coexisting phases and the type of phases that can be formed increases. The hydrate phase (H), liquid phase other than liquid water (L_V or L_G) and solid phase of the guest component (S) which are not present in the phase behaviour of unary water system might be appearing in the phase diagram of the binary hydrate forming system. Application of the Gibbs' phase rule on the binary hydrate forming system is summarized in Table 2.2.

Table 2.2 The representation of phase(s) in a phase $P-T$ plane for binary hydrate forming system.

π	\emptyset	Example	F	Representation in P, T, x surface
1	0	I, L_W , V, L_V	3	volume
2	0	I- L_W , H-V, H- L_W	2	region, surface
3	0	H- L_W -V, I-H-V, H- L_W - L_V	1	curve, line
4	0	I-H- L_W -V, H- L_W - L_V -V	0	point

As pointed out by Mooijer - van den Heuvel [2004], two types of schematic phase diagrams can be encountered if binary systems of water and a gas are considered in the hydrate forming region. The difference is mainly due to the location of the critical temperature of the gas in the phase diagram. Gases with critical temperatures lower or close to the triple point of water are referred to as 'gas-like' while gases with critical temperatures above the triple point of water are referred to as 'liquid-like'. Carbon dioxide

has a critical temperature of 304.2 K, which is appreciably above the triple point of water (273.16 K). Thus, the binary system of water and carbon dioxide has a 'liquid-like' behaviour in the hydrate forming region. The schematic P-T projection of 'liquid-like' behaviour is presented in Figure 2.2 and the selected cross sections at constant pressures and temperatures are depicted in Figures 2.3 and 2.4 respectively.

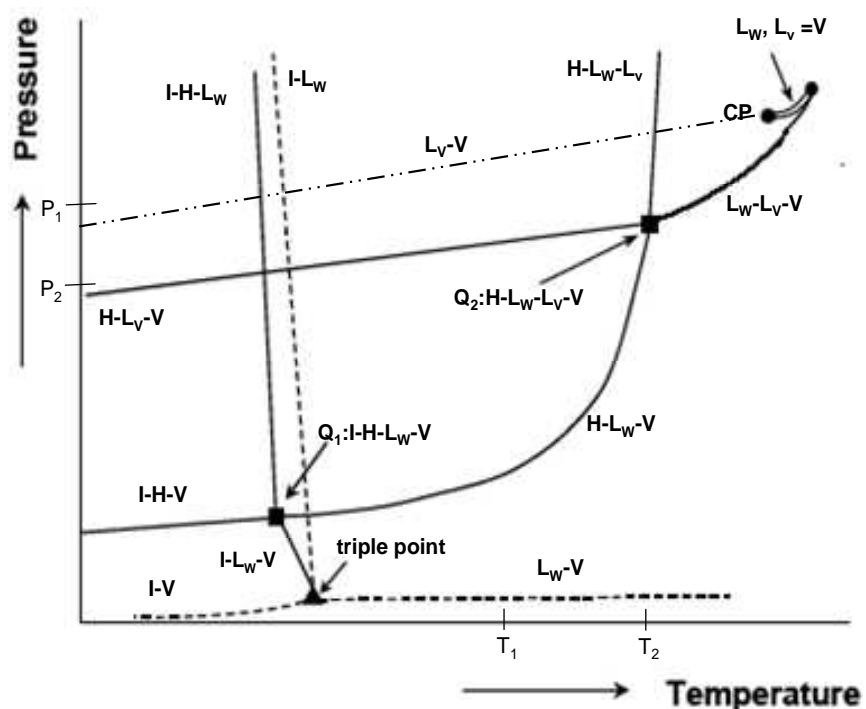


Figure 2.2 Schematic P-T projection of the phase behaviour of the binary system water + gas (solid line) in the hydrate forming region. The gas has a relatively high T_c compared to T_{Q1} . The phase behaviour of the unary systems of water (---) and carbon dioxide (-.-.-) are also included [modified from Mooijer-van den Heuvel, 2004].

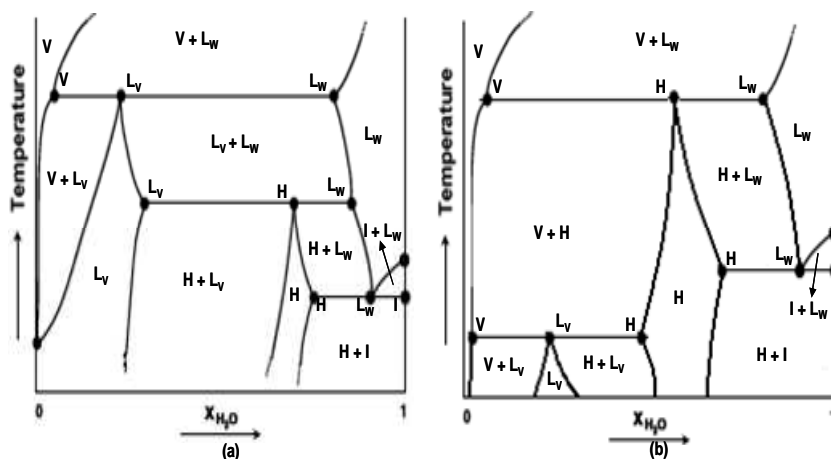


Figure 2.3 Schematic T-x cross sections of the phase behaviour in the binary system water + gas at pressures P_1 (a) and P_2 (b) as indicated in Figure 2.2.

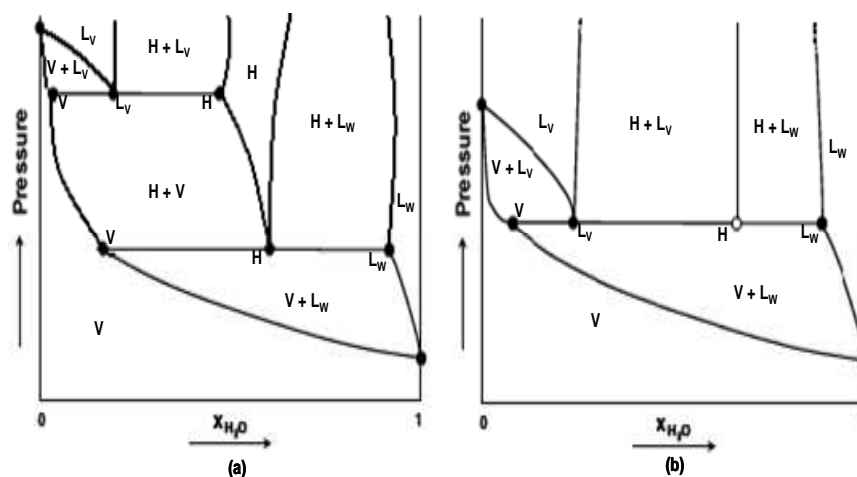


Figure 2.4 Schematic P-x cross-sections of the phase behaviour in the binary system water + gas at temperatures T_1 (a) and T_2 (b) as indicated in Figure 2.2.

As depicted in Figure 2.2, two quadruple points exist in the binary system with 'liquid-like' behaviour, namely Q_1 and Q_2 , respectively. The

quadruple point is a point where four-phases exist in equilibrium in a binary system ($F = 0$). At Q_1 , the four phases in equilibrium are ice (I), hydrate (H), liquid water (L_W) and vapour (V). The three-phase equilibrium curves emerging from Q_1 are H- L_W -V, I-H-V, I-H- L_W and I- L_W -V. The triple point of water is connected to quadruple point Q_1 of the binary system by the three-phase equilibrium curve I- L_W -V. At Q_2 , the four phases in equilibrium are hydrate (H), liquid water (L_W), condensed gas (L_V) and vapour (V). The equilibrium curves emerging from quadruple point Q_2 are H- L_W -V, H- L_V -V, H- L_W - L_V and L_W - L_V -V. It is also clearly shown in Figure 2.2 that the hydrate stability region is confined by the I-H-V, H- L_W -V and H- L_W - L_V equilibrium curves.

The T-x and P-x cross-sections at P_1 , P_2 , T_1 and T_2 are presented in Figures 2.3 and 2.4, respectively. In the cross-sections, univariant equilibria, which are the three-phase equilibria in binary systems ($F=1$), are represented by a horizontal line. Each one of the horizontal lines shown in Figures 2.3 and 2.4 (a) connect three points, which location represents the composition of three coexisting phases. The regions where two phases are stable, are obtained by connecting the points for the same phases on the different horizontal lines. The composition of the various phases and the length of the horizontal lines are dependent on the pressure or temperature at which the cross-section is made. For example, it may be expected that for most conditions, the V phase is relatively rich in the gaseous component, L_W is rich in water, and the I-phase is pure water. It is also possible to represent a quadruple point in the T-x or P-x cross sections. In this case, the four phases are located on a horizontal line at which one of the points represents the fourth phase as depicted in Figure 2.4 (b). From this point, a vertical line is drawn, which separates two regions where two phases are coexisting. From the constructed cross-sections shown in Figures 2.3 and 2.4 at selected fixed pressures or temperature, it can be observed that there are regions where a single phase is stable (V, L_W and L_G), including a single

hydrate phase (H). Besides gases, hydrate forming components that are present in the liquid state at ambient conditions such as tetrahydrofuran, 1,3-dioxolane and 1,4-dioxane, also have similar phase behaviour in the P-T projection as shown in Figure 2.2. This is due to their relatively high values of the critical temperature T_C . However, for these liquids, the H-L_W-V curve will be narrow due to the relatively low vapour pressure of these components. Moreover, the formation of the solid phase of these liquids occurs at relatively low pressures and high temperatures. This may lead to formation of different crystalline solid phases (S, I, and H) in the vicinity the triple point of water [Mooijer-van den Heuvel, 2004; Nakayana and Tahara, 1967].

2.1.4 Ternary and Multi-component Systems in the Hydrate Forming Region

In a ternary system or a multi-component system ($F_{\max} \geq 4$), the representation of the complete phase behaviour requires four or more dimensions. Often, this is not feasible to work with. However, if some of the variables are kept constant, a better representation of the phase diagrams can be obtained. In the case of ternary systems, triangular diagrams at constant pressure and temperature, and prisms with pressure or temperature being constant are two examples of such representations of the phase behaviour. Moreover, if phase transitions are measured for a number of overall-compositions of the system, construction of a surface for three-phase equilibrium curves is possible.

In the hydrate forming region, the appearance of phase diagrams in ternary systems such as water-carbon dioxide-promoter depends on several factors. The phase behaviour of binary system of each guest component with water including the possibility of clathrate hydrates formation have

some impacts on the appearance of the phase behaviour in the ternary system. Moreover, the occurrence and the size of regions of immiscibility of liquid phases also has some influence on the phase behaviour of the ternary systems. One is referred to Mooijer-van den Heuvel [2004] for a detailed discussion on the types of phase behaviour of ternary systems in the hydrate forming region.

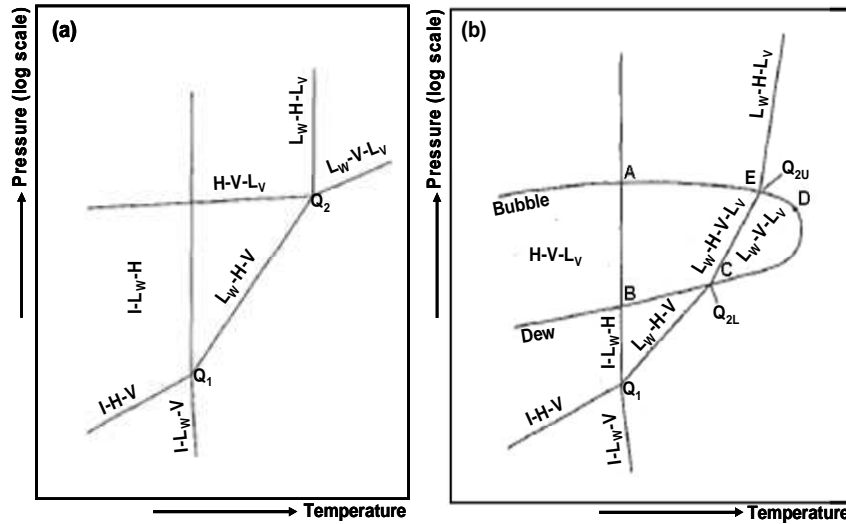


Figure 2.5 Schematic representation of the P-T diagram of two multi-component natural gas + water systems [adapted from Sloan and Koh, 2007].

For a multi-component system, the complete phase behaviour cannot be represented in P-T diagrams. However, similar to ternary systems, if the composition of each component is fixed, then the phase behaviour at this fixed composition can be depicted in a P-T diagram. As examples of the phase behaviour of multi-component systems, Figure 2.5 represents the P-T diagrams of two mixtures of natural gas and water. For the case in which

the multi-component natural gases contain heavier components but no liquid hydrocarbon is present, the phase diagram is presented by Figure 2.5(a). In this case, the two quadruple points, Q_1 and Q_2 are connected by the three-phase L_W -H-V equilibrium curve. However, if liquid hydrocarbon is present in the hydrate forming region, the line L_W -V- L_V in Figure 2.5(a) broadens and becomes a region as labelled CDE in Figure 2.5(b). The formation of this region is caused by the combination of hydrocarbon (and water) vapour pressures which creates a broader phase envelope. Consequently, the upper quadruple point (Q_2) evolves into a four phase equilibrium line of H- L_W - L_V -V. The upper and lower limits of this four-phase equilibrium locus are Q_{2U} and Q_{2L} , respectively.

2.2 HYDRATE FORMATION AND DISSOCIATION

2.2.1 Hydrate Formation

The formation of clathrate hydrates is generally divided into two processes, the nucleation process and the stable growth process [Vysniaskas and Bishnoi, 1983; Englezos et al., 1987; Skovborg et al., 1993; Natarajan et al., 1994; Kashchiev and Firoozabadi, 2003]. Gas hydrate nucleation and growth have been investigated experimentally using different experimental techniques and expressions have been developed to describe the acquired data. Due to the stochastic and time-dependent nature of clathrate hydrate nucleation and growth, there is still a lot of on-going scientific discussion pertaining to these issues. In the next sections, the theoretical background of hydrate nucleation and growth are discussed.

2.2.1.1 Hydrate nucleation

The hydrate nucleation process refers to the formation and growth of hydrate nuclei to a critical size. The growing clusters of gas and water molecules are acting as the precursors to hydrate nuclei formation [Englezos and Bishnoi, 1988; Englezos et al., 1990; Natarajan et al., 1994; Vysniauskas and Bisnoi, 1985]. A growing hydrate nucleus that attains the critical size is a stable nucleus and immediately leads to the formation of crystal hydrate. Experimental and calculated results showed that a stable hydrate nucleus should have a radii between 25 -170 Å [Nerheim et al., 1992; Englezos et al, 1987].

The formation of gas hydrates is a phase transformation which requires a supersaturated environment in order for it to occur. It is a crystallization process. Gas molecules dissolved in liquid water build the supersaturated environment, throughout the liquid phase or locally near the interface. At some point during the dissolution, the precursors to the hydrate phase (nuclei) appear. The nuclei subsequently grow if sufficient gas is present in the structured water environment. Nucleation of hydrates is a microscopic stochastic phenomenon where gas-water clusters (nuclei) grow and disperse until the nuclei have grown to a critical size [Natarajan et al., 1994]. Based on a series of measurements performed for natural gas and carbon dioxide hydrate, Long and Sloan [1996] suggested that the site of hydrate nucleation is located at the water-gas interface. This suggestion is supported by a number of other researchers based on observations made on methane hydrate [Huo et al., 2001; Østergaard et al., 2001] and carbon dioxide hydrate [Kimuro et al., 1993; Fujioka et al., 1994; Hirai et al., 1995; Mori, 1998] nucleation. Sloan and Koh [2007] explained the vapour-liquid interface is preferred for the hydrate formation not only due to the lowering of the Gibbs free energy of nucleation but also due to high concentration of

water and guest molecules, which is required for hydrate nucleation. Thus, theories dealing with describing the hydrate nucleation have focused on this interface. Currently, there are two hypothetical theories dealing with describing the nucleation mechanism have gained acceptance in literature. One of these theories is the cluster nucleation theory [Christiansen and Sloan, 1994] which proposes that water molecules form labile clusters around dissolved gas molecules. These clusters of dissolved species combine to form hydrate unit cells. The other theory assumes that nucleation is taking place at the vapour side of the vapour-liquid interface [Long and Sloan, 1996; Kvamme, 1996]. In this theory, the gas molecules are firstly transported to the interface and absorbed by the aqueous surface. At suitable adsorption sites, water molecules first will form partial and then complete cages around the adsorbed gas molecules. Then, the clusters will join and grow on the vapour side until the critical size is reached. In order to verify which of the above mechanisms accurately represents hydrate nucleation, experimental validation is required. Unfortunately, to date, there is very limited experimental verification of the above hypotheses due to both the stochastic and microscopic nature and the timescale resolution of most experimental techniques.

One of the important parameters used to characterize hydrate nucleation is the induction time. The induction time is the time elapsed during the nucleation processes which include formation of gas-water clusters and their growth to stable nuclei with a critical size. The induction time can be obtained by observing the pressure-time relationship for a hydrate forming system such as presented Figure 2.6. In Figure 2.6, the dissolution of gas in the liquid aqueous phase causes the initial pressure drop from P_0 to P_{sol} . After a steady-state condition is reached, the pressure stabilizes until t_{ind} at which a sudden pressure drop is detected as hydrate starts to form. This point is also known as turbidity point. The pressure keeps decreasing as gas is consumed during the hydrate formation process

until it reaches P_{lim} where no more hydrate forms. The induction time is calculated as

$$\text{Induction time} = t_{ind} - t_{sol} \quad (2.4)$$

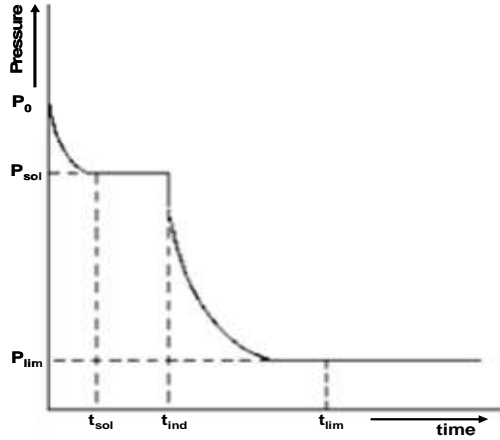


Figure 2.6 Schematic representation of the pressure changes with time during a typical kinetic hydrate formation experiment [adapted from Jensen et al., 2008].

The curve presented in Figure 2.6 is slightly idealized for illustration purposes. Deviation from the shape can appear for example when t_{ind} is lower than t_{sol} or if the gas solubility in water is sufficiently low. Moreover, if temperature of the systems is decreasing with increasing time, the line between t_{sol} and t_{ind} is not straight due to gas contraction upon cooling. The induction time is also dependent on the supersaturation of the guest component in the aqueous phase [Jensen et al., 2008]. A typical relationship between the induction time and the supersaturation is presented in Figure 2.7. In the plot shown in Figure 2.7, it is shown that as the supersaturation decreases, the induction time becomes longer until a

critical point at which the induction time goes to infinity. This trend indicates that no hydrate is formed below this supersaturation critical point.

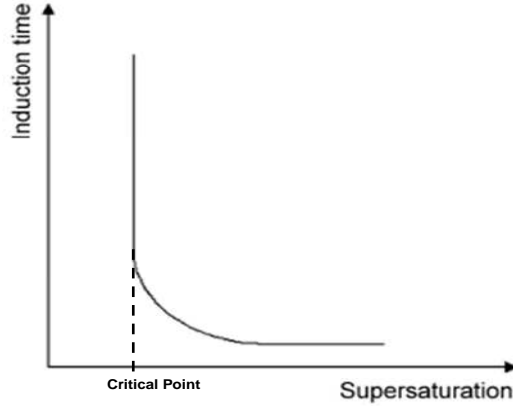


Figure 2.7 Schematic representation of the typical relationship between the induction time and the supersaturation for a nucleating gas hydrate system. When the supersaturation reaches a critical value, the induction time increases dramatically [from Jensen et al., 2008].

Similarly, North et al. [1998] showed that there is a critical value for a gas loading at which below this value, no hydrate will be formed in the system. They calculated the critical value as:

$$Y_{\text{CO}_2} = \frac{\text{total mol of CO}_2}{\text{total mol of CO}_2 + \text{total mol of H}_2\text{O}} \quad (2.5)$$

The authors showed that for carbon dioxide hydrate, this value is about 0.036. Moreover, they hypothesized that carbon dioxide in the liquid phase exists in two categories: dissolved carbon dioxide and carbon dioxide combined with structured water. If the two categories are regarded as reservoirs that must be filled to saturation before hydrate can be formed,

then the dissolved carbon dioxide reservoir should accommodate additional carbon dioxide as pressure increases.

Furthermore, heterogeneous nucleation, which plays an important role in the formation of ice [Mullin, 2004], has also been shown also to be thermodynamically favoured over homogeneous nucleation of gas hydrates [Kashchiev and Firoozabadi, 2002]. This causes the induction time to be very sensitive to any heterogeneities in solution, i.e., impurities can possibly cause significant deviation from the measured induction times.

Table 2.3 Different driving forces used to describe hydrate nucleation.

Investigators	Year	Driving force
Vysniauskas and Bishnoi	1983	$T^{eq} - T^{exp}$
Skovborg and Rasmussen	1994	$\mu_{WH}^{exp} - \mu_{WL}^{exp}$
Natarajan et al.	1994	$f_i^{exp} / f_i^{eq} - 1$
Christiansen and Sloan	1995	Δg^{exp}
Kaschiev and Firoozabadi	2002	$\Delta\mu$, supersaturation
Anklam and Firoozabadi	2004	Δg
Armandi et al.	2005	$T^{eq} - T^{exp}$

In literature, a number of options have been used to describe the driving force for the hydrate nucleation process as summarized in Table 2.3. A comparison and justifications of the selected driving forces have been thoroughly discussed by Sloan and Koh [2007], resulting in the general equation for the hydrate nucleation driving force to be:

$$\Delta g = \nu_L (P^{eq} - P^{exp}) + RT \sum x_i \ln(f_i^{eq} / f_i^{exp}) + \nu_H (P^{exp} - P^{eq}). \quad (2.6)$$

The authors have argued that Equation 2.6 is the general case for all driving forces for hydrate nucleation due to three reasons:

- a. The $(\mu_{WH}^{\text{exp}} - \mu_{WL}^{\text{exp}})$ driving force of Skovborg and Rasmussen [1992] is included in the $\nu_L (P^{\text{ep}} - P^{\text{exp}})$ and $\nu_H (P^{\text{exp}} - P^{\text{eq}})$ terms of Equation 2.6
- b. For all hydrates, the second term on the right dominates Equation 2.6, whereas the first and the last term effectively cancel because the molar volume of water is within 15% of that of hydrates.
- c. The ΔT driving force is the isobaric equivalent of the isothermal Δg in Equation 2.6.

2.2.1.2 Hydrate growth

The hydrate growth process refers to the growth of stable hydrate nuclei as solid hydrates. Mass and heat transfers play important roles in hydrate growth process although most of the nucleation parameters such as displacement from equilibrium conditions, surface area, agitation and gas composition continue to be important during the process. Vysniauskas and Bishnoi [1983, 1985] developed a semi-empirical model to correlate experimental kinetic data which were taken by contacting gas with water at temperatures above the freezing point of water. Their study was the first attempt to describe quantitatively and to model the formation kinetics of gas hydrates. These studies indicated that hydrate formation consists of the appearance of nuclei and their subsequent growth. The growth is dependent on the interfacial area, pressure, temperature and the degree of supercooling. Moreover, the history of the water affects the induction period, but it does not have any observable effect on the growth of the nuclei.

Later, an intrinsic kinetic model for hydrate growth with only one adjustable parameter was formulated by Englezos et al. [1987]. The model is a mechanistic model based on crystallization and mass transfer theories.

It visualized the solid hydrate particle as being surrounded by an adsorption "reaction" layer followed by a stagnant liquid diffusion layer as schematically shown in Figure 2.8.

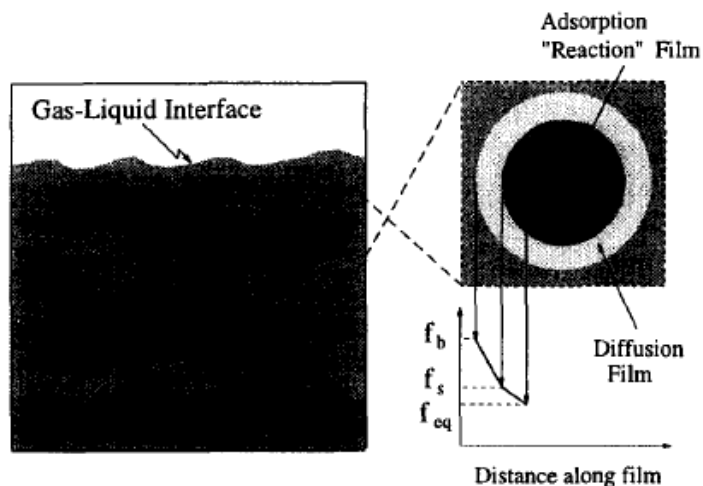


Figure 2.8 Fugacity profile in the diffusion and adsorption "reaction" film around a growing hydrate particle [from Vishnoi and Natarajan, 1996]

The authors proposed the following two consecutive steps for the hydrate particle growth:

- Step 1: Diffusion of the dissolved gas from the bulk of the solution to the crystal-liquid interface through the laminar diffusion layer around a particle.
- Step 2: "Reaction" at the interface, which is an adsorption process describing the incorporation of the gas molecules into the water molecules and the subsequent stabilization of the framework of the structured water.

Since no accumulation is allowed in the diffusion layer around the particle, the above two rates are equal. Hence, the rate of growth per particle in terms of the overall driving force is obtained as

$$\left(\frac{dn}{dt}\right)_p = K^* A_p (f - f_{eq}) \quad (2.7)$$

where A_p is the hydrate surface area per particle, $f - f_{eq}$ is the difference in the fugacity of the dissolved gas and its fugacity at the three phase equilibrium and K^* is expressed in terms of the coefficients for diffusion (k_d) and reaction (k_s) as:

$$\frac{1}{K^*} = \frac{1}{k_r} + \frac{1}{k_d} \quad (2.8)$$

When bulk techniques such as gas uptake measurements are used for determining the kinetics of hydrate formation, a gradual conversion of gas to hydrate is normally shown suggesting a relatively homogenous process that could be modelled using a set of intrinsic kinetics parameter. Recently, Moudrakovski et al. [2004] studied methane and carbon dioxide hydrates formation in water droplets through measurement from magnetic resonance microimaging. Based on their ^1H magnetic resonance microimages such as shown in Figure 2.9, they showed that the hydrate growth process is inhomogeneous process and the smaller the experimental volume observed, the more inhomogeneous the process appeared to be. Based on these observations, they argued that in the quiescent systems studied, the definition of intrinsic kinetic parameters will be difficult, if possible at all, because of a stochastic component that competes with more gradual conversion processes.

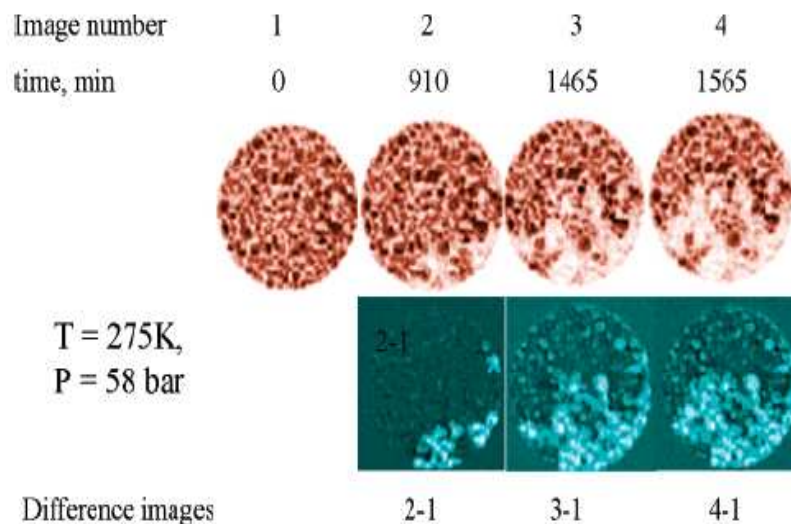


Figure 2.9 ^1H images of CO_2 hydrate formation as a function of time. The images shown are for one of three slices, with the difference images indicated below. Top, hydrate is white; bottom, hydrate is blue [taken from Moudrakovski et al., 2004].

2.2.2 Hydrate Dissociation

Hydrate dissociation is an endothermic process. For hydrate dissociation to take place, heat must be supplied externally to break the hydrogen bonds between water molecules and the van der Waals interaction forces between the guest and water molecules of the hydrate lattice to decompose the hydrate into water and gas. Kamath et al. [1984] have studied the heat transfer during the hydrate decomposition process and observed that the process is analogy with the nucleate boiling phenomena. Based on this analogy, they developed an expression of heat transfer rate during propane hydrate decomposition to be a power function of ΔT , which is the temperature difference between the bulk fluid and the hydrate surface. Later, Kamath and Holder [1987] generalized the correlation and applied it to methane hydrate decomposition. Kim et al.

[1987] suggested that the hydrate decomposition may be viewed as a two step process: the destruction of the clathrate host lattice at the particle surface followed by desorption of the guest molecule from the surface. Based on this view, they developed an intrinsic kinetic model for hydrate decomposition. In the model, the decomposing hydrate particle is assumed to be spherical and a cloud of gas, as shown schematically in Figure 2.10.

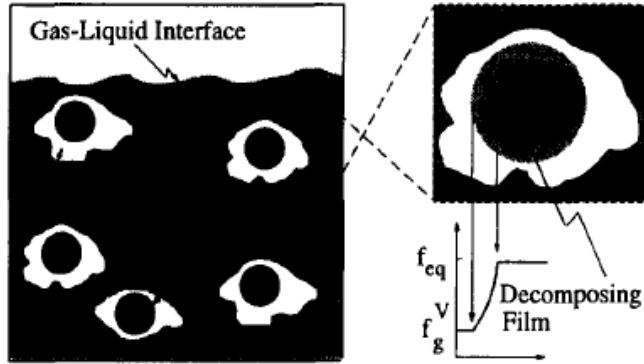


Figure 2.10 Schematic representation of the decomposition of hydrate particles [from Vishnoi and Natarajan, 1996]

The rate of decomposition for a hydrate particle is given by,

$$-\left(\frac{dn_H}{dt}\right)_p = K_d A_p (f_{eq} - f_g^V) \quad (2.9)$$

where K_d is the decomposition rate constant and A_p is the surface area of the hydrate particle. The three phase equilibrium fugacity of the gas, f_{eq} , is obtained at the particle surface temperature and the three-phase equilibrium

pressure while the fugacity of the gas, f_g^V , is obtained at the particle surface temperature and the experimental pressure.

In the last decade, it has been generally agreed that heat transfer plays a more dominant role in hydrate dissociation compared to intrinsic kinetics [Hong et al., 2003; Davies et al., 2006; Sloan and Koh, 2007]. Hong et al. [2003] suggested that the intrinsic kinetics controls the very early stage of hydrate dissociation. However, the existing temperature gradient at the hydrate zone, due to the removal of heat during decomposition, forces heat to be conducted from the hydrate zone to the interface. Hence, the dissociation process is controlled by heat transfer throughout the later stages. Sloan and Koh [2007] have shown a heat transfer model based on Fourier's Law that is able to most accurately predict dissociation time without any adjustable parameters. One is referred to Sloan and Koh [2007] for the details and examples of the developed model (CSMPlug).

2.3 REFERENCES

- Anklam, A.F. and Firoozabadi, A., J. Chem. Phys., 2004, 121, pg. 11867.
- Armandi, M., Ren, S., Tohidi, B., Danesh, A., Todd, A.C., Chem. Eng. Sci., 1994, 715, pg. 177
- Choukrouna, M. and Grasset, O., J. Chem. Phys., 2007, 127(12), pg. 124506-1-11.
- Christiansen, R.L. and Sloan, E.D. in Proc. First International Conference Natural Gas Hydrates, (Sloan, E.D., Happel, J., Hnatow, M.A., eds) Ann. N.Y. Acad. Sci., New Paltz, NY. June 13-16, 1993 (1994).
- Davies, S.R., Selim, M.S., Sloan, E.D., Bollavaram, P., Peters, D.J., AIChE J., 2006, 52, pg. 4016
- Loos, Th.W. de, Understanding Phase Diagrams, In: Supercritical Fluids, Kiran, E., Levelt – Sengers, J.M.H., Applied Sciences, 1994, 273, p. 65-88.

- Englezos, P. and Bishnoi, P.R., Fluid Phase Equilibria, 1988, 42, pg. 129.
- Englezos, P., Kalogerakis, N., Dholabhai, P.D., and Bishnoi, P.R., Chem. Eng. Sci., 1987, 42, pg. 2647.
- Englezos, P., Kalogerakis, N., and Bishnoi, P.R., Journal of Inclusion Phenomena and Molecular Recognition in Chemistry, 1990, 8, pg. 89.
- Fujioka, Y., Takeuchi, K., Shindo, Y., Komiyama., Intl. J. energy res., 1994, 19, pg. 765-769.
- Hirai, S., Okazaki, K., Araki, N., Yoshimoto, K., Ito, H., Hijikata, K., Energy Convers. Manag., 1995, 36, pg. 471.
- Hong, H., Pooladi-Darvish, M., Bishnoi, P.R., J. Can. Petrol. Technol., 2003, 42, pg. 45.
- Huo, Z., Freer, E., Lamar, M., Sannigrahi, B., Knauss, D.M., Sloan, E.D., Chem. Eng. Sci., 2001, 56, 4979-4991.
- Jensen, L., Thomsen, K., von Solms, N., Chem. Eng. Science, 2008, 63, pg. 3069-3080.
- Kamath, V.A. and Holder, G.D., AIChE J., 1987, 33, pg. 347-350.
- Kamath, V.A., Holder, G.D., Angert, P.F., Chem. Eng. Sci., 1984, 39, pg. 1435-1442
- Kashchiev, D., Firoozabadi, A., 2002. Nucleation of gas hydrates. Journal of Crystal Growth 243, pg. 476-489.
- Kashchiev, D and Firoozabadi, A. J. Crystal Growth, 2003, 250, pg. 499-515
- Kim, H.C, Bishnoi, P.R., Heideman, R.A., Rizvi, S.S.H., Chem. Eng. Sci., 1987, 42, pg. 1645.
- Kimuro, H., Yamaguchi, F., Ohtsubo, K., Kusayanagi, T., Morishita, M., Energy Convers. Manag., 1993, 34(9-11), pg. 1089-1094.
- Kvamme, B., in Proc. Second International Conference on Gas Hydrates, Toulouse, France, June 2-5, 1995, pg. 139.
- Long, J.P. and Sloan, E.D., Int. J. Thermophysics, 1996, 17, pg. 1-13

Mooijer-van den Heuvel, M.M. "Phase Behaviour and Structural Aspects of Ternary Clathrate Hydrate Systems: The Role of Additives". Ph.D thesis, Delft Uni. of Technology, January, 2004.

Mori, Y.H., Energy Convers. Manag., 1998, 37, pg. 1537

Moudrakovski, I.L, McLaurin, G.E., Ratcliffe, C.I. and Ripmeester, J.A. J. Phys. Chem. B., 2004, 108, pg. 17591-17595

Mullin, J.W., 2004. Crystallization. Elsevier-Butterworth Heinemann, London.

Nakayama, H. and Tahara, M., Bul. Chem. Soc. Japan, 1973, 46(10), pg. 2965 -2968.

Natarajan, V., Bishnoi, P.R., and Kalogerakis, N., Chem. Eng. Science., 1994, 49, pg. 2075.

Nerheim, A.R., Svartaas, T.M., Samuelsen, E.K., In Proceedings of the Second International Offshore and Polar Engineering Conference, San Francisco, USA, 14-19 June 1992, pg. 620-627.

North, W.J., Blackwell, V.R., Morgan, J.J., Environ. Sci. Technol., 1998, 32, pg. 676-681.

Østergaard, K.K., Tohidi, B., Burgass, R.W., Danesh, A., Todd, A.C., J. Chem. Eng. Data, 2001, 46, pg. 703-708

Skovborg, P., Ng, H.J., Rasmussen, P., and Mohn, U., Chem. Eng. Sci., 1993, 48, pg. 445.

Skovborg, P., and Rasmussen, P., Chem. Eng. Sci., 1994, 49, pg. 1131-1143.

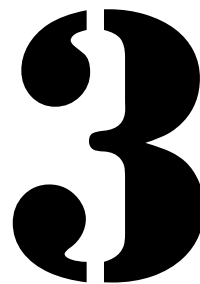
Smith J.M., Van Ness, H.C, Abbott, M.M. "Introduction to Chemical Engineering Thermodynamics", 6th ed. Mc Graw Hill, Singapore, 2001.

Sloan Jr., E.D. and Koh, C.A. "Clathrate Hydrates of Natural Gas", 3rd ed., CRC Press, Florida, 2007.

Vishnoi, P.R. and Natarajan, V., Fluid Phase Equilibr., 1996, 117, pg. 168-177.

Vysniauskas, A. and Bishnoi, P.R., Chem. Eng. Sci., 1983, 38, pg. 1061.

Vysniauskas, A. and Bishnoi, P.R., Chem. Eng. Sci., 1985, 40, pg. 299.



Experimental Methodology

The details of all chemicals used in the present work are given in section 3.1. In order to accurately measure the phase transitions and investigate the phase behaviour of system at hydrate formation conditions, the Cailletet apparatus was used to gather experimental data. This has previously been proven to be amongst the most accurate phase behaviour techniques and suitable for measurements of clathrate hydrate equilibria. The description of the apparatus and experimental procedures are provided in section 3.2. For the measurement of formation of clathrate hydrate kinetic, an in-house designed high-pressure system was employed. The description of the high pressure system and the experimental procedures are detailed out in section 3.3.

3.1 CHEMICALS

The main chemicals used in the present work are demineralised and distilled water (H₂O), carbon dioxide (CO₂) and tetrahydrofuran (THF). The rest of the chemicals used are metal halides. The supplier, the purity and the phase of each chemical used are tabulated in Table 3.1. Carbon dioxide and tetrahydrofuran were used without any further purification. In order to reduce moisture contamination of the metal halide samples especially in the case of CaCl₂, all metal halides were dried at 80°C for 24 hours in a vacuum oven prior to their usage in sample preparation. Distilled and de-ionised water were used after careful degassing.

Table 3.1 Chemicals used with their purities, their phases and suppliers.

Component	Purity (%)	Supplier	Phase
H ₂ O	Distilled & demineralised	Own	Liquid
CO ₂	99.95	Messer-Griesheim	Gas
THF	99.95	Sigma-Aldrich	Liquid
MgCl ₂	> 99.00	Sigma-Aldrich	Solid
CaCl ₂	> 96.00	Sigma-Aldrich	Solid
NaBr	> 99.00	Sigma-Aldrich	Solid
KBr	> 99.00	Sigma-Aldrich	Solid
KCl	> 99.00	Sigma-Aldrich	Solid
NaF	≥ 99.00	Sigma-Aldrich	Solid
NaCl	> 99.00	Sigma-Aldrich	Solid

3.2 PHASE BEHAVIOUR MEASUREMENT

The measurement of phase equilibria was done by using Cailletet apparatus. The equilibrium conditions were measured based on the visual observation of the phases and their transitions. A 'synthetic method' was implied in sample preparation with the help of a gas-rack. A brief explanation of the gas rack and the preparation of the sample are elucidated in Section 3.2.1. The Cailletet apparatus is briefly discussed in Section 3.2.2 and the details of the phase behaviour measurement procedures are presented in Section 3.2.3.

3.2.1 Sample Preparation

The gas-rack apparatus is a necessary facility to be used in the sample preparation process. A schematic representation of the gas-rack apparatus is shown in Figure 3.1. The apparatus is operated based on the principle of communicating vessels. The design of the apparatus allows to be used for liquid sample degassing, measurement of the amount of gaseous sample and filling the sample tube with gaseous sample and confining the sample with mercury.

The samples are prepared according to the synthetic method. Firstly, a liquid sample is prepared depending on the requirement of the system to be studied. This liquid sample can either be pure water, an aqueous solution of water and tetrahydrofuran or an aqueous solution consisting of water, tetrahydrofuran and an electrolyte. For each of the aqueous solutions prepared, the composition of each component in the solution is well-defined. Next, a quantity of the liquid sample is injected into a high-pressure tube, also known as Cailletet tube, using a micrometer syringe. The

Cailletet tube serves as an equilibrium cell for the phase behaviour measurements. The tube is about 50 cm in length, has an open lower end and a closed upper end. Prior to this, a stainless ball is placed into the Cailletet tube, which has a function to magnetically stir the sample. The amount of liquid sample injected is determined by weighing on a scale (Sartorius), with an accuracy of 0.0001g. The tube is then connected to the gas-rack apparatus and the liquid sample is kept frozen by liquid nitrogen. Subsequently, the air inside the tube is evacuated under high vacuum while the liquid sample is kept frozen. Then, the liquid sample is subjected to degassing by successive steps of freezing with liquid nitrogen, imposing high vacuum, and melting.

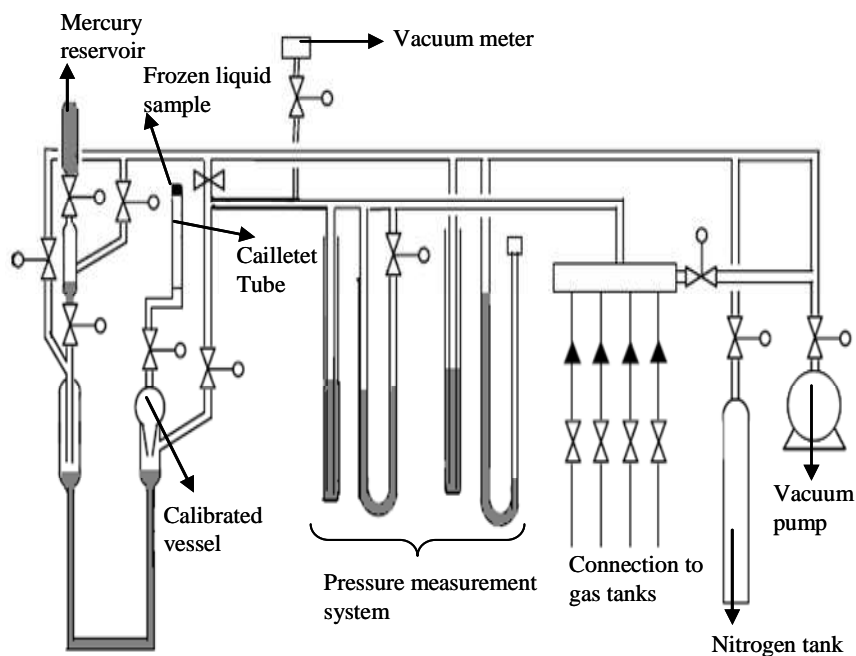


Figure 3.1 Schematic representation of the gas-rack [adapted from Kroon, 2006].

When de-gassing is completed, the gaseous component is added into the tube while the liquid sample is kept frozen. In the present work, the gas used is carbon dioxide. The volumetric calibrated vessel (57.43 cm^3) on the gas-rack apparatus is filled with carbon dioxide. Once the valve connecting the vessel to the carbon dioxide tank is closed, the mercury level is raised by pressurizing the mercury with nitrogen. The carbon dioxide is confined in the vessel by sealing the vessel with mercury. Then, the temperature and pressure readings are taken. Next, carbon dioxide is allowed to flow in the tube and the tube is sealed with mercury. As the volume, pressure and temperature of the amount of carbon dioxide is known, the number of moles of carbon dioxide is easily calculated by applying an appropriate p-V-T relation such as ideal gas law.

3.2.2 Cailletet Apparatus

Once the sample is prepared, the Cailletet tube is transferred to the Cailletet apparatus for the phase behaviour measurements. The overall schematic diagram of the Cailletet apparatus is depicted in Figure 3.2. In this apparatus, phase equilibrium conditions can be measured within a pressure range of 0.35 to 15 MPa and temperature from 255 to 470 K, depending on the fluid chosen as heat-transferring medium. As shown in Figure 3.2, a sample with fixed composition is placed in the top of the Cailletet tube and sealed by a mercury column. The mercury column also acts as a part of the pressure transferring mediums. Pressure is generated by pressing the hydraulic oil into the system with a screw type hand pump. A dead-weight pressure gauge is used to monitor the pressure with an accuracy of $\pm 0.0025 \text{ MPa}$. The temperature of the sample is kept constant by the circulating thermostat liquid through a thermostat jacket surrounding the Cailletet tube. In the present work, ethanol is used as the thermostat liquid with operating temperature ranges from -20°C to 55°C . The

temperature measurement is realized by using a platinum resistance thermometer with an accuracy of $\pm 0.01\text{K}$, located in the jacket near the top of the Cailletet tube. Homogeneous mixing is obtained by moving a stainless ball with two moving magnets driven by an electrical motor. An arrangement consisting of a microscope, which is placed in front of the Cailletet tube and an adjustable light source, which is placed behind the tube is used to achieve a higher visual clarity.

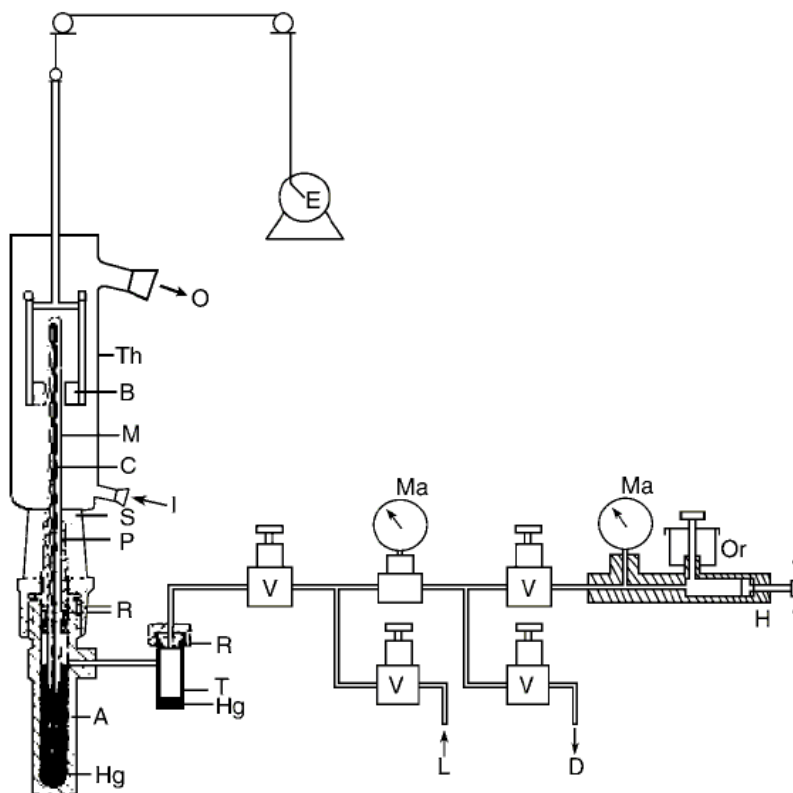


Figure 3.2 Schematic representations of the Cailletet apparatus: A, autoclave; B, magnets; C, Cailletet tube; D, drain; E, stirring motor; H, hydraulic pump; Hg, mercury; I, inlet thermostat liquid; L, connection with dead-weight pressure gauge; M, sample of mercury; Ma, manometers; O, outlet thermostat liquid; Or, oil reservoir; P, closing plug; R, O-rings; S, silicone rubber stopper; T, mercury trap; Th, glass thermostat; V, valve [taken from Raeissi, 2004].

3.2.3 Phase Behaviour Measurement Procedure

The main working principle of Cailletet apparatus for phase behaviour measurements is based on the observation of the number and types of phases present at known temperature and pressure conditions.

3.2.3.1 Hydrate equilibrium points measurement

For the hydrate phase measurements, the equilibrium line is measured by monitoring the disappearance of the hydrate phase. In general, the sample is cooled to form the clathrate hydrate (H) phase at elevated pressure. The pressure is kept constant as much as possible to prevent changes in the level of mercury column, which may result in enclosure of clathrate hydrate crystals in the mercury and changes the overall composition of the sample. By controlled stirring and keeping the sub-cooling of the sample as minimum as possible, formation of plugs or agglomerated hydrate crystals is prevented. Measurement of the equilibrium or transition involving a clathrate hydrate phase can only be accomplished when the clathrate hydrate crystals are moving freely in the fluid phases.

For the measurement of hydrate equilibrium dissociation lines, i.e., $H + L_W + V \rightarrow L_W + V$, $H + L_W + L_V \rightarrow L_W + L_V$, $H + L_W + L_V + V \rightarrow L_W + L_V + V$, the pressure is fixed at a constant value by means of the dead-weight pressure gauge. The starting point is at a pressure where a hydrate phase (H), a vapour phase (V), a liquid water phase (L_W) and/or a liquid organic phase (L_V) are present. Subsequently, the temperature is elevated in small steps, typically at a rate of 0.5 K per 10 minutes, until the dissociation of the hydrate phase can be observed. Small bubbles appear around the hydrate crystals and the temperature is kept constant as long as these bubbles are observed. When the bubbles disappear and the hydrate phase is still

present, the temperature is increased by small steps of 0.1 K until no hydrate crystal is observed. The temperature where the hydrate phase disappears is taken as the phase equilibrium temperature. A schematic representation of a phase transition comprising a clathrate hydrate phase is depicted in Figure 3.3.

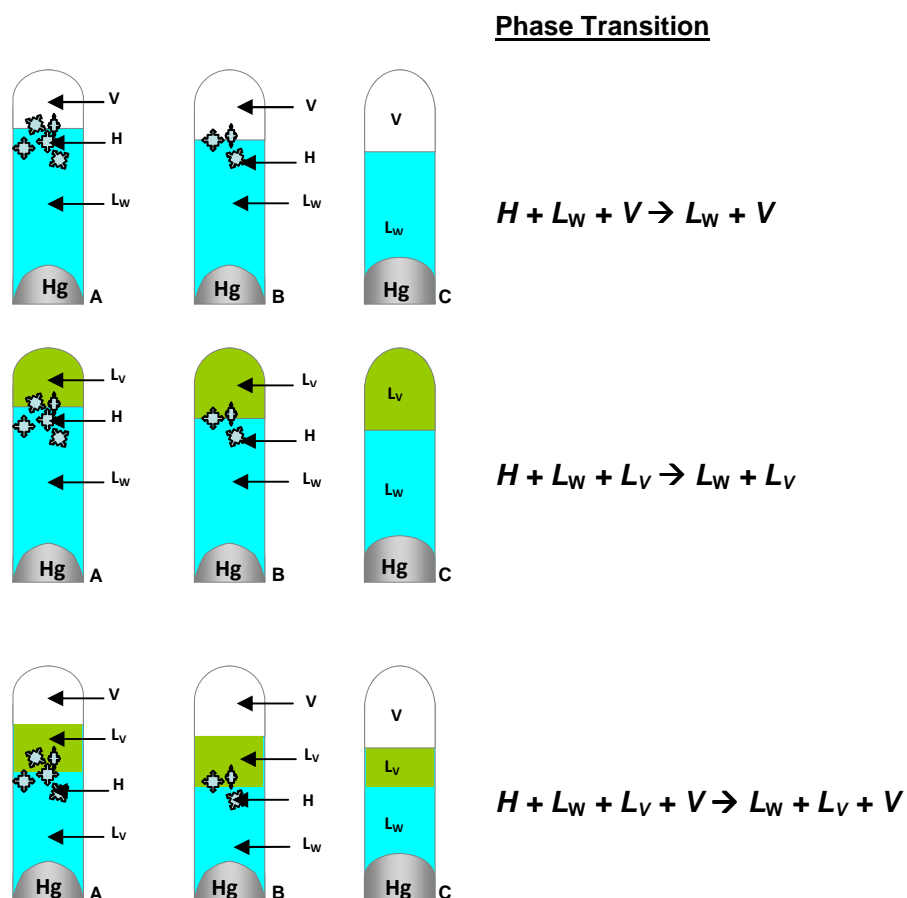


Figure 3.3 Schematic representation of a phase transition comprising a clathrate hydrate phase.

3.2.3.2 Bubble- and dew points measurement

In the present work, fluid phase boundary curves and clathrate hydrate equilibria are used to determine quadruple points. The quadruple points measured are Q_2 or Q_{2U} and Q_{2L} depending on whether a liquid-liquid phase split occurs in the system measured. The fluid phase boundary curves measured are comparable to bubble- and dew point measurements. A schematic representation of the bubble- and dew point measurements is depicted in Figure 3.4.

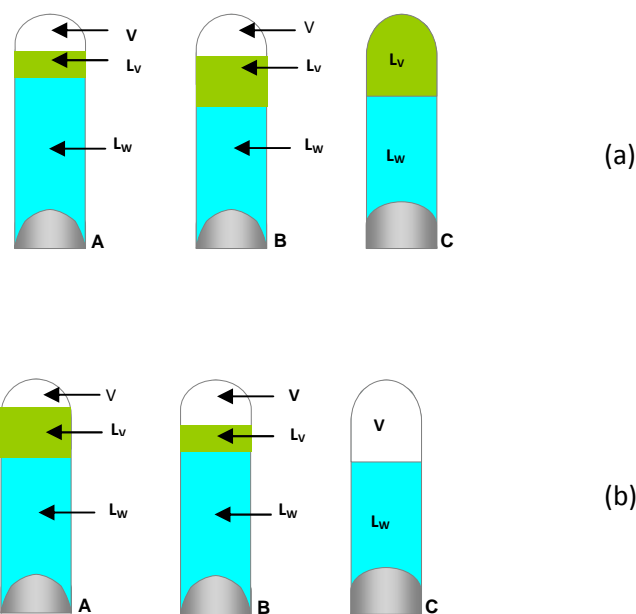


Figure 3.4 Schematic representation of a fluid phase transition: (a) bubble and (b) dew points [adapted from Kühne, 2008].

For the measurement of bubble point curves, the temperature is fixed at a constant value and the pressure is adjusted using the dead-weight pressure gauge. The starting point is at a pressure where a vapour phase

(V), liquid water (L_W), liquid organic (L_V) are present. From this point, the pressure is increased gradually until the last bubbles of the vapour phase disappears, i.e., $L_W + L_V + V \rightarrow L_W + L_V$. Similarly, the starting point for the dew point measurements is the same. However, the pressure is reduced until the last droplets of the condensed gas phase disappears, i.e., $L_W + L_V + V \rightarrow L_W + V$. For all types of phase transition measurements, the pressure is corrected for the pressure generated by the height of the mercury column and the atmospheric pressure as well.

3.3 KINETICS OF HYDRATE FORMATION MEASUREMENT

The measurement of kinetic of hydrate formations was also conducted in a high-pressure system. A semi-batch stirred tank reactor was designed and built for the experimental work. A brief explanation of the apparatus is elucidated in section 3.3.1. The details of the kinetic of hydrate formation measurement procedures are presented in Section 3.3.2.

3.3.1 High Pressure Kinetics Measurement Apparatus

A schematic representation of the high-pressure system used for the measurement of kinetics of formation and decomposition of clathrate hydrate in the present work is depicted in Figure 3.5. The main part of the system is a high-pressure stainless steel vessel with an internal volume of approximately 150 cm^3 . The maximum working pressure for the vessel is 100 MPa. To maintain the temperature at a desired value, the vessel is immersed in a thermostatic bath. The temperature of the thermostatic bath is controlled by a PID controller that maintained the temperature within $\pm 0.1^\circ\text{C}$. The thermostat liquid used is a mixture of ethylene glycol + water

and the heating and cooling of the thermostat liquid is carried out by a cryostat. The temperature inside the vessel was monitored both in the gas phase and in the liquid phase by two thermocouples (New Port Omega type T) with an accuracy of ± 0.01 °C. To achieve proper mixing in the liquid sample, a magnetic stirrer is placed in the vessel. The pressure inside the cell is measured with a pressure transducer (a piezo-resistive AE SML series pressure sensor) with pressure reading range between 0 to 250 bars. The pressure and temperatures readings are recorded and stored in a data acquisition system.

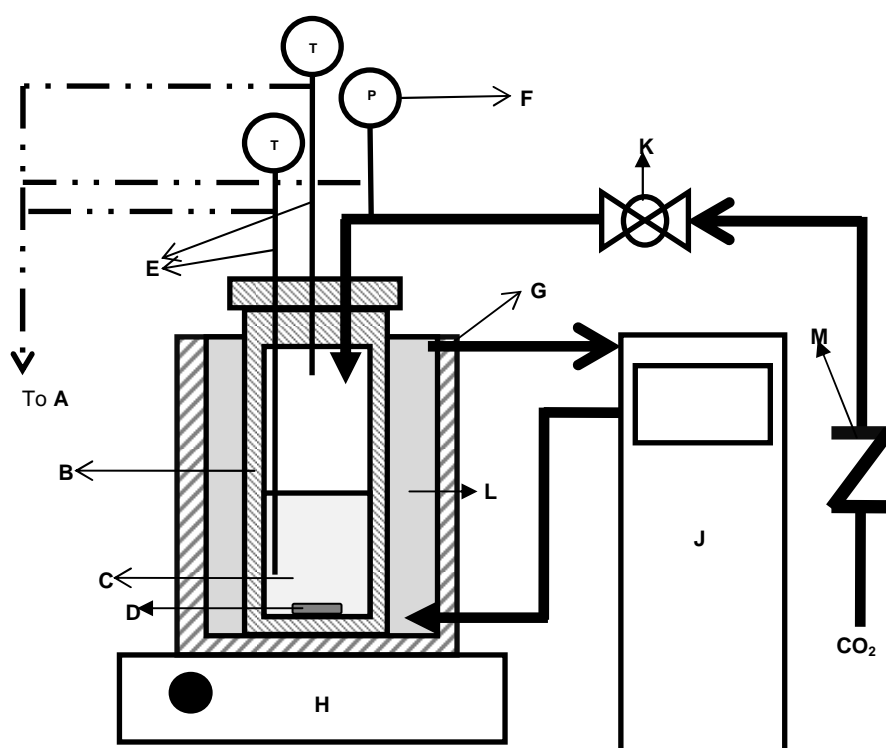


Figure 3.5 Schematic representation of the high pressure kinetics measurement apparatus: A: Data Acquisition System, B: High Pressure Vessel, C: Liquid Sample, D: Stirrer, E: Thermocouple, F: Pressure Gauge, G: Thermostatic Bath, H: RPM controller, J: Cryostat, K: Valve, L: Thermostatic Liquid, M: One-way Valve

3.3.2 Kinetics Measurement Procedure

In the present work, a closed loop cycle method [Sloan, 1998] is employed for the measurement of formation and decomposition of clathrate hydrate kinetics. In this method, the amount of carbon dioxide and liquid sample are fixed and neither carbon dioxide nor liquid are added to the system during the experiment. For each one of the cycles, the high pressure vessel is loaded with a known volume and mass of a liquid sample. Throughout the present work, three different liquid samples are used depending on the systems measured. The liquid samples are demineralized water, a mixture of water and tetrahydrofuran (5 mol%) or a mixture of water, tetrahydrofuran (5 mol%) and sodium chloride (1 mol%). Then, the vessel is flushed with carbon dioxide by loading of carbon dioxide and subsequently releasing the pressure. Since the presence of other gases may effects temperature and pressure values at which hydrate will be formed, the type of hydrate formed and the occupation of hydrate cavities, the procedure is repeated five times to ensure that the presence of other gases in the vessel is in the order of ppm or as minimum as possible. During the flushing, the stirrer is switched off to prevent solubility of carbon dioxide in the aqueous sample. After the flushing procedure is completed, the vessel is ready to be used for the kinetic measurements.

Due to high solubility of carbon dioxide in the aqueous mixture, the loading of carbon dioxide is conducted at initial temperature 2-3 K higher than the hydrate equilibrium temperature at a specified pressure. Firstly, when the temperature is stabilized, the vessel is pressurized with carbon dioxide to the desired pressure value. When the pressure and the temperature in the liquid and vapor phases in the vessel are relatively constant, the stirrer is switched on. The rate of stirring is kept at 500 rpm. This value is chosen because the stirring rate is sufficient to remove the clathrate hydrates from the gas-liquid interface and to keep the hydrate

particles as small crystals in solution (slurry) but not high enough to induce excessive rippling at the surface or bubble entrapment by vortex [Vysniauskas and Bishnoi, 1983]. Throughout the experimental work, a decrease of pressure is observed during this step suggesting that the dissolution of carbon dioxide in the aqueous mixture is taking place. When the pressure regains stability, the temperature of the system is slowly reduced to 5 K below the hydrate equilibrium temperature of the system. Meanwhile the system was stirred. The temperature was never decreased below 273 K to prevent the formation of ice instead of the gas hydrate. When the desired final temperature condition is achieved, the system is left for 2 to 3 hours to ensure that the clathrate hydrate formation is completed. Throughout the process, pressure and temperature changes are monitored and recorded by the data acquisition system every second. When the pressure and temperature values stabilized, the measurement of clathrate hydrate formation kinetic is completed.

When the clathrate hydrate formation is completed, i.e., the pressure of the system is stabilized at a preset temperature below the hydrate equilibrium temperature, the stirring is switched off. Then, the system is slowly heated up to the initial temperature, which is 2-3 K higher than the hydrate equilibrium temperature. The system is allowed to reach equilibrium, normally in about 2-3 hours while the pressure and temperature data are collected by the data acquisition system.

3.4 REFERENCES

Kroon, M.C. "Combined reactions and separations using ionic liquids and carbon dioxide". PhD thesis, Delft University of Technology, December, 2006.

Kühne, E. "Fluid phase behaviour of ionic liquid-based systems of interest for green processes: experiments and modelling". PhD thesis, Delft University of Technology, June, 2008.

Raeissi, S. "On the phenomenon of double retrograde vaporization within a study on supercritical deterpenation of orange oils with ethane". PhD thesis, Delft University of Technology, November, 2004.

Sloan Jr., E.D. "Clathrate Hydrates of Natural Gas". 2nd ed., Marcel Dekker, New York, 1998. pg. 66.

Vysniauskas, A. and Bishnoi, P.R. Chem. Eng. Sci., 1983, 38 (7), pg. 1061-1972.

4

Phase Behaviour of Simple Carbon Dioxide and Mixed Carbon Dioxide and Tetrahydrofuran Hydrates

Phase equilibria and phase transitions comprising a clathrate hydrate phase are determined experimentally based on the methodology discussed in Sections 3.1 and 3.2. In this chapter, the H-L_W-V, H-L_W-L_V-V and H-L_W-L_V equilibrium data and the phase transitions L_W-L_V-V → L_W-L_V and L_W-L_V-V → L_W-V are reported when available. As a method to verify the accuracy of the experimental techniques and the basis for comparison, the phase behaviour of the binary system consisting water and carbon dioxide is measured experimentally and reported in Section 4.1. The data are compared with literature data. Next, the phase behaviour of the ternary system of water, carbon dioxide and tetrahydrofuran is measured experimentally and reported in Section 4.2. In Sections 4.2.1 and 4.2.2, the effects of carbon dioxide and tetrahydrofuran concentrations on the phase equilibria of the ternary system in the hydrate forming region are reported and thoroughly discussed, respectively.

4.1 INTRODUCTION

It is well established that the inclusion of a hydrate promoter in hydrate forming systems reduces the hydrate formation pressure significantly. Promoters or additives can be divided into two categories depending on their solubility in water, i.e., water-soluble and water-insoluble additives respectively. THF, propylene oxide, 1,4-dioxane are some examples of water-soluble additives. The equilibrium pressure reduction effect by water-soluble compounds differs from the pressure effect of water-insoluble compounds by their concentration dependency [de Deugd et al., 2001]. Insoluble additives like benzene, cyclohexane, cyclopentane and neopentane [Tohidi et al., 1997] form an extra liquid phase in the system, which reduces the number of degrees of freedom by one according to the Gibbs phase rule. However, if the solubility limit of the water-soluble compounds is reached, the systems will lose their concentration dependency of the hydrate equilibrium conditions.

In general, it is normally agreed that for a system with single gas components such as methane, carbon dioxide, ethane and hydrogen with a soluble promoter, the three-phase H-L_W-V equilibrium line is dependent on the pressure or temperature and concentration of the promoter in the hydrate forming systems. However, due to the limited number of data for such systems at higher pressure conditions, a complete understanding of the phase behaviour of these systems in the hydrate forming region is still desirable. In the case of carbon dioxide, the possibility of a liquid-liquid phase split in the water and cyclic organic ethers such as tetrahydrofuran when pressurized with carbon dioxide [Lazzaroni et al., 2004] is among the considerations that might increase the complexity of the phase behaviour in hydrate forming system. In order to get a better understanding of these systems, in the present work, an attempt is made to carefully measure the

hydrate equilibrium lines in a large range of temperature and pressure conditions and at different compositions of the ternary systems. As a basis for comparison, in Section 4.2, the hydrate equilibrium conditions for the binary system water and carbon dioxide are measured and reported. In Section 4.3, the hydrate equilibrium conditions for the ternary system carbon dioxide-tetrahydrofuran-water are presented. The effect of carbon dioxide and tetrahydrofuran on the phase behaviour of the ternary systems are shown and discussed in Section 4.3.1 and 4.3.2 respectively. All the measured equilibrium data are tabulated in Appendix A. In this work, the aqueous-composition of THF is converted to the overall composition as follows:

$$\text{Overall composition (\%THF)} = \left[\frac{\left(\frac{\text{aqueous composition (\%THF)}}{100} \right) \times \text{no. of mole of liquid sample}}{\text{total no. of mole}} \right] \times 100 \quad (4.1)$$

4.2 PHASE BEHAVIOUR OF THE BINARY WATER AND CARBON DIOXIDE SYSTEM IN THE HYDRATE FORMING REGION

As a basis for comparison with systems with promoter and inhibitors, the phase behaviour of the binary system water and carbon dioxide in the clathrate hydrate forming region is measured in the temperature and pressure ranges of 272–292 K and 1.0–7.5 MPa, respectively. The equilibrium conditions measured are the hydrate equilibrium line, H-L_W-V, the high pressure hydrate equilibrium line, H-L_W-L_V and bubble-point line, L_W-L_V-V → L_W-L_V. Moreover, the accuracy of the measurement is verified with available literature data. The measured data are presented in Table A1, appendix A. The results together with literature data are presented in Figure 4.1. From Figure 4.1, it can be observed that

the measured data agree very well with those reported in literature in the temperature and pressure ranges studied. In this system, the L_V phase is a condensed carbon dioxide phase. The measurement of the $H-L_V-V$ equilibrium line is achieved by taking advantage of the metastability condition of clathrate hydrate formation, which required sub-cooling of the system to force the hydrate formation to take place. Due to this phenomenon, the bubble point measurement is employed to obtain the $H-L_V-V$ equilibrium line until hydrate is formed in the system at about 5 K below the clathrate hydrate equilibrium temperature. As shown in Figure 4.1, the $H-L_V-V$ data obtained in this work by taking advantage of the metastability conditions agree very well with that of Ohgaki et al. [1993] and Vlahakis et al. [1972], which are obtained from direct measurement.

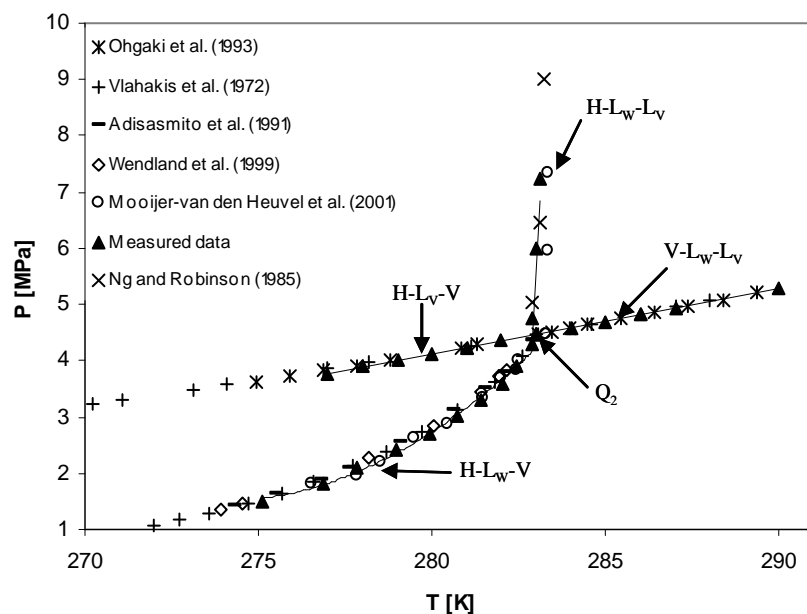


Figure 4.1 Three-phase equilibrium data for the carbon dioxide hydrate system.

The upper quadruple point, Q_2 (see Figure 4.1) at which hydrate, vapour, condensed carbon dioxide and liquid water phases exist in equilibrium is measured at 283.0 K and 4.47 MPa. The experimental value of Q_2 is similar to the reported literature values of Mooijer-van den Heuvel et al. [2001] at 283.27 K and 4.48 MPa and Unruh and Katz (1949) at 283.1 K and 4.502 MPa. As shown in Figure 4.1, it is obvious that the hydrate formation region is bounded by the H-L_W-V and H-L_W-L_V equilibrium lines. At any specified pressure and temperature higher than the clathrate hydrate equilibrium temperature, no clathrate hydrate will be present in the binary water and carbon dioxide system. By taking this as a consideration, the H-L_V-V equilibrium data reported by Vlahakis et al. (1972) is actually a combination of H-L_V-V and L_W-L_V-V equilibrium data. Since no hydrate can be present in the system at temperatures higher than the Q_2 temperature, the hydrate phase is changed into a liquid phase at a temperature higher than the Q_2 temperature.

4.3 PHASE BEHAVIOUR OF THE TERNARY SYSTEM WATER, TETRAHYDROFURAN AND CARBON DIOXIDE IN THE HYDRATE FORMING REGION

The measured hydrate equilibrium data for the ternary system of carbon dioxide-tetrahydrofuran-water with 5 mol % of tetrahydrofuran in the aqueous solution and 2 mol% of carbon dioxide in the overall composition are shown graphically and compared in Figure 4.2 with the binary system of carbon dioxide-water. As depicted in Figure 4.2, the addition of a small amount of tetrahydrofuran expands the hydrate stability region significantly to higher temperature at a constant pressure. As comparison, reported H-L_W-V equilibria for CO₂ + THF + water [Delahaye et al., 2006] and methane + THF + water [de Deugd et al., 2001] systems in literature are depicted in Figures 4.3 and 4.4 respectively.

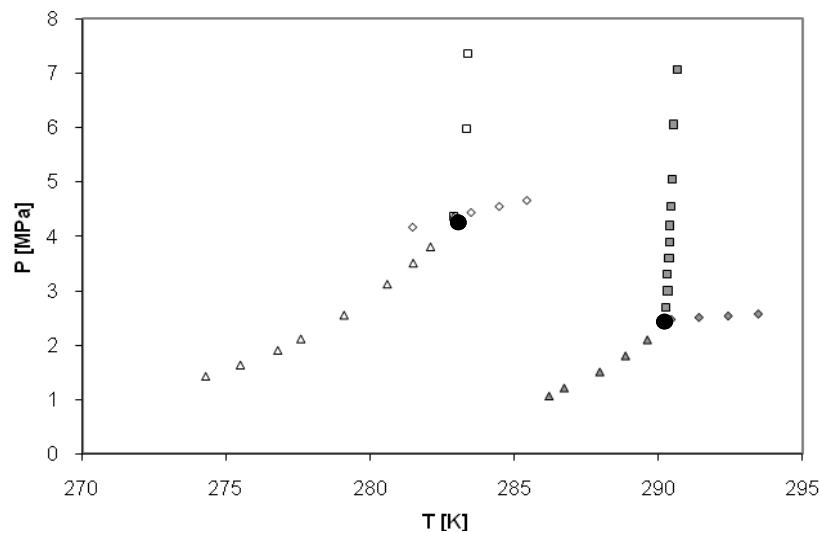


Figure 4.2 Experimental phase equilibrium data of the binary system $\text{H}_2\text{O} + \text{CO}_2$ (open markers) and the system ternary $\text{H}_2\text{O} + \text{CO}_2 + \text{THF}$ with 5 mol% THF in the aqueous solution and 2 mol% CO_2 in overall concentration (filled markers). The various three-phase equilibria are indicated as follows: H-L_W-V (Δ), H-L_W-L_V (\square), L_W-L_V \rightarrow L_W-L_V (\diamond) and Q₂ (\bullet).

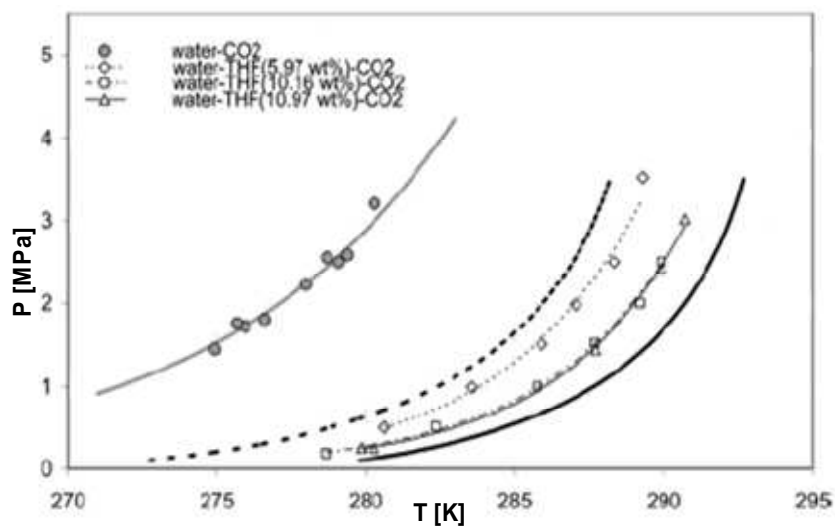


Figure 4.3 L_W-H-V equilibria for water-CO₂ (literature1 and previous work4) and water-THF-CO₂ systems [taken from Delahaye et al., 2006].

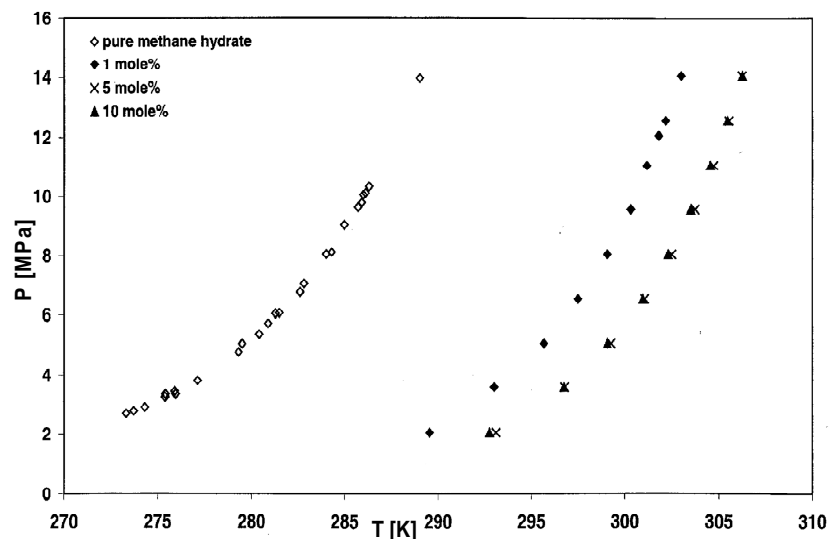


Figure 4.4 p,T-diagram of the $\text{H-L}_W\text{-V} \rightarrow \text{L}_W\text{-V}$ transitions in the water–methane–THF system [taken from de Deugd et al., 2001].

At a specified pressure, the equilibrium temperature of the system with tetrahydrofuran is shifted to higher temperature by ~ 10 K. Similar results were found by Delahaye et al. [2006] for the $\text{H-L}_W\text{-V}$ equilibrium conditions as depicted in Figure 4.3. This temperature shift is found to be less than that of methane hydrates systems as depicted in Figure 4.4. Nonetheless, it is clearly shown that the inclusion of tetrahydrofuran increases the hydrate stability region in both systems. It should be noted that both systems have two types of hydrate equilibrium lines i.e., $\text{H-L}_W\text{-V}$ and $\text{H-L}_W\text{-L}_V$. The changes of the vapour phase (V) into condensed phase (L_V) occurred at a quadruple point (Q_2). This point is located at the intersection between the $\text{H-L}_W\text{-V}$ line and the $\text{L}_W\text{-L}_V\text{-V}$ line. Due to the incompressibility of the three phases of the $\text{H-L}_W\text{-L}_V$ equilibrium line, the pressure increases steeply with increasing temperature. Moreover, the upper quadruple point, Q_2 , in the ternary system is shifted to much lower pressure compared to that of the binary system.

This observation confirms that the presence of tetrahydrofuran in the system increased the stability of the hydrate phase. In pure water, carbon dioxide forms sl simple hydrate with its molecules occupying the large cavities ($5^{12}6^2$). Meanwhile, tetrahydrofuran is known to form sII hydrate as simple hydrate and its molecules occupy the large cavities ($5^{12}6^4$) of sII hydrate. However, since the van der Waals diameter of the carbon dioxide (5.12 Å) is smaller than the free diameters (~ 5.76 Å) of most cavities in the hydrate lattice, carbon dioxide molecules can migrate in the hydrate lattice [Teng, 1996]. Studies by Ripmeester and Ratcliffe [1998] and Mooijer-van den Heuvel [2004] have shown that carbon dioxide molecules will occupy the small cage in sII hydrate when there is a larger hydrate former presents in the system. Thus, in the ternary system of carbon dioxide-tetrahydrofuran-water, since tetrahydrofuran molecules cannot enter any of the sl cavities, sII hydrates are formed as its molecules occupy the large cavities ($5^{12}6^4$), while carbon dioxide molecules occupy the smaller cavities (5^{12}) of structure sII. Since, hydrate stability, to certain extent, is dependent on the fractional occupancy of the hydrate lattices, the stability of the hydrate will be increased as more cavities are filled with guest molecules. Thus, the addition of tetrahydrofuran in the aqueous solution results in more favourable conditions for the formation of gas hydrates at a lower pressure and elevated temperature.

In order to get a better understanding of the effects of different concentrations of carbon dioxide and tetrahydrofuran on the phase behaviour of the ternary system in the clathrate hydrate forming region, the hydrate equilibrium lines and phase transitions at different compositions of carbon dioxide and tetrahydrofuran in the ternary system have been measured. The phase behaviour of the ternary system in the clathrate hydrate forming region at different concentrations of carbon dioxide and at a constant tetrahydrofuran concentration of 5 mol% in the aqueous solution are presented in Section 4.3.1 while the phase behaviour of the ternary system in the clathrate hydrate forming region at different concentrations of

tetrahydrofuran and a constant carbon dioxide of 9 mol% are presented in Section 4.3.2.

4.3.1 Effects of Carbon Dioxide Concentration

To gain some insight in the effects of carbon dioxide concentration on the phase behaviour of the ternary system in the hydrate forming region, the hydrate equilibrium data and phase transitions for systems with overall carbon dioxide concentration of 1, 3, 4, 9, 19 and 29 mol% are depicted in Figure 4.5. In all systems studied, the composition of tetrahydrofuran is kept constant at 5 mol% in the aqueous solution (CO₂ free basis). As depicted in Figures 4.5, at very low overall compositions of carbon dioxide of 1 mol%, the three-phase hydrate equilibrium line of H-L_W-V is connected directly to the H-L_W-L_V equilibrium line at a quadruple point, Q₂. However, as the overall composition of CO₂ is increased to higher values as shown in Figure 4.5, a four-phase equilibrium line H-L_W-L_V-V is observed to appear in between the H-L_W-V and H-L_W-L_V lines.

The formation of the four-phase equilibrium line is due to a liquid-liquid phase split which normally occurs in mixtures of water and a hydrophilic organic solvent such as THF when pressurized with carbon dioxide [Lazzaroni et al., 2004]. Addition of carbon dioxide to a miscible binary liquid mixture of tetrahydrofuran + water at a temperature near the critical temperature of carbon dioxide results in the formation of two distinct liquid phases, i.e., a water-rich phase with a nearly constant amount of carbon dioxide present and a carbon dioxide + organic-rich phase where the carbon dioxide concentration increases with increasing pressure. Since the bubble point (L_W-L_V-V → L_W-L_V) and dew point (L_W-L_V-V → L_W-V) lines are observed by the disappearance of either one of the vapour (V) or condensed gas phase (L_V), the four-phase equilibrium line is bounded by

those two equilibrium lines. Also, since the condensed gas phase is dependent on the amount of carbon dioxide available in the system, the region where the two liquid phases ($L_W + L_V$) and the vapour phase (V) can exist in equilibrium is extended by the increase of the overall composition of CO_2 in the system and consequently the $\text{H-L}_W\text{-L}_V\text{-V}$ is extended to higher pressure and temperature.

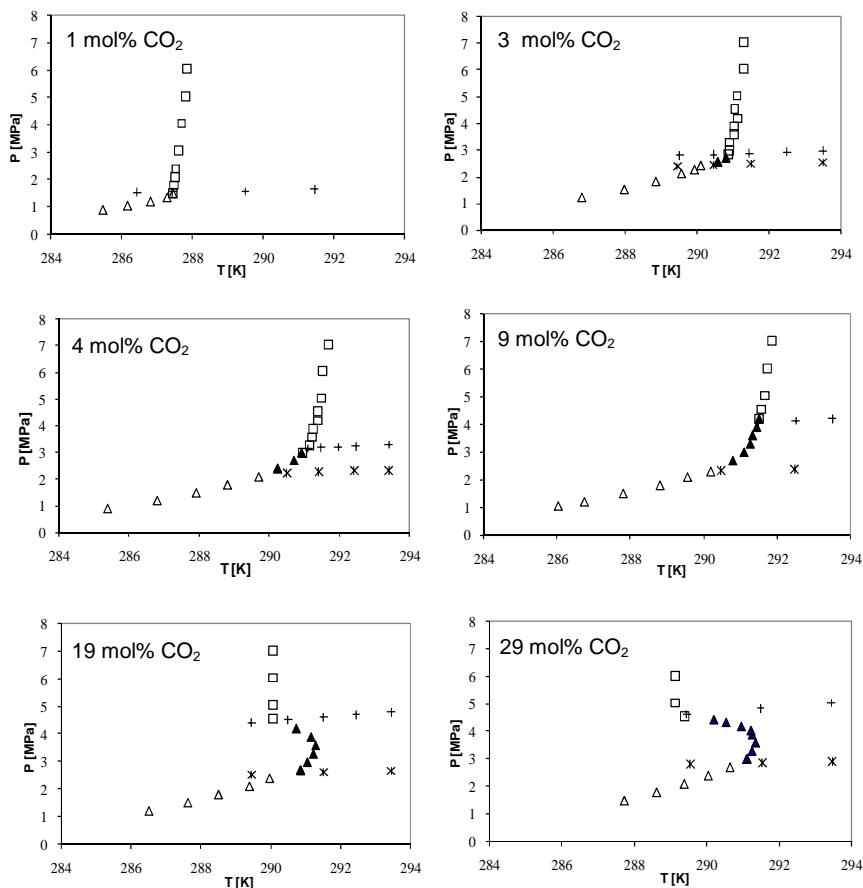


Figure 4.5 Experimental data of the phase behaviour in the ternary system $\text{H}_2\text{O} + \text{CO}_2$ with 5 mol% THF in the aqueous solution. The various equilibria are indicated as follows: $\text{H-L}_W\text{-V}$ (Δ), $\text{H-L}_W\text{-L}_V\text{-V}$ (\blacktriangle), $\text{H-L}_W\text{-L}_V$ (\square), $\text{L}_W\text{-L}_V\text{-V} \rightarrow \text{L}_W\text{-L}_V$ (+), $\text{L}_W\text{-L}_V\text{-V} \rightarrow \text{L}_W\text{-V}$ (\times).

In general, according to the Gibbs phase rule, for a ternary system consisting of water-soluble additive + gas + water, the three-phase equilibrium has two degrees of freedom. Consequently, the temperature of the equilibrium $H-L_W-V$ and $H-L_W-L_V$ are dependent on the overall composition of the system at a constant pressure. Figure 4.6 shows the $H-L_W-V$ equilibrium data for different overall compositions of carbon dioxide in the ternary system while the concentration of THF in the aqueous phase is kept constant at 5 mol%. Within the experimental error, the $H-L_W-V$ equilibrium line seems to be independent on the overall composition of carbon dioxide in the system at pressures in the range studied. Since there are two degrees of freedom for the above three-phase equilibrium, the phase equilibrium is suspected to be dependent on the overall composition of THF in the ternary system.

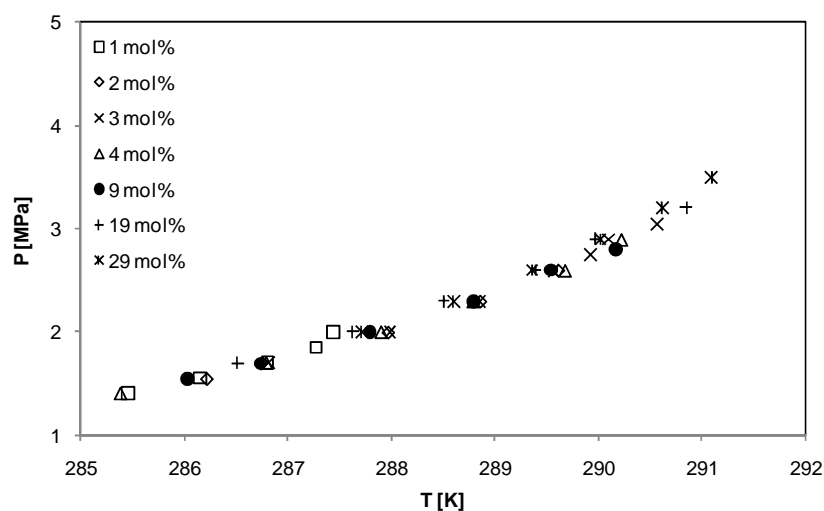


Figure 4.6 Experimental data of the $H-L_W-V$ equilibrium line for the ternary system H_2O-CO_2-THF at different concentrations of CO_2 . The concentration of THF is kept constant at 5 mol% in the aqueous solution.

The $H-L_W-L_V-V$ and $H-L_W-L_V$ equilibrium lines at 3, 4 and 9 mol% of overall composition of carbon dioxide are depicted in Figure 4.7. For the

four-phase equilibrium $H-L_W-L_V-V$, since there is only one degree of freedom, the temperature of the equilibrium is independent of the overall-composition of the system when pressure is kept constant. However, since the region where the formation of a liquid-liquid phase split is limited by the bubble and dew point lines, which are dependent on the amount of carbon dioxide concentration, the extension of $H-L_W-L_V-V$ line that can be observed visually is affected by the amount of CO_2 available in the system. At higher pressure where only incompressibility phases appear, it can be clearly seen that the $H-L_W-L_V$ equilibrium line is dependent on the overall composition of carbon dioxide in the system.

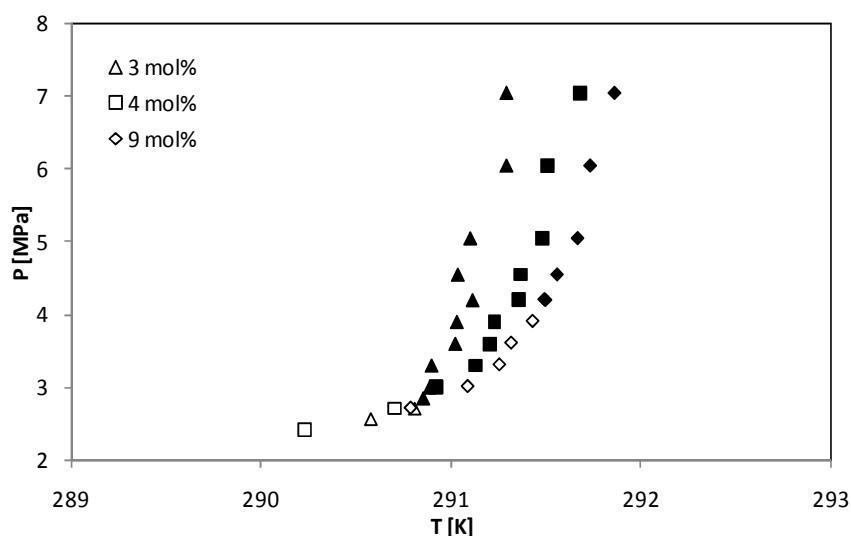


Figure 4.7 Experimental data of the $H-L_W-L_V-V$ and $H-L_W-L_V$ equilibrium lines in the ternary system H_2O-CO_2-THF at different concentrations of CO_2 . The concentration of THF is kept constant at 5 mol% in aqueous solution. The equilibria are indicated as follows: $H-L_W-L_V-V$ (open markers) and $H-L_W-L_V$ (filled markers).

As the overall composition of carbon dioxide is further increased to 19 and 29 mol% respectively, interesting phase behaviour of the carbon dioxide-tetrahydrofuran-water system is observed as shown in Figure 4.6. As presented in Figure 4.8, pressurization at $T \approx 291$ K results in the

subsequent phase transitions $L_W + V \rightarrow H + L_W + V \rightarrow L_W + L_V + V \rightarrow L_W + L_V$. The phase changes can be characterized as clathrate hydrate phase appearances followed by clathrate hydrate phase disappearances and finally bubble point.

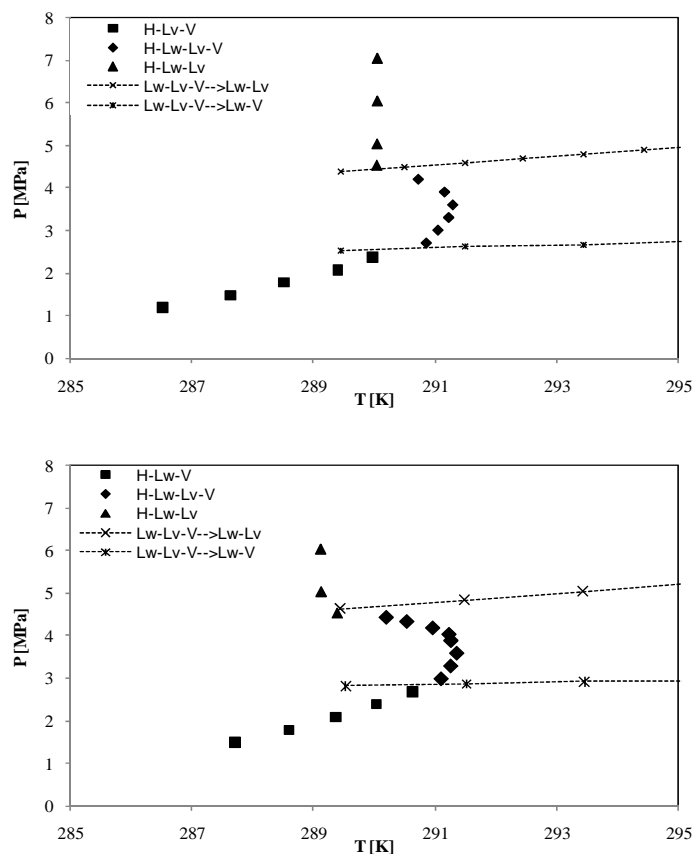


Figure 4.8 Experimental data of the phase equilibria of the ternary system H_2O - CO_2 -THF for (a) 19 mol% and (b) 29 mol% of CO_2 in the hydrate forming region. The concentration of THF is kept constant at 5 mol% in the aqueous solution.

The phenomenon observed in this work is different from the retrograde behaviour reported in the carbon dioxide-water system at pressure more than 300MPa and T at ~ 294 K [Ballard and Sloan, 2001]. In the retrograde behaviour, the number and types of phases coexisting before

and after the sequence of a phase transition are the same. However, the number and types of phases observed in this work are different at the initial and the final pressure of the sequence phase transitions. This phenomenon is characterized as pseudo-retrograde hydrate behaviour and has been previously reported in literature for systems consisting of ethane (C_2H_6) and propane (C_3H_8) as the guest components [Mooijer-van den Heuvel, 2004; Ballard et al., 2001]. Ballard et al. [2001] hypothesized that pseudo-retrograde phenomena will occur, but not constrain to any pseudo-binary system in which sl and sII hydrate formers that have fairly low vapour pressures are present. As mentioned earlier, in the ternary system of carbon dioxide-tetrahydrofuran-water, it is believed that sII hydrate will be formed. However, it should be noted that carbon dioxide also acts as an inhibitor to sII hydrate formation due to competition with THF to occupy the large cages in the structure. Thus, as the overall composition of carbon dioxide increases or the THF concentration decreases, more carbon dioxide molecules are expected to fill the larger cavities and since carbon dioxide hydrate will be more stable in the form of sl hydrate, a structural transition will occur from sII into sl hydrate in the system. This structural transformation from sII to sl hydrate is believed to lead to the pseudo-retrograde behaviour in the system.

4.3.2 Effects of Tetrahydrofuran concentration

In this section, the phase behaviours of the ternary system are measured at different concentrations of tetrahydrofuran in the aqueous phase. The overall composition of carbon dioxide is kept constant at 9 mol% in all samples. To investigate the effects of the tetrahydrofuran concentration on the three-phase equilibrium line H-L_W-V, the data for the H-L_W-V equilibrium at different concentrations of tetrahydrofuran in the system are presented in Figure 4.9. Data for the tetrahydrofuran-free system of carbon dioxide-water are included as a comparison. Figure 4.9 clearly

shows that the addition of tetrahydrofuran extends the equilibrium conditions for mixed hydrates of tetrahydrofuran and carbon dioxide to higher temperature at a fixed pressure.

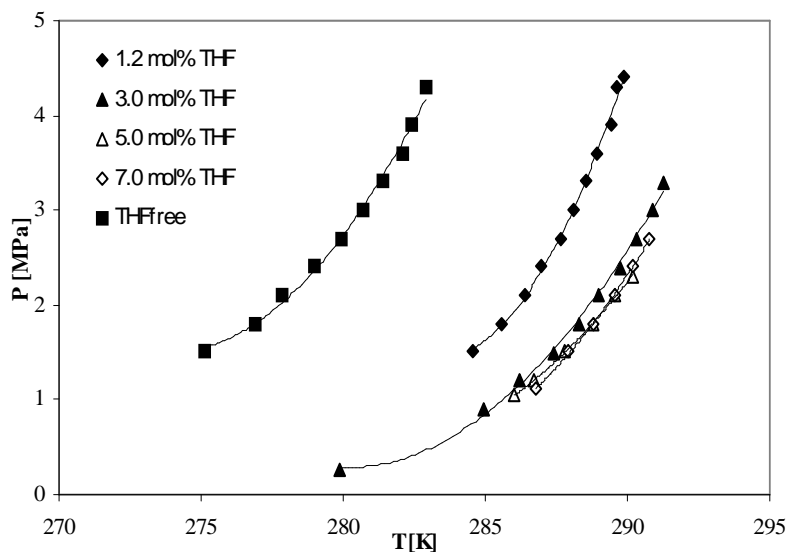


Figure 4.9 H-L_W-V equilibrium data for CO₂-water-THF systems at different concentrations of THF.

Table 4.1 Fitted equilibrium pressures of hydrates formed from CO₂ + water and CO₂ + Water + THF (3 mol%) systems and relative Pressure Decrease $\Delta P_{rel.}$

T (K)	CO ₂ in water	CO ₂ in aqueous solution of 3 mol % THF	ΔP (%)
	P (MPa)	P (MPa)	
280.15	2.80	0.29	89.51
281.15	3.24	0.30	90.74
282.15	3.75	0.36	90.43
283.15	4.33	0.47	89.15
284.15	4.98	0.63	87.28
$\Delta P_{avg.} =$			89.42

Moreover, a significant hydrate formation pressure reduction up to more than 80% can be obtained when tetrahydrofuran is present in the hydrate formation system. An example for the pressure reduction is presented in Table 4.1 for hydrate formation in pure water and for an aqueous solution of 3 mol% tetrahydrofuran. Once again, this finding confirms that the mixed hydrate of tetrahydrofuran and carbon dioxide are more stable than the single carbon dioxide hydrate.

In contrast to the carbon dioxide concentration, the concentration of tetrahydrofuran in the system is clearly affecting the conditions of the H-L_W-V equilibrium line. To get a better representation of the dependency of the hydrate stability to the concentration of tetrahydrofuran in the system, three hydrate equilibrium isobars have been calculated from the data and are presented in Figure 4.10. The isobars are calculated by fitting the exponential curve to the data sets at each composition. The sum of squares of the regression was better than 0.9993 for each data set. The data shows clearly that the mixed hydrates of tetrahydrofuran and carbon dioxide are more stable than structure I carbon dioxide hydrates. From the isobars, it is clear that at a fixed pressure, the temperature of the hydrate equilibrium increases drastically when a small amount of tetrahydrofuran is present in the hydrate forming system (1 mol%). Then, the temperature increases steadily until it reaches a maximum when between 5 and 7 mol% of tetrahydrofuran is present in the aqueous solution. At higher concentration of tetrahydrofuran, the equilibrium temperature starts to decrease again as shown for the 1.0 MPa isobar. No value is shown for higher pressure because at these conditions, a four-phase equilibrium line H-L_W-L_V-V is observed and will be discussed later. This behaviour is expected as the ratio of large cages to water molecules in a structure II hydrate is 1/17 or 0.0588. This means that the mixed hydrate is most stable in a stoichiometric mixture of water and the soluble hydrate former, in this case, tetrahydrofuran. Similarly findings on the influence of concentration of soluble promoters on

hydrate stability have been reported in literature [Jager et al., 1999; de Deugd et al., 2001; Jager et al., 2000].

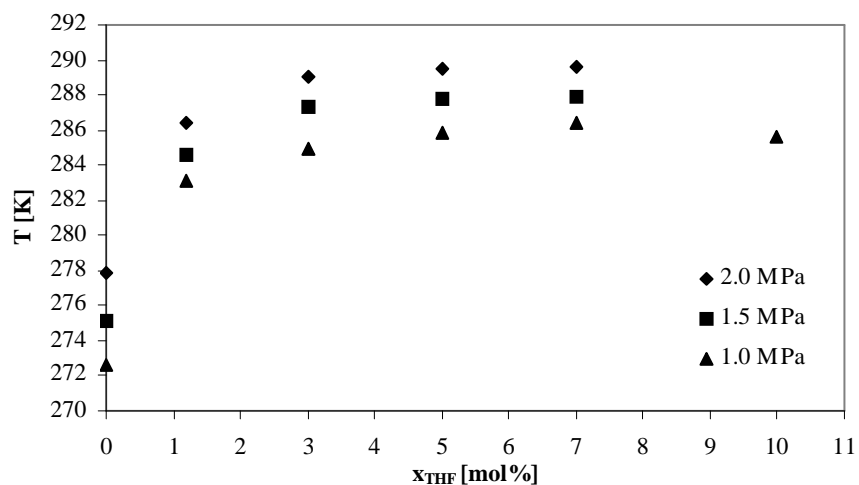


Figure 4.10 T-x projection of H-L_W-V equilibrium line for the CO_2 -water-THF system at different tetrahydrofuran concentrations.

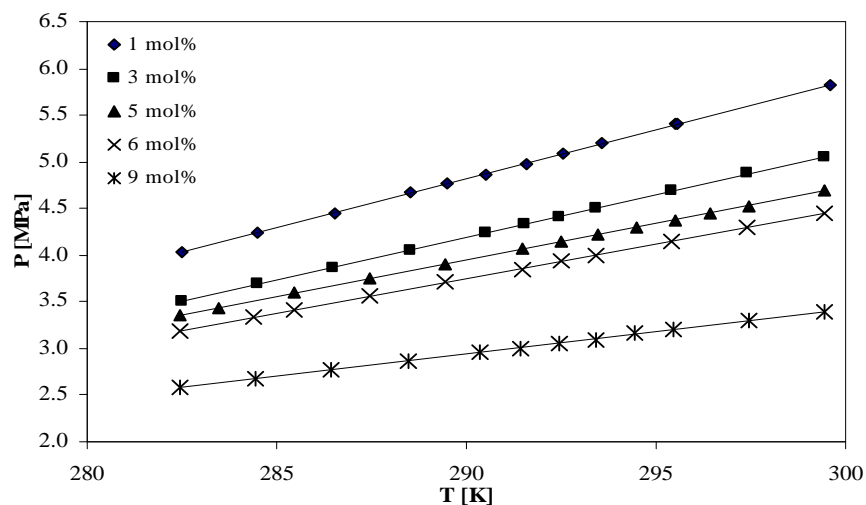


Figure 4.11 p-T representations of $\text{L}_W\text{-L}_V\text{-V} \rightarrow \text{L}_W\text{-L}_V$ (bubble point) phase transitions in the ternary system $\text{H}_2\text{O} + \text{CO}_2 + \text{THF}$ at different THF concentrations in the aqueous solution while CO_2 is kept constant at 9 mol%.

As discussed earlier, a mixture of water and tetrahydrofuran is subjected to a liquid-liquid phase split when pressurized with carbon dioxide. As a method to determine the boundaries of the liquid-liquid phase split, the bubble point ($L_W-L_V-V \rightarrow L_W-V$) and dew point ($L_W-L_V-V \rightarrow L_W-V$) lines are measured for the ternary system at different tetrahydrofuran concentrations and the results are presented in Figure 4.11 and Figure 4.12 respectively. As shown clearly in Figures 4.11 and 4.12, the bubble point and dew point lines for the ternary system depend on the concentration of tetrahydrofuran.

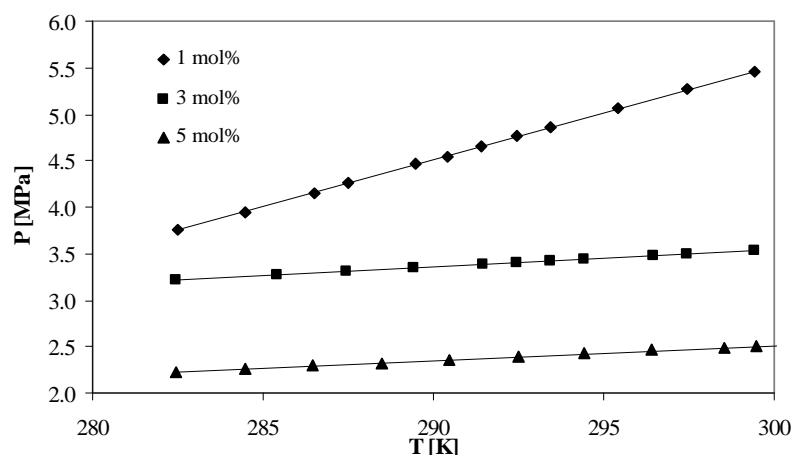


Figure 4.12 p-T representations of $L_W-L_V-V \rightarrow L_W-V$ phase transitions in the ternary system $H_2O + CO_2 + THF$ at different THF concentrations in the aqueous solution while CO_2 is kept constant at 9 mol%.

As a result of the liquid-liquid phase split, a four-phase $H-L_W-L_V-V$ equilibrium line is observed in the systems at temperature and pressure conditions at which two distinct liquid phases together with the vapour and hydrate phases are present. It should be emphasized that the formation of the $H-L_W-L_V-V$ equilibrium line depends on the appearance of the two liquid phases. In the present work, the appearance and the disappearance of one of the liquid phases depends on the bubble and dew point lines as

presented in Figures 4.11 and 4.12 respectively. Thus, the temperature-pressure region where it is possible to measure the four-phase equilibrium is different for each concentration of tetrahydrofuran in the system.

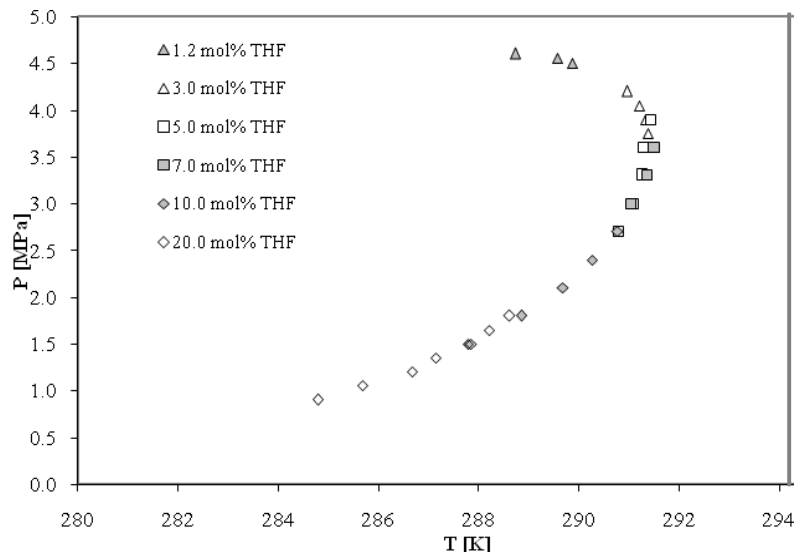


Figure 4.13 H-L_W-L_V-V equilibrium data for the ternary CO_2 -water-THF system at different THF concentrations. The CO_2 concentration is kept at 9 mol%.

By combining all the data measured at different THF concentrations in the ternary system, the four-phase H-L_W-L_V-V equilibrium line is constructed and depicted in Figure 4.13. From this figure, it is clear that the four-phase H-L_W-L_V-V equilibrium line is independent of the tetrahydrofuran concentration. Once again, the measured data is in line with Gibb's phase rule. Since there are four phases and three components in the system, there should be only one degree of freedom. Thus, it is clearly shown that systems containing water-soluble additives such as tetrahydrofuran lose their concentration dependency when the solubility limit is reached. Moreover, due to the pseudo-retrograde behaviour of the system as discussed in section 4.2.1, the four-phase equilibrium line shows that there is a maximum temperature where hydrates are possibly formed in the

system. Further pressurization of the system will result in the decrease of the temperature at which hydrates are stable.

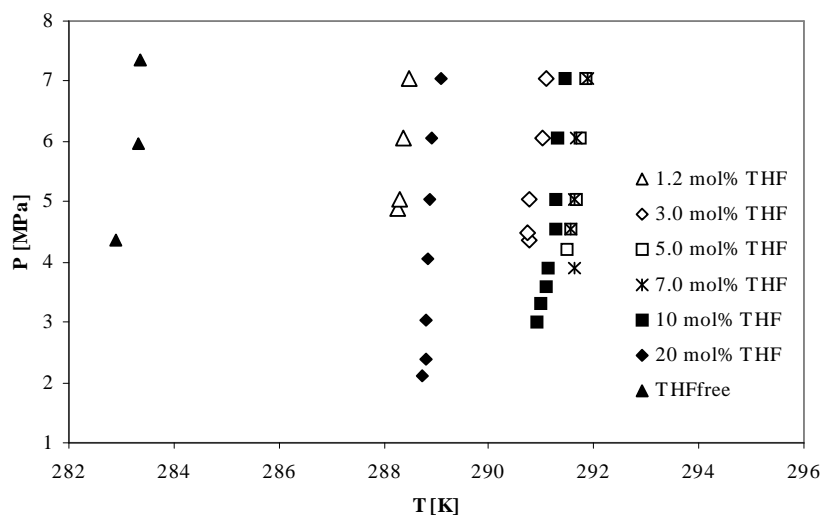


Figure 4.14 Pressure vs. temperature plot of the H-L_W-L_V equilibrium data of the CO₂-water-THF system at different concentrations of THF. The CO₂ concentration is kept constant at 9 mol%.

The pressure versus temperature plot of the high-pressure three-phase hydrate equilibrium line of H-L_W-L_V is shown in Figure 4.14 while the T-x projection is depicted in Figure 4.15. Similar to the H-L_W-V equilibrium line, the H-L_W-L_V equilibrium is dependent on the concentration of tetrahydrofuran in the system. By comparing the isobars presented in Figure 4.14, a sharp increase of temperature of about 5 K is observed when 1.2 mol% of tetrahydrofuran is added to the system. Then, the hydrate equilibrium temperature increases to a maximum at about 5-6 mol% of tetrahydrofuran in the system. Further increase in tetrahydrofuran resulted in a decrease of the hydrate equilibrium temperature. The observed behaviour further proves that the mixed hydrates formed are most stable at the stoichiometric ratio of water and tetrahydrofuran in the system. Due to the

incompressibility of the phases belonging to the $\text{H-L}_\text{W-L}_\text{V}$ equilibrium line, the pressure increases steeply with a small increase of the temperature.

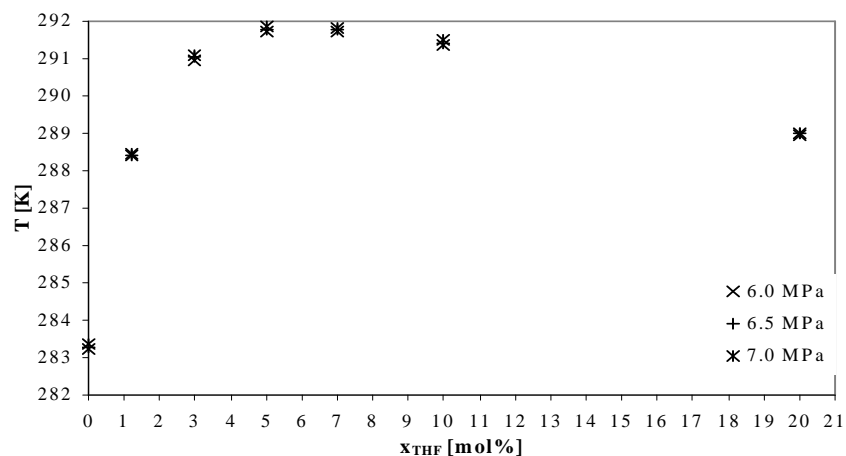


Figure 4.15 T-x projection of the $\text{H-L}_\text{W-L}_\text{V}$ equilibrium line of the CO_2 -water-THF system at different concentrations of THF. The CO_2 concentration is kept constant at 9 mol%.

4.4 REFERENCES

- Adisasmito, S., Frank, R.J., Sloan Jr., E.D. J. Chem. Eng. Data, 1991, 36, pg. 68-71.
- Ballard, L. and Sloan Jr., E.D. Fluid Phase Equilibria, 2004, 216, pg. 257-270.
- de Deugd, R.M., Jager, M.D, de Swaan Arons, J. AIChE J., 2001, 47, pg. 693-704.
- Delahaye, A.; Fournaison, L.; Marinhas, S.; Chatti, I.; Petitet, J.-P.; Dalmazzone, D.; Frst, W. Ind. Eng. Chem. Res., 2006, 45, pg. 391-397.
- Jager, M.D., de Deugd, R.M., Peters, C.J., de Swaan Arons, J., Sloan, E.D. Fluid Phase Equilibria, 1999, 165, pg. 209-223.

Jager, M.D., De Deugd, R.M., Peters, C.J., Arons, J.D., Sloan, E.D. A model for systems with soluble hydrate formers in "Gas Hydrates: Challenges for the Future", Annals of The New York Academy of Sciences 2000, 912, pg. 917-923.

Lazzaroni, M.J., Bush, D., Jones, R., Hallett, J.P., Liotta, C.I., Eckert, C.A. Fluid Phase Equilibria, 2004, 224, pg. 143-154.

Mooijer-van den Heuvel, M.M., Witteman, R., Peters, C.J. Fluid Phase Equilibria, 2001, 182, pg. 97-110.

Mooijer-van den Heuvel, M.M. "Phase Behaviour and Structural Aspects of Ternary Clathrate Hydrate Systems: The Role of Additives". Ph.D thesis, Delft Uni. of Technology, January, 2004.

Ng, H.-J. and Robinson, D.B. Fluid Phase Equilibria, 1985, 21, pg. 145-155.

Ohgaki, K., Makihara, Y., Takano, K. J. Chem. Eng. Japan, 1993, 26 (5), pg. 558-564.

Ripmeester, J.A. and Ratcliffe, C.I. Energy & Fuels, 1998, 12, pg. 197-200.

Sloan Jr., E.D. "Clathrate Hydrates of Natural Gas", 2nd ed., Marcel Dekker, New York, 1998.

Teng, H. Int. J. Chem. Kinetics, 1996, 28, pg. 935-937.

Tohidi, B. , Danesh, A., Todd, A.C., Burgass, R.W. , Østergaard, K.K. Fluid Phase Equilibria, 1997, 138, pg. 241-250.

Unruh, C.H. and Katz, D.L. Trans. American Institute of Mining and Metallurgical Engineers, 1949, 186(4), pg. 83-86.

Vlahakis, J.G., Chen, H.-S., Suwandi, M.S., Barduhn, A.J. "The growth rate of ice crystals: Properties of carbon dioxide hydrate, a review of properties of 51 gas hydrates". Syracuse U. research and development report 830, prepared for US Department of Interior, 1972.

Wendland, M., Hasse, H., Maurer, G. J. Chem. Eng. Data, 1999, 44, pg. 901-906.

5

Phase Behaviour of Mixed Hydrates in Aqueous Electrolyte Solutions and the Strength of Hydrate Inhibition by Metal Halides

In this chapter the effects of electrolytes on the phase behaviour of carbon dioxide hydrate forming systems are thoroughly investigated. In Section 5.2, the phase behaviour of the simple carbon dioxide and mixed carbon dioxide and tetrahydrofuran hydrates at different overall concentrations in sodium chloride solutions are presented. In Section 5.3, the competing effect between tetrahydrofuran and an electrolyte of the metal halide homologous series and their impacts on the phase behaviour of the hydrate forming systems are discussed. The strength of hydrate inhibition among metal halides is compared and quantitative analyses between the anions and cations are made in order to gain some understanding of the mechanism of electrolyte inhibition on the hydrate formation.

5.1 INTRODUCTION

It is well established that electrolytes inhibit clathrate hydrate formation. In our laboratory, this phenomenon was first studied in ternary system of water-methane-sodium chloride [Roo et al., 1983]. The inhibition of hydrate formation by electrolytes is due to the lowering of the activity of water in the coexisting liquid phase, causing hydrates to form at lower temperatures and higher pressures compared to their formation in pure water [Duan and Sun, 2006]. Many phase equilibrium data especially on H-L_w-V equilibrium line have been reported for carbon dioxide in the presence of electrolytes. A compilation of these data can be found in Sloan and Koh [2007]. In contrast, as shown in Chapter 4, cyclic organics such as tetrahydrofuran reduce the pressure requirement for hydrate formation at a specified temperature when presents in small quantity in aqueous solutions up to about 5 – 7 mol%. The usage of such organics at low concentration may provide an alternative solution to overcome the inhibiting effects of electrolytes. Unfortunately, no available reported data for hydrate equilibria of mixed carbon dioxide and tetrahydrofuran hydrates in aqueous solution have been found in literature. Realizing the potential benefits of such data for the development of hydrate-based processes, an attempt has been made to measure the hydrate equilibrium data for such systems. For consistency, tetrahydrofuran is chosen as a representative of hydrate promoter in the present work. In section 5.1, phase behaviour of mixed carbon dioxide and tetrahydrofuran hydrates in sodium chloride (NaCl) solutions are presented. Sodium chloride is chosen to represent electrolytes that are present in naturally occurring water. In section 5.2, the measurement of hydrate equilibrium conditions for mixed carbon dioxide and tetrahydrofuran hydrates are extended to another six electrolytes from the metal halide homologous series. Besides NaCl, the electrolytes used in this work are calcium chloride (CaCl₂), magnesium chloride (MgCl₂), potassium bromide (KBr), sodium fluoride (NaF), sodium bromide (NaBr)

and potassium chloride (KCl). Based on the experimental data, a comparison is made to quantitatively evaluate the inhibiting effect of different salts on the hydrate formation. All measured equilibrium data are tabulated in Appendix B.

5.2 Phase Equilibria of Mixed Carbon Dioxide and Tetrahydrofuran Hydrates in Aqueous Solutions of Sodium Chloride

As a method to verify the accuracy of the experimental apparatus and procedure adapted in this work, the H-L_W-V equilibrium lines of carbon dioxide-water and carbon dioxide-water-sodium chloride at 5 and 10 mass% sodium chloride concentration systems are measured and compared with literature data [Dholabhai et al., 1993; Fan and Guo, 1999]. The measured data are compared with literature data and depicted in Figure 5.1. The carbon dioxide vapour pressure line is included to indicate the upper limit of the H-L_W-V equilibrium line. As depicted in Figure 5.1, the data measured in this work agree very well with earlier reported data in the whole region where a comparison could be made, i.e. up to the carbon dioxide vapour pressure curve. It should be emphasized that the reproducibility of the hydrate equilibrium conditions reported in this work is very good. The data presented in Figure 5.1 show that the addition of sodium chloride inhibits the formation of carbon dioxide and the inhibition effect of sodium chloride is concentration dependent. A closer inspection of Figure 5.1 reveals that the temperature depression of hydrate formation increases with increasing pressure.

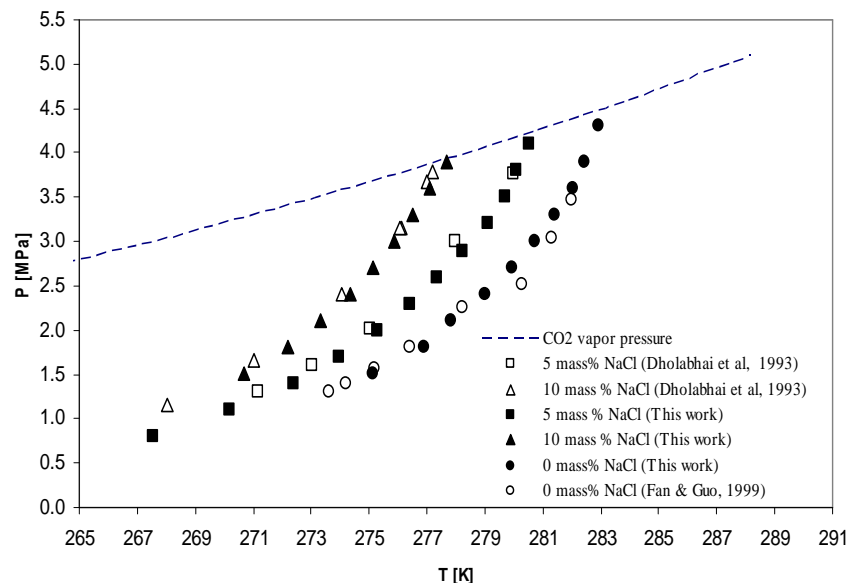


Figure 5.1 Measured hydrate equilibrium data of simple carbon dioxide hydrates in water and sodium chloride solutions and comparison with literature data.

The hydrate equilibrium conditions of mixed carbon dioxide and tetrahydrofuran hydrates in aqueous sodium chloride solutions are measured systematically at different overall concentrations of each component in the quaternary system. The experimental temperature range is from 267.55 K up to 289.82 K, and the pressure ranges from 0.80 MPa up to 7.05 MPa. The measured data for the $\text{H-L}_W\text{-V} \rightarrow \text{L}_W\text{-V}$, $\text{H-L}_W\text{-L}_V\text{-V} \rightarrow \text{L}_W\text{-L}_V\text{-V}$ and $\text{H-L}_W\text{-LV} \rightarrow \text{L}_W\text{-LV}$ transitions in the quaternary systems at different compositions are presented in Appendix B. To gain the insight on the effects of tetrahydrofuran on the phase behaviour of the system in the hydrate forming region, a series of three-phase equilibrium data of $\text{H-L}_W\text{-V}$ is compared with hydrate equilibrium data of simple carbon dioxide in water and aqueous sodium chloride solutions and mixed carbon dioxide and tetrahydrofuran hydrates. These data are graphically shown as isopleths in the pressure vs. temperature plot in Figure 5.2. It can be clearly seen in this

figure that the presence of tetrahydrofuran leads to a substantial extension of hydrate equilibrium temperature in the quaternary system. Although the equilibrium temperature is less than that of mixed carbon dioxide and tetrahydrofuran hydrates in water for any specified pressure, it is more than 10 K higher than that of water-carbon dioxide-sodium chloride system and it is much higher than that of simple carbon dioxide hydrates. This shows that the presence of tetrahydrofuran in the system is able to suppress the inhibiting effect of sodium chloride on the hydrate formation.

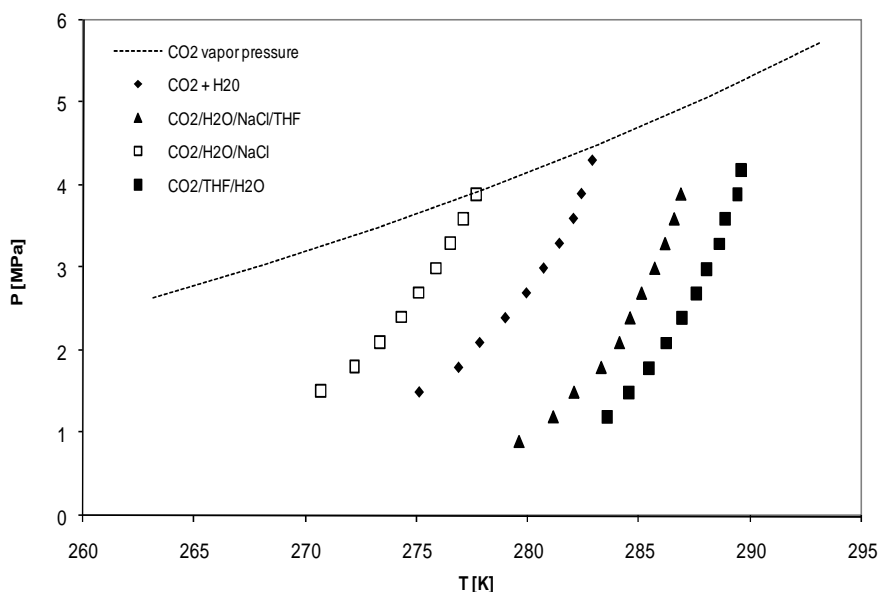


Figure 5.2 Hydrate equilibrium lines of simple CO₂ hydrate in water, in a aqueous NaCl solution and in mixed CO₂ and THF hydrates in water and in aqueous NaCl solutions. Composition: CO₂, 0.4; NaCl, 0.2 and THF, 0.1 mol fraction when present.

Figure 5.3 represents in a p,T-diagram the experimental hydrate equilibrium data of the mixed hydrate in a 2 mol% aqueous solution of sodium chloride and various concentrations of tetrahydrofuran. In the diagram, each line represents a combination of three-phase H-L_W-V and

four-phase H-L_W-L_V-V hydrate equilibrium conditions. As observed already in Chapter 4, the formation of the four-phase equilibrium is mainly due to a liquid-liquid phase split, which creates two immiscible liquids in the system studied. However, a detailed comparison of hydrate equilibrium data in system with and without sodium chloride, presented in Appendix A and B respectively, shows that the split between the two liquids is enhanced by the present of sodium chloride and it depends on the sodium chloride concentration. In this work, it is observed that at sodium chloride concentrations of more than 5 mol%, the second liquid phase is already present at ambient pressure and temperature conditions (1 bar and 293 K, respectively). Sloan [1998] pointed out that the clustering of ions by water molecules is responsible for that as it causes a decrease in the solubility of the potential hydrate guest molecules in the water.

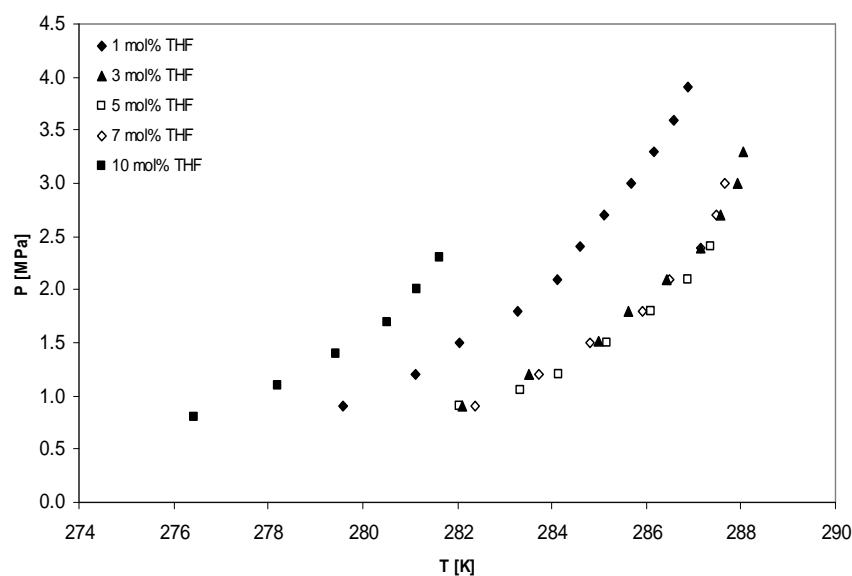


Figure 5.3 P-T projection of hydrate equilibrium lines (H-L_w-V and H-L_w-L_v-V) for mixed CO₂ and THF hydrates in aqueous NaCl solutions at different THF concentrations. The CO₂ and NaCl compositions are fixed at mole fractions of 0.4 and 0.2 respectively.

Due to the formation of the organic-rich liquid phase, the upper quadruple point (Q_2) of the hydrate line evolves into a line consisting of four phases comprising hydrate (H), liquid water (L_W), liquid organic (L_V) and vapour (V). The extension of this four-phase H- L_W - L_V -V line is bounded by the quadruple points Q_{2U} and Q_{2L} at which the hydrate equilibrium line intersects the bubble and dew point lines of the system respectively as depicted in Figure 5.4. As shown in Figure 5.3, similar to the electrolyte-free system, the promoting effect of tetrahydrofuran is concentration dependent with an observed optimum promoting effect between 5 to 7 mol% of tetrahydrofuran in the aqueous solution. At concentrations higher than 7 mol% the promoting effect of tetrahydrofuran changes into an inhibiting effect. The change from the promoting effect to the inhibiting effect may be due to the anti-freeze effect of tetrahydrofuran on the formation of mixed hydrate, which is concentration dependent.

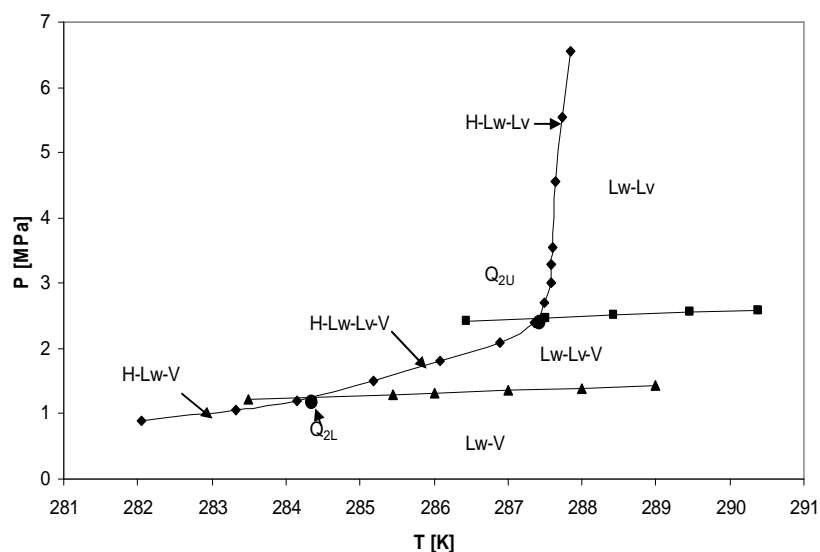


Figure 5.4 P-T-diagram of the quaternary system of mixed CO₂ and THF hydrates in an aqueous NaCl solution. The global composition of each component is as follows: $z_1 = 0.89$, $z_2 = 0.04$, $z_3 = 0.02$, $z_4 = 0.05$.

To further investigate the effect of the sodium chloride concentration on the phase behaviour in the quaternary system in the hydrate forming region, p-T-curves of the mixed carbon dioxide and tetrahydrofuran systems in sodium chloride solutions are plotted in Figure 5.5. The concentration of sodium chloride in the aqueous solution is varied from 1 to 5 mol%, while the concentrations of carbon dioxide and tetrahydrofuran are fixed at 4 mol% and 5 mol%, respectively.

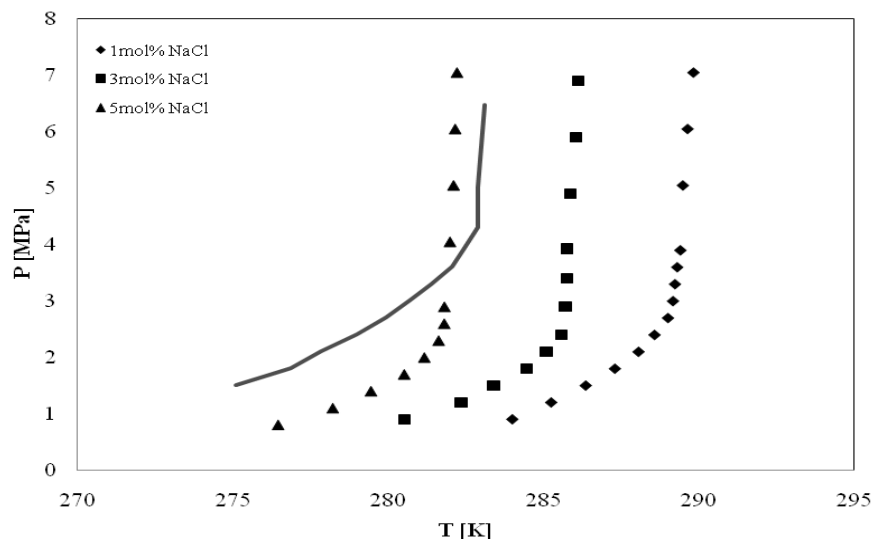


Figure 5.5 P-T-diagram of the equilibrium lines of mixed CO₂ and THF hydrates in aqueous NaCl systems. The concentration of THF is 5 mol% and the P-T-curves are given for various concentrations of NaCl. The solid line is the hydrate equilibrium curve of the simple system H₂O + CO₂.

In the range studied, it is found that the promoting effect of tetrahydrofuran is still stronger than the inhibiting effect of sodium chloride up to a concentration of sodium chloride of 5 mol% in the aqueous solution. However, as the concentration of sodium chloride increases, the pressure reduction effect of tetrahydrofuran decreases. It is known that salts ionize in aqueous solutions and the ions interact with the dipoles of water molecules forming a coulombic bond. The formation of these strong bonds between

ions and water causes water molecules to cluster around the ions. This cluster formation inhibits the formation of hydrate since water is more attracted by ions than the hydrate structure. Thus, as more ions are present in the solution, the larger hydrate inhibiting effect can be noticed. It is believed that both ion clustering and salting-out causes that a more substantial sub-cooling is required for the formation of hydrate [Sloan and Koh, 2007]. Thus, as the concentration of sodium chloride increases, the inhibition effect of sodium chloride increases and overcomes the pressure reduction effect of tetrahydrofuran in the quaternary system.

5.3 Competing Effect of Tetrahydrofuran and an Electrolyte and the Strength of Hydrate Inhibition by Metal Halides in Mixed Carbon Dioxide Hydrate Systems

In the present study, the hydrate equilibrium conditions coupled with the corresponding bubble point line of several quaternary systems of carbon dioxide-water-tetrahydrofuran-electrolyte are measured in pressure and temperature ranges of 0.90-7.10 MPa and 275-305 K respectively. The type of electrolyte, the system compositions both in mol% and mass%, the molality and the ionic strength of each system are summarized in Table 5.1. The ionic strength is calculated by:

$$I_m = \frac{1}{2} \sum_{B=1}^n m_B z_B^2 \quad (5.1)$$

where m_B is the molality of ion B (mol/ kg solvent), Z_B is the charge number of that ion, and the sum is taken over all ions in the solution.

The mixed carbon dioxide and tetrahydrofuran phase equilibria are determined for several electrolytes at different concentrations and in temperature and pressure ranges of 275-295 K and 0.5–7.10 MPa,

respectively. Since it is already known that the hydrate promoting effect of tetrahydrofuran is concentration dependent and the maximum hydrate promoting effect is achieved at a concentration of the promoter of 5-7 mol% (section 5.2), the concentration of tetrahydrofuran is fixed at 5 mol%.

Table 5.1 Compositions and ionic strength of the ternary aqueous solutions

Sample	Composition, mol% on wet basis			Composition, mass% on wet basis			Molality, (mol/kg solvent)	Ionic strength, molal
	Electrolyte	H ₂ O	THF	Electrolyte	H ₂ O	THF		
1.0 mol% NaCl	1.00	94.00	5.00	2.77	80.17	17.07	0.01028	0.01028
3.0 mol% NaCl	3.00	92.00	5.00	7.99	75.57	16.44	0.03261	0.03261
5.0 mol% NaCl	5.00	90.00	5.00	12.85	71.30	15.85	0.05737	0.05737
0.5 mol% NaBr	0.50	94.50	5.00	2.43	80.51	17.05	0.00512	0.00512
1.0 mol% NaBr	1.00	94.00	5.00	4.77	78.51	16.72	0.01050	0.01050
3.0 mol% NaBr	3.00	92.00	5.00	13.27	71.24	15.50	0.03459	0.03459
0.5 mol% NaF	0.50	94.50	5.00	1.01	81.69	17.30	0.00505	0.00505
1.0 mol% NaF	1.00	94.00	5.00	2.00	80.79	17.20	0.01020	0.01020
0.5 mol% KCl	0.50	94.50	5.00	1.77	81.06	17.17	0.00509	0.00509
0.5 mol% CaCl ₂	0.50	94.50	5.00	2.62	80.36	17.02	0.00513	0.01284
1.0 mol% CaCl ₂	1.00	94.00	5.00	5.13	78.22	16.65	0.01054	0.02635
0.2 mol% MgCl ₂	0.20	94.80	5.00	0.91	81.82	17.27	0.00202	0.00505
0.5 mol% MgCl ₂	0.50	94.50	5.00	2.26	80.66	17.08	0.00512	0.01279
1.0 mol% MgCl ₂	1.00	94.00	5.00	4.43	78.79	16.78	0.01046	0.02616
0.5 mol% KBr	0.50	94.50	5.00	2.80	80.21	16.99	0.00514	0.00514
1.0 mol% KBr	1.00	94.00	5.00	5.48	77.93	16.59	0.01058	0.01058

To further examine the competing effect of tetrahydrofuran and electrolytes in the hydrate forming systems, the measured mixed hydrates equilibrium data in aqueous solutions of NaCl, CaCl_2 and MgCl_2 are compared with literature data for simple carbon dioxide hydrates in the similar electrolyte solutions and are presented in Figures 5.6, 5.7 and 5.8, respectively.

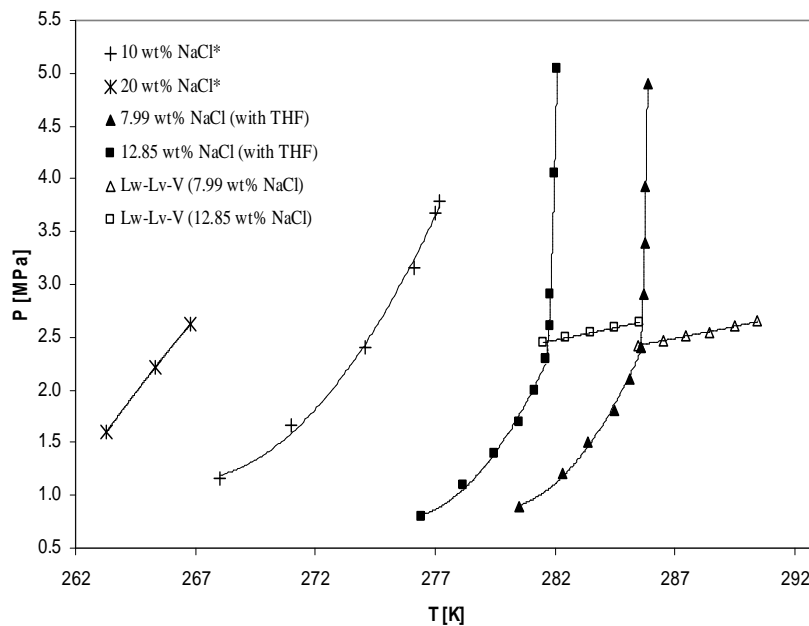


Figure 5.6 P,T-projection of simple CO_2 and mixed CO_2 and THF hydrates in aqueous NaCl solutions for different NaCl concentrations. *Data taken from Dholabhai et. al [1993]

In all figures, the $\text{H-L}_W\text{-V}$, $\text{H-L}_V\text{-L}_W\text{-V}$ and $\text{H-L}_W\text{-L}_V$ lines of the measured data are combined as a single hydrate equilibrium line for simplification. The upper limit of the upper quadruple points, Q_{2u} , of the measured systems where hydrate (H), water-rich liquid (L_W), organic-rich liquid (L_V) and vapour (V) phases coexist, are also included in the figures. When available, literature data for the upper quadruple points, Q_2 , of the

ternary water-carbon dioxide-electrolyte are also included for comparison. Based on Figure 5.6, 5.7 and 5.8, regardless of the type of electrolyte used, the promoting effect of tetrahydrofuran is found to be large enough to overrule the inhibiting effect of all electrolytes studied. Thus, the promoting effect of tetrahydrofuran on the carbon dioxide hydrate equilibrium shows promising results to combat the hydrate inhibition effects of electrolytes for practical applications that require reduction of the hydrate equilibrium pressure or, alternatively, increase of the hydrate equilibrium temperature. Moreover, it is found that the Q_{2u} for the mixed hydrates are formed at much lower pressure compared to the Q_2 of simple carbon dioxide hydrates such as clearly shown in Figure 5.8. Thus, the presence of tetrahydrofuran not only increases the hydrate equilibrium temperature, it also shifts the upper quadruple point to significantly lower pressure.

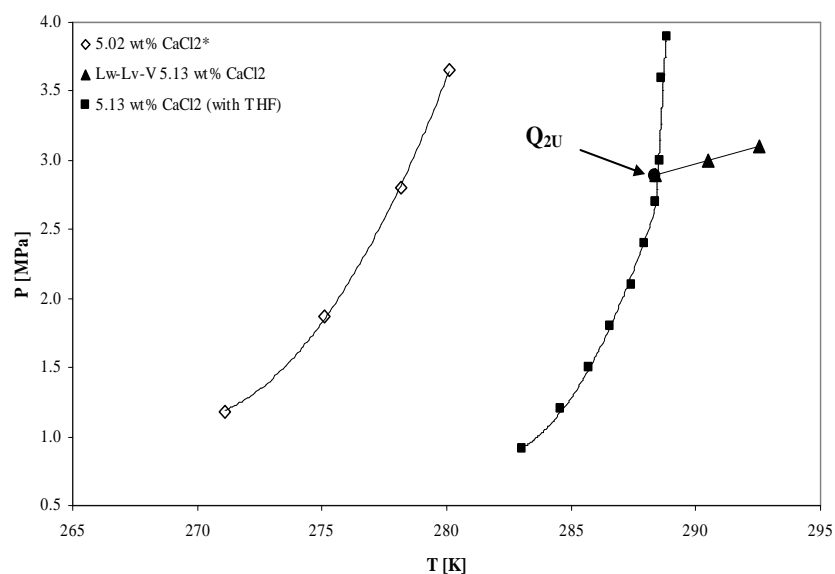


Figure 5.7 P-T-projection for simple CO_2 and mixed CO_2 and THF hydrates in aqueous CaCl_2 solutions for different CaCl_2 concentrations. *Data taken from Dholabhai et. al [1993].

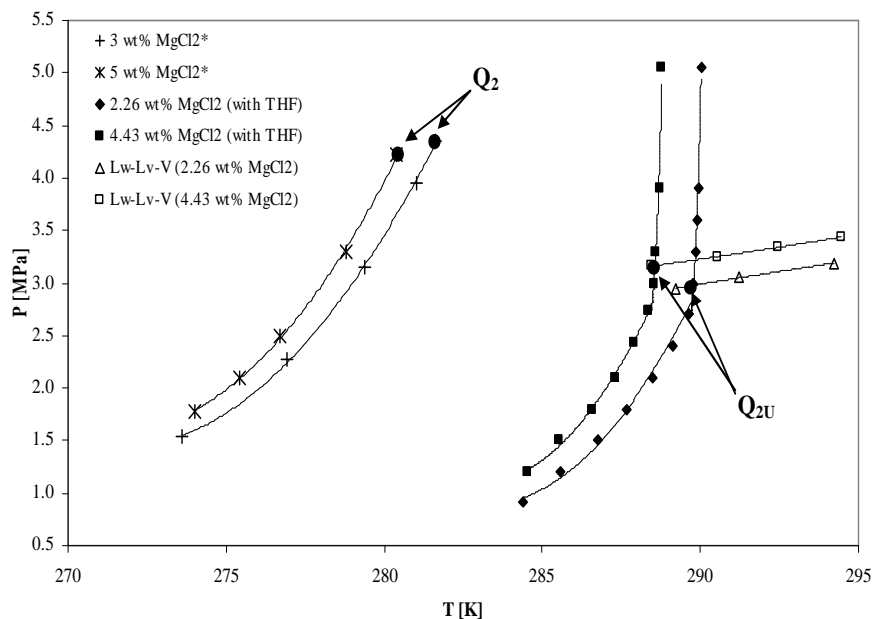


Figure 5.8 P-T-projection for simple CO₂ and mixed CO₂ and THF hydrates in aqueous MgCl₂ solutions for different MgCl₂ concentrations. *Data taken from Kang et. al [1998].

It is also known that different salts have different hydrate inhibition strength. Thus, the hydrate stability region is affected by the type of salts presence in the hydrate forming system. In order to make a comparison of the hydrate inhibiting effects between the various metal halides, hydrate equilibrium conditions are measured for seven different salts at overall salt concentrations of 0.5 and 1 mol% respectively. Carbon dioxide and tetrahydrofuran concentrations are kept fixed at 0.04 and 0.05 mol fraction respectively. The unit of mol% or mol fraction is used in this work because it gives a better representation of the ionic strength and molality compared to mass% as shown in Table 5.1. The measured hydrate equilibrium data at 0.5 mol% and 1 mol% are depicted in Figure 5.9 and 5.10 respectively.

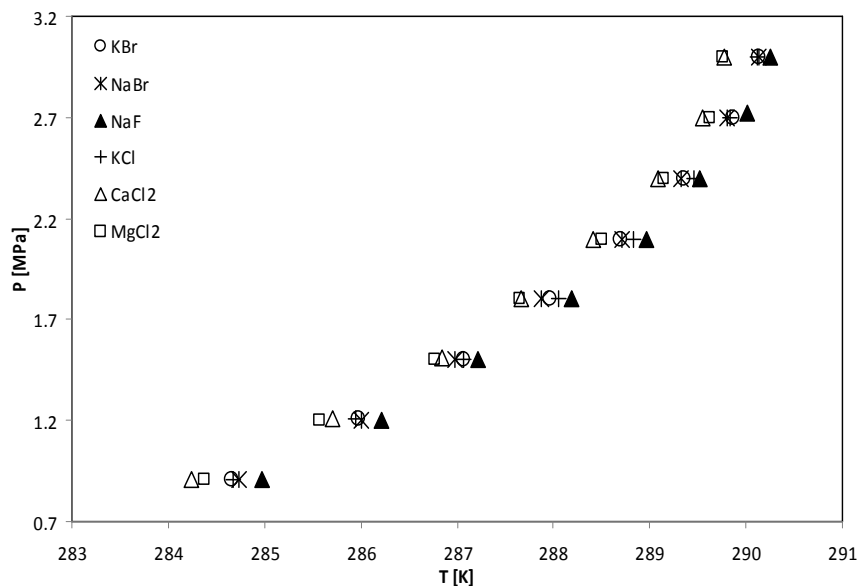


Figure 5.9 P-T projection of hydrate equilibrium lines for mixed CO₂ and THF hydrate in different electrolyte solutions at 0.5 mol% electrolyte concentration.

The hydrate inhibition strength on an electrolyte is a measure for the temperature depression caused by the particular electrolyte for hydrate formation to take place. This means that the stronger the hydrate inhibiting effect of an electrolyte is, the lower is the hydrate equilibrium temperature. In general, at an electrolyte concentration of 0.5 mol%, the different strength of hydrate inhibition between the various electrolytes studied in the present work is not very clear. Nonetheless, in the range studied, it is found that NaF has relatively the least hydrate inhibition strength while CaCl₂ and MgCl₂ are the two electrolytes with the highest inhibition strength. KBr, KCl and NaBr are found to have more or less similar hydrate inhibition strength with KCl has slightly a lower value compared to the other two electrolytes. As the concentration of the electrolytes increases to higher values, the difference of the hydrate inhibition strength between the electrolytes is becoming more apparent. As shown in Figure 5.10, the hydrate equilibrium temperature of the mixed hydrate in electrolyte solution is decreasing in the following

electrolyte order: $\text{NaF} > \text{KBr} > \text{NaCl} > \text{NaBr} > \text{CaCl}_2 \approx \text{MgCl}_2$. This trend indicates that both CaCl_2 and MgCl_2 have the strongest inhibition effect while NaF has the weakest inhibition effect for hydrate formation. The trend observed among metal chlorides in this work is similar to that of simple carbon dioxide hydrate in aqueous electrolyte solution as reported in literature [Dholabhai et al. 1996; Kang et al., 1998].

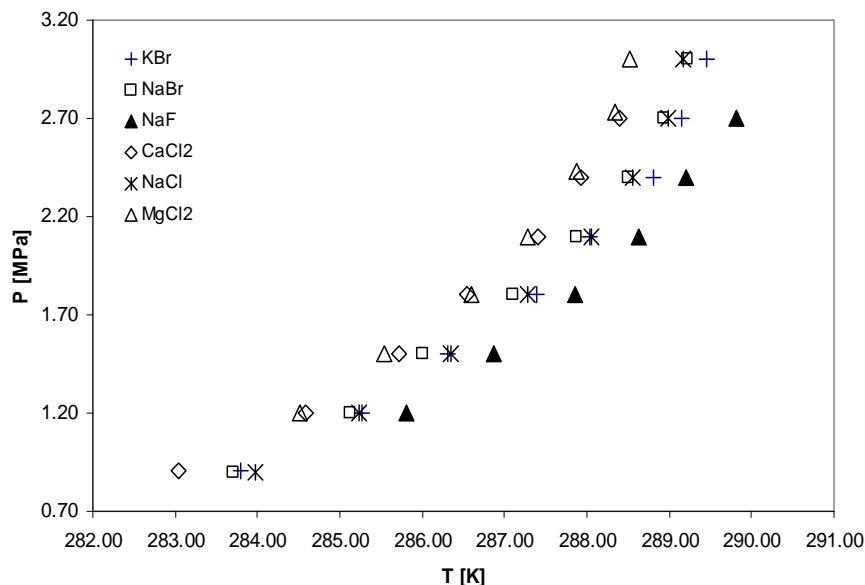


Figure 5.10 P-T projection of hydrate equilibrium lines for mixed CO_2 and THF hydrate in different electrolyte solutions at 1mol% electrolyte concentration.

It is our interest to gain the understanding on the different strength of the metal halides studied. Firstly, through a comparison between the cations of the same acid, Makogon [1981] stated that salting-out effect, a phenomenon that reduced the solubility of a certain non-electrolyte compound in water by the addition of a salt, is the main reason which make electrolytes effective inhibitors for hydrate formation. Makogon [1981] pointed out that the salting-out effect is practically caused by the hydration of ion with water molecules in electrolyte solution. Thus, the salting-out

effect of individual ions increases with the ion charge and also depends on the ionic radius. With the decrease in ion size, the bond between the water molecules and the ions becomes stronger. In contrast, the co-ordination number of the ions decreases with the reduction in ion size which will result in a shrink of the size of water coating around the ion. However, the first tendency is stronger and, therefore, the ion's salting-out effect is usually decreasing with increasing ion radius. As a result, salt inhibition is suggested to be approximately a direct function of charge and an inverse function of ion radius, implicating that the best electrolyte inhibitor must have the maximum charge and a minimum radius.

The trend observed for the hydrate inhibition strength between the metal chlorides as measured in this study, i.e. MgCl_2 , CaCl_2 and KCl at 0.5 mol% and MgCl_2 , CaCl_2 and NaCl at 1.0 mol% of electrolyte concentration, agrees well with the suggested trend by Makogon. It is found that the hydrate inhibiting strength decreases in the following order: $\text{MgCl}_2 > \text{CaCl}_2 > \text{NaCl}$ or KCl . It is also apparent that the hydrate equilibrium temperature in solutions of NaCl or KCl is significantly higher than either CaCl_2 or MgCl_2 at any specified pressure, while the hydrate equilibrium temperature for MgCl_2 is almost similar to that of CaCl_2 at lower pressure and slightly higher as the pressure increases. Since Na^+ and K^+ have +1 charge while both Mg^{2+} and Ca^{2+} have +2 charge, it is proven that the anion with higher charge will have the stronger hydrate inhibition. Due to the fact that Mg^{2+} (0.78 Å) has a smaller radius than Ca^{2+} (1.06 Å), the hydrate inhibition of Mg^{2+} is predicted to be higher than that of Ca^{2+} . Unfortunately, no conclusive evidence can be found from the experimental data to support this trend although there is a slight decrease of the hydrate equilibrium temperature for the MgCl_2 system compared to that of CaCl_2 at higher pressure. A better result can be obtained by comparing the series of NaBr and KBr at 1.0 mol%. Since Na^+ (0.98 Å) has a smaller ionic radius compared to K^+ (1.38 Å), Na^+ should have a stronger inhibiting effect for hydrate formation. In Figure 5.10, it can

be clearly seen that the hydrate equilibrium temperature for NaBr solution is always lower than that of KBr supporting the trend proposed by Makogon [1983]. All these observations indicate that the charge of an ion has a much stronger effect compared to its size in hydrate inhibition.

In contrast, in a series of sodium halide studies, i.e. NaF, NaCl and NaBr, the strength of the hydrate inhibiting effect reduces in the following order: NaBr > NaCl > NaF. Since all halogen ions have a -1 charge, Br⁻, which has the largest ion radius (182 pm), showed the highest inhibiting effect compared to Cl⁻ (167 pm) and F⁻ (119 pm). Furthermore, there is a significant increase in the hydrate equilibrium temperature in NaF solutions compared to the other two solutions as shown in Figure 5.10. Thus, it is obvious that the observed trend cannot be explained by the salting-out effect. In this case, the basic understanding of gas hydrate formation is required. Gas hydrate is formed by the stabilizing effect of gas molecules in cages formed by hydrogen bonded water molecules. Therefore, if the water network is disturbed, the formation of hydrate might be disturbed as well. When ions are solvated by water, the ionic hydrogen bonds act to affect the ambient water networks, as result a hydrogen bonds is lost for every direction association of a water molecule with an ion [Lu et al., 2001]. The decrease of the hydrogen bonds in ambient water will reduce the possibility of water molecules to form clusters for hydrate formation. Thus, the strength of hydrate inhibition of an ion depends on the probability of the ion to have a hydrogen bond with a water molecule.

Mizuno et al. [1995, 1996] have studied the water structure in binary aqueous mixtures of halogenated alcohols. Based on their NMR results, they showed that hydrogen bonds of the water molecules become weak and the water structure breaks down with an increase in the alcohol concentration, the number of halogen atoms and the size of halogen atom in the alcohols. Furthermore, the halogen atoms behave as weak proton

acceptors in hydrogen-bonding interaction with the surrounding water molecules, which results in the reduction of the polarity and hydrogen-bonding strength of other water molecules in the vicinity of the halogen atoms. This is the main mechanism of the ambient water structure breakdown although a dipole-dipole interaction between the halogen atoms and the surrounding water molecules is responsible for the breakdown as well [Mizuno et al., 1995]. The study of IR measurements for the same water-halogenated alcohol mixtures [Mizuno et al., 1997] indicates conclusively that a breakdown of water structure occurred in the water-halogenated alcohol mixtures and the effects of the alcohols on the breakdown is found to increase in the order $\text{ClC}_2\text{H}_4\text{OH} < \text{BrC}_2\text{H}_4\text{OH} < \text{IC}_2\text{H}_4\text{OH}$.

Based on these findings, it can be deduced that the effect of the halogen ions on the water structure breakdown is decreasing in the following order $\text{I}^- > \text{Br}^- > \text{Cl}^- > \text{F}^-$. Since Br^- is stronger in breaking down the water structure compared to Cl^- and F^- , it can be predicted that hydrate formation will be suppressed more in solutions containing Br^- compare to that of Cl^- and F^- . This explains the trend observed in the present work, which shows that NaBr is a more effective hydrate inhibitor compared to NaCl and NaF. Moreover, when anions are solvated by water, the ionic hydrogen-bonds act to either disrupt or reinforce the ambient water networks depending on the particular ion involved. The fluoride ion acts as a so-called “structure-maker”, reducing the entropy of water, while “structure breakers” like iodide decrease the order, suggesting a qualitative difference in the solvation morphologies for the different halides [Ayotte et al., 199]. Since hydrate formation requires a structured ambient water network for the formation of hydrate cages, the “structure-maker” ion is preferable for hydrate formation. This may explain the significant increase of the hydrate equilibrium temperature for the mixed THF- CO_2 hydrate in a NaF solution compared to that of in NaCl and NaBr solutions.

Due to the difference of cation and anion hydration characteristics, Lu et. al [2001] suggested that the anion plays a more important role than the cation in affecting hydrate stability in electrolyte solutions. They argued that asymmetrical distribution of water molecules around an anion allows the anion to exert an eminent influence on the ambient water network. Meanwhile, the symmetrical arrangement of water molecules around the cation reduces the influence of the cation on the water molecules, mainly in the first and second hydration layer. However, they emphasized that the recognized phenomenon is not conclusive due to limited data used in their study. A qualitative comparison of the mixed hydrate equilibrium temperature in MgCl_2 , NaCl and NaF aqueous solutions as presented in Figures 5.9 and 5.10 showed that the substitution of Na^+ by Mg^{2+} in a metal chloride solution shifts the hydrate equilibrium temperature to a lower value being more or less similar to the shift of the equilibrium temperature to a higher value when Cl^- is substituted by F^- in a sodium halide solution. As a result, in the present study no conclusive evidence is observed showing that the anion plays a more important role in hydrate inhibition. However, it should be noted that in the present study, the concentration of electrolytes used in the quaternary system is low at 0.5 mol% and 1 mol%, respectively. Since hydrate inhibiting effect of electrolyte is concentration dependent, higher concentration of electrolyte in the quaternary system may have different quantitative effects on the phase equilibrium conditions, if compared to non-electrolyte equilibrium conditions.

5.4 REFERENCES

- Ayotte, P., Nielsen, S. B., Weddle, G. H., Johnson, M. A., Xantheas, S. S. J. *Phys. Chem. A*. 1999. 103 (50), pg. 10665-10669.
- Dholabhai, P.D., Kalogerakis, N. and Bishnoi, P.R. *Fluid Phase Equilibria*, 1993, 38(4), pg. 650-654.

Dholabhai, P.D. Perent, J.S., Bishnoi, P.R. Ind. Eng. Chem. Res. 1996, 35, pg. 819-823.

Duan, Z. and Sun, R. American Mineralogist, 2006, 91, pg. 1346-1354.

Fan, S.S. and Guo, T.M. J. Chem. Eng. Data, 1999, 44(4), pg. 829-832.

Kang, S.-P., Chun, M.-K. and Lee, H. Fluid Phase Equilibria, 1998, 147, pg. 229-238.

Lu, H., Matsumoto, R., Tsuji, Y., Oda, H. Fluid Phase Equilibria. 2001, 178, pg. 225-232.

Makogon, Y.F. "Hydrates of natural gas", Penwell Books, Tulsa, Oklahoma, 1981.

Mizuno, K., Oda, K., Maeda, S., Shindo, Y., Okumura, A. J. Phys. Chem., 1995, 99 (10), pg. 3056-3059.

Mizuno, K., Oda, K., Shindo, Y., Okumura, A. J. Phys. Chem., 1996, 100 (24), pg. 10310-10315.

Mizuno, K., Mabuchi, K., Miyagawa, T., Matsuda, Y., Kita, S., Kaida, M., Shinda, Y. J. Phys. Chem. A. 1997, 101, pg. 1366-1369.

Sabil, K. M., Román, V. R., Witkamp, G.-J., Peters, C.J. "Tetrahydrofuran-promoted clathrate hydrate phase equilibria of CO₂ in aqueous electrolyte solutions" In Proc. Sixth International Conference on Gas Hydrate, Vancouver, Canada, July 7-10, 2008.

Sloan Jr., E.D. and Koh, C.A. "Clathrate Hydrates of Natural Gas", 2nd ed., CRC Press, Florida, 2007.

Roo, J.L. de, Peters, C.J., Lichtenthaler, R.N., Diepen, G.A.M., AIChE J., 1983, 29, pg. 651-657.

6

ENTHALPIES OF DISSOCIATION OF SIMPLE AND MIXED CARBON DIOXIDE CLATHRATE HYDRATES

In this Chapter, the enthalpies of dissociation for simple and mixed carbon dioxide clathrate hydrates are presented. The Clausius-Clapeyron equation is used to calculate the enthalpies of dissociation. In Section 6.1, the results of the calculated enthalpies of dissociation for simple carbon dioxide hydrates are presented and discussed. The hydration number for simple carbon dioxide is also calculated and presented in this section. In Section 6.2, the results of the calculated enthalpy of dissociation for mixed carbon dioxide and tetrahydrofuran are presented. The effects of carbon dioxide and tetrahydrofuran concentration on the enthalpy of dissociation are discussed as well. In Section 6.3, the enthalpies of dissociation for simple carbon dioxide and mixed carbon dioxide and tetrahydrofuran hydrates in electrolyte solutions are calculated and presented. The effects of the concentration and type of the electrolyte, present in the hydrate forming system, are shown and discussed.

6.1 INTRODUCTION

Enthalpies of dissociation for clathrate hydrates can be measured either by direct or indirect methods. In the direct method, the enthalpy of dissociation is measured calorimetrically. Handa [1986a and 1986b], Reuff et al. [1988] and Leivois et al. [1990] are among the first who reported enthalpy of dissociation measurements for clathrate hydrates through calorimetric techniques. More recently, Kang et al. [2001], Delahaye et al. [2006], Lin et al. [2007] and Martínez et al. [2008] have measured the enthalpy of dissociation of carbon dioxide or mixed carbon dioxide hydrates by similar techniques. Although the calorimetric techniques arguably produce the most accurate enthalpy data, the measurements are often painstakingly difficult and therefore, the data are limited in number.

A simpler and easier method to calculate the enthalpy of dissociation is via the indirect method. By taking advantage of the wide availability of three-phase hydrate equilibrium data of I (Ice) - H (Hydrate) - V (Vapour) or L_w (Liquid water) – H (Hydrate) – V (Vapour) of hydrate forming systems, the Clausius-Clapeyron equation can be applied to calculate the enthalpies of dissociation of the clathrate hydrates. The Clausius-Clapeyron equation [Smith et al., 2001] is stated below:

$$\frac{d \ln P}{d(1/T)} = \frac{-\Delta H}{zR} \quad (6.1)$$

where P is the pressure, T is temperature, ΔH is the enthalpy of dissociation, z is the gas compressibility factor and R is the universal gas constant. If the compressibility factor does not change rapidly, this equation can provide the ΔH value over a narrow temperature and pressure range.

The application of the Clausius-Clapeyron equation for the determination of the hydrate enthalpy of dissociation has been correctly argued to produce less accurate data. This is due to factors such as the phase volume changes, gas imperfections, gas solubility and water saturation which should be taken into account and corrected for more accurate results [Glew, 1959; Barrer, 1959 and Yamamura and Suga, 1989]. However, as pointed out by Sloan and Fleyfel [1992], consensus has been reached that the equation is valid for a univariant system (water + gas \leftrightarrow hydrate) with restrictions as follows: a. the fractional guest occupation of each cavity should not change appreciably, b) the condensed phase volume changes should be negligible relative to gas volume, and c) the gas composition should be constant. The authors have successfully demonstrated that the method provides acceptable results by comparing their data with that of Handa [1986a and 1986b] for similar clathrate hydrates. Furthermore, comparisons between the enthalpy data obtained from the direct and indirect methods such as reported by Kang et al. [2001] and Delahaye et al. [2006] for single and mixed carbon dioxide hydrates provide supplementary evidence on the suitability of the Clausius-Clapeyron equation for the calculation of the enthalpy of dissociation of clathrate hydrates.

By taking advantage of the vast number of three-phase equilibrium data (H-L_W-V) measured in the present work for simple carbon dioxide and mixed carbon dioxide and tetrahydrofuran hydrates in water and aqueous solutions, the enthalpy of dissociation is determined from the slope of these three-phase equilibria and subsequently substituted in the Clausius-Clapeyron equation. In this work, the compressibility factor, z , is calculated from Pitzer's correlation as shown below:

$$z = z^0 + \omega z^1 \quad (6.2)$$

where z^0 and z^1 are functions of both the reduced temperature (T_r), the reduced pressure (P_r) and ω , which is the acentric factor of carbon dioxide. The values of z^0 and z^1 are obtained from the Lee/Kesler Generalized-correlation Tables presented in Appendix E in Smith et al. [2001]. All the H-Lw-V data used in the current work are similar to those reported in Chapters 4 and 5.

6.2 SIMPLE CARBON DIOXIDE HYDRATE

As mentioned earlier, the enthalpy of dissociation for clathrate hydrates can be obtained by plotting $\ln P$ vs. $1/T$ of the three-phase H-Lw-V equilibrium data. In this work, the plot is constructed and depicted in Figure 6.1 for simple carbon dioxide hydrates. As presented in Figure 6.1, it can be seen that within experimental error all the experimental data points appear to fall on a line, indicating a constant enthalpy of dissociation. However, ΔH also depends on the compressibility factor, z . Since z is dependent on temperature and pressure and its values vary throughout the data series, the ΔH values will vary accordingly throughout the series as shown in Figure 6.2. It can be seen clearly from Figure 6.2 that the value of ΔH changes with the same order of magnitude as the compressibility factor. The trend observed supports the argument made by Skovborg and Rasmussen [1994] that ΔH and compressibility factor, z , must display a change of the same order of magnitude for the slope of $\ln P$ vs. $1/T$ to be constant. Thus, it must be emphasized that the compressibility factor must be evaluated in the P-T region of interest when ΔH is calculated from the Clausius-Clapeyron equation.

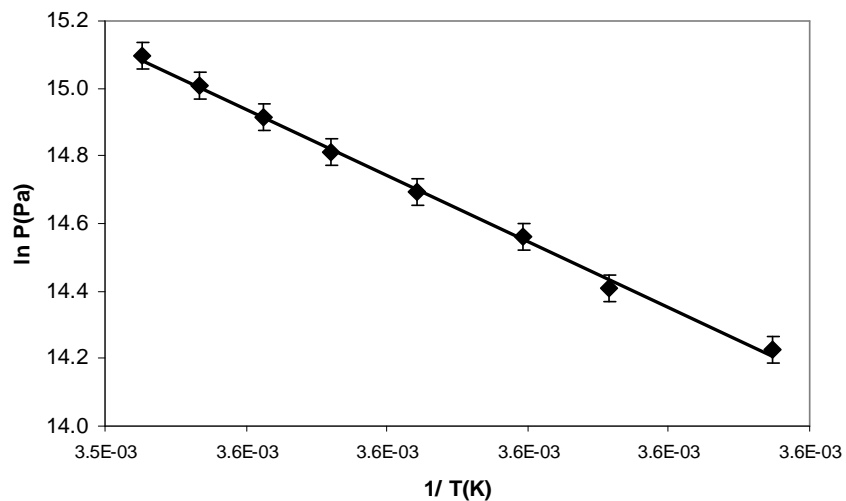


Figure 6.1 Three-phase H-L_W-V equilibrium data of simple carbon dioxide hydrate, represented in a Clausius-Clapeyron ($\ln P$ vs $1/T$) plot.

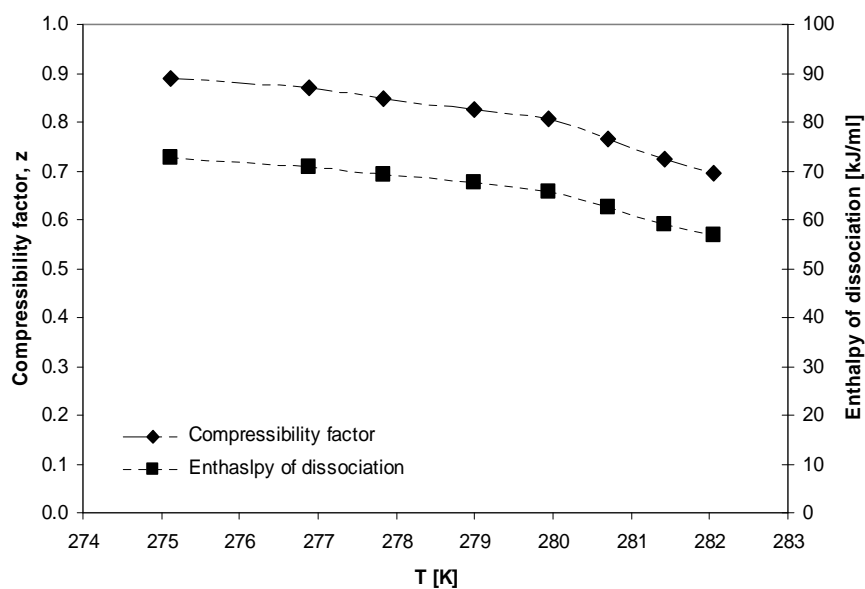


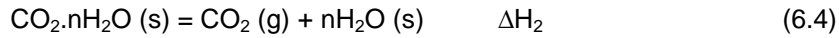
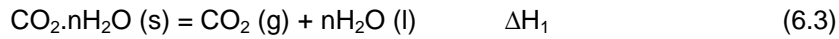
Figure 6.2 Compressibility factors z and enthalpies of dissociation ΔH for simple carbon dioxide hydrates, calculated at various temperatures.

Table 6.1 Enthalpies of dissociation of simple carbon dioxide at different H-L_W-V equilibrium points.

T [K]	P [MPa]	z	ΔH [kJ/mol]
273.15	1.05	0.92	75.37
273.65	1.22	0.91	74.44
275.12	1.51	0.89	72.66
276.88	1.81	0.87	70.93
277.83	2.11	0.85	69.15
278.99	2.40	0.83	67.48
279.94	2.70	0.81	65.81
280.71	3.00	0.77	62.48
281.42	3.30	0.72	59.06
282.06	3.60	0.70	56.85

The calculated values of ΔH for simple carbon dioxide hydrates between the quadruple points Q_1 and Q_2 are tabulated in Table 6.1. The unit of ΔH used throughout this work is kJ/mol_{CO₂}. The dissociation enthalpies of the hydrate vary between the Q_1 and Q_2 quadruple points. There is a significant increase of about 20 kJ/mol of ΔH as the equilibrium temperature drops from 282.06 to 273.15 K.

The hydration number of simple carbon dioxide hydrate is calculated based on the de Forcrand method [Sloan and Koh, 2007]. This method considers two scenarios representing the dissociation of hydrate to gaseous vapour and liquid water, and to vapour and ice. The two equations representing the two scenarios are as follows:



At quadruple point Q_1 , the number of liquid water converted to ice can be calculated as:



where

$$\Delta H_3 = \Delta H_1 - \Delta H_2 = n\Delta H_s^l(\text{H}_2\text{O}) \quad (6.6)$$

Since the enthalpy of fusion of water (ΔH_s^l) is well-known (6.01 kJ/mol), the number of moles of water converted to hydrate (n) can be calculated from Equation 6.6. Strictly, Eq. 6.6 is only valid only at the quadruple point Q_1 , where both reactions presented by Equations 6.3 and 6.4 occur simultaneously. However, Anderson [2003] stated that since the pressure and temperature range of the H-L_w-V region is modest for carbon dioxide hydrate, the equation is valid to determine the hydration number for this hydrate. ΔH_2 is calculated from reported H-I-V equilibrium data [Larson, 1955]. The results are tabulated in Table 6.2. As reported in Table 6.2, the enthalpy of dissociation of carbon dioxide hydrate to ice and vapour seems to be fairly constant throughout the region covered in this study. This is mainly due to the fact that the compressibility factor for carbon dioxide is reasonably constant in the region studied.

Table 6.2 Enthalpy of dissociation ΔH_2 of simple carbon dioxide hydrate for various H-I-V equilibrium points.

T [K]	P [MPa]	z	ΔH_2 [kJ/mol]
256.80	0.55	0.9526	24.03
264.00	0.75	0.9387	23.68
267.40	0.87	0.9319	23.51
268.90	0.92	0.9289	23.43
270.00	0.97	0.9263	23.36
270.70	1.00	0.9248	23.33
271.40	1.03	0.9235	23.29
271.70	1.04	0.9228	23.28
271.80	1.05	0.9224	23.27

Table 6.3 Hydration number n of simple carbon dioxide hydrate for various H-L_W-V equilibrium points.

T [K]	P [MPa]	Hydration Number (n)
273.65	1.22	8.54
275.12	1.51	8.25
276.88	1.81	7.96
277.83	2.11	7.66
278.99	2.40	7.38
279.94	2.70	7.11
280.71	3.00	6.55
281.42	3.30	5.98

The calculated hydration number at various temperatures obtained in this work is tabulated in Table 6.3. As reported in Table 6.3, a significant variation of the hydration number is obtained when Eq. 6.6 is used to calculate its value for simple carbon dioxide hydrate. A similar trend is observed by Anderson [2003]. The theoretical considerations and observations reported in literature on cage occupancy of the hydrate structures can be used to justify the reported hydration number. The hydration number is calculated based on the number of cavities occupied by carbon dioxide molecules in the hydrate. Structure I hydrate consists of 6 large cavities and 2 small cavities and the unit cell comprises 46 molecules of water. If all cavities are occupied, the hydration number is $n = 46/8 = 5.75$. If only the large cages are filled, the hydration number is $n = 46/6 = 7.67$. Since the van der Waals diameter of a carbon dioxide molecule (5.12 Å) is smaller than the free diameters (~ 5.76 Å) of most cavities in the hydrate lattice, carbon dioxide molecules can occupy either the small or large cavities, depending on the conditions of the hydrate formation [Teng, 1996; Ripmeester and Ratcliffe, 1998 and Mooijer-van den Heuvel, 2004]. Moreover, as pointed out by Sloan and Koh [2008], the typical occupancies of large cavities are usually greater than 95% while occupancy of the small cavities are usually of the order of magnitude of 50%. The present study implies that at 281.42 K, almost all cages are filled with carbon dioxide molecules, while at

273.15 K, only about 90 % of the large cavities of structure I hydrate are filled with carbon dioxide molecules. By comparing the equilibrium pressure at 281.42 K and 273.65 K, there is 2 MPa pressure increment, implying that the pressure of the system at 281.42 K is more than three times higher than at 273.15 K. Thus, it is not surprising that more carbon dioxide molecules are present in the hydrate structure and, consequently, the hydration number is found to be dependent on the equilibrium pressure of the system.

Table 6.4 Reported values of the enthalpy of dissociation and hydration number for simple carbon dioxide hydrate.

Reference	T (K)	ΔH (kJ. mol ⁻¹)	n	Method
Vlahakis et al. (1972)	273.15	59.90	7.30	Clausius-Clapeyron Eq.
Kamath (1984)	-	80.10	-	Clausius-Clapeyron Eq.
Long (1994)	-	73.00	-	Clausius-Clapeyron Eq.
Skovborg and Rasmussen (1994)	273.65	68.71	-	Clausius-Clapeyron Eq.
Uchida et al. (1995)	-	-	7.24 to 7.68	Raman
Aya et al. (1997)	-	-	6.0 to 7.8	Pressure drop
Ripmeester and Ratcliffe (1998)	-	-	≥ 7.0	NMR
Udachin et al. (2001)	-	-	6.20	X-ray diffraction
Kang et al. (2001)	273.65	65.22	7.23	Calorimetry
Yoon et al. (2003)	Q1	57.66	6.21	Clausius-Clapeyron Eq.
Anderson (2003)	282.15 to 274.15	58.2 to 62.5	5.7 to 6.4	Clapeyron Eq.
Delahaye et al. (2006)	280.3	65.22	-	DSC

As comparison, reported literature data on the enthalpy of dissociation and hydration number for simple carbon dioxide hydrate are presented in Table 6.4. As shown in Table 6.4, there is a significant variation

in the reported data in literature concerning enthalpy of dissociation and hydration number of simple carbon dioxide hydrate. The enthalpy of dissociation varies from 57.66 up to 80 kJ/mol and the hydration number varies from 5.7 to 7.8, depending on the methods used to obtain these data. At higher temperature, the enthalpy of dissociation obtained from the present study agrees most closely with those of Anderson [2003] whose values at 281.15 and 282.15 K are 59.4 and 58.2 kJ/mol, respectively. However, at lower temperature, i.e., 273.15 and 273.65 K, the calculated enthalpies are much closer to the reported value of Long [1994]. A similar trend is also found for the hydration number. Anderson [2003] argued that both the enthalpy of dissociation and hydration number as calculated by Clausius-Clapeyron equation suffer from errors caused by the volume changes, the non-ideality of the vapour phase and the solubility of carbon dioxide in water. Moreover, Uchida [1995] pointed out that the direct methods used to measure the hydration number, such as NMR and X-ray diffraction, suffer from the difficulties in the sample preparation and assumptions made during the analysis. Given the uncertainties on which method is the most accurate for the measurements based on data presented in Table 6.3 and the simplicity of the Clausius-Clapeyron equation, it is found that this equation can be used to obtain approximate values of the enthalpy of dissociation and hydration number for simple carbon dioxide hydrate with reasonable errors.

6.3 MIXED CARBON DIOXIDE AND TETRAHYDROFURAN HYDRATE

In the present work, the Clausius-Clapeyron equation is also used to calculate the enthalpy of dissociation for mixed carbon dioxide and tetrahydrofuran hydrates. From the previous sections, it is known that the

presence of tetrahydrofuran in carbon dioxide forming systems changes the phase behaviour of the systems. The pressure reduction, the liquid-liquid phase split and the pseudo-retrograde behaviour that might occur in the systems depend on the concentration of tetrahydrofuran. It is our interest to gain some information on how the inclusion of tetrahydrofuran in the system affects the enthalpy of dissociation.

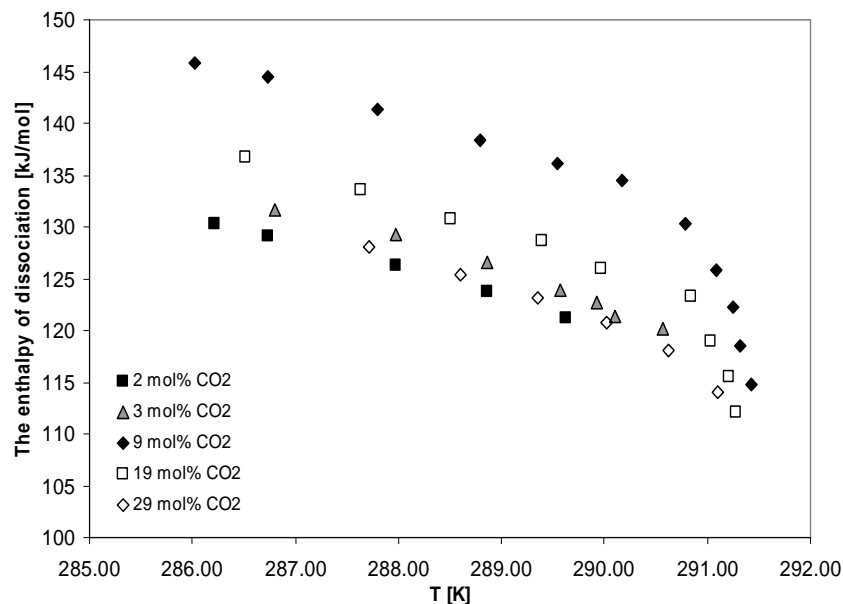


Figure 6.3 Dissociation enthalpy of mixed carbon dioxide and tetrahydrofuran hydrates at different concentrations of CO₂. The concentration of tetrahydrofuran is kept constant at 5.013 mol%.

Firstly, the calculated data for the enthalpy of dissociation for mixed carbon dioxide and tetrahydrofuran clathrate hydrates for different carbon dioxide concentrations in the hydrate forming systems are plotted in Figure 6.3. In this figure, the concentration of tetrahydrofuran is fixed at 5.0 mol% in the aqueous solution. As can be seen in Figure 6.3, at low concentration of carbon dioxide the enthalpy of dissociation seems to be independent of the concentration of carbon dioxide. However, as the concentration of carbon

dioxide increases to 9 mol%, a sharp increase of the enthalpy of dissociation is observed, especially in the low temperature region. As the concentration of carbon dioxide increases further to 19 mol% and 29 mol% respectively, a significant decrease of the enthalpy of dissociation is observed. The observed trend suggests that the enthalpy of dissociation of the mixed hydrates is dependent on the concentration of carbon dioxide in the system.

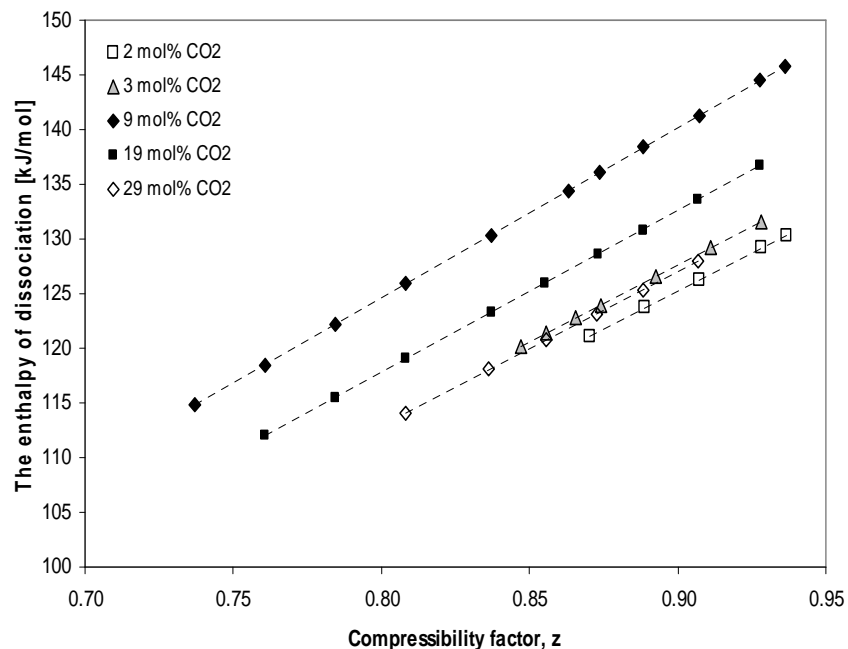


Figure 6.4 Dissociation enthalpy of mixed carbon dioxide and tetrahydrofuran hydrates vs. compressibility factor at different concentrations of CO₂. The concentration of tetrahydrofuran is kept constant at 5.013 mol%.

To get a better view, a plot of the enthalpy of dissociation versus the compressibility factor is presented in Figure 6.4. From this figure it becomes apparent that at a fixed value of the compressibility factor, the enthalpy of dissociation is dependent on the concentration of carbon dioxide in the

system. This observation further proves that the enthalpy of dissociation of mixed hydrate is dependent on the concentration of carbon dioxide available in the hydrate forming systems. Moreover, it seems that there is an optimum value for the carbon dioxide concentration to have the highest value of enthalpy of dissociation.

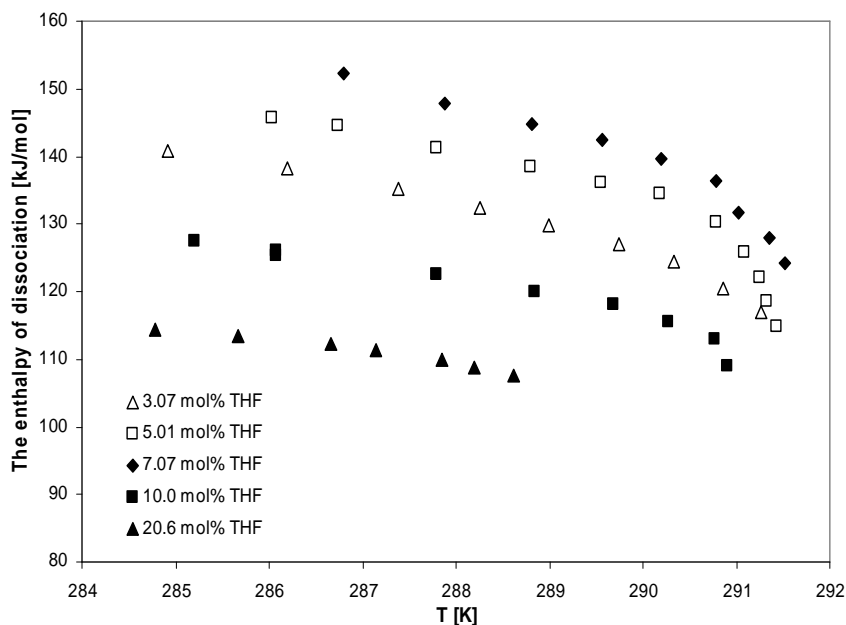


Figure 6.5 Enthalpies of dissociation of mixed carbon dioxide and tetrahydrofuran hydrates at different concentrations of tetrahydrofuran in the aqueous solutions. The concentration of carbon dioxide is kept constant at ~ 9 mol%.

In Figure 6.5, the enthalpy of dissociation of the mixed carbon dioxide and tetrahydrofuran hydrates is plotted against temperature at different concentrations of tetrahydrofuran, while the concentration of carbon dioxide is fixed at 9 mol%. The plot of the enthalpy of dissociation versus the compressibility factor is given in Figure 6.6. Based on Figures 6.5 and 6.6, it is clear that the enthalpy of dissociation is dependent on the concentration of tetrahydrofuran in the hydrate forming system. It is also found that the

maximum enthalpy of dissociation is achieved at 7 mol% tetrahydrofuran in the system. In Chapter 5, it has been shown that above 7 mol% the hydrate promoting effect of tetrahydrofuran changes into an inhibiting effect, which reduces the hydrate stability. With the decrease in stability, a lesser amount of energy is required to dissociate the hydrate structure which, in turn, produces less enthalpy of dissociation. Thus, it can be deduced that for the mixed carbon dioxide and tetrahydrofuran hydrates, the maximum hydrate enthalpy of dissociation is obtained at the stoichiometric tetrahydrofuran concentration in the aqueous solution. Similar findings on the dependency of the enthalpy of dissociation on the tetrahydrofuran concentration have been reported by Delahaye et al. [2006] for mixed carbon dioxide and tetrahydrofuran hydrates and by Kang et al. [2001] for mixed carbon dioxide, nitrogen and tetrahydrofuran hydrates.

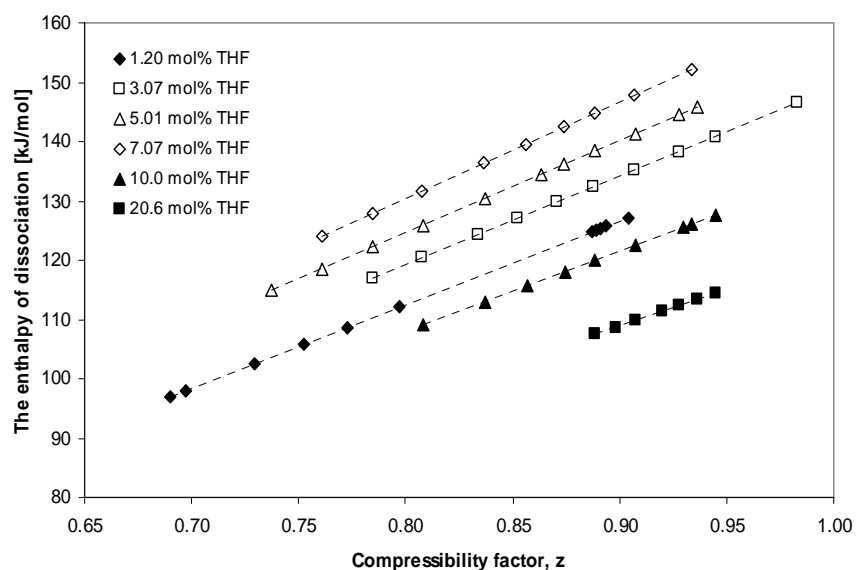


Figure 6.6 Dissociation enthalpies of mixed carbon dioxide and tetrahydrofuran hydrates vs. the compressibility factor at different concentrations of tetrahydrofuran. The concentration of carbon dioxide is kept constant at ~ 9 mol%.

Table 6.5 Enthalpies of dissociation for simple and mixed carbon dioxide and tetrahydrofuran hydrates at selected temperatures and tetrahydrofuran concentrations.

System	T [K]	Con. of THF (mol%)	ΔH (kJ. mol ⁻¹)
CO ₂ + H ₂ O	280.71	-	62.48
CO ₂ + THF + H ₂ O*	283.96	1.2	116.95
-identical-	284.91	3.1	140.83
-identical-	286.03	5.0	145.82
-identical-	286.79	7.0	152.27
-identical-	286.07	10.0	125.49
-identical-	286.67	20.6	112.37

* The concentration of carbon dioxide is kept constant at 9 mol%.

Selected data for the enthalpy of dissociation of simple carbon dioxide and mixed hydrates are tabulated in Table 6.5. As shown in Table 6.5, the dissociation enthalpies of the mixed carbon dioxide and tetrahydrofuran hydrates are much higher than that of simple carbon dioxide hydrate. In presence of 1.2 mol% of tetrahydrofuran, the dissociation enthalpy value increases from 62.48 kJ/mol to 116.95 kJ/mol. At 7.0 mol% of tetrahydrofuran, the enthalpy of dissociation for mixed hydrate is 152.27 kJ/mol. This large increase of the enthalpy of dissociation is attributed to the hydrate structural change. In case of the simple carbon dioxide hydrates, structure I hydrates are formed while in the case of mixed carbon dioxide and tetrahydrofuran hydrates, structure II hydrate is formed. Since the enthalpy of dissociation to the larger extent depends on the amount of water relative to the amount of guest species in the hydrate structure (Skovborg and Rasmussen, 1994), it is not surprising that the enthalpy of dissociation for structure II hydrate (136 water molecules per unit cell) is much higher compared to structure I hydrate (46 water molecules per unit cell). Moreover, the change from structure I to structure II hydrates increases the total amount of entrapped guest species, leading to enhanced hydrate stability. Thus, it is expected that an increase in guest molecule occupancy

in the hydrate cavities increases the hydrate stability, which increases the enthalpy of dissociation.

As addition, reference data on the enthalpies of dissociation for mixed carbon dioxide hydrates are tabulated in Table 6.6. The data reported by Delahaye et al. [2006] for mixed carbon dioxide and tetrahydrofuran hydrates is in the similar range of the results obtained in this work. Their enthalpy value of 155 kJ/mol at 280 K and 2.99 mol% tetrahydrofuran is very similar to our values at 279.9 K and 3.07 mol% tetrahydrofuran of 146.57 kJ/mol. The dependency of the enthalpy on carbon dioxide concentration might play a significant role in the discrepancy of the between the reported data and calculated values. Moreover, the enthalpy of mixed carbon dioxide and tetrahydrofuran hydrates is found to be consistently higher than that of mixed carbon dioxide, nitrogen and tetrahydrofuran hydrate.

Table 6.6 Literature data of the enthalpies of dissociation for mixed carbon dioxide tetrahydrofuran hydrates.

Ref.	System	T (K)	THF concentration (mol%)	ΔH (kJ. mol ⁻¹)
a	CO ₂ + THF + H ₂ O	280	0.98	130
		280	1.56	142
		280	2.74	147
		280	2.99	155
		280	4.22	163
b	CO ₂ + N ₂ +THF + H ₂ O (70% CO ₂ + 30% N ₂)	273.65	1.00	107.18
		273.65	3.00	113.66

a = Delahaye et al. (2006) and b = Kang et al. (2001)

6.4 MIXED CARBON DIOXIDE AND TETRAHYDROFURAN HYDRATES IN AQUEOUS ELECTROLYTES SOLUTION

In order to obtain some information on the effects of electrolytes on the enthalpy of hydrate dissociation, the enthalpies of dissociation for the simple carbon dioxide hydrates in water and aqueous sodium chloride solution are plotted against the compressibility factor and are represented in Figure 6.7.

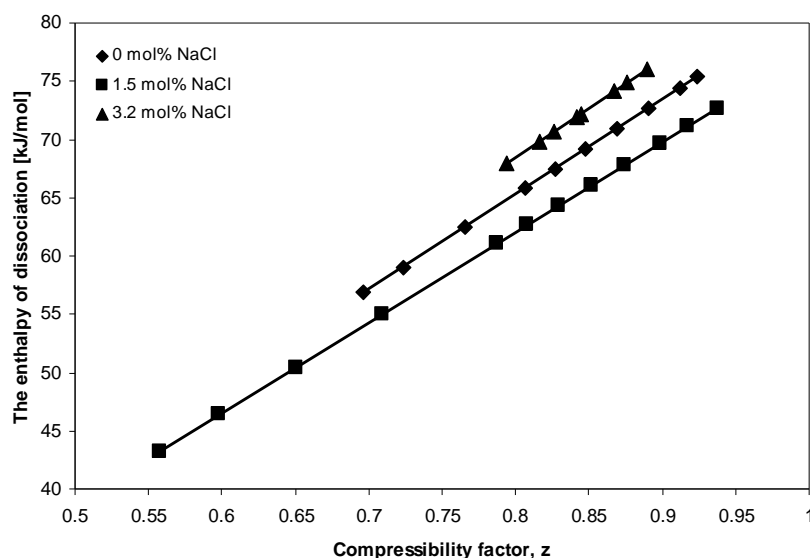


Figure 6.7 Dissociation enthalpy of simple carbon dioxide hydrates vs. the compressibility factor at different concentrations of sodium chloride. The concentration of carbon dioxide is kept constant at ~ 9 mol%.

It is shown in Figure 6.7 that the presence of sodium chloride changes the enthalpy of hydrate dissociation. De Roo et al. (1983) suggested that the enthalpy of dissociation and hydration number depend on the distribution of dissolved ions in the solution. Moreover, as pointed out by Elwood Madden et al. (2007), the depression of hydrate formation temperature by salts

shows that the addition of salts may have varying affects on the activity of water and, therefore, affects both the freezing point of pure water and the stability of gas hydrates to varying degrees. Consequently, a change in hydrate stability, caused by the presence of salts, also may affect the hydrate enthalpy of dissociation as a function of the salt concentration in the system.

In the present work, no conclusive evidence can be found from the available experimental data on either the presence of sodium chloride gives a positive or negative impact on the enthalpy of hydrate dissociation. This is because at 1.5 mol% of sodium chloride in the aqueous solution, the enthalpy of dissociation of the carbon dioxide hydrate is lower than that of pure water at any given compressibility factor. However, at 3 mol% of sodium chloride, the enthalpy of the carbon dioxide hydrate dissociation is higher than that of pure water. Based on the results of his study, Le [2002] suggested that the presence of electrolyte in the system requires a higher energy to form hydrate and similarly, a higher energy to dissociate the hydrate formation. Although this agreement may be valid to a high concentration of sodium chloride, it is not valid for an aqueous solution with low concentrations of sodium chloride.

To further investigate the effects of sodium chloride, the calculation of the enthalpy of dissociation is extended to mixed carbon dioxide and tetrahydrofuran hydrates. Figure 6.8 depicts the plot of enthalpy of dissociation for the mixed hydrate against compressibility factor at different concentrations of the aqueous sodium chloride solutions. Contrary to the tetrahydrofuran-free system, the presence of 1 mol% of sodium chloride in the hydrate forming system increases the enthalpy of hydrate dissociation for about ≈ 10 kJ/mol more than that of NaCl free system for any given compressibility factor. However, if the concentration of sodium chloride increases to 2 mol%, the enthalpy of dissociation decreases drastically to

less than that of NaCl free system (about ≈ 8 kJ/mol) for any given compressibility factor. Then, the enthalpy of dissociation slightly increases to higher values if the concentration of sodium chloride increases from 2 mol% to 5 mol% in the aqueous solutions.

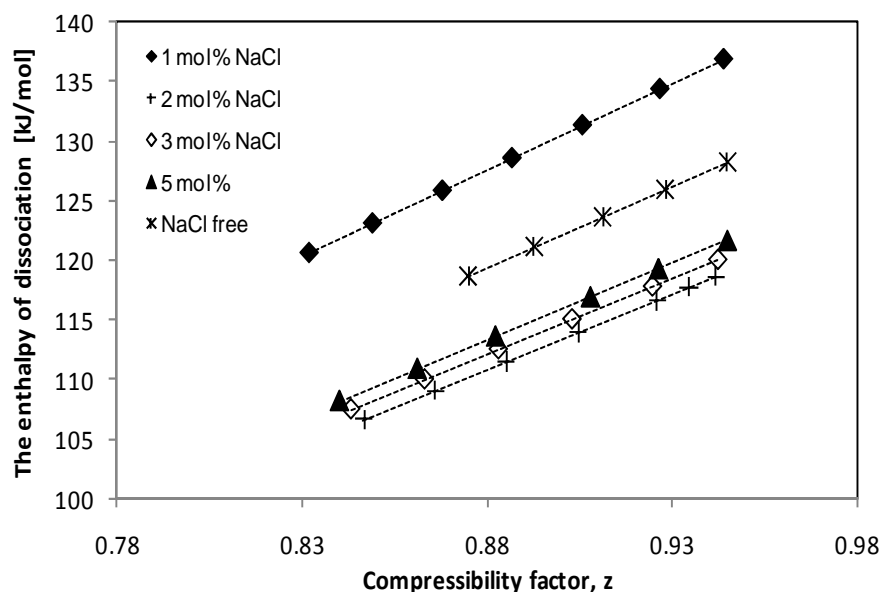


Figure 6.8 Dissociation enthalpies of mixed carbon dioxide and tetrahydrofuran hydrates vs. compressibility factor at different concentrations of sodium chloride. The concentrations of carbon dioxide and tetrahydrofuran are kept constant at 4 mol% and 5 mol%, respectively.

Further investigation of the effects of electrolytes on the enthalpy of hydrate dissociation is extended to different electrolytes. In Figure 6.9, the enthalpy of dissociation of mixed carbon dioxide and tetrahydrofuran is plotted against the compressibility factor for three different electrolytes, namely potassium bromide (KBr), sodium bromide (NaBr) and sodium fluoride (NaF), and at two different concentrations of 0.5 mol% and 1.0 mol% of the electrolyte in the aqueous solution. As depicted in Figure 6.9, regardless of the type of the electrolytes, the enthalpy of dissociation is found to decrease with increasing concentration of the electrolyte from 0.5

mol% to 1 mol%. Moreover, as clearly shown in Figure 6.9, the enthalpy of dissociation is also dependent on the type of electrolyte present in the hydrate forming system.

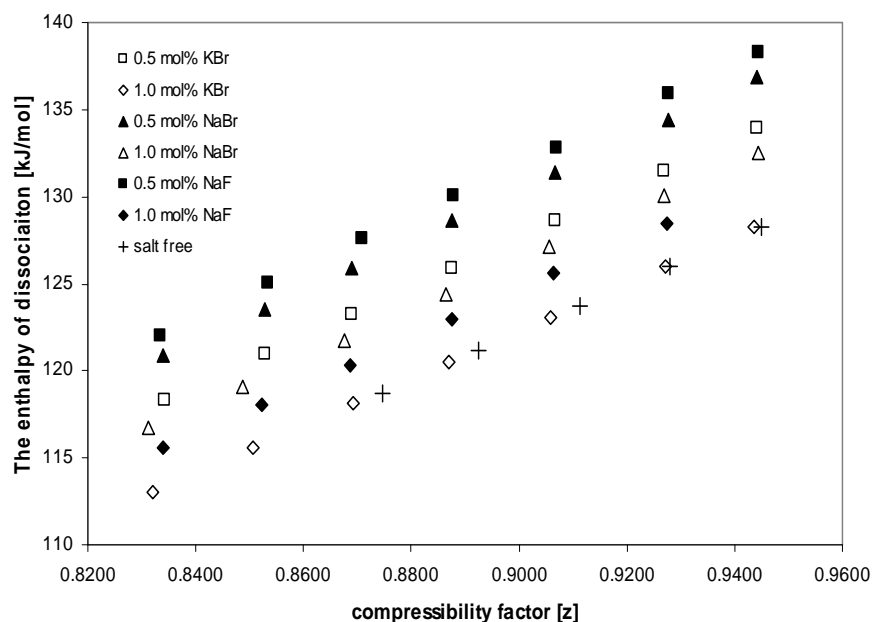


Figure 6.9 Dissociation enthalpies of mixed carbon dioxide and tetrahydrofuran hydrates vs. the compressibility factor for different concentrations of the electrolyte in the aqueous solutions. The concentration of carbon dioxide and tetrahydrofuran are kept constant at 4 mol% and 5 mol%, respectively

6.5 REFERENCES

- Anderson, G.K. J. Chem. Thermodynamics, 2003, 35, pg. 1171-1183.
- Aya, I., Yamane, K., Nariai, H. Energy, Int. J., 1997, 22, pg. 263-271.
- Barrer, R.M. Nature, 1959, 183, pg. 462-463.
- de Roo, J.L., Peters, C.J., Lichtenthaler, R.N., Diepen, G.A. AIChE J., 1983, 29, pg. 651-657.

- Delahaye, A., Fournaison, L., Marinhas, S., Chatti, I., Petitet, J.-P., Dalmazzone, D., Fürst, W. *Ind. Eng. Chem. Res.*, 2006, 45, pg. 391-397.
- Elwood Madden, M.E., Ulrich, S.M., Onstott, T.C., Phelps, T.J. *Geophys. Res. Letters*, 2007, 34, L11202.
- Glew, D.N. *Nature*, 1959, 184, pg 545-546.
- Handa Y.P. *J. Chem. Thermodynamics*, 1986a, 18 (9), pg. 915-921.
- Handa Y.P. *J. Chem. Thermodynamics*, 1986b, 18(10), pg. 891-902.
- Kamath, V.A. "A study of heat transfer characteristics during dissociation of gas hydrates". PhD thesis, Uni. Of Pittsburgh, 1984.
- Kang, S.-P., Lee, H., Ryu, B.-J. *J. Chem. Thermodynamics*, 2001, 33, pg 513-521.
- Larson, S.D. "Phase studies of the two-component carbon dioxide-water system, involving the carbon dioxide hydrate". PhD thesis, Uni. of Illinois, 1955.
- Le, H.Q. "An experimental study on CO₂ hydrate formation and dissociation". MSc thesis, Uni. of Oklahoma, 2002.
- Liegeois, J.S., Perkins, R., Martin, R.J., Kobayashi, R. *Fluid Phase Equilibria*, 1990, 59 (1), pg. 73-97.
- Lin, W., Delahaye, A. and Fournaison, L. *Fluid Phase Equilibria*, 2008, 264, pg. 220-227.
- Long, J.P. "Gas hydrate formation mechanism and kinetic inhibition". PhD thesis, Colorado School of Mines, 1994.
- Martínez, M.C., Dalmazzone, D., Fürst, W., Delahaye, A., Fournaison, L. *AIChE journal*, 2008, 54(4), pg. 1088-1095.
- Mooijer-van den Heuvel, M.M. "Phase Behaviour and Structural Aspects of Ternary Clathrate Hydrate Systems: The Role of Additives". PhD thesis, Delft Uni. of Technology, January, 2004.
- Ripmeester, J.A. and Ratcliffe, C.I. *Energy & Fuels*, 1998, 12, pg. 197-200.
- Rueff, R.M., Sloan, E.D., Yesavage, V.F. *AIChE Journal*, 1988, 34(9), pg. 1468-1476.

Skovborg, P. and Rasmussen, P. Fluid Phase Equilibria, 1994, 96, pg. 223-231.

Smith J.M., Van Ness, H.C, Abbott, M.M. "Introduction to Chemical Engineering Thermodynamics", 6th ed. Mc Graw Hill, Singapore, 2001.

Sloan, E.D. and Fleyfel, F. Fluid Phase Equilibria, 1992, 76, pg. 123-140.

Sloan Jr., E.D. and Koh, C.A. "Clathrate Hydrates of Natural Gas", 3rd ed., CRC Press, Florida, 2007.

Smith, J.M., Van Ness, H.C., Abbott, M.M. "Introduction to Chemical Engineering Thermodynamics", 6th, McGraw-Hill, New York, 2001.

Teng, H. Int. J. Chem. Kinetics, 1996, 28, pg. 935-937.

Uchida, T., Takagi, A., Kawabata, J., Mae, S., Hondoh, T. Energy Convers. Manage., 1995, 36, pg. 547-550.

Udachin, K.A., Ratcliffe, C.I., Ripmeester, J.A. J. Phys. Chem. B, 2001, 105, pg. 4200-4204.

Vlahakis, J.G., Chen, H.-S., Suwandi, M.S., Barduhn, A.J. "The growth rate of ice crystals: Properties of carbon dioxide hydrate, a review of properties of 51 gas hydrates". Syracuse U. research and development report 830, prepared for US Department of Interior, 1972.

Yamamura, O. and Suga, H. J. Therm. Analysis, 1989, 35, pg. 2025-2064.

Yoon, J.H., Yamamoto, Y., Komai, T., Haneda, H. Ind. Eng. Chem. Res, 2003, 42, pg. 1111-1114.



Modelling of the Phase Behaviour of the Hydrate Forming Systems

In this chapter, the thermodynamic modelling of the phase equilibria including a clathrate hydrate phase is described. The principles of modelling clathrate hydrate phase behaviour are described in Section 7.1. The selected equation of state with selected mixing rule used to model the fluid phases are detailed out in Section 7.2, while the thermodynamic model for the solid hydrate phase is presented in Section 7.3. The modelling results are presented and discussed in Section 7.4.

7.1 PRINCIPLES OF THERMODYNAMIC MODELLING

A system is in thermodynamic equilibrium when it is in thermal, mechanical and chemical equilibrium. For a system at constant pressure and temperature, thermodynamic equilibrium can be characterized by the Gibbs energy to be minimum. For a transfer of dn_i moles of a substance between two phases 1 and 2, in equilibrium at constant temperature and pressure, the change in Gibbs energy (G) is

$$dG = (\mu_i^2 - \mu_i^1)dn_i \quad (7.1)$$

where μ_i is the chemical potential of a substance i , and n_i is the number of moles of i . At equilibrium G is minimum, thus:

$$\left(\frac{\partial G}{\partial n_i} \right)_{T,P,n_j} = 0 \quad (7.2)$$

resulting in

$$\mu_i^1 = \mu_i^2 \quad (7.3)$$

For multiphase – multicomponent equilibria, Equation 7.2 can be extended to

$$\mu_i^1 = \mu_i^2 = \dots = \mu_i^k, \text{ for } i = 1, 2, \dots, N \quad (7.4)$$

and k is the number of coexisting phases.

Based on the above equations, the equilibrium condition may be calculated either by direct minimization of the Gibbs energy or by using the principle of equality of chemical potentials [Walas, 1985]. The chemical

potential can be expressed in terms of the fugacity of a component by the following equation:

$$\mu = \mu^0 + RT \ln \frac{f(p)}{P^0} \quad (7.5)$$

where μ^0 is the chemical potential at reference state, T is the temperature, R is the universal gas constant, P^0 is the pressure at the reference state and $f(P)$ is the fugacity as a function of pressure.

Combination of Eqs. 7.4 and 7.5 results in the equality of fugacities for the thermodynamic equilibrium under consideration:

$$f_A^1 = f_A^2, f_B^1 = f_B^2 \quad (7.6)$$

where f is the fugacity of component A or B in phase 1 or 2.

In the present work, the hydrate phase equilibrium is modelled by using the fugacity approach as proposed by Klauda and Sandler [2000, 2002, 2003]. This approach is based on solving the condition of equal fugacities of water in the hydrate phase and the fluid phases:

$$f_w^H(T, P) = f_w^\pi(T, P, x) \quad (7.7)$$

For solving these conditions, the fugacity of water in the fluid phase is calculated with an equation of state (EoS), while the fugacity of water in the hydrate phase is calculated from Equation 7.8.

$$f_w^H(T, P) = f_w^\beta(T, P) \exp\left(\frac{-\Delta\mu_w^H(T, P)}{RT}\right) \quad (7.8)$$

where

$$f_w^\beta(T, P) = f_w^{sat, \beta}(T, P) \exp\left(\frac{V_w^\beta(T, P)(P - P_w^{sat, \beta}(T))}{RT}\right) \quad (7.9)$$

In Equation 7.9, f_w^β is the fugacity of the hypothetical, empty hydrate lattice. This fugacity depends on the guest molecule(s) of the clathrate hydrate cavities, which takes into account the different degree of lattice distortion caused by different guests [Klauda and Sandler, 2000]. The chemical potential difference between the empty and occupied cage of the hydrate $\Delta\mu_w^H$ is calculated according to the van der Waals and Platteeuw (VdWP) statistical thermodynamic theory [van der Waals and Platteeuw, 1959].

7.2 THERMODYNAMIC MODELS OF FLUID PHASES

In order to calculate the fugacity of different components in various fluid phases, thermodynamic models are used. Conventional methods for hydrate phase equilibrium calculations [John et al., 1985; Klauda and Sandler, 2000; Cao et al., 2001] used different thermodynamic models to calculate the fugacity of water in the fluid phases. Based on this approach, the Peng-Robinson equation of state (EoS) as modified by Stryjek and Vera (PRSV EoS) [1986] in combination with Huron-Vidal-Orbey-Sandler mixing rules [Orbey and Sandler, 1995] is used to model the fluid phases. The UNIQUAC model is used to calculate the excess Gibbs free energy, which is incorporated in the attractive term of the selected mixing rules [Larsen et al.,

1987]. The main advantage of this method is its simplicity and it can be easily extended to more complicated systems.

7.2.1 The Peng-Robinson-Stryjek-Vera Equation of State

In the present work, the Peng-Robinson EoS with the modification by Stryjek and Vera (PRSV EoS) [1986] is used for the phase equilibrium calculations for the fluid phases. The PRSV EoS is defined represented as follows:

$$P = \frac{RT}{v-b} - \frac{a}{v^2 + 2bv - b^2} \quad (7.10)$$

where R is the universal gas constant, P is the pressure, T is the temperature, v is the molar volume, a and b are the attractive and excluded volume parameters, respectively. The parameters a and b can be calculated from as:

$$a = 0.457235 \frac{R^2 T_c^2}{P_c} \alpha \quad (7.11)$$

$$b = 0.077796 \frac{RT_c}{P_c} \quad (7.12)$$

In Equations 7.11 and 7.12, T_c and P_c are the critical temperature and pressure, respectively, and α is the Stryjek-Vera temperature dependency, which is defined as:

$$\alpha = [1 + \kappa(1 + \sqrt{T/T_c})]^2 \quad (7.13)$$

where κ is a function of temperature and it is defined as:

$$\kappa = \kappa_0 + \kappa_1(1 + \sqrt{T/T_c})(0.7 - T/T_c) \quad (7.14)$$

with

$$\kappa_0 = 0.378893 + 1.4897153\omega - 0.17131848\omega^2 + 0.0196554\omega^3 \quad (7.15)$$

In this equation, ω is the acentric factor and κ_1 is an additional adjustable characteristic of each pure compound. The pure component parameters for PRSV EoS used in this work are tabulated in Table 7.1. In this table, r is UNIQUAC pure component volume parameter and q is UNIQUAC pure component area parameter.

Table 7.1 Pure component parameters for the PRSV EoS.

Compounds	T_c (K)	P_c (bar)	ω	κ_1	r	q
CO ₂	304.21	73.6	0.2250	0.04285	1.299	1.292
H ₂ O	647.13	220.55	0.3438	-0.06635	0.920	1.400
THF	540.15	51.9	0.2255	0.03961	2.866	2.172

The compressibility of the liquid phase and the compressibility of the vapour phase are the smallest and largest roots, respectively of the cubic:

$$Z^3 - (1 - B)Z^2 + (A - 3B^2 - 2B)Z - (AB - B^2 - B^3) = 0 \quad (7.16)$$

A and B are dimensionless forms of a and b , respectively:

$$A = \frac{aP}{R^2T^2} \quad (7.17)$$

$$B = \frac{bP}{RT} \quad (7.18)$$

For a multicomponent system, the Huron-Vidal-Orbey-Sandler (HVOS) mixing rule [Orbey and Sandler, 1995] is used. For this mixing rule, the a parameter of the mixture is calculated from:

$$a = bRT \left[\sum_i x_i \frac{a_i}{b_i RT} + \frac{1}{C^*} \left(\frac{G^E}{RT} + \sum_i x_i \ln \left(\frac{b}{b_i} \right) \right) \right] \quad (7.19)$$

This model takes the advantage of the pressure independence of the excess Helmholtz energy and its relation to the readily obtained g^E , as shown in Equation 7.20.

$$g^E(x, T, P = low) = a^E(x, T, P = low) = a^E(x, T, P = \infty) \quad (7.20)$$

At the limit of infinite pressure, the ratio V/b goes to unity, therefore C^* is equal to -0.623225. The b parameter of the mixture is calculated from:

$$b = \sum x_i b_i \quad (7.21)$$

7.2.2 UNIQUAC model

In this work the UNIQUAC (Universal Quasi-Chemical Activity Coefficient Model) is chosen to represent the excess Gibbs free energy. Within this approach a liquid is considered as a three-dimensional lattice of equi-spaced sites in which the immediate vicinity of a site is called a *cell*.

Each molecule in the liquid is divided into attached segments such that each segment occupies one cell and it is assumed that the total number of cells is equal to the total number of segments. Thus, for a binary solution of components 1 and 2, it is considered that there are, respectively, r_1 and r_2 segments for molecule of each component. Also, it is assumed that all segments have the same size but different external contact area. Hence, for any component i the number of nearest neighbours is zq_i where z is the coordination number of the lattice and q_i is a parameter proportional to the molecule's external surface area.

The UNIQUAC contribution to the excess Gibbs energy consists of a combinatorial part and a residual part. The excess Gibbs free energy of a component i , in a multi-component mixture is obtained from the following equation:

$$\frac{g^E}{RT} = \underbrace{\sum_i^n x_i \ln \left(\frac{\Phi_i}{x_i} \right) + \frac{z}{2} \sum_i^n q_i x_i \ln \left(\frac{\theta_i}{\Phi_i} \right)}_{\frac{g^{E,C}}{RT}} - \underbrace{\sum_i^n q_i x_i \ln \sum_j^n \theta_j \tau_{ji}}_{\frac{g^{E,R}}{RT}} \quad (7.22)$$

In this equation, the combinatorial part is marked by superscript C and the residual part by superscript R. In Equation 7.22, x_i is the mole fraction of component i , Φ_i is the volume fraction of component i , and θ_i is the surface area fraction of component i . The volume and surface area fractions of component i , are calculated from:

$$\Phi_i = \frac{r_i x_i}{\sum_j^n r_j x_j} \quad \theta_i = \frac{q_i x_i}{\sum_j^n q_j x_j} \quad \tau_{ij} = \exp \left(-\frac{u_{ij}}{RT} \right) \quad (7.23)$$

In this work, the energy parameters, u_{ij} for the G^E model are obtained by fitting the data obtained from Lazzaroni et al. [2004]. The fitted equations are tabulated in Table 7.2.

Table 7.2 Energy parameters used in HVOS mixing rule with UNIQUAC g^E model.

System	u_{12} (cal/mol)	u_{21} (cal/mol)
H ₂ O (1) + THF (2)	$4.308 \cdot T - 1553.951$	$-9.505 \cdot T + 4057.368$
THF (1) + CO ₂ (2)	$-13.197 \cdot T + 3940.916$	$17.077 \cdot T - 5233.738$
H ₂ O (1) + CO ₂ (2)	$-0.03095 \cdot (T^2) + 17.24524 \cdot T - 1412.38571$	$-0.66048 \cdot (T^2) + 443.01762 \cdot T - 72510.32286$

The activity coefficient of component i in a multi-component mixture iscalculated from:

$$\ln \gamma_i = \ln \left(\frac{\Phi_i}{x_i} \right) + \frac{z}{2} q_i \ln \left(\frac{\theta_i}{\Phi_i} \right) + \ell_i - \frac{\Phi_i}{x_i} \sum_i^n x_i \ell_i - q_i \ln \left(\sum_j^n \theta_j \tau_{ji} \right) + q_i - q_i \sum_j^n \frac{\theta_j \tau_{ij}}{\sum_k^n \theta_k \tau_{kj}} \quad (7.24)$$

with

$$\ell_i = \frac{z}{2} (r_i - q_i) - (r_i - 1) \quad (7.25)$$

With these mixing and combining rules and the PRSV EOS, the fugacity in a homogeneous phase f_i of component i can be expressed as

$$f_i = P \phi_i x_i \quad (7.26)$$

where P is the pressure, x_i is the mole fraction and ϕ_i is the fugacity coefficient of component i , which is given by

$$\ln \phi_i = \frac{b_i}{b} (Z-1) - \ln(Z-B) - \frac{1}{2\sqrt{2}} \left(\frac{a_i}{b_i RT} + \frac{\ln \gamma_i}{C^*} + \frac{1}{C^*} \ln \left(\frac{b_i}{b} \right) + \frac{1}{C^*} \left(\frac{b_i}{b} - 1 \right) \right) \ln \left(\frac{Z + (1+\sqrt{2})B}{Z + (1-\sqrt{2})B} \right) \quad (7.27)$$

where $A, B, Z, a_i, b_i, \gamma_i$ and C^* has been defined previously.

7.3 THERMODYNAMIC MODEL FOR THE HYDRATE PHASE

The hydrate phase is modelled based on the van der Waals and Platteeuw model [van der Waals and Platteeuw, 1959; Sloan and Koh, 2007], combined with a fugacity approach as proposed by Chen and Guo [1996] and Klauda and Sandler [2000]. The equilibrium criteria of the hydrate-forming mixture are based on the equality of fugacity of the specified component i in all phases which coexist simultaneously:

$$f_i^H = f_i^L = f_i^V (= f_w^I) \quad (7.28)$$

In this equation, H is the hydrate phase either structure I, II or H, L is the liquid phase such as the water-rich or guest-rich liquid phases, V is the vapour phase, and I is the ice phase. Each of the possible hydrate structures I, II or H has to be considered as one independent phase because the mixed or double hydrates can possibly exist for the systems containing one or more guest components [Jager et al., 2005]. The fugacity of water in the hydrate phase $f_w^H(T, P)$ is given by:

$$f_W^H(T, P) = f_W^{MT}(T, P) \exp\left(\frac{-\Delta\mu_w^{MT-H}}{RT}\right) \quad (7.29)$$

Here, $f_W^{MT}(T, P)$ represents the fugacity of water in the hypothetical empty hydrate cavity and $\Delta\mu_w^{MT-H}$ is the chemical potential difference of water in the empty hydrate lattice, μ_w^β and the hydrate phase, μ_w^H . $\Delta\mu_w^{MT-H}$ is calculated from the following equation:

$$\Delta\mu_w^{MT-H} = RT \sum_m \nu_m \ln\left(1 - \sum_j \theta_{mj}\right) \quad (7.30)$$

where ν_m is the number of cavities of type m per water molecule in the hydrate phase (which are: $\nu_1 = 1/23$ and $\nu_2 = 3/23$ for structure I hydrate and $\nu_1 = 2/17$ and $\nu_2 = 1/17$ for structure II hydrate) and θ_{mj} the fraction of cavities of type m occupied by the molecules of component j . This fractional occupancy is determined by a Langmuir-type expression:

$$\theta_{mj} = \frac{C_{mj} f_j^V}{1 + \sum_k C_{mk} f_k^V} \quad (7.31)$$

In Eq. 7.31, C_{mj} is the Langmuir constant of component j in a cavity of type m and f_j^V is the fugacity of component j in the vapour phase in equilibrium with the hydrate. In the present work, the Langmuir constants C_{mj} are estimated by assuming the following temperature dependence:

$$C_{mj} = \frac{A_{mj}}{T} \exp\left(\frac{B_{mj}}{T}\right) \quad (7.32)$$

The values of the parameters A_{mj} and B_{mj} are given by Munck et al. [1988] and Delahaye et al. [2006] and are tabulated in Table 7.3.

Table 7.3 The optimized A_{mj} and B_{mj} parameters for the calculation of *Langmuir constants*.

		CO ₂		THF	
		A (K·Pa ⁻¹)	B (K ⁻¹)	A (K·Pa ⁻¹)	B (K ⁻¹)
Structure I	Large cavities	4.19E-07	2813	-	-
	Small cavities	2.44E-09	3410	-	-
Structure II	Large cavities	8.40E-06	2025	6.5972	1003.22
	Small cavities	8.34E-10	3615	-	-

The fugacity of water in the empty hydrate lattice, $f_w^{MT}(T, P)$, is calculated from:

$$f_w^{MT} = P_w^{sat, MT} \phi_w^{sat, MT}(T) \exp\left(\frac{v_w^{MT}(P - P_w^{sat, MT}(T))}{RT}\right) \quad (7.33)$$

with $P_w^{sat, MT}$ and $\phi_w^{sat, MT}$ respectively as the saturation vapour pressure and fugacity coefficient of the hypothetical empty hydrate lattice at temperature T.

Based on X-ray diffraction data obtained by Tse [1987] and Hirai et al. [2000], Klauda and Sandler [2000] expressed the molar volume of the empty

hydrate lattice, v_w^{MT} for each structure as a function of the temperature and pressure as:

$$v_{w,I}^{MT}(T,P) = (11.835 + 2.217 \times 10^{-5} T + 2.242 \times 10^{-6} T^2)^3 \frac{10^{-30} N_A}{46} - 8.006 \times 10^{-9} P + 5.448 \times 10^{-12} P^2 \quad (7.34)$$

$$v_{w,II}^{MT}(T,P) = (17.13 + 2.249 \times 10^{-4} T + 2.013 \times 10^{-6} T^2 + 1.009 \times 10^{-9} T^3)^3 \frac{10^{-30} N_A}{136} - 8.006 \times 10^{-9} P + 5.448 \times 10^{-12} P^2 \quad (7.35)$$

The saturation vapour pressure $P_w^{sat,MT}$ is modelled based on Ruzicka and Majer [1996]. This expression is chosen because of its accuracy in extrapolation. The expression is shown below:

$$\ln(P_w^{sat,MT}) = A \ln(T) + \frac{B}{T} + C + DT \quad (7.36)$$

where A, B, C and D are adjustable parameters and their values are regressed from phase equilibrium data. The adjustable parameter C is fixed at 2.7789. This is done to enable a comparison with the data of Klauda and Sandler [2000].

7.4 RESULTS AND DISCUSSION

The modelling programme created for this work is based on the programme previously developed by Mooijer-van den Heuvel [2004] and Martin and Peters [2009]. In the MATLAB programme (version 7.3.0), calculations are performed for all phases that could occur in the region for all

selected systems studied in the thesis. The main criterion of this model is the equality of the fugacity of water in the clathrate hydrate and aqueous phase ($f_w^H = f_w^L$). For convergence of the flash calculations, the Rachford-Rice equation was used, with the Newton-Raphson algorithm applied for solving this equation.

7.4.1 Modelling Results for the Fluid Phases

For the bubble point conditions ($L_W-L_V-V \rightarrow L_W-L_V$), the experimental data of the ternary system of carbon dioxide-tetrahydrofuran-water system together with the modelling results at a constant tetrahydrofuran concentration of 5 mol% in the aqueous solution are visualized in Figure 7.1 as isopleths, i.e. as loci for a constant overall-composition. The concentration of carbon dioxide is varied from 1 mol% to 27 mol%. In order to examine the consistency of the various isopleths, each isopleth of the ternary system is fitted to a second order polynomial with an average correlation coefficient of 0.998. From the fitted function, the bubble point pressure can be calculated for various values of the temperature as a function of the composition of the system as shown in Figure 7.2. As can be seen in Figures 7.1 and 7.2, the calculated and measured data are in good agreement throughout the temperature, pressure and concentration ranges studied. In general, the model slightly underpredicts the equilibrium pressure of the system at specified overall concentration of carbon dioxide. This error might be caused by the experimental error during the sample preparation due to very low concentrations of carbon dioxide used. The average absolute relative deviation (AARD%) is found to be 3.73%. The AAD% is calculated from:

$$AARD\% = \frac{1}{N_{\text{exp}}} \sum_{i=1}^{N_{\text{exp}}} \left(\frac{|P_{i,\text{exp}} - P_{i,\text{cal}}|}{P_{i,\text{exp}}} \right) \quad (7.37)$$

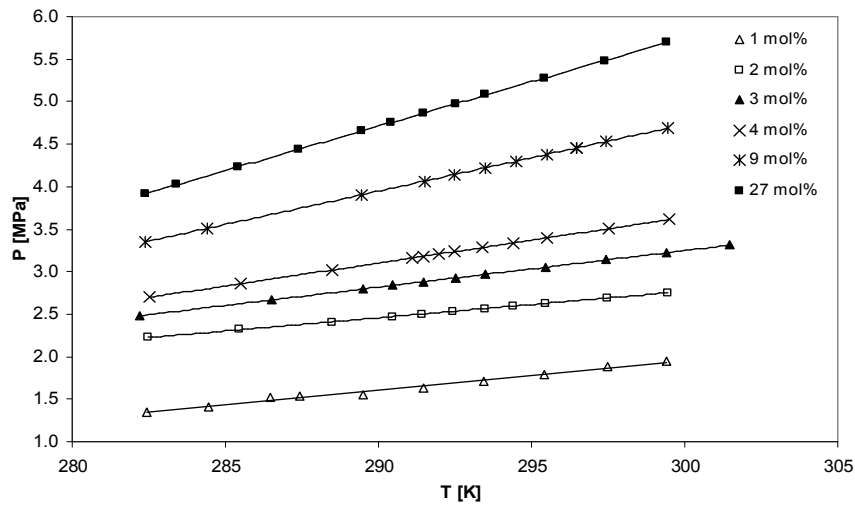


Figure 7.1 P, T-projection of bubble points ($L_W-L_V-V \rightarrow L_W-L_V$) for the system CO_2 -THF- H_2O at 5 mol% THF. The experimental bubble point data are represented by the markers for the overall-compositions that are given in mol% CO_2 and the modelled data are represented by solid lines.

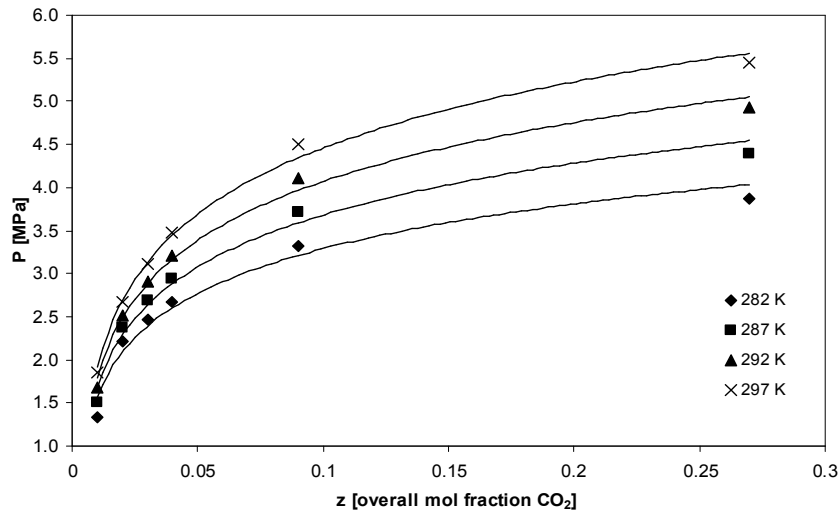


Figure 7.2 P,z section for bubble points ($L_W-L_V-V \rightarrow L_W-L_V$) at various temperatures for the system CO_2 -THF- H_2O at 5 mol% THF. The modelled data are represented by solid lines and the data that are calculated from the fitted isopleths are represented by markers.

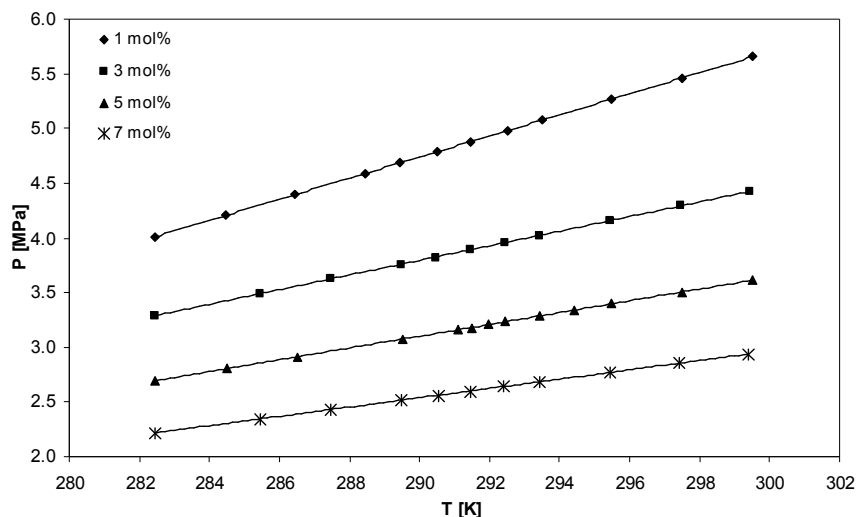


Figure 7.3 P,T-projection of bubble points ($L_W-L_V-V \rightarrow L_W-L_V$) for the system CO_2 -THF- H_2O at 4 mol% CO_2 . The experimental bubble point data are represented by the markers for the overall-compositions that are given in mol% THF and the modelled data are represented by solid lines.

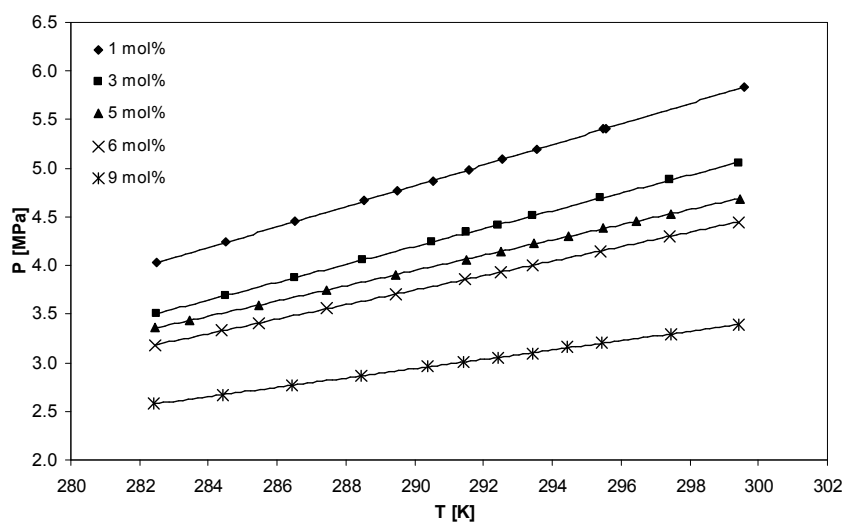


Figure 7.4 P,T-projection of bubble points ($L_W-L_V-V \rightarrow L_W-L_V$) for the system CO_2 -THF- H_2O at 9 mol% CO_2 . The experimental bubble point data are represented by the markers for the overall-compositions that are given in mol% THF and the modelled data are represented by solid lines.

Next, the measured and modelled bubble point conditions ($L_W-L_V-V \rightarrow L_W-L_V$) of the ternary system at overall constant carbon dioxide concentration of 4 and 9 mol% are visualized as isopleths in Figures 7.3 and 7.4, respectively. The P,x section for both systems are constructed as previously discussed and represented together with the modelling results in Figures 7.5 and 7.6 respectively.

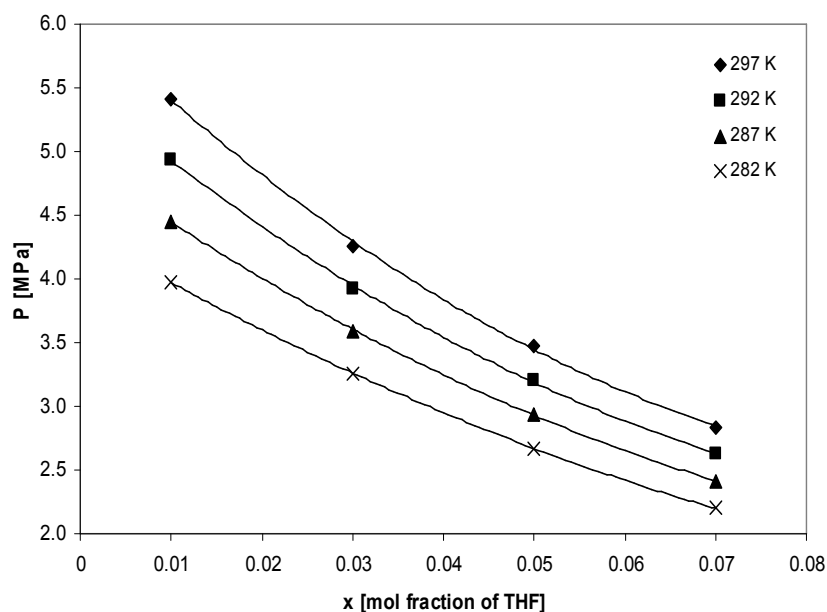


Figure 7.5 P,x section for bubble points ($L_W-L_V-V \rightarrow L_W-L_V$) at various temperatures for the system CO_2 -THF- H_2O at 4 mol% CO_2 . The modelled data are represented by solid lines and the data that are calculated from the fitted curves through the isopleths are represented by markers.

The calculated AARD% for both cases is 0.31756% and 2.5727% respectively. The good agreement of the predicted isopleths and isotherms lines in all cases demonstrates the ability of the models to capture the bubble point pressure dependencies on concentration and temperature. In general, as the temperature increased from 282 to 297 K, the pressure

required for the last bubble to disappear is also increasing. With regard to the carbon dioxide concentration, the bubble point pressure also increases with its concentration. In contrast, if the concentration of tetrahydrofuran increases, the bubble point pressure decreases. The lowering of the bubble point pressure with the increasing amount of tetrahydrofuran may be explained based on the high solubility of carbon dioxide in tetrahydrofuran [Lazzaroni et al, 2005]. The authors attributed the high solubility of carbon dioxide in tetrahydrofuran to the possibility of carbon dioxide acting like a Lewis acid and thus likely to interact with the basic ether functionality of tetrahydrofuran, i.e. the higher the amount of tetrahydrofuran in the system, the easier it will be for carbon dioxide to dissolve in the liquid organic aqueous phase (L_V).

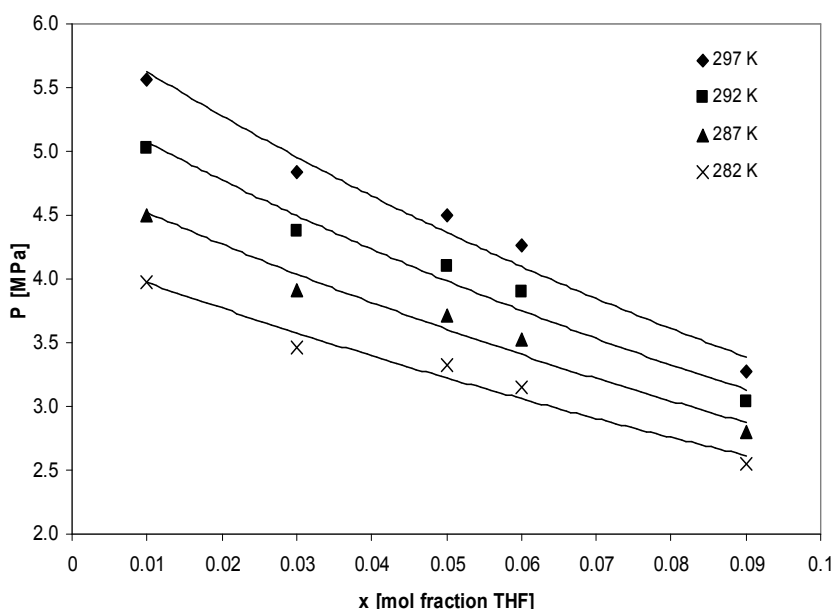


Figure 7.6 P,x-cross section for bubble points ($L_W-L_V-V \rightarrow L_W-L_V$) at various temperatures for the system CO_2 -THF- H_2O at 9 mol% CO_2 . The modelled data are represented by solid lines and the data that are calculated from the fitting curves through the isopleths are represented by markers.

Similarly, the dew point line ($L_W-L_V-V \rightarrow L_W-V$) is modelled for the ternary systems at fixed composition of carbon dioxide while the concentration of tetrahydrofuran is varied from 1 to 9 mol% in the aqueous phase. Two systems with a fixed carbon dioxide concentration of 4 mol% and 9 mol% are presented to demonstrate the ability of the model to predict dew points in the ternary system. The P,T-representations of the systems are depicted in Figures 7.7 and 7.8 respectively. In addition, four isotherms for each system are represented in Figures 7.9 and 7.10.

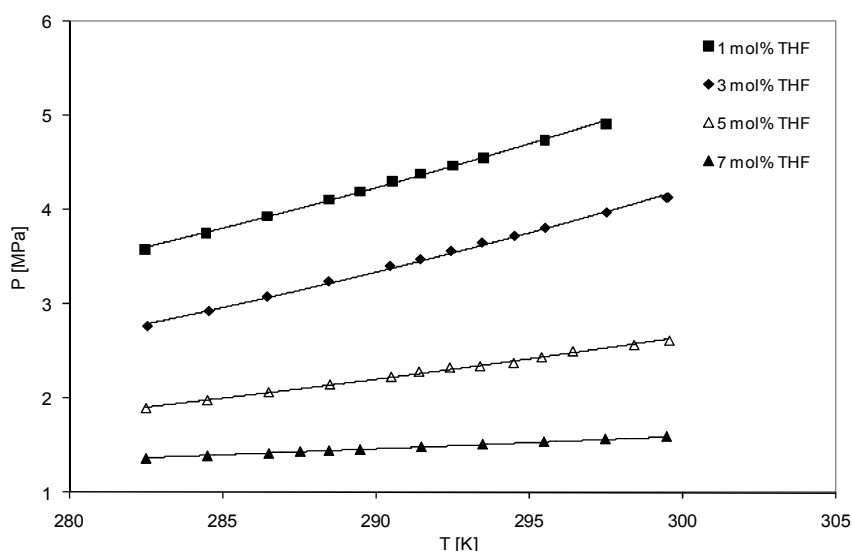


Figure 7.7 P,T-projection of dew points ($L_W-L_V-V \rightarrow L_W-V$) for the system CO_2 -THF- H_2O at 4 mol% CO_2 . The experimental data are represented by the markers for the overall-compositions that are given in mol% THF and the modelled data are represented by solid lines.

Again, it is shown that the model used in the work is able to represent the phase boundary between all the fluid phases of the systems studied with AAD% of 3.36% and 1.75% respective to the two examples used in this work. In general, the AARD% is increasing with a decreasing amount of carbon dioxide in the system. Once again, this trend might be attributed to

the inaccuracies occurring during sample preparation for very low concentrations of carbon dioxide.

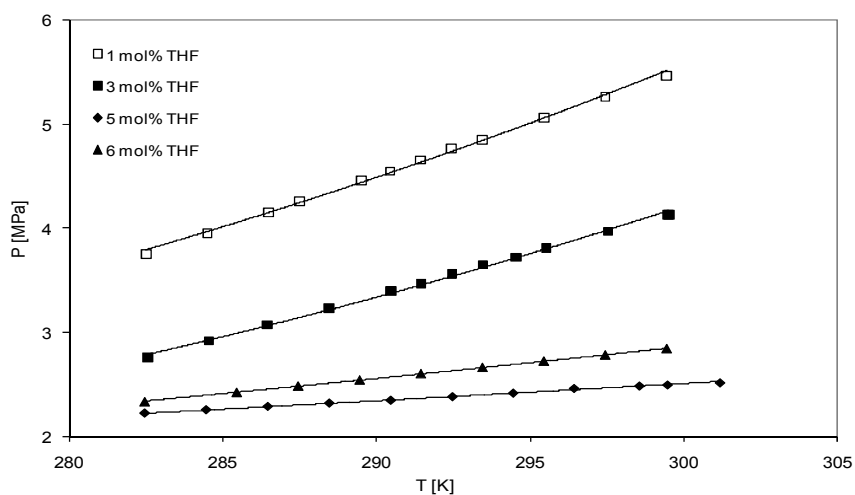


Figure 7.8 P,T-projection of dew points ($L_W-L_V-V \rightarrow L_W-V$) for the system CO_2 -THF- H_2O at 9 mol% CO_2 . The experimental data are represented by the markers for the overall-compositions that are given in mol% THF and the modelled data are represented by solid lines.

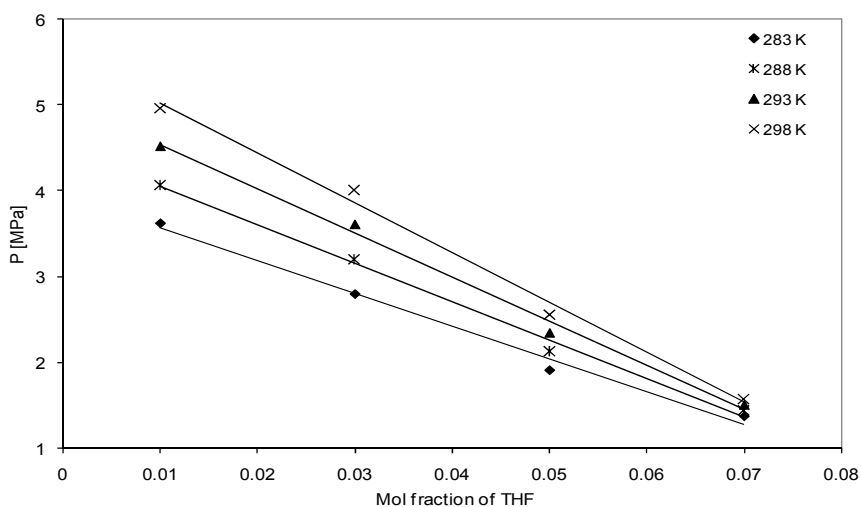


Figure 7.9 P,x-projection of dew points ($L_W-L_V-V \rightarrow L_W-V$) for the system CO_2 -THF- H_2O at 4 mol% CO_2 . The modelled data are represented by solid lines and the data that are calculated from the fitted curves through the isopleths are represented by markers.

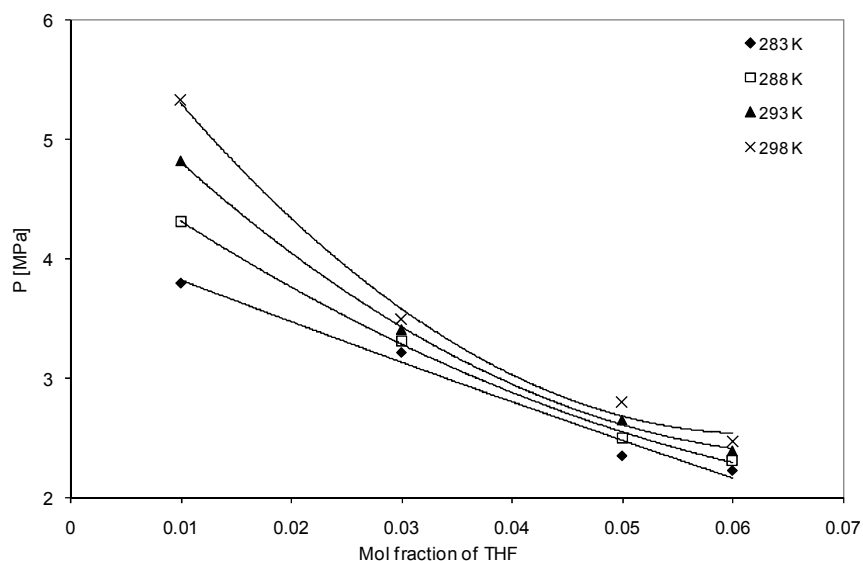


Figure 7.10 P, x-projection of dew points ($L_W-L_V-V \rightarrow L_W-V$) for the system CO_2 -THF- H_2O at 9 mol% CO_2 . The modelled data are represented by solid lines and the data that are calculated from the fitted curves through the isopleths are represented by markers.

Both predicted and experimental results show that the carbon dioxide + tetrahydrofuran + water system requires a very little amount of carbon dioxide for a liquid-liquid phase split to occur. The infinite dilution activity coefficient (γ^∞) of tetrahydrofuran in water at 298 K measured by Sherman et al. [1996] is 17.01. This value shows that, although tetrahydrofuran is completely miscible in water, the system strongly deviates from ideality and, therefore, is susceptible to a phase split upon addition of carbon dioxide to the system. Moreover, it is clearly observed that the dew point line is becoming more horizontal as the concentration of tetrahydrofuran is increasing in the system. As the dew point line is used to indicate the occurrence of a liquid-liquid phase split in the ternary system, the trend shows that the liquid phase is becoming more susceptible to a liquid-liquid phase split when higher amounts of tetrahydrofuran are present in the system.

7.4.2 Modelling Results of the Hydrate Equilibria in the Ternary Systems Water, Carbon Dioxide and Tetrahydrofuran

The PRSV-HVOS in combination with fugacity based hydrate model has been used to model the different phase transitions involving a hydrate phase found experimentally in ternary systems of water-carbon dioxide-tetrahydrofuran. In total, there are three different types of equilibria that have been modelled namely H-L_W-L_V, H-L_W-L_V-V and H-L_W-L_V. The concentration of carbon dioxide is varied from 2 mol% to 27 mol% while the concentration of tetrahydrofuran is varied from 1.2 mol% to 20.6 mol% in the ternary systems studied. This is carried out in order to observe the changes of the phase behaviour caused by changing the overall concentration in the ternary system. The necessary parameters for the model used are those reported already in sections 7.2 and 7.3. Table 7.5 presents the type of phase equilibrium modelled and the average absolute values of the relative deviation (AARD%) between the experimental and predicted values. The AARD% is calculated similarly as mentioned in Equation 7.37. Figures 7.11 to 7.15 present the graphical comparison between the experimental data points and the predicted ones for a whole range of overall compositions in the ternary system. The predicted bubble and dew point lines are also included when available.

Table 7.5 Summary of the results of the phase equilibria modelled and the overall values of the relative deviation (AARD%) between the experimental and calculated values for the ternary water-carbon dioxide-tetrahydrofuran systems.

Type of equilibrium	Number of exp. data points	AARD (%)
H-L _W -V	124	3.46%
H-L _W -L _V -V	90	9.01%
H-L _W -L _V	125	11.75%

In general, it can be concluded from the comparison of the AARD% values that the model presents acceptable agreements between predicted and experimental values. When the region of H-L_W-V phase boundaries is considered, the predicted equilibrium data comply with the experimental data with overall AARD% of 3.46% when averaged over the whole composition range. This trend can be observed throughout the whole composition range as shown in Figures 7.11 to 7.15.

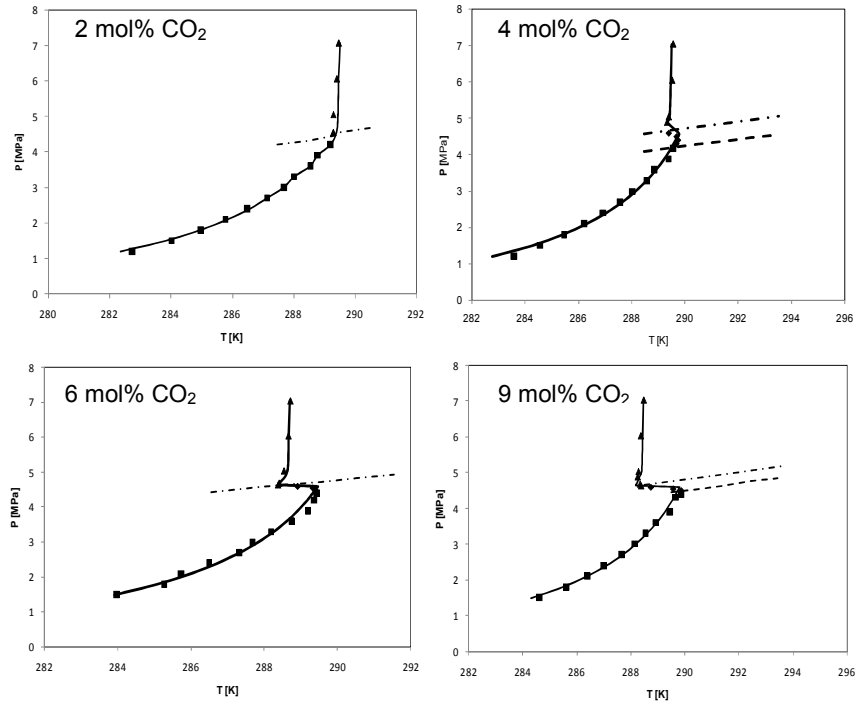


Figure 7.11 Experimental data for the various equilibria H-L_W-V (■), H-L_W-L_V-V (◆), H-L_W-L_V (▲) and predicted equilibrium conditions for those equilibria in the system of H₂O + CO₂ + tetrahydrofuran at 1.2 mol% of tetrahydrofuran in the aqueous solution. The equilibrium conditions of L_W-L_V-V → L_W-L_V (---) and L_W-L_V-V → L_W-V (----) are also included.

Slightly larger deviations between the predicted and experimental values are obtained when the pressure of the system is less than 1.0 MPa. For this lower pressure region, the model tends to overpredict the

equilibrium pressure. In terms of the deviation between the calculated temperatures and measured temperatures, the average deviation throughout the range studied is 0.53 K. This deviation is much smaller than that of Delahaye et al. [2006]. In their work, the deviation is lower than 1.51 K when the system is modelled with a combination of the van der Waals and Platteeuw hydrate model together with the Redlich-Kwong equation of state associated to a modified Huron-Vidal (MHV2) mixing rule. This shows that the combining model used in this work has a better predictive capability than that of Delahaye et al. [2006].

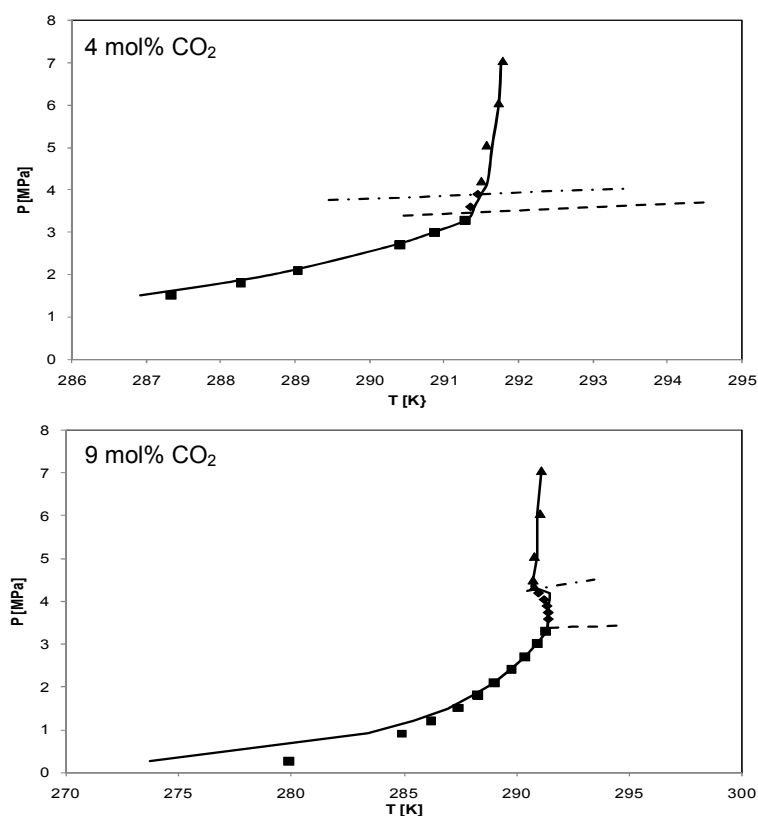


Figure 7.12 Experimental data for the various equilibria H-L_W-V (■), H-L_W-L_V-V (◆), H-L_W-L_V (▲) and with predicted equilibrium conditions for those equilibria in the system of H₂O + CO₂ + tetrahydrofuran at 3.0 mol% of tetrahydrofuran in the aqueous solution. The equilibrium conditions of L_W-L_V-V → L_W-L_V (-.-.-) and L_W-L_V-V → L_W-V (---) are also included.

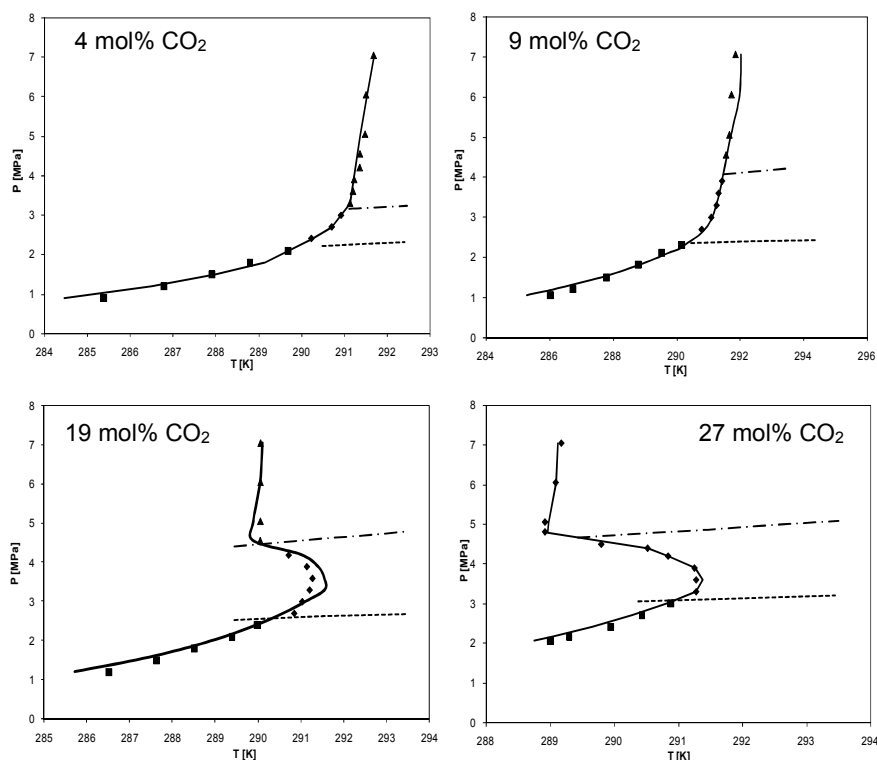


Figure 7.13 Experimental data for the various equilibria $H-L_W-V$ (■), $H-L_W-L_V-V$ (◆), $H-L_W-L_V$ (▲) and predicted equilibrium conditions for those equilibria in the system of $H_2O + CO_2 +$ tetrahydrofuran at 5.0 mol% of tetrahydrofuran in the aqueous solution. The equilibrium conditions of $L_W-L_V-V \rightarrow L_W-L_V$ (---) and $L_W-L_V-V \rightarrow L_W-V$ (----) are also included.

In comparison with the prediction of the $H-L_W-V$ three-phase equilibrium line, the prediction of the four-phase $H-L_W-L_V-V$ equilibrium line is less accurate as a higher AARD% of 9.01% was obtained. As a comparison, Mooijer-van den Heuvel [2004] reported that deviations of 4 to 9 % between the predicted and experimental data are typical for $H-L_W-L_V-V$ equilibria in the ternary system of water, carbon dioxide and a cyclic organic compound such as tetrahydropyran, cyclobutanone and methylcyclohexane. In her work, the prediction was carried out by using a combination of Soave-Redlich-Kwong Equation of state and the van der Waals and Platteuw model with the solubility of other components in the aqueous phase corrected by

using the Henry coefficient model of Krichevsky and Kasarnovsky [Krichevsky and Kasarnovsky, 1935]. It is worth to mention that in her work, no pseudo-retrograde data were modelled.

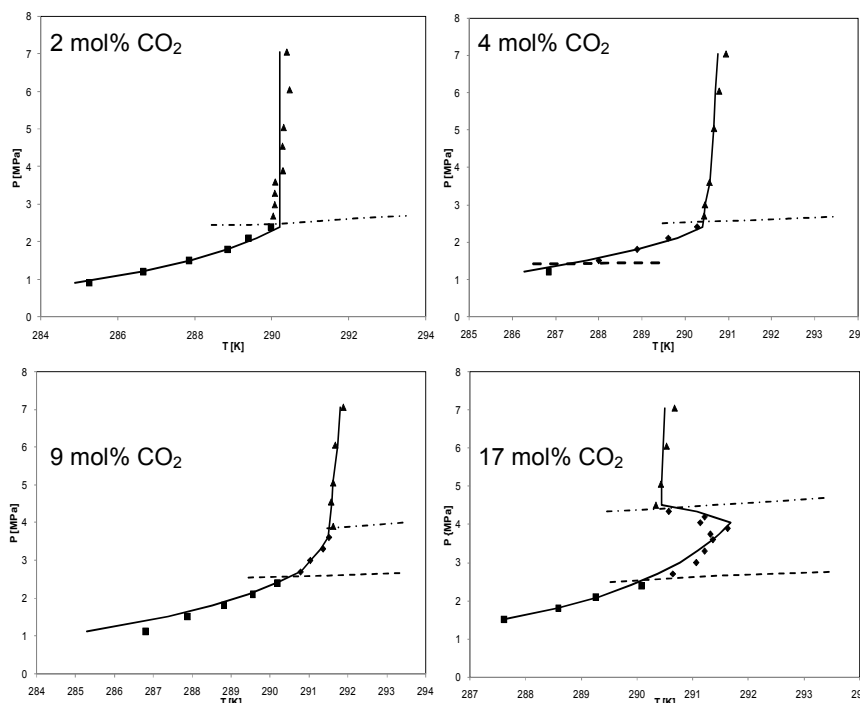


Figure 7.14 Experimental data for the various equilibria H-L_W-V (■), H-L_W-L_V-V (◆), H-L_W-L_V (▲) and predicted equilibrium conditions for those equilibria in the system of H₂O + CO₂ + tetrahydrofuran at 7.0 mol% of tetrahydrofuran in the aqueous solution. The equilibrium conditions of L_W-L_V-V → L_W-L_V (-.-.-) and L_W-L_V-V → L_W-V (----) are also included.

In this work, the hydrate pseudo-retrograde behaviour is observed to occur in the ternary system at certain overall concentrations of carbon dioxide and tetrahydrofuran as can be seen in Figures 7.11 to 7.15. In most cases, it is found that the model is able to predict the occurrence of the pseudo-retrograde behaviour in the ternary system. However, as shown in Figures 7.11 to 7.15, the prediction of the equilibrium pressure or temperature is becoming less accurate when pseudo-retrograde behaviour

occurs in the ternary system, especially at higher concentration of tetrahydrofuran in the system (5 mol% and 7 mol%, respectively). If the predicted values of the H-L_W-L_V-V equilibrium are omitted when pseudo-retrograde behaviour is observed, the AARD% for the H-L_W-L_V-V equilibrium is significantly reduced to 3.92%. Thus, it is shown that the higher values of the overall AARD% for the H-L_W-L_V-V equilibrium is mainly caused by the occurrence of the pseudo-retrograde behaviour.

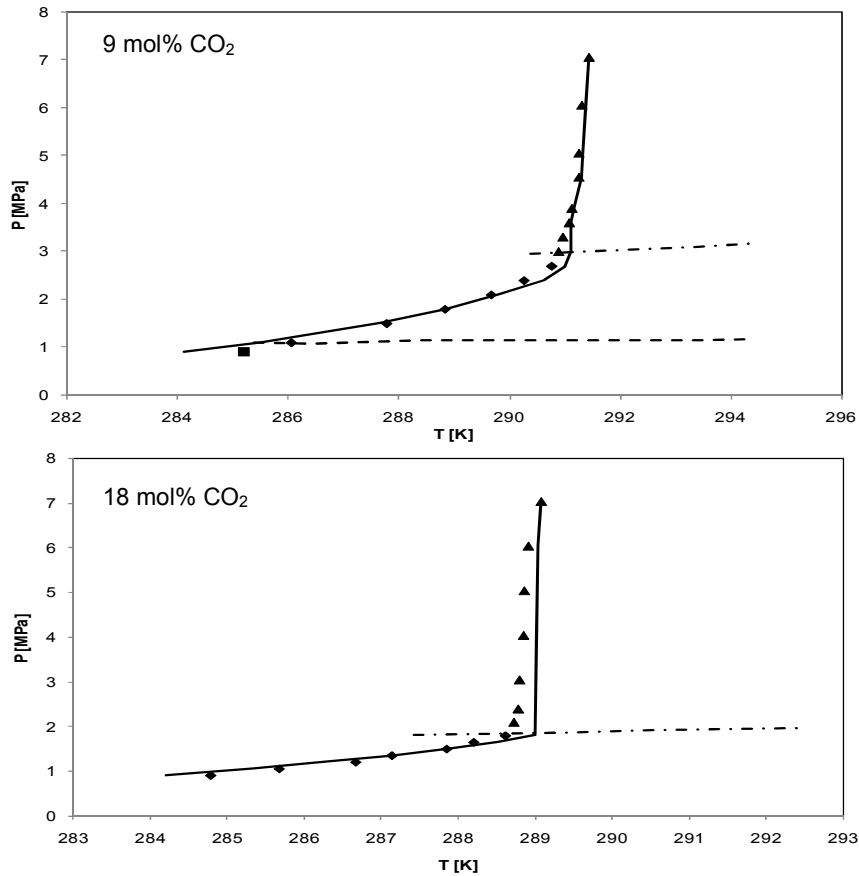


Figure 7.15 Experimental data for the various equilibria H-L_W-V (■), H-L_W-L_V-V (◆), H-L_W-L_V (▲) and predicted equilibrium conditions for those equilibria in the system of H₂O + CO₂ + tetrahydrofuran at 10.0 mol% of tetrahydrofuran in the aqueous system. The equilibrium conditions of L_W-L_V-V → L_W-L_V (---) and L_W-L_V-V → L_W-V (----) are also included.

In a similar way, the high-pressure $H-L_W-L_V$ equilibrium of the ternary system has also been modelled. As expected, the prediction of the equilibrium data is less accurate compared to that of the $H-L_W-V$ and $H-L_W-L_V-V$ equilibria with AARD% of 11.75% respectively. In this region, the equilibrium pressure increases significantly with a very small increase of the equilibrium temperature. This results in slightly less accuracies in the measurement of the experimental data in this region by using the Cailletet apparatus. Moreover, the AARD% is calculated based on the difference between the experimental and predicted pressure values which does not give a clear representation of the accuracy of the model for an equilibrium line with a very steep slope. Considering that the difference between the predicted and experimentally determined temperatures is less than 0.5K for most of the data points studied, except at a very low concentration of carbon dioxide or at pressures higher than 6 MPa, the model used gives a good representation of the high-pressure $H-L_W-L_V$ equilibrium in the concentration, pressure and temperature region studied.

7.4.3 Modelling Results for the Hydrate Equilibria in of Mixed Carbon Dioxide and Tetrahydrofuran in Aqueous Sodium Chloride Solutions

As the combination of PRSV-HVOS with UNIQUAC and fugacity based hydrate model used in this work successfully predicts the hydrate phase equilibria for the ternary system of water, carbon dioxide and tetrahydrofuran with acceptable accuracy in the range studied, the use of the model is extended to the mixed hydrate phase equilibria in aqueous sodium chloride solutions. In order to take into account the presence of electrolyte in the quaternary systems, the Debye-Hückel (D-H) electrostatic term as proposed by Aasberg-Petersen et al. [1991] is added to the PRSV EoS for the calculation of the fugacity of non-electrolyte components in the aqueous phase. The fugacity coefficient is then calculated as follows:

$$\ln \phi_i = \ln \phi_i^{EoS} + \ln \gamma_i^{EL} \quad (7.38)$$

where ϕ_i is the fugacity coefficient of a non-electrolyte component i in the aqueous solution, ϕ_i^{EoS} is the fugacity coefficient of a non-electrolyte component i using an EoS, neglecting the electrostatic effect, and γ_i^{EL} is the contribution of the electrostatic term. Using the D-H activity coefficient model, the second term at the right hand side in Equation 7.38 is calculated from:

$$\ln \gamma_i^{EL} = \ln \gamma_i^{DH} = \frac{2AM_m h_{is}}{B^3} f(BI^{1/2}) \quad (7.39)$$

where M_m is the salt-free mixture molecular weight determined as a molar average, and h_{is} is the binary interaction parameter between the dissolved salt and a non-electrolyte component (e.g. water-salt, gas-salt,). The function $f(BI^{1/2})$ is defined by:

$$f(BI^{1/2}) = 1 + BI^{1/2} - \frac{1}{(1 + BI^{1/2})} - 2 \ln(1 + BI^{1/2}) \quad (7.40)$$

with I as the ionic strength of the salt in pure water. The ionic strength I is calculated from:

$$I_i = \frac{1}{2} \sum_{i=1}^N m_i \cdot z_i^2 \quad (7.41)$$

where m is the molality of ion i (mol/kg H₂O) and z is the charge number. The parameters A and B are given by Aasberg-Petersen et al. [1991]:

$$A = \frac{1.327757 \times 10^{-5} d_m^{1/2}}{(\eta_m T)^{3/2}} \quad (7.42)$$

$$B = \frac{6.359696 d_m^{1/2}}{(\eta_m T)^{1/2}} \quad (7.43)$$

where d_m is the density of the salt-free mixture and η_m is the salt-free mixture dielectric constant, which can be calculated for a mixture of salt and water from:

$$\eta_m = x_w \eta_w \quad (7.44)$$

where x_w and η_w are the salt-free mole fraction and dielectric constant of water, respectively. The dielectric constants of dissolved non-electrolyte components have been neglected.

The binary interaction parameter between the dissolved sodium chloride and a non-electrolyte component, h_{is} is calculated based on the method proposed by Tohidi and Kalorazi [1995]. The expression used to calculate these binary interaction parameters reads:

$$h_{is} = (-1.191 + 1.037 \times 10^{-2} T - 6.043 \times 10^{-2} w - 5.814 \times 10^{-3} w^2 + 3.861 \times 10^{-4} T w) / 1000 \quad (7.45)$$

In this equation, T is the temperature in K and w is the salt concentration in weight percentage relative to water.

To check the suitability of the model to predict a system containing electrolyte, it is first applied to predict the hydrate equilibria for simple carbon dioxide hydrate in sodium chloride solution. The overall concentration of carbon dioxide is 4 mol% while the concentration of sodium chloride in the

aqueous solution is 1.5 mol%. For this ternary system, only two different hydrate equilibria are available namely the three-phase equilibria H-L_W-V and H-L_W-L_V. The predicted data together with the experimental data are plotted in Figure 7.16. As shown in Figure 7.16, good agreement between the predicted and experimental data is achieved with an overall AARD% less than 3.5%. In the low pressure region (less than 2 MPa), the model slightly under-predicts the equilibrium pressure.

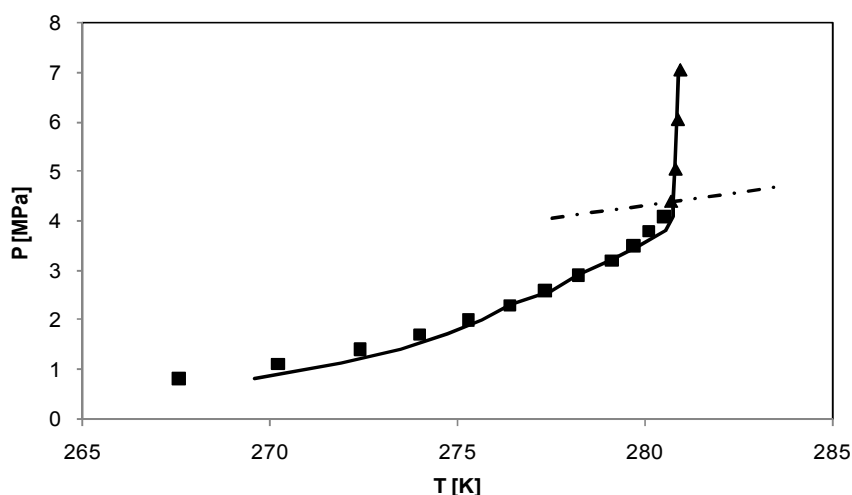


Figure 7.16 Experimental data for the various equilibria H-L_W-V (■), and, H-L_W-L_V (▲) and predicted equilibrium conditions for those equilibria in the system of H₂O + CO₂ + sodium chloride at 1.5 mol% of sodium chloride in the aqueous solution. The equilibrium conditions of L_W-L_V-V → L_W-L_V (---) are also included.

The predicted and experimental data for the equilibrium conditions for mixed carbon dioxide and tetrahydrofuran hydrate in sodium chloride solutions are presented in Figures 7.17 and 7.18. In Figure 7.17, all the samples are kept at 2 mol% and 4 mol% of sodium chloride and carbon dioxide in the overall concentration, respectively, while the concentration of tetrahydrofuran is varied from 1 mol% to 7 mol% in the overall concentration. In contrast, all samples shown in Figure 7.18 are kept fixed at 4 mol% and 5 mol% of carbon dioxide and tetrahydrofuran, respectively, while the

concentration of sodium chloride is varied from 1 mol% to 9 mol%. The calculated AARD% for the H-L_W-V, H-L_W-L_V-V and H-L_W-L_V equilibria are presented in Table 7.6 along with the number of experimentally determined data points.

Table 7.6 Summary of the modelling results and the average absolute values of the relative deviation (AARD%) between the experimental and calculated values for mixed carbon dioxide and tetrahydrofuran hydrates in sodium chloride solutions.

Type of equilibrium	Number of exp. data point	AARD (%)
H-L _W -V	37	11.76%
H-L _W -L _V -V	49	7.56%
H-L _W -V	42	14.37%

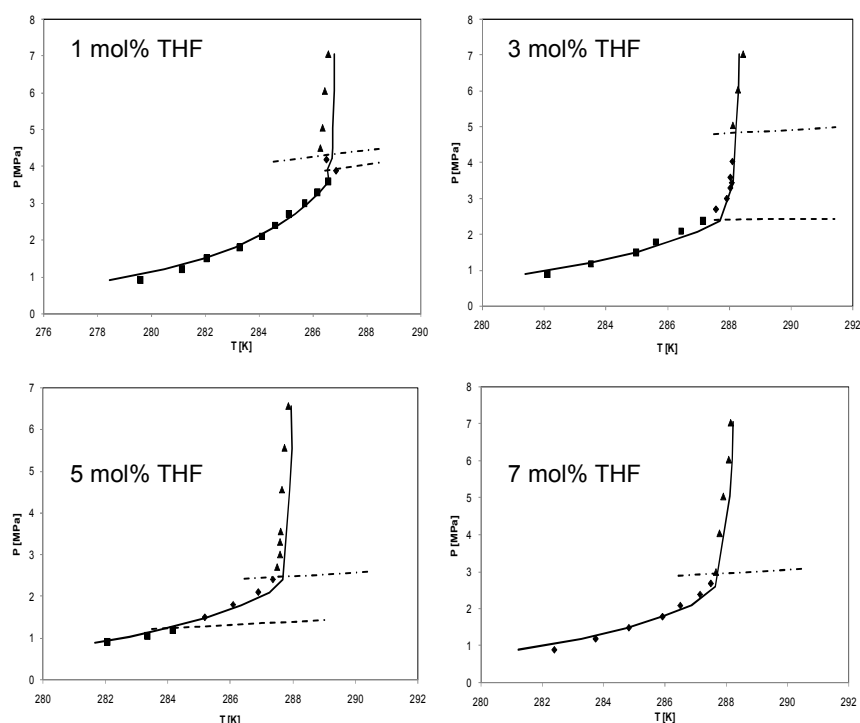


Figure 7.17 Experimental data for the various equilibria H-L_W-V (■), H-L_W-L_V-V (◆), H-L_W-L_V (▲) and predicted equilibrium conditions for those equilibria in the system of H₂O + CO₂ + tetrahydrofuran at 2.0 mol% of sodium chloride in the aqueous system. The concentration of carbon dioxide is fixed at 4.0 mol%. The phase equilibria L_W-L_V-V → L_W-L_V (---) and L_W-L_V-V → L_W-V (----) are also included.

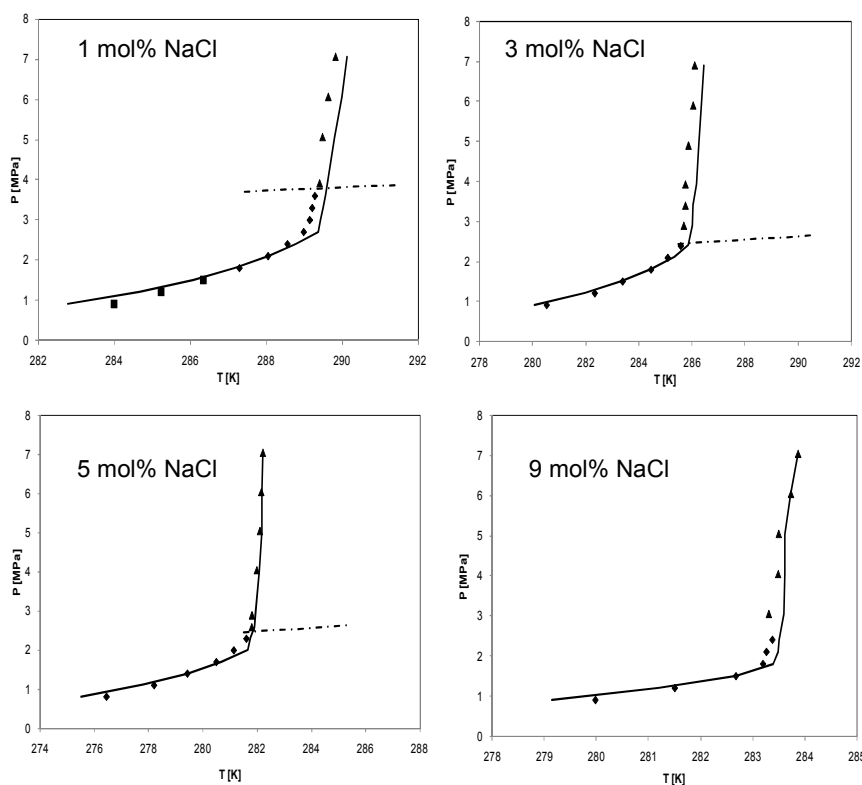


Figure 7.18 Experimental data for the various equilibria H-L_W-V (■), H-L_W-L_V-V (◆), H-L_W-L_V (▲) and with predicted equilibrium conditions for those equilibria in the system of H₂O + CO₂ + tetrahydrofuran at 7.0 mol% of carbon dioxide in the system. The phase equilibria L_W-L_V-V → L_W-L_V (---) are also included when available.

In general, it is found that the deviations between the experimental data and predicted values for the systems containing sodium chloride are higher compared to that of the ternary water-carbon dioxide-tetrahydrofuran systems, especially for the H-L_W-V and H-L_W-L_V equilibria. This suggests that the predictive model used has lower ability to accurately predict the phase behaviour of the hydrate systems when electrolytes are present. In fact, the model is unable to capture the pseudo-retrograde hydrate behaviour that occurs at very low concentrations of tetrahydrofuran as shown in Figure 7.17 at an overall concentration of 1 mol% THF. However, the highest AARD%

calculated which is for H-L_W-L_V equilibrium is still within an acceptable range of error for clathrate hydrate modelling [Mooijer-van Den Heuvel, 2004]. Moreover, it is also noted that the presence of sodium chloride in the hydrate systems increases the possibility of a liquid-liquid phase split in the aqueous water-tetrahydrofuran phase. This trend suggests that the presence of electrolytes in hydrate forming systems with miscible promoter is more susceptible to a liquid-liquid phase split in the aqueous water-promoter phase due to the reduced activity and, in addition, it is suspected to be dependent on the strength of the activity between these two components.

Taking into account that there is no information known in literature on methods that is able to predict the carbon dioxide hydrate equilibrium in the presence of both an electrolyte and a promoter, the model used in this work gives at least a good initial estimation of the phase behaviour of such systems. Nevertheless, the model can be improved to obtain a better prediction of the hydrate equilibria. One way to achieve this is by fitting the parameters a , b , c , d and e used to calculate the binary interaction parameters between sodium chloride and non-electrolyte components, h_{is} , from experimental data on vapour pressure depression in aqueous solutions. Unfortunately, this suggestion cannot be implemented in this work due to lack of experimental data, mainly for the vapour pressure depression of sodium chloride on tetrahydrofuran. Secondly, the energy parameters used in the HVOS mixing rule with the UNIQUAC g^E model should be optimized by fitting to bubble point data of the hydrate forming systems. Moreover, an extended electrolyte model can be used to replace the D-H model used in this work.

7.5 REFERENCES

- Aasberg-Petersen, K., Stenby, E., Fredenslund, A.A., *Ind. Eng. Chem. Res.*, 1991, 30(9), pg. 2180-2185.
- Cao, Z.T., Tester, J.W., Sparks, K.A., Trout, B.L., *J. Phys. Chem. B*, 2001, 105(44), pg. 10950-10960.
- Chen, G.J., Guo, T.M., *Fluid Phase Equilibr.*, 1996, 122(1-2), pg. 43-65.
- Delahaye, A., Fournaison, L., Marinha, S., I. Chatti, J.-P. Petit, D. Dalmazzone, W. Fürst. *Ind. Eng. Chem. Res.*, 2006, 45, pg. 391-397.
- Jager, M.D., Ballard, A.L., Sloan, E.D., *Fluid Phase Equilibr.*, 2005, 232, pg. 25-36.
- John, V.T., Papadopoulos, K.D., holder, G.D., *AIChE J.*, 1985, 31(2), pg. 252-259.
- Klauda, J.B. and Sandler, S.I., *Ind. Eng. Chem. Res.*, 2000, 39, pg. 3377-3386.
- Klauda, J.B. and Sandler, S.I., *J. Phys. Chem. B.*, 2002, 106, pg. 5722-5732.
- Klauda, J.B. and Sandler, S.I., *Chem. Eng. Sci.*, 2003, 58, pg. 27-41.
- Krichevsky, I.R., and Kasarnavsky, J.S., *J. Am. Chem. Soc.*, 1935, 57, pg. 2168-2171.
- Lazzaroni, M.J., Bush, D., Jones, R., Hallett, J.P., Liotta, C.L., Eckert, C.A., *Fluid Phase Equilibria*, 2004, 224, pg. 143-154.
- Lazzaroni, M.J., Bush, D., Brown, J.S., Eckert, C.A., *J. Chem. Eng. Data*, 2005, 50(1), pg. 60-65.
- Martin, A. And Peters, C.J., *J. Phys. Chem. C*, 2009, 113(1), pg. 442-430.
- Mooijer-van den Heuvel, M.M. "Phase Behaviour and Structural Aspects of Ternary Clathrate Hydrate Systems: The Role of Additives". Ph.D thesis, Delft Uni. of Technology, January, 2004.
- Munck, J., Skjold-Jorgensen, S, Rasmussen, P., *Chem. Eng. Sci.*, 1988, 43, pg. 2661-2667.

Orbey, H., and Sandler, S.I., Fluid Phase Equilibria, 1995, 111, pg. 53-70.

Ruzicka, K., Majer, V., AIChE J., 1996, 42 (6), pg. 1723-1740.

Sherman, S.R., Trampe, D.B., Bush, D.M., Schiller, M., Eckert, C.A., Dallas, A.J., Li, J.J., Carr, P.W., Fluid Phase Equilib., 1996, 35(4), pg. 1044-1058.

Sloan Jr., E.D. and Koh, C.A. "Clathrate Hydrates of Natural Gas", 3rd ed., CRC Press, Florida, 2007.

Stryjek, R., Vera, J.H., Can. J. Chem. Eng., 1986, 64(2), pg. 323-333.

Tohidi, B., A. Danesh and A.C. Todd, Chem. Eng. Res. Des., 1995, 73, pg. 464-472.

Tse, J.S., and Klein, J.S., J. Phys. Chem., 1987, 91, pg. 5789.

Van der Waals, J.H., Platteeuw, J.C., Adv. Chem. Phys., 1959, 2, pg. 1-57.

Walas, S.M., "Phase Equilibria in Chemical Engineering", Butterworth Publisher, 1985.

8

Kinetics of Formation of Single and Mixed Carbon Dioxide Hydrates in Water and NaCl Aqueous Solution

In this chapter, the experimental work on the kinetics of formation of simple carbon dioxide and mixed carbon dioxide hydrates is presented. The T-cycle method, which is used to collect the kinetic data, is briefly discussed in section 8.1. The experimental results on the induction time and temperature for clathrate hydrate nucleation are presented and discussed in Section 8.2. Based on the amount of carbon dioxide consumed, the hydrate growth process, the apparent rate constant and the activation energy for each system is considered. The data are reported and discussed in Section 8.3.

8.1 INTRODUCTION

Besides the thermodynamic properties, other important aspects to be considered in order to successfully develop CO₂ hydrate based technology for industrial applications are the insights of the kinetics of formation and dissociation of either single or mixed carbon dioxide hydrate in water and aqueous electrolyte solutions. Unfortunately, time-dependent hydrate phenomena are more difficult to measure compared to time-independent phenomena, i.e. structural and thermodynamic information [Sloan and Koh, 2007]. Therefore it is not surprising that the reported kinetic data of either formation or dissociation of carbon dioxide hydrates in literature are rather scarce. Some of the available literature sources on carbon dioxide hydrate are summarized in the following paragraph.

Ohgaki et al. [1993] measured the formation of carbon dioxide hydrate in pure water and in seawater. They obtained the apparent rate constant of hydration under the assumption of dealing with a pseudo-first order reaction with respect to the CO₂ concentration. Shindo et al. [1993] proposed a mechanism of the formation of CO₂ hydrate at the interface between liquid CO₂ and water. Chun and Lee [1996] carefully measured the kinetics of carbon dioxide hydrate formation in a semi-batch stirred tank reactor with stirring rate of 500 rpm at three different temperatures between 275.2 and 279.2 K, and at pressures ranging from 2.0 to 3.5 MPa. They concluded that the hydrate kinetic model developed by Englezos et al. [1987] adopted in their study, was able to predict the kinetic curves of formation of carbon dioxide hydrate as obtained in their study. Malegaonkar et al. [1997] measured the kinetics of carbon dioxide hydrate formation and its solubility in distilled water in a semi-batch stirred tank reactor. With these data, they tested a modified kinetic model of Englezos et al. [1987] and determined the intrinsic kinetic rate constant for the carbon dioxide hydrate formation. They established that the rate is higher than that of methane hydrate. A similar

study was conducted by North et al. [1998], and it was found that there must be a minimum amount of carbon dioxide available in all phases in order to form gas hydrate, and this amount varied with pressure. To simulate the deep ocean sediment, Lee et al. [2002] studied the kinetics of carbon dioxide hydrate in sodium chloride solution in a clay system. They discovered that when clay was included, the final consumption of carbon dioxide for hydrate formation decreased but the initial formation rate increased compared to the system without clay. A Raman spectroscopy study conducted by Kawamura et al. [2002] showed that the mechanism of carbon dioxide hydrate formation depends on the temperature. Clarke and Bishnoi [2004] presented a method for calculating the moments of the particle size distribution. In their study, they used a semi-batch stirred tank reactor with an in-situ particle analyzer to determine the intrinsic rate of carbon dioxide hydrate and its activation energy. The effect of pressure and vessel size on the formation of gas hydrate was studied by McCallum et al. [2007] using a 72 L vessel. Based on their experimental work, the reduction in overpressure and/or induction time required for the accumulation of hydrates may be attributed to increase in bubble surface area, increased gas concentration, increased lifetime of bubbles, increased total volume of the vessel, or a combination of all these factors. Giavarini et al. [2007] studied the formation and dissociation of carbon dioxide hydrate and found that carbon dioxide hydrate does not present any anomalous self-preservation effect (memory effect). They also found that the dissociation of carbon dioxide is not affected by subcooling before storage. However, they pointed out that the preservation of carbon dioxide hydrate is more affected by temperature rather than by pressure, which is the opposite of that of methane hydrate.

As summarized in the previous paragraph, although there have been studies reported on the formation and dissociation of carbon dioxide hydrate in water and seawater, there is no such information of mixed carbon dioxide with tetrahydrofuran or any other promoters available in the open literature.

It is our goal to fill this gap by measuring the kinetics of formation of simple carbon dioxide and mixed carbon dioxide and tetrahydrofuran hydrates in water and aqueous electrolyte solutions. The main focus of this study is to obtain the kinetic data under rapid formation of simple and mixed carbon dioxide hydrates. In this work, an apparatus for the measurement of the pressure-temperature data during hydrate formation was designed and built, and was already discussed in Chapter 3. The kinetics of formation of simple carbon dioxide and mixed carbon dioxide and tetrahydrofuran hydrates were studied in water and aqueous solutions of sodium chloride. In Section 8.1, the closed loop method to obtain kinetic data on hydrate formation is briefly discussed. In Section 8.2, the induction time and induction temperature for hydrate nucleation are presented and discussed. In Section 8.3, the hydrate growth data, including the carbon dioxide consumption, the apparent rate constant and the activation energy for simple carbon dioxide and mixed carbon dioxide and tetrahydrofuran hydrates in water and sodium chloride solution are reported and discussed.

8.1 THE CLOSED LOOP (T-CYCLE) METHOD

In this work, the closed loop (T-cycle) method used by Ohgaki et al. [1993] was adapted for the measurement of the kinetics of formation of single and mixed carbon dioxide hydrates. An example of a working diagram of the method for the determination of the formation, turbidity point and stationary point of carbon dioxide hydration is represented in Figure 8.1. For the formation of gas hydrates, a sharp decrease of pressure is observed at the beginning of the experiment although the temperature is kept constant. This is due to the solubility of carbon dioxide in water. Then, the pressure stabilizes at constant temperature indicating a steady-state is achieved at point A. All the experiments were conducted with a stirring rate of 500 rpm.

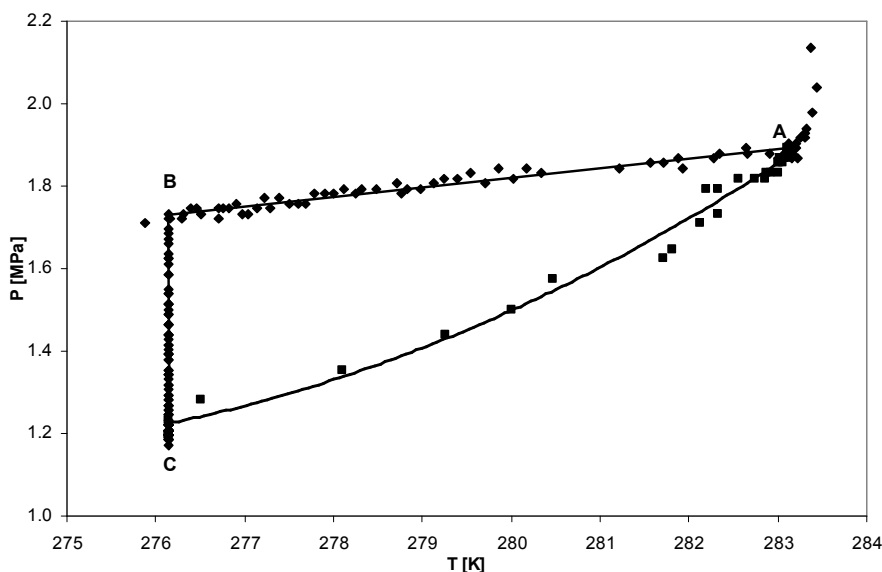


Figure 8.1 Pressure and temperature trajectory during formation and decomposition of simple carbon dioxide hydrate starting at an initial pressure of 2.25 MPa

From A to B, it was observed that the pressure was decreasing as the temperature decreased. This trend is mainly due to two main factors: the solubility of the gas in the liquid phase and gas contraction upon cooling. At point B, which is also known as the turbidity point, a sudden decrease of pressure was observed. This pressure drop was mainly due to the hydrate formation during which a rapid entrapment of the gas molecules in the solid phase occurred. In general, the formation of gas hydrates starts rapidly and the rate then decreases with time until maximum sorption is attained at point C. Point C is adopted at the stationary point of the reaction. After the formation of the hydrate is completed, the process was reversed to let the formed hydrate to dissociate again. The dissociation of the gas hydrates is achieved by heating the system from Point C to Point A. During the heating process, an increase of pressure is observed until all carbon dioxide molecules that were entrapped in the solid phase is completely released at Point A.

To calculate the number of moles of carbon dioxide at each point, the p,T data are converted into the number of moles using the following equation for real gases:

$$P \cdot V = n \cdot Z \cdot R \cdot T \quad (8.1)$$

where P is the pressure, V is the volume of the gas phase, n is the number of moles of hydrogen present in the gas phase, Z is the compressibility factor, R is the universal gas constant and T is the temperature of the gas phase.

The compressibility factor Z is calculated from the Peng-Robinson Equation of state:

$$Z = \frac{1}{(1 - b/V)} - \frac{a(T)}{RT} \frac{1}{(V + 2b - b^2/V)} \quad (8.2)$$

$a(T)$ and b are defined as:

$$b = \frac{0.07780RT_c}{P_c} \quad (8.3)$$

$$a(T) = 0.45724 \frac{(RT_c)^2}{P_c} \left[1 + \beta(1 - \sqrt{T/T_c}) \right]^2 \quad (8.4)$$

$$\beta = 0.37464 + 1.5422\omega - 0.26992\omega^2 \quad (8.5)$$

T_c is the critical temperature, P_c is the critical pressure and ω is the acentric factor of carbon dioxide.

In the present work, three different hydrate formation systems are studied, i.e. carbon dioxide-water, carbon dioxide-tetrahydrofuran-water and carbon dioxide-tetrahydrofuran-sodium chloride-water systems. The concentration of tetrahydrofuran and sodium chloride are fixed at 5 and 1 mol% respectively in the aqueous solution when they are present in the systems studied. The ratio is selected due to the availability of phase equilibria data as presented in Chapter 5. The amount of aqueous solutions (water or aqueous THF or aqueous THF-NaCl solutions) used in each experiment is 50 ml. As discussed in Chapter 2, the clathrate hydrate formation is generally divided into two processes namely the hydrate nucleation and the hydrate growth processes. In this study, the hydrate nucleation process is studied through the measurement of the induction time and the induction temperature for hydrate nucleation and the results are presented and discussed in Section 8.2. The hydrate growth process is studied through the measurements of gas consumption and the calculation of apparent rate constant and the activation energy and the results are presented and discussed in Section 8.3.

8.2 NUCLEATION OF SIMPLE CARBON DIOXIDE AND MIXED CARBON DIOXIDE AND TETRAHYDROFURAN HYDRATES

One of the advantages of the T-cycle method or measurement of the kinetic data through a constant cooling rate is that the hydrate formation is less stochastic [Sloan and Koh, 2007]. This enables the measurement of the induction time, i.e. the time required for hydrates to be detected macroscopically after nucleation and onset of growth have occurred to take place. The induction time of hydrate nucleation for simple carbon dioxide and mixed carbon dioxide and tetrahydrofuran hydrates in water and an aqueous sodium chloride solution at different initial pressures are plotted in

Figure 8.2. The induction time is calculated from the point where the dissolution of carbon dioxide in the aqueous phase is completed and the turbidity point has been reached. Due to the stochastic nature of hydrate nucleation, the experiment was repeated at least five times and the values of the induction time falls within ± 2 minutes of each others for each initial carbon dioxide pressure. The average values of the induction times are then plotted in Figure 8.2.

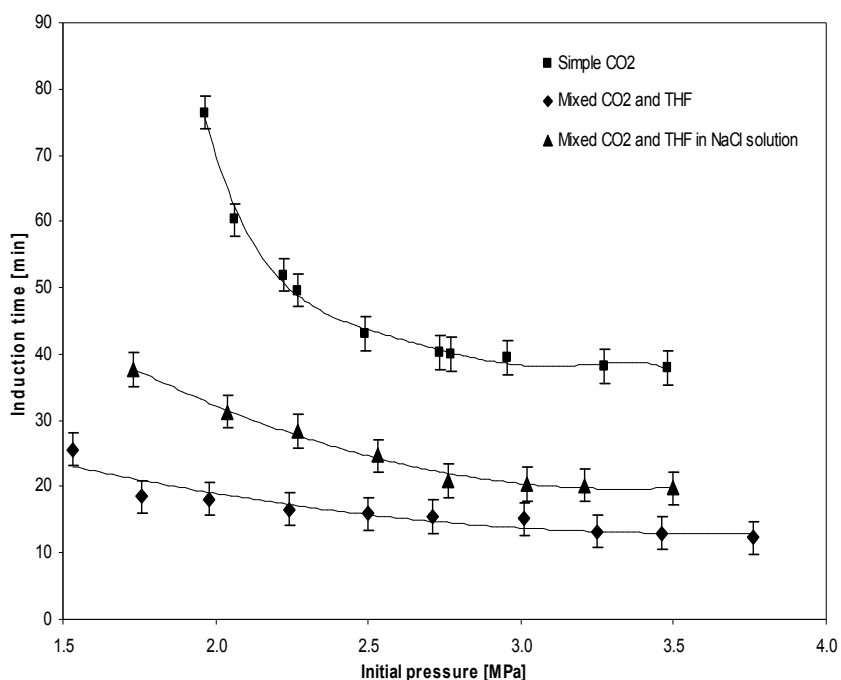


Figure 8.2 The induction time of hydrate nucleation for simple carbon dioxide and mixed carbon dioxide and THF in water and an aqueous solution of NaCl.

As depicted in Figure 8.2, for the system of carbon dioxide and water, at an initial pressure of carbon dioxide lower than 1.95 MPa, no hydrate formation is observed. For hydrate nucleation, the induction time is dependent on the supersaturation of the guest component in the aqueous

phase [North et. al., 1998; Jensen et al., 2008] and if the supersaturation critical point is not achieved, no hydrate will be formed in the system. From a comparison of Figures 8.2 and 2.7, it can be deducted that below an initial pressure of 1.95 MPa, a critical point of supersaturation of the carbon dioxide in water is not achieved; resulting in no hydrate formation and the induction time goes to infinity. As the initial carbon dioxide pressure increases from 1.95 MPa to 2.96 MPa, the induction time decreases from 76.4 minutes to almost half of its value of 39.5 minutes. At higher pressure values, the induction time is achieved at ± 38 minutes. This trend shows that the supersaturation of carbon dioxide is increasing with the increasing initial pressure of carbon dioxide until a pressure of 2.96 MPa where the liquid phase is completely supersaturated with carbon dioxide. Above this value, the induction time is becoming relatively constant with increasing initial carbon dioxide pressure.

For the carbon dioxide-tetrahydrofuran-water system, it was observed that clathrate hydrates are formed for all the initial carbon dioxide pressures used in this study even at an initial carbon dioxide pressure of 1.53 MPa. Since tetrahydrofuran is also a hydrate former and it is completely miscible in water, the amount of carbon dioxide required to achieve the supersaturation condition for hydrate nucleation is reduced significantly. Moreover, the induction time for hydrate formation is found to be decreasing from 25.62 minutes to 12.25 minutes as the initial pressure increases from 1.53 MPa to 3.76 MPa. For a comparison, the induction time for the ternary system at initial carbon dioxide of 1.93 MPa is approximately four times lower than that of the binary system. As the initial pressure increases, the difference between the induction times of the ternary and binary systems decreases. These values show that the induction time required for hydrate nucleation is much lower in the ternary system of carbon dioxide-tetrahydrofuran-water compared to that of binary system of carbon dioxide-

water. This comparison indicates that the hydrate nucleation process is more readily to occur in presence of tetrahydrofuran in the aqueous solution.

As shown in Figure 8.2, the presence of sodium chloride prolongs the induction time for hydrate nucleation in the mixed carbon dioxide and tetrahydrofuran hydrate forming system. The difference in the induction times for the mixed hydrate forming system in water and sodium chloride solution is larger at lower initial carbon dioxide pressure in the system and becoming smaller at higher initial carbon dioxide pressure. As discussed in chapters 4 and 5, the presence of ions in the aqueous phase hinders hydrate formation due to the clustering of water molecules with the ions and the salting-out effect, which reduce the solubility of both tetrahydrofuran and carbon dioxide in water. These two factors are suspected to create a mass transfer resistance that prolonged the process of hydrate nucleation when electrolytes are present in the hydrate forming system. Although the induction time increases, it is still significantly lower than the induction time of simple carbon dioxide hydrates. Based on this, it is shown that the inclusion of tetrahydrofuran in hydrate forming systems is not only thermodynamically favourable for hydrate formation but it also reduces the induction time for hydrate nucleation significantly.

The temperature at the turbidity point for each initial carbon dioxide pressure is taken as an average value of the five experimental repetitions used to calculate the induction time. The average error in these temperatures is $\pm 1^{\circ}\text{C}$. These average temperature values are plotted against the initial carbon dioxide pressures and depicted in Figures 8.3, 8.4 and 8.5 for carbon dioxide-water, carbon dioxide-tetrahydrofuran-water and carbon dioxide-tetrahydrofuran in sodium chloride solution systems respectively. From these figures, it becomes apparent that for the formation of clathrate hydrate, subcooling is required to overcome the metastability in the hydrate forming system. Since hydrate nucleation is a stochastic

process, it is surprising that there is a general linear trend between the initial carbon dioxide pressure and the temperature at the turbidity point as observed in this study. Furthermore, it is shown that for all systems investigated in this study, the temperature at the turbidity point increases when the initial carbon dioxide pressure in the system increases. This behaviour is expected as an increase in carbon dioxide causes a richer environment of supersaturation at the liquid-vapour interface, which is required in order for the hydrate nucleation process to take place. Due to this factor, the degree of subcooling required to enrich the interface with carbon dioxide molecules for higher initial concentrations of carbon dioxide, i.e. higher initial carbon dioxide pressure, is expected to be less than at lower carbon dioxide concentrations.

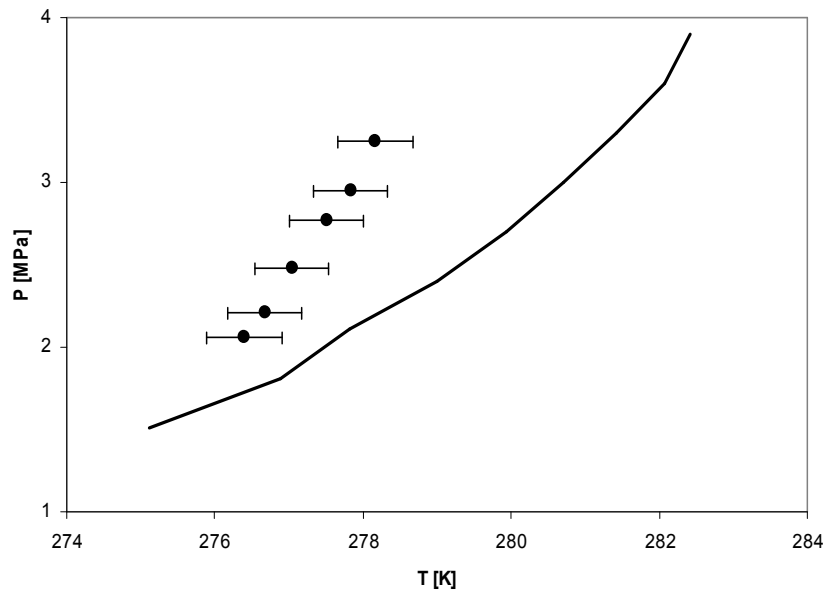


Figure 8.3 The temperature at the turbidity point for different initial carbon dioxide pressures for the CO₂ + water system. The corresponding hydrate equilibrium curve for each system is also included (solid line).

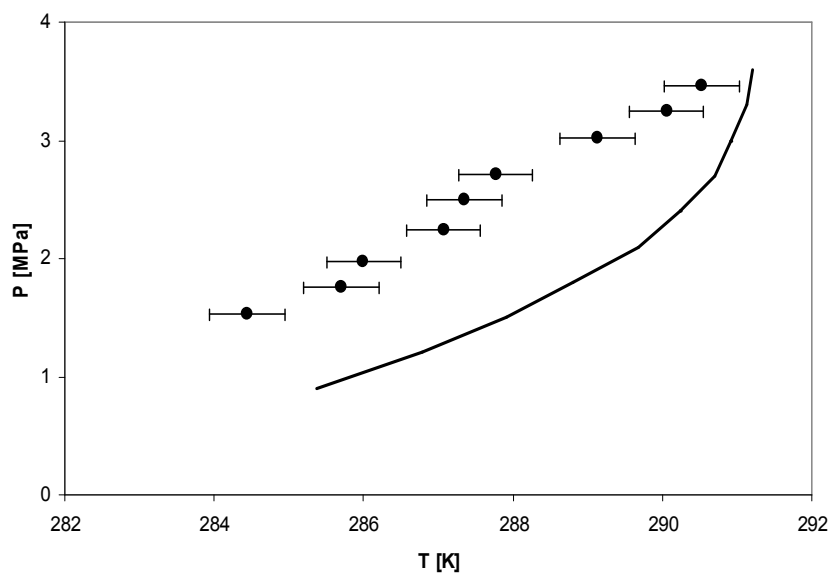


Figure 8.4 The temperature at the turbidity point for different initial carbon dioxide pressures for the CO_2 + THF + water system. The corresponding hydrate equilibrium curve for each system is also included (solid line).

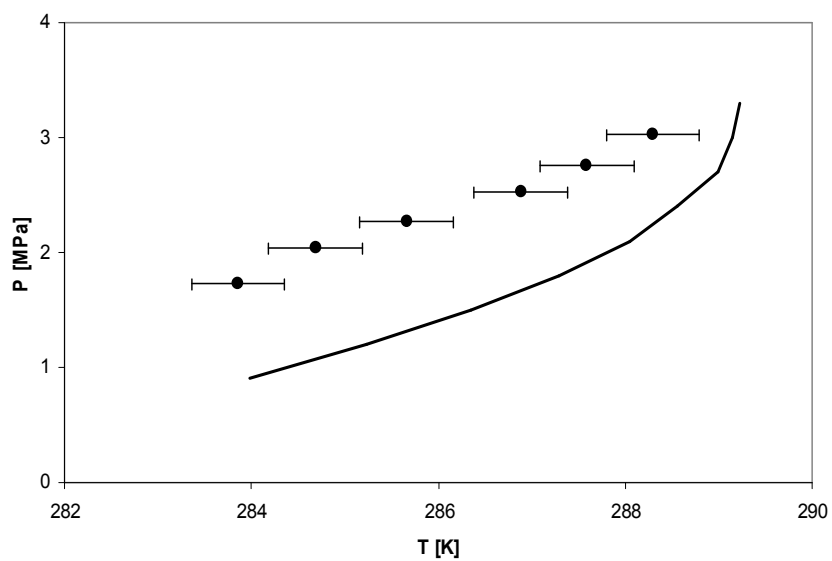


Figure 8.5 The temperature at turbidity point for different initial carbon dioxide pressures CO_2 + THF in NaCl solution system. The corresponding hydrate equilibrium curve for each system is also included (solid line).

Table 8.1 The required sub-cooling (ΔT_{sub}) for hydrate formation in different carbon dioxide hydrate forming systems.

CO ₂ + water		CO ₂ + THF + water		CO ₂ + THF in NaCl solution	
Pressure	ΔT_{sub}	Pressure	ΔT_{sub}	Pressure	ΔT_{sub}
-	-	1.53	3.91	-	-
-	-	1.76	3.17	1.73	3.29
2.06	1.49	1.98	3.31	2.04	3.05
2.21	1.75	2.25	2.70	2.27	2.47
2.48	2.22	2.50	2.82	2.53	1.65
2.77	2.56	2.71	2.70	2.76	1.27
2.95	2.70	3.02	1.75	3.03	0.92
3.25	3.05	3.25	1.12	-	-
-	-	3.47	0.91	-	-

To gain some insights in the degree of subcooling required for the clathrate hydrate formation, the differences between the hydrate equilibrium temperature and the temperature at the turbidity point, ΔT_{sub} , at a specified pressure are calculated and tabulated in Table 8.1 for each initial pressure and different type of hydrate formation system. In the case of simple carbon dioxide, the degree of subcooling is increasing with the increase in initial pressure of carbon dioxide. Arjmandi et al. [2005] showed that for a simple hydrate such as carbon dioxide hydrate, subcooling is proportional to the driving force for hydrate formation. In this case, the higher degree of subcooling, due to the increase of the initial carbon dioxide pressure, results in a higher driving force for hydrate formation. With the increase of driving force for hydrate formation, it is expected that the system is more susceptible for hydrate formation resulting in the reduction of the induction time as shown in Figure 8.2.

In contrast, the degree of subcooling required for hydrate formation is found to decrease with the increasing initial carbon dioxide pressure for mixed carbon dioxide and tetrahydrofuran hydrates in water and an aqueous sodium chloride solution. For both cases, a significant reduction of more than 2°C of the degree of subcooling is observed when pressure of the system increases from ~1.7 MPa to ~3.0 MPa. From Figure 8.2, it can be

seen that the induction time also decreases in this pressure region. This behaviour might be explained by considering the degree of supersaturation in the hydrate forming systems. It is supposed that the presence of tetrahydrofuran in both systems reduces the driving force required for hydrate formation. As the initial carbon dioxide pressure increases in the systems, the amount of carbon dioxide molecules at the liquid-vapour interface will also increase. The combination of these two factors results in a reduced driving force required for hydrate formation. As the driving force of the hydrate formation can be related to the degree of sub-cooling, at least to some extent [Arjmandi et al., 1995], the subcooling requirement for hydrate formation decreases with the decrease of the required driving force. It also can be observed that no significant effect of the presence of electrolytes can be observed in the hydrate forming systems on the degree of subcooling requirement for hydrate formation.

8.3 GROWTH OF SIMPLE CARBON DIOXIDE AND MIXED CARBON DIOXIDE AND TETRAHYDROFURAN HYDRATES

In this section, the hydrate growth process is considered in the region from the turbidity point, at which the hydrate formation is noticeable based on the sharp pressure decrease in the system, to the stationary point, at which the maximum amount of carbon dioxide consumed for the hydrate formation is observed. The amount of carbon dioxide dissolved in the liquid phase is not considered during hydrate growth because it is assumed that the supersaturation condition is maintained throughout the hydrate formation process [North et al., 1998] and the hydrate particles formed are in three-phase equilibrium with the liquid and vapour phases [Englezos et al., 1987]. The amount of carbon dioxide consumed during the growth process for simple carbon dioxide hydrates and both mixed carbon dioxide and tetrahydrofuran hydrates in water and sodium chloride at different initial

pressure of carbon dioxide are plotted in Figures 8.6, 8.7 and 8.8, respectively. For all the hydrate forming systems, the carbon dioxide consumption during the hydrate growth process is found to be dependent on the initial pressure of carbon dioxide in the system, which relates to the initial amount of carbon dioxide in the system. By comparing all the figures, it is noticed that the time taken from the turbidity point to the stationary point for simple carbon dioxide hydrates (~60 minutes) is about three times longer that that of mixed carbon dioxide and tetrahydrofuran hydrates (~20 minutes) regardless of the initial carbon dioxide pressure in the systems. The time is slightly prolonged with the presence of sodium chloride in the system for the mixed carbon dioxide and tetrahydrofuran hydrates (~30 minutes). This observation implies that the rate of hydrate growth is much faster with the introduction of tetrahydrofuran in the system.

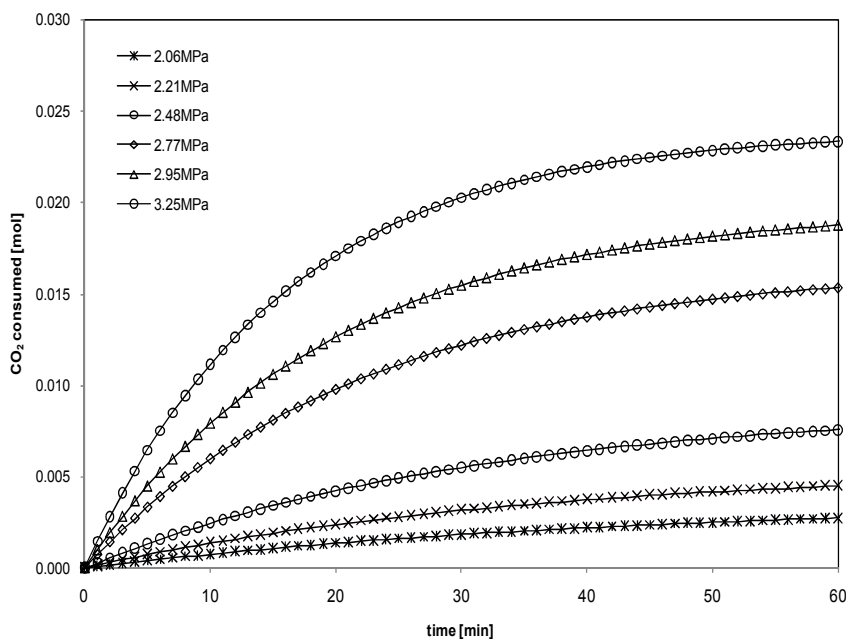


Figure 8.6 Experimental carbon dioxide consumption for the formation of simple carbon dioxide hydrates at different initial pressures of carbon dioxide.

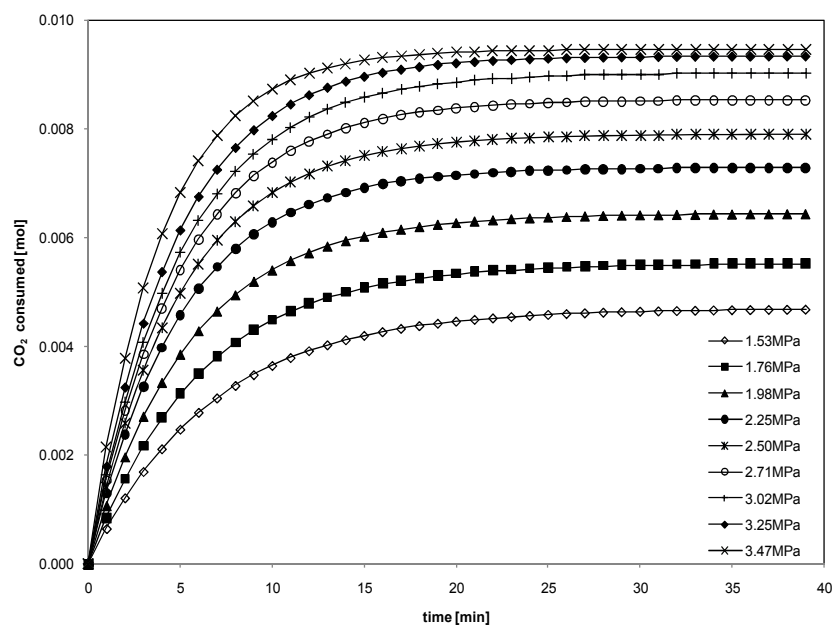


Figure 8.7 Experimental carbon dioxide consumption for the formation of mixed carbon dioxide and tetrahydrofuran hydrates at different initial pressures of carbon dioxide.

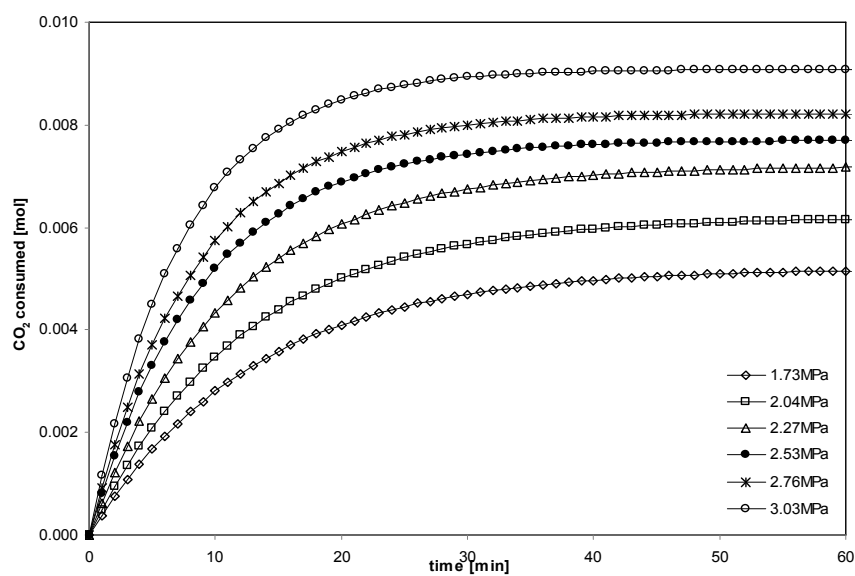


Figure 8.8 Experimental carbon dioxide consumption for formation of mixed carbon dioxide and tetrahydrofuran hydrates in an aqueous sodium chloride solution at different initial pressures of carbon dioxide.

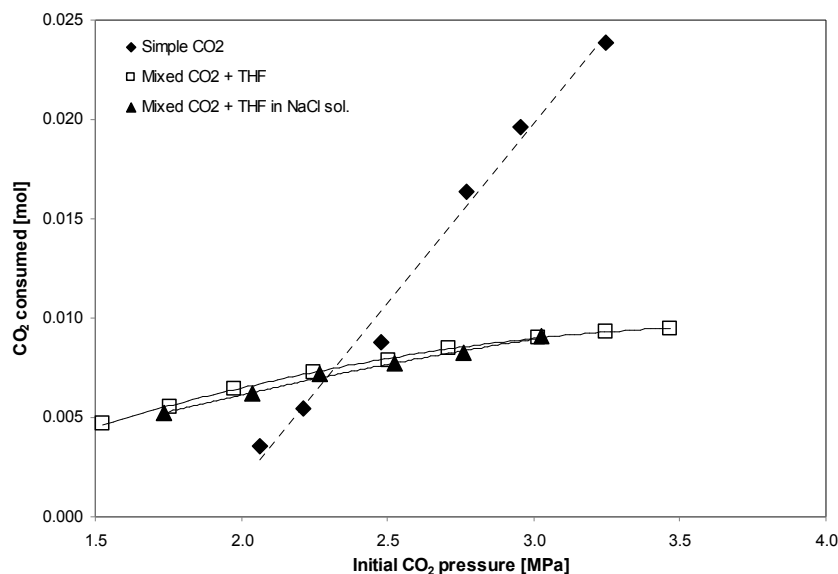


Figure 8.9 Maximum carbon dioxide consumptions during hydrate growth in different hydrate forming systems at different initial carbon dioxide pressures.

For comparison, the maximum carbon dioxide consumption during the hydrate growth process at different initial carbon dioxide pressures for each system studied is plotted in Figure 8.9. As can be seen in this figure, at initial pressures higher than 2.5 MPa, the amount of carbon dioxide consumed during hydrate growth in the simple carbon dioxide hydrate system is higher than that of mixed carbon dioxide and tetrahydrofuran hydrate system at similar initial pressures. This observation shows that the inclusion of tetrahydrofuran in the hydrate forming systems reduces the amount of carbon dioxide entrapped in the hydrate structure.

The reduction of carbon dioxide consumption in those two might be explained by considering the type of hydrate structure in each system. In the case of simple carbon dioxide hydrate, structure I will be formed and carbon dioxide molecules will fill the large cavities of the structure and possibly some of the small cavities because the ratio of carbon dioxide molecule

diameter versus the effective diameter of the 5^{12} is equal to 1 [Sloan and Koh, 2007]. If all cavities are occupied, 8 molecules of carbon dioxide molecules are entrapped per unit cell of clathrate hydrate with 46 molecules of water giving a ratio of carbon dioxide to water per unit cell of 0.1304. In contrast, structure II hydrate will be formed in the case of the mixed carbon dioxide and tetrahydrofuran hydrates where 136 water molecules are present per unit cell of the structure. Due to their size, tetrahydrofuran molecules will only occupy the large cavities of this structure, leaving the smaller cavities for the carbon dioxide molecules. Although the size ratio of carbon dioxide molecule is slightly larger than that of the small cavity of structure II hydrate, there is evidence showing that carbon dioxide molecule can fit in the small cavities of structure II hydrate, especially when there is a larger hydrate former present in the system [Teng, 1996; Ripmeester and Ratcliffe, 1998; Mooijer van den Heuvel, 2004]. If the small cavities are fully occupied by carbon dioxide, the ratio of carbon dioxide versus water per unit cell is equal to 0.118. This simple calculation shows that there is a reduction of carbon dioxide consumption among the formation of different hydrate structures, even if all possible cavities are occupied with carbon dioxide. Obviously, if the size ratio of carbon dioxide is slightly larger than the diameter of the small cavity of structure II hydrate, the occupancy of carbon dioxide in this cavity is expected to be less than in the ideal case which leads to a significantly less carbon dioxide consumption in the mixed carbon dioxide and tetrahydrofuran hydrate.

At initial pressure of less than 2.20 MPa, the consumption of carbon dioxide in simple carbon dioxide hydrate is found to be less than that of the mixed carbon dioxide and tetrahydrofuran hydrate. Referring to Figures 8.5 and 8.6, at these lower initial pressure conditions the hydrate formation of simple carbon dioxide hydrate occurs at a temperature near to that of the equilibrium temperature of the hydrate equilibrium, resulting in a smaller driving force for hydrate formation. Furthermore, the equilibrium condition

limits the formation of more hydrate in the system. The combination of these two factors reduces the amount of carbon dioxide consumption for hydrate formation in the case of simple carbon dioxide at these low initial pressure values.

As shown in Figures 8.7 and 8.8 for the mixed carbon dioxide and tetrahydrofuran systems, the presence of sodium chloride in the aqueous solution is found to prolong the hydrate growth period by ~30%, regardless the initial pressure of carbon dioxide in the system. Moreover, the amount of carbon dioxide consumed is also found to be slightly less in the presence of sodium chloride in the system, especially at lower initial pressure conditions as shown in Figure 8.11. These observations might be attributed to the clustering and salting out effects of electrolytes in hydrate formation as discussed in section 8.2.

In this work, the hydration rate is calculated based on the assumption of pressure independency [Ohgaki et. al, 1993]. It is assumed that the hydrate formation is a first-order reaction. In this case, the apparent rate constant can be calculated from:

$$\frac{dC_h}{dt} = k(C - C_s) \quad (8.6)$$

In this equation, k is the apparent rate constant, C is the concentration of carbon dioxide at time t , C_s is the saturated concentration of carbon dioxide at the stationary point and C_h is the concentration of carbon dioxide in hydrate at time t . The plots of $\ln (C_0 - C_s / C - C_s)$ versus time for the three different systems studied in this work are presented in Figure 8.10, 8.11 and 8.12 respectively.

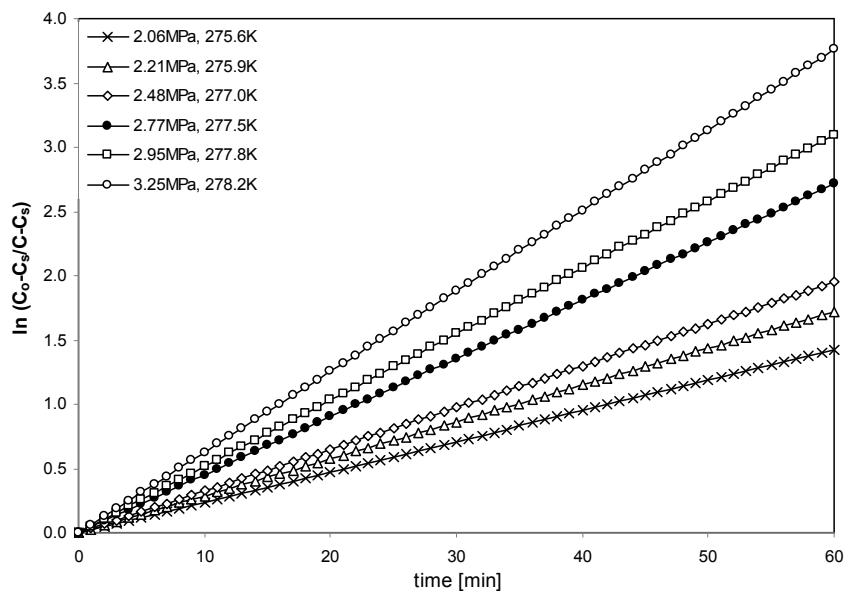


Figure 8.10 Plot of $\ln [C_0 - C_s / C - C_s]$ versus time in pure water at different initial pressures of carbon dioxide for the formation of simple carbon dioxide hydrates.

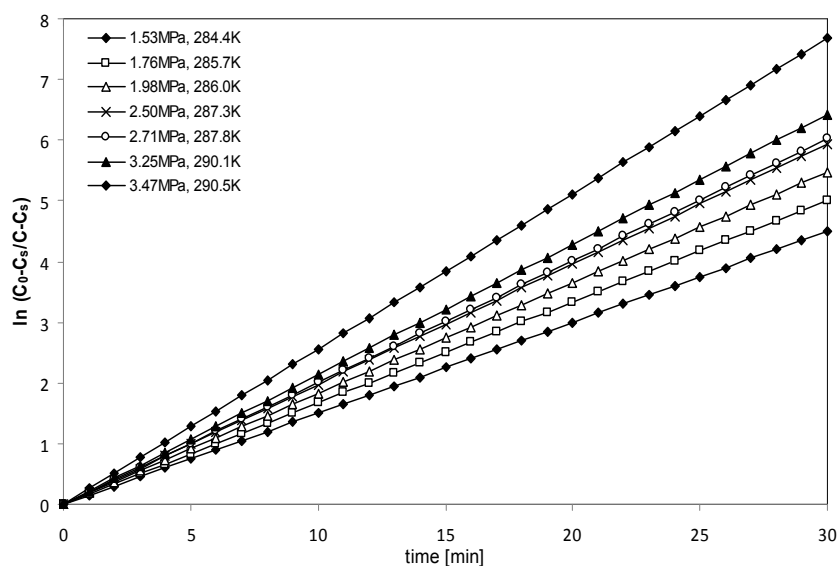


Figure 8.11 Plot of $\ln [C_0 - C_s / C - C_s]$ versus time in pure water at different initial pressures of carbon dioxide for the formation of mixed carbon dioxide and tetrahydrofuran hydrates.

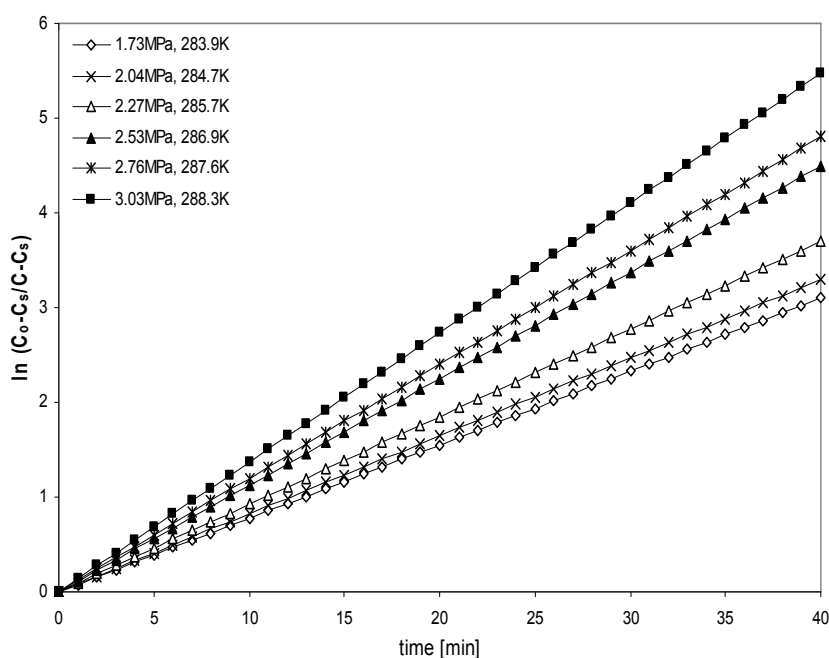


Figure 8.12 Plot of $\ln [C_0 - C_s / C - C_s]$ versus time in sodium chloride solution at different initial pressures of carbon dioxide for the formation of mixed carbon dioxide and tetrahydrofuran hydrates.

From these plots, the apparent rate constant k is calculated from the slope of each line and the calculated data are tabulated in Table 8.2. From the calculated data, it is shown that the apparent rate constant is dependent on the initial pressure of carbon dioxide in the system. Moreover, the apparent rate constant for the mixed carbon dioxide hydrate is found to be higher than that of the simple carbon dioxide hydrate at similar initial pressure values. The presence of sodium chloride in the hydrate forming system reduces the apparent rate constant of the system.

Table 8.2 The apparent rate constant for the hydration of simple carbon dioxide and mixed carbon dioxide and tetrahydrofuran hydrates.

Simple CO ₂ hydrate			Mixed CO ₂ and THF hydrate		
T	P _{int.}	k	T	P _{int.}	k
275.6	2.06	0.0237	284.4	1.53	0.1500
275.9	2.21	0.0287	285.7	1.76	0.1670
277.0	2.48	0.0325	286.0	1.98	0.1825
277.5	2.77	0.0452	287.1	2.25	0.1980
277.8	2.95	0.0516	287.3	2.50	0.1989
278.2	3.25	0.0627	287.8	2.71	0.2007
			289.1	3.02	0.2008
			290.1	3.25	0.2142
			290.5	3.47	0.2559
Mixed CO ₂ and THF hydrate in NaCl solution					
T	P _{int.}	k			
283.9	1.73	0.0775			
284.7	2.04	0.0823			
285.7	2.27	0.0924			
286.9	2.53	0.1200			
287.6	2.76	0.1124			
288.3	3.03	0.1367			

Following the Arrhenius equation, the apparent rate constant for the hydrate growth k can also be expressed as:

$$k = k^0 \exp\left(\frac{-E_a}{RT}\right) \quad (8.7)$$

In this equation, k^0 is the initial rate constant, E_a the activation energy, T the temperature at isothermal conditions and R is the universal gas constant. The Arrhenius plot of the apparent rate constant of the hydrate growth for each one of the system studied are presented in Figure 8.13. From these plots, the activation energy E_a and the initial rate constant k^0 for each system are calculated and tabulated in Table 8.3. Some literature data are also included in the table for comparison.

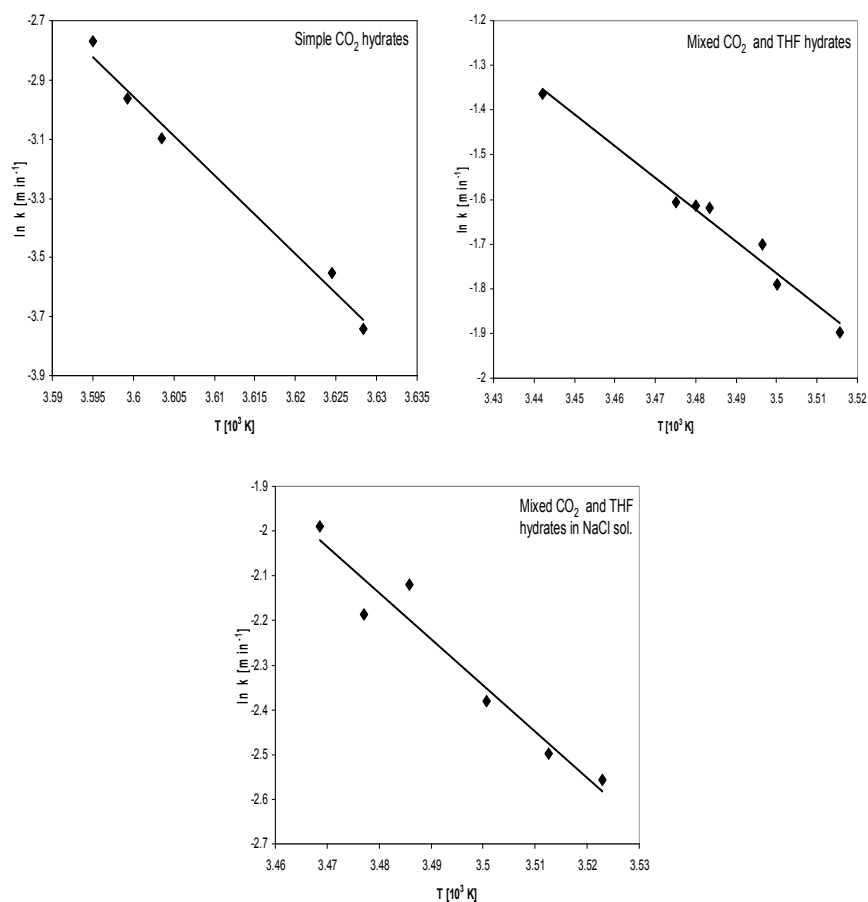


Figure 8.13 Arrhenius plots of apparent rate constant of hydrate growth for different hydrate forming systems.

Table 8.3 The activation energy E_a and the initial apparent rate constant k^0 calculated from the Arrhenius equation for hydrate growth.

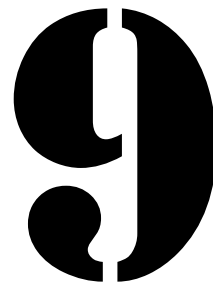
System	E_a (kJ/mol _{CO2})	k^0 (min ⁻¹)	Ref.
CO ₂ + water	221	1.64×10^{40}	This work
CO ₂ + water	241	5.92×10^{43}	Ohgaki et al., 1993
CO ₂ + THF + Water	59	1.2×10^{10}	This work
CO ₂ + THF + NaCl + water	86	5.14×10^{14}	This work

In this work, the activation energy E_a is defined as the energy that must be overcome in order for a hydrate growth process to occur. As shown in Table 8.3, the calculated activation energy for simple carbon dioxide hydrate growth is 221 kJ/mol_{CO₂}. This value is in good agreement with the value reported by Ohgaki et al. [1993] of 241 kJ/mol_{CO₂}. In comparison, the activation energy for the mixed carbon dioxide and tetrahydrofuran is found to be 59 kJ/mol, which is significantly lower. This shows that hydrate formation is more readily to occur in the mixed hydrate forming system compared to that of simple carbon dioxide system. The activation energy of the hydrate growth is found to slightly increase to 86 kJ/mol in the presence of sodium chloride in the mixed hydrates systems. This finding implies that the presence of ions in the solution create some mass transfer resistance for hydrate growth process to occur due to clustering of water molecules with these ions. However, the activation energy is still much lower than for the simple carbon dioxide hydrate.

8.4 REFERENCES

- Arjmandi, M., Tohidi, B., Danesh, A., Todd, A.C. Chem. Eng. Sci., 2005, 60, pg. 1313-1321.
- Chun, M.-K., and Lee, H. Korean J. Chem. Eng., 1996, 13, pg. 620-626.
- Clarke, M. A. and Bishnoi, P.R. Chem. Eng. Sci., 2004, 59, pg. 2983-2993.
- Englezos, P., Kalogerakis, N., Dholabhai, P.D., Bishnoi, P.R. Chem. Eng. Sci., 1987, 42, pg. 2647-2658.
- Giavarini, C., Maccioni, F., Politi, M., Santarelli, M.L., Energy & Fuels, 2007, 21, pg. 3284-3291.
- Jensen, L., Thomsen, K., von Solms, N., Chem. Eng. Sci., 2008, 63, pg. 3069-3080.

- Kawamura, T., Komai, T., Yamamoto, Y., Nagashima, K., Ohga, K., Higuchi, K., J. Crystal Growth, 2002, 234, pg. 220-226.
- Lee, K. M., Lee, H., Lee, J., Kang, J.M., Geophysical Res. Letters, 2002, 29, 30(1-4).
- Malegaonkar, M. B., Dholabhai, P.D., Bishnoi, P.R., Canadian J. Chem. Eng., 1997, 75, pg. 1090-1099.
- McCallum, S. D., Riestenberg, D. E., Zatsepina, O. Y., Phelps, T. J., J. Petroleum Sci. Eng., 2007, 56, pg. 54-64.
- Mooijer-van den Heuvel, M.M. "Phase Behaviour and Structural Aspects of Ternary Clathrate Hydrate Systems: The Role of Additives". Ph.D thesis, Delft Uni. of Technology, January, 2004.
- North, W.J., Blackwell, V.R., Morgan, J.J., Environ. Sci. Technol., 1998, 32, pg. 6767-681.
- Ohgaki, K., Makiyama, Y., Takano, K. J. Chem. Eng. Japan, 1993, 26, pg. 558-564.
- Ripmeester, J.A. and Ratcliffe, C.I. Energy & Fuels, 1998, 12, pg. 197-200.
- Shindo, Y., Lund, P.C., Fujioka, Y., Komiyama, H., Energy Convers. Mgmt., 1993, 34, pg. 1073-1079.
- Sloan Jr., E.D. and Koh, C.A. "Clathrate Hydrates of Natural Gas", 2nd ed., CRC Press, Florida, 2007.
- Teng, H. Int. J. Chem. Kinetics, 1996, 28, pg. 935-937.



Conclusions and Outlook

The major conclusions from the study presented in this thesis are given in this chapter. Experimental and modelling results for the phase behaviour in the hydrate forming region are discussed. The changes of the phase behaviour due to the presence of electrolytes are also discussed. The applicability of the Clausius-Clayperon equation for estimating the enthalpy of dissociation of simple carbon dioxide and mixed carbon dioxide hydrates are reported. The kinetics of clathrate hydrate formation in selected systems is presented. A brief perspective of recommended future research is briefly highlighted.

9.1 CONCLUSIONS

The phase equilibria determined in ternary systems of carbon dioxide + tetrahydrofuran + water and quaternary systems of carbon dioxide + tetrahydrofuran + electrolyte + water is compared with the corresponding equilibria in the binary system carbon dioxide + water. The hydrate phase equilibrium dissociation pressures were largely shifted to higher temperature conditions by the addition of tetrahydrofuran. Moreover, a drastic pressure reduction of the hydrate equilibrium pressure up to ~90% can be obtained with the introduction of THF in the aqueous solution. Accordingly, tetrahydrofuran was confirmed to act as a hydrate promoter and able to extend the stability region of clathrate hydrates. It was found that the promoting effect of tetrahydrofuran is concentration dependent.

The three-phase hydrate equilibrium line of $H-L_W-V$ is found to be independent of the concentration of carbon dioxide in the system. In contrast, the high-pressure three-phase hydrate equilibrium line $H-L_W-L_V$ is greatly affected by the overall concentration of carbon dioxide in the system, especially at overall concentrations of carbon dioxide of more than 3 mol%. With an overall CO_2 concentration as low as 3 mol% in the system, a liquid-liquid phase split occurs. In this case, a water rich (L_W) phase and a condensed gas + organic (L_V) phase occurs, creating a region where a three-phase equilibrium L_W-L_V-V exists. In this region, the four-phase hydrate equilibrium line ($H-L_W-L_V-V$) loses its dependency on the concentration of tetrahydrofuran in the system.

Pseudo-retrograde hydrate behaviour has been observed in the ternary system at several selected compositions in the region where a four-phase hydrate equilibrium line ($H-L_W-L_V-V$) is determined. This phenomenon can be characterized as the appearance of the clathrate hydrate, followed

by clathrate hydrate disappearance and finally a bubble point. Due to this behaviour, there is a maximum temperature at which the mixed carbon dioxide and tetrahydrofuran hydrates stable in the system. Further pressurization of the system will result in the decrease of temperature at which hydrates are stable.

In the quaternary system studied, the presence of an electrolyte in the system enhanced the liquid-liquid phase split creating two distinct liquid phases, i.e. a water-rich phase and a phase rich in tetrahydrofuran and carbon dioxide. This behaviour is attributed to the salting-out effect, which is a phenomenon caused by the presence of ions. In general, it is found that the hydrate promoting effect of tetrahydrofuran suppresses the inhibiting effect of an electrolyte when both species are present in the hydrate forming system.

The strength of the hydrate inhibiting effect among the investigated electrolytes was compared. The results show that the hydrate inhibiting effect of the metal halides is increasing in the order $\text{NaF} < \text{KBr} < \text{NaCl} < \text{NaBr} < \text{CaCl}_2 < \text{MgCl}_2$. Among the cations studied, the strength of hydrate inhibition increases in the following order: $\text{K}^+ < \text{Na}^+ < \text{Ca}^{2+} < \text{Mg}^{2+}$. On the other hand, the strength of hydrate inhibition caused by the halogen anions studied decreases in the following order: $\text{Br}^- > \text{Cl}^- > \text{F}^-$. Based on these results, it is suggested that the inhibiting effect of electrolytes on the hydrate formation is highly affected by the strength of the ionic-hydrogen bond between an ion and a water molecule and the effects of this bond on the surrounding network of water molecules.

As an alternative for the time-consuming hydrate phase equilibrium measurements, the van der Waals and Platteeuw model, specifically suitable for a gas hydrate phase, is combined with an equation of state model to predict the clathrate hydrate phase equilibria investigated in this study. The

phase behaviour of the fluid phases is modelled with the Peng-Robinson-Stryjek-Vera Equation of State (PRSV EoS) with Huron-Vidal-Orbey-Sandler (HVOS) mixing rules. In order to take into account the presence of electrolyte in the quaternary systems, a Debye-Hückel (D-H) electrostatic term is added to the PRSV EoS, allowing the calculation of the fugacity of non-electrolyte components in the aqueous phase. Excellent agreement has been found between the experimental and predicted values for the bubble point and dew point curves in the ternary carbon dioxide + tetrahydrofuran + water at different overall composition ratios. Similarly, the H-L_W-V equilibrium is very well predicted by the model with an AARD% less than 3.5%. However, the predictions of the high pressure three-phase H-L_W-V, and the four-phase H-L_W-L_V-V hydrate equilibria are less accurate, resulting in higher AARD% values of ~12% and 9% respectively. Nevertheless, taking into account the complexity of the systems, the errors are still within an acceptable region. In the presence of sodium chloride the predictive model is becoming less accurate with AARD% as high as 7 up to 15 % of the experimental values, depending on the type of the equilibrium line. Considering that up to now, there is no comparable predictive method available in literature that is able to predict the carbon dioxide hydrate equilibrium in the presence of an electrolyte and a promoter, the model provides a good basis for further improvement.

The estimation of the enthalpy of dissociation of simple carbon dioxide and mixed carbon dioxide hydrates are made by applying the Clausius-Clapeyron equation. Moreover, the hydration number of simple carbon dioxide hydrate is calculated based on the de Forcrand method. It was found that the enthalpy of dissociation and the hydration numbers for carbon dioxide hydrates, calculated in this work, agree well with those reported in literature. Throughout the work, it has been consistently shown that the compressibility factor z has significant effects on the values of these properties. Moreover, in the range of pressure and temperature studied, the

enthalpy of dissociation for mixed carbon dioxide and tetrahydrofuran hydrate is found to be consistently higher than that of simple carbon dioxide hydrate. It is also shown that the presence of electrolytes also affects the enthalpy of dissociation for both the simple carbon dioxide and the mixed carbon dioxide hydrates. Furthermore, it was observed that the effects depend on the type of ions present in the system.

Furthermore, in this study measurements on the kinetics of formation in the hydrate forming systems have been carried out. For that purpose, the so-called T-cycle method was applied. The induction time for hydrate nucleation was found to be much lower in the ternary system of carbon dioxide + tetrahydrofuran + water compared to that of the binary system of carbon dioxide + water. This comparison indicates that the hydrate nucleation process is more readily to occur in the presence of tetrahydrofuran in the aqueous solution. The presence of sodium chloride is found to slightly prolong the induction time in the mixed hydrate system. In general, the carbon dioxide consumption is found to be higher for simple carbon dioxide hydrates compared to mixed carbon dioxide and tetrahydrofuran hydrates. In contrast, the activation energy of mixed carbon dioxide and tetrahydrofuran hydrates is found to be significantly lower than that of simple carbon dioxide hydrate. This implies that the mixed system is more susceptible for hydrate formation. The presence of sodium chloride is found to slightly reduce the carbon dioxide consumption during the hydrate formation process. On the other hand, an increase of the activation energy for hydrate formation in the mixed hydrates systems was observed.

9.2 OUTLOOK

The aims of the present work are to provide some information on the phase behaviour and kinetics of formation of simple carbon dioxide and

mixed carbon dioxide and tetrahydrofuran hydrates in water or aqueous electrolyte solutions. Although some interesting observations are made throughout this work, further research is required to get a better understanding of the complexity encountered in such hydrate forming systems.

Regarding the phase behaviour and taking into account the limited available information in literature, special attention should be paid to the occurrence of the pseudo-retrograde phenomenon in the hydrate forming systems. Experimental investigations should be made in order to perceive if this phenomenon is common in hydrate forming systems of carbon dioxide and a miscible promoter such as propylene oxide, 1,4-dioxane and acetone.

As reported in this work, anions and cations showed different inhibiting effects on clathrate hydrate stability/formation. However, due to the limited data available, no concrete conclusion can be achieved. To get a better understanding on the inhibition effects of electrolytes on clathrate hydrate, the effects of anions and cations should be more systematically studied.

Since research on the kinetics of formation and dissociation of gas hydrates are relatively new fields compared to the thermodynamics of these systems, more experimental work and modelling work should be conducted to obtain reliable data and to come up with a better understanding of the kinetics of gas hydrate systems. The type of reactors, operation modes, type of feeding systems are among major research areas to be focused on in order to obtain better fundamental insights on the reliability of future processes based on carbon dioxide hydrates.

For a proper interpretation of the experimental data on the phase behaviour and kinetics of formation as obtained in this study on a

microscopic level, more knowledge of the formed clathrate hydrate structure and its occupancy is essential. In this work, due to the unavailability of physical characterization techniques, the growth and the stability of hydrate nucleus and the consistency of the crystalline size are not monitored. Therefore, application of various physical characterization techniques to analyze the clathrate hydrates formed is strongly recommended.

The ultimate long term main objective of this kind of research is to successfully develop environmentally friendly carbon dioxide hydrate based processes. To ensure the success of these processes, the process designs and the economical aspects should be further investigated. This underlying study aims to provide a sound basis of new knowledge for novel future processes where carbon dioxide hydrates will play a central role.

APPENDIX A

**Measured Equilibrium Data for
Binary CO₂ + Water and Ternary CO₂
+ THF + Water**

Table A-1 Experimental data for H-L_W-V and L_W-V--->L_W-L_V equilibrium curves in the system CO₂ + water

H-L _W -V		L _W -V--->L _W -L _V	
T (K)	P(MPa)	T (K)	P(MPa)
275.12	1.51	277.00	3.77
276.88	1.81	278.00	3.89
277.83	2.11	279.00	4.01
278.99	2.40	280.00	4.12
279.94	2.70	281.00	4.24
280.71	3.00	282.00	4.35
281.42	3.30	283.00	4.47
282.06	3.60	284.00	4.59
282.41	3.90	285.00	4.70
282.90	4.30	286.00	4.82
		286.00	4.82
Q ₂ (283.07 K, 4.47 MPa)		287.00	4.93
		290.00	5.28

Table A-2 Experimental data for H-L_W-V, H-L_W-L_V and L_W -V--->L_W-L_V equilibrium curves in the system CO₂ + THF + water at 1 mol% of CO₂ and 5 mol% THF.

H-L _W -V		H-L _W -L _V		L _W -V--->L _W -L _V	
T (K)	P(MPa)	T (K)	P(MPa)	T (K)	P(MPa)
285.46	0.90	287.44	1.50	286.45	1.52
286.16	1.05	287.48	1.80	287.44	1.53
286.81	1.20	287.52	2.10	289.50	1.56
287.28	1.35	287.52	2.40	291.45	1.63
		287.60	3.05	293.43	1.71
Q ₂ (287.44 K, 1.50 MPa)		287.68	4.05	295.43	1.79
Mole fraction CO ₂ : 0.010		287.79	5.05	297.49	1.88
Mole fraction water: 0.940		287.83	6.05	299.41	1.94
Mole fraction THF: 0.050					

Table A-3 Experimental data for different equilibrium curves in the system containing CO₂ + THF + water at 2 mol% of CO₂ and 5 mol% THF.

H-L _W -V		H-L _W -L _V -V		H-L _W -L _V	
T (K)	P(MPa)	T (K)	P(MPa)	T (K)	P(MPa)
286.21	1.05	289.62	2.10	290.27	2.70
286.74	1.20	290.21	2.40	290.34	3.00
287.97	1.50			290.32	3.30
288.86	1.80	L _W -L _V -V--->L _W -V		290.37	3.60
		T (K)	P(MPa)	290.38	3.90
L _W -L _V -V--->L _W -L _V		289.43	2.08	290.39	4.20
T (K)	P(MPa)	290.43	2.10	290.44	4.55
290.45	2.47	291.42	2.14	290.47	5.05
291.41	2.51	292.43	2.16	290.54	6.05
292.43	2.53	294.42	2.23	290.67	7.05
293.48	2.57	296.40	2.29		
294.42	2.60			Mole fraction CO ₂ : 0.020	
295.47	2.63			Mole fraction water: 0.930	
Q ₂ (290.21 K, 2.40 Mpa)				Mole fraction THF: 0.050	

Table A-4 Experimental data for different equilibrium curves in the system containing CO₂ + THF + water at 3 mol% of CO₂ and 5 mol% THF.

H-L _W -V		H-L _W -L _V -V		H-L _W -L _V	
T (K)	P(MPa)	T (K)	P(MPa)	T (K)	P(MPa)
286.81	1.20	290.57	2.55	290.85	2.85
287.98	1.50	290.81	2.70	290.89	3.00
288.86	1.80			290.90	3.30
289.57	2.10	L _W -L _V -V--->L _W -V		291.02	3.60
289.93	2.25	T (K)	P(MPa)	291.03	3.90
290.10	2.40	289.45	2.41	291.11	4.20
290.57	2.55	290.45	2.45	291.03	4.55
		291.49	2.48	291.10	5.05
L _W -L _V -V--->L _W -L _V		293.50	2.53	291.29	6.05
T (K)	P(MPa)	295.43	2.58	291.29	7.05
289.52	2.80	297.49	2.65		
290.45	2.84	299.42	2.67		
291.45	2.88				
292.51	2.92				
293.50	2.97				

Table A-4 (Cont.)

295.44	3.05	Mole fraction CO ₂ : 0.030
297.43	3.14	Mole fraction water: 0.920
299.42	3.22	Mole fraction THF: 0.050
301.47	3.31	

Table A-5 Experimental data for different equilibrium curves in the system containing CO₂ + THF + water at 4 mol% of CO₂ and 5 mol% THF.

H-L _W -V		H-L _W -L _V -V		H-L _W -L _V	
T (K)	P(MPa)	T (K)	P(MPa)	T (K)	P(MPa)
285.38	0.90	290.23	2.40	291.13	3.30
286.79	1.20	290.70	2.70	291.20	3.60
287.90	1.50	290.92	3.00	291.23	3.90
288.79	1.80			291.35	4.20
289.68	2.10	L _W -L _V -V--->L _W -V		291.36	4.55
		T (K)	P(MPa)	291.48	5.05
L _W -L _V -V---->L _W -L _V		290.49	2.22	291.50	6.05
T (K)	P(MPa)	291.39	2.28	291.67	7.05
291.10	3.16	292.40	2.32		
291.48	3.18	293.39	2.34	Mole fraction CO ₂ : 0.040	
291.96	3.21	294.48	2.37	Mole fraction water: 0.910	
292.46	3.23	295.39	2.43	Mole fraction THF: 0.050	
293.41	3.29	296.41	2.50		
294.40	3.34				
295.50	3.40				

Table A-6 Experimental data for different equilibrium curves in the system containing CO₂ + THF + water at 9 mol% of CO₂ and 5 mol% THF.

H-L _W -V		H-L _W -L _V -V		H-L _W -L _V	
T (K)	P(MPa)	T (K)	P(MPa)	T (K)	P(MPa)
286.03	1.06	290.79	2.70	291.49	4.20
286.74	1.20	291.09	3.00	291.55	4.55
287.80	1.50	291.26	3.30	291.66	5.05
288.80	1.80	291.32	3.60	291.73	6.05
289.55	2.10	291.43	3.90	291.86	7.05
290.18	2.30				
290.79	2.70				

Table A-6 (Cont.)

		L _W -L _V -V---->L _W -V		Mole fraction CO ₂ : 0.090
				Mole fraction water: 0.860
L _W -L _V -V---->L _W -L _V		T (K)	P(MPa)	Mole fraction THF: 0.050
T (K)	P(MPa)			
291.49	4.06	290.47	2.35	
292.49	4.14	292.47	2.39	
293.48	4.22	294.45	2.42	
294.50	4.30	296.43	2.47	
295.49	4.38	298.55	2.49	
296.45	4.45	299.47	2.50	
		301.17	2.52	

Table A-7 Experimental data for different equilibrium curves in the system containing CO₂ + THF + water at 19 mol% of CO₂ and 4 mol% THF.

H-L _W -V		H-L _W -L _V -V		H-L _W -L _V	
T (K)	P(MPa)	T (K)	P(MPa)	T (K)	P(MPa)
286.51	1.21	290.84	2.70	290.05	4.55
287.63	1.50	291.03	3.00	290.05	5.05
288.50	1.80	291.21	3.30	290.05	6.05
289.39	2.10	291.28	3.60	290.05	7.05
289.97	2.40	291.14	3.90		
		290.71	4.20		
L _W -L _V -V---->L _W -L _V				Mole fraction CO ₂ : 0.190	
				Mole fraction water: 0.770	
				Mole fraction THF: 0.040	
T (K)	P(MPa)	L _W -L _V -V---->L _W -V			
		T (K)	P(MPa)		
289.45	4.40				
290.49	4.51	289.45	2.53		
291.50	4.60	291.50	2.63		
292.44	4.69	293.44	2.67		
293.44	4.79	295.43	2.77		
294.43	4.89	297.42	2.87		
295.43	4.99				

Table A-8 Experimental data for different equilibrium curves in the system containing CO₂ + THF + water at 29 mol% of CO₂ and 4 mol% THF.

H-L _W -V		H-L _W -L _V -V		H-L _W -L _V	
T (K)	P(MPa)	T (K)	P(MPa)	T (K)	P(MPa)
287.71	1.50	291.10	3.00	289.13	5.05
288.60	1.80	291.25	3.30	289.12	6.05
289.36	2.10	291.35	3.60		
290.02	2.40	291.26	3.90	L _W -L _V -V---->L _W -V	
290.62	2.70	291.22	4.05	T (K)	P(MPa)
		290.96	4.20	289.53	2.83
L _W -L _V -V---->L _W -L _V		290.54	4.35	291.52	2.88
T (K)	P(MPa)	290.20	4.45	293.45	2.93
289.44	4.63			295.42	2.95
291.49	4.84	Mole fraction CO ₂ : 0.290		297.49	2.98
293.43	5.04	Mole fraction water: 0.670		299.42	3.02
295.49	5.27	Mole fraction THF: 0.040		301.46	3.05
297.43	5.48				
299.47	5.72				
301.46	5.95				

Table A-9 Experimental data for different equilibrium curves in the system containing CO₂ + THF + water at 1 mol% of CO₂ and 1.2 mol% THF.

H-L _W -V		H-L _W -L _V		L _W -L _V -V---->L _W -L _V	
T (K)	P(MPa)	T (K)	P(MPa)	T (K)	P(MPa)
281.76	0.90	283.79	1.50	280.46	1.23
282.39	1.00	283.80	1.80	281.52	1.28
282.93	1.10	283.80	2.10	282.51	1.33
283.26	1.20	283.91	2.40	283.50	1.38
		283.89	2.70	284.45	1.43
		283.92	2.95	285.50	1.48
		283.96	3.30	286.50	1.53
		283.95	3.60		
		284.03	3.90	Mole fraction CO ₂ : 0.010	
		283.96	4.20	Mole fraction water: 0.980	
		283.96	4.55	Mole fraction THF: 0.010	
		284.08	5.05		
		284.15	6.05		
		284.21	7.05		

Table A-10 Experimental data for different equilibrium curves in the system containing CO₂ + THF + water at 2 mol% of CO₂ and 1.2 mol% THF.

H-L _W -V		H-L _W -L _V		L _W -L _V -V---->L _W -L _V	
T (K)	P(MPa)	T (K)	P(MPa)	T (K)	P(MPa)
282.73	1.20	289.30	4.55	287.49	4.20
284.02	1.50	289.31	5.05	288.49	4.31
284.96	1.80	289.42	6.05	289.43	4.46
285.78	2.10	289.49	7.05	289.49	4.55
286.49	2.40			290.54	4.67
287.14	2.70	Mole fraction CO ₂ : 0.020			
287.68	3.00	Mole fraction water: 0.970			
288.02	3.30	Mole fraction THF: 0.010			
288.55	3.60				
288.78	3.90				
289.20	4.20				

Table A-11 Experimental data for different equilibrium curves in the system containing CO₂ + THF + water at 4 mol% of CO₂ and 1.2 mol% THF.

H-L _W -V		H-L _W -L _V -V		H-L _W -L _V	
T (K)	P(MPa)	T (K)	P(MPa)	T (K)	P(MPa)
283.56	1.20	289.68	4.30	289.39	4.70
284.55	1.50	289.74	4.40	289.33	4.90
285.45	1.80	289.68	4.50	289.40	5.05
286.21	2.10	289.39	4.60	289.39	5.55
286.92	2.40			289.53	6.05
287.56	2.70	L _W -L _V -V---->L _W -V		289.57	7.05
288.03	3.00	T (K)	P(MPa)		
288.57	3.30	288.46	4.10	L _W -L _V -V---->L _W -L _V	
288.86	3.60	289.46	4.19	T (K)	P(MPa)
289.39	3.90	290.51	4.29	288.45	4.59
289.56	4.20	291.45	4.38	289.46	4.69
		292.50	4.46	290.51	4.79
Mole fraction CO ₂ : 0.040		293.50	4.55	291.45	4.87
Mole fraction water: 0.950				292.51	4.98
Mole fraction THF: 0.010				293.50	5.08

Table A-12 Experimental data for different equilibrium curves in the system containing CO₂ + THF + water at 6 mol% of CO₂ and 1.2 mol% THF.

H-L _W -V		H-L _W -L _V -V		H-L _W -L _V	
T (K)	P(MPa)	T (K)	P(MPa)	T (K)	P(MPa)
283.96	1.50	289.38	4.50	288.38	4.65
285.26	1.80	289.32	4.55	288.41	4.70
285.73	2.10	288.91	4.60	288.54	5.05
286.49	2.40			288.66	6.05
287.32	2.70	L _W -L _V -V---->L _W -L _V		288.71	7.05
287.67	3.00	T (K)	P(MPa)		
288.19	3.30	286.55	4.44	Mole fraction CO ₂ : 0.060	
288.74	3.60	287.49	4.54	Mole fraction water: 0.930	
289.19	3.90	288.48	4.65	Mole fraction THF: 0.010	
289.36	4.20	289.55	4.74		
289.42	4.40	290.49	4.83		
		291.54	4.94		

Table A-13 Experimental data for different equilibrium curves in the system containing CO₂ + THF + water at 9 mol% of CO₂ and 1.2 mol% THF.

H-L _W -V		H-L _W -L _V -V		H-L _W -L _V	
T (K)	P(MPa)	T (K)	P(MPa)	T (K)	P(MPa)
284.59	1.51	289.86	4.50	288.39	4.65
285.59	1.81	289.56	4.55	288.35	4.70
286.38	2.11	288.73	4.60	288.26	4.90
286.99	2.41			288.29	5.05
287.66	2.71	L _W -L _V -V---->L _W -L _V		288.38	6.05
288.13	3.00	T (K)	P(MPa)	288.49	7.05
288.55	3.30	288.51	4.67		
288.92	3.60	289.50	4.77	L _W -L _V -V---->L _W -V	
289.43	3.90	290.52	4.87	T (K)	P(MPa)
289.64	4.30	291.57	4.98	289.49	4.46
289.87	4.40	292.56	5.09	290.44	4.55
		293.57	5.20	291.43	4.66
Mole fraction CO ₂ : 0.090				292.43	4.77
Mole fraction water: 0.900				293.43	4.85
Mole fraction THF: 0.010					

Table A-14 Experimental data for different equilibrium curves in the system containing CO₂ + THF + water at 2 mol% of CO₂ and 7 mol% THF.

H-L _W -V		H-L _W -L _V		L _W -L _V -V---->L _W -L _V	
T (K)	P(MPa)	T (K)	P(MPa)	T (K)	P(MPa)
285.25	0.90	290.02	2.70	288.44	2.45
286.66	1.20	290.07	3.00	289.46	2.45
287.84	1.50	290.07	3.30	290.46	2.50
288.85	1.80	290.08	3.60	291.49	2.57
289.39	2.10	290.28	3.90	292.47	2.64
289.99	2.40	290.27	4.55	293.47	2.69
		290.30	5.05		
Mole fraction CO ₂ : 0.020		290.46	6.05		
Mole fraction water: 0.910		290.38	7.05		
Mole fraction THF: 0.070					

Table A-15 Experimental data for different equilibrium curves in the system containing CO₂ + THF + water at 4 mol% of CO₂ and 7 mol% THF

H-L _W -V		H-L _W -L _V -V		H-L _W -L _V	
T (K)	P(MPa)	T (K)	P(MPa)	T (K)	P(MPa)
286.84	1.21	288.01	1.50	290.44	2.70
		288.89	1.80	290.46	3.00
L _W -L _V -V---->L _W -L _V		289.61	2.10	290.56	3.60
T (K)	P(MPa)	290.27	2.40	290.67	5.05
289.48	2.52			290.78	6.05
290.54	2.56	L _W -L _V -V---->L _W -V		290.94	7.05
291.44	2.60	T (K)	P(MPa)		
292.40	2.64	286.49	1.42	Mole fraction CO ₂ : 0.040	
293.43	2.68	287.52	1.44	Mole fraction water: 0.890	
		288.46	1.45	Mole fraction THF: 0.070	
		289.47	1.46		

Table A-16 Experimental data for different equilibrium curves in the system containing CO₂ + THF + water at 9 mol% of CO₂ and 6 mol% THF.

H-L _w -V		H-L _w -L _v -V		H-L _w -L _v	
T (K)	P(MPa)	T (K)	P(MPa)	T (K)	P(MPa)
286.79	1.11	291.03	3.00	291.62	3.90
287.88	1.51	291.36	3.30	291.57	4.55
288.82	1.81	291.51	3.60	291.62	5.05
289.56	2.11			291.67	6.05
290.20	2.41	L _w -L _v -V---->L _w -V		291.88	7.05
290.78	2.70	T (K)	P(MPa)		
		289.44	2.55	Mole fraction CO ₂ : 0.090	
L _w -L _v -V---->L _w -L _v		291.44	2.60	Mole fraction water: 0.850	
T (K)	P(MPa)	293.44	2.66	Mole fraction THF: 0.060	
291.47	3.85				
292.49	3.93				
293.42	4.00				

Table A-17 Experimental data for different equilibrium curves in the system containing CO₂ + THF + water at 17 mol% of CO₂ and 6 mol% THF.

H-L _w -V		H-L _w -L _v -V		H-L _w -L _v	
T (K)	P(MPa)	T (K)	P(MPa)	T (K)	P(MPa)
287.61	1.51	291.06	3.00	290.33	4.50
288.58	1.81	291.21	3.30	290.42	5.05
289.25	2.11	291.35	3.60	290.52	6.05
290.07	2.40	291.31	3.75	290.67	7.05
290.64	2.70	291.62	3.90		
		291.13	4.05		
L _w -L _v -V---->L _w -L _v		291.21	4.20	Mole fraction CO ₂ : 0.170	
T (K)	P(MPa)	290.57	4.35	Mole fraction water: 0.780	
289.46	4.33			Mole fraction THF: 0.060	
290.42	4.41	L _w -L _v -V---->L _w -V			
291.36	4.50	T (K)	P(MPa)		
292.49	4.61	293.43	2.75		
293.43	4.70	291.45	2.65		
		289.48	2.48		

Table A-18 Experimental data for different equilibrium curves in the system containing CO₂ + THF + water at 27 mol% of CO₂ and 5 mol% THF.

H-L _W -V		H-L _W -L _V -V		H-L _W -L _V	
T (K)	P(MPa)	T (K)	P(MPa)	T (K)	P(MPa)
289.01	2.06	291.28	3.31	288.92	4.80
289.30	2.16	291.28	3.61	288.92	5.05
289.95	2.41	291.26	3.90	289.09	6.05
290.44	2.71	290.85	4.20	289.18	7.05
290.89	3.01	290.53	4.40		
		289.80	4.50		
L _W -L _V -V---->L _W -L _V			Mole fraction CO ₂ : 0.270		
T (K)	P(MPa)	L _W -L _V -V---->L _W -V		Mole fraction water: 0.680	
		T (K)	P(MPa)	Mole fraction THF: 0.050	
289.44	4.65				
290.40	4.76	290.38	3.06		
291.46	4.86	291.45	3.11		
292.50	4.97	292.44	3.16		
293.50	5.08	293.45	3.21		

Table A-19 Experimental data for different equilibrium curves in the system containing CO₂ + THF + water at 4 mol% of CO₂ and 3 mol% THF.

H-L _W -V		H-L _W -L _V -V		H-L _W -L _V	
T (K)	P(MPa)	T (K)	P(MPa)	T (K)	P(MPa)
287.33	1.50	291.34	3.60	291.50	4.20
288.27	1.80	291.44	3.90	291.57	5.05
289.03	2.10			291.73	6.05
290.40	2.70	L _W -L _V -V---->L _W -V		291.79	7.05
290.86	3.00	T (K)	P(MPa)		
291.27	3.30	290.46	3.40		
		291.45	3.47	Mole fraction CO ₂ : 0.040	
L _W -L _V -V---->L _W -L _V		292.44	3.56	Mole fraction water: 0.930	
T (K)	P(MPa)	293.45	3.65	Mole fraction THF: 0.030	
289.46	3.76	294.51	3.72		
290.46	3.82				
291.45	3.89				
292.45	3.96				
293.44	4.02				

Table A-20 Experimental data for different equilibrium curves in the system containing CO₂ + THF + water at 9 mol% of CO₂ and 3 mol% THF.

H-L _W -V		H-L _W -L _V -V		H-L _W -L _V	
T (K)	P(MPa)	T (K)	P(MPa)	T (K)	P(MPa)
279.9	0.26	291.38	3.60	290.79	4.35
284.91	0.90	291.38	3.75	290.73	4.50
286.20	1.20	291.32	3.90	290.79	5.05
287.38	1.50	291.20	4.05	291.03	6.05
288.26	1.80	290.96	4.20	291.08	7.05
288.99	2.10				
289.74	2.40	L _W -L _V -V---->L _W -L _V		L _W -L _V -V---->L _W -V	
290.33	2.70	T (K)	P(MPa)	T (K)	P(MPa)
290.86	3.00	290.49	4.24	291.44	3.38
291.26	3.30	291.52	4.34	292.44	3.40
		292.44	4.42	293.44	3.42
Mole fraction CO ₂ : 0.090		293.42	4.51	294.45	3.43
Mole fraction water: 0.880					
Mole fraction THF: 0.030					

Table A-21 Experimental data for different equilibrium curves in the system containing CO₂ + THF + water at 9 mol% of CO₂ and 9 mol% THF.

H-L _W -V		H-L _W -L _V -V		H-L _W -L _V	
T (K)	P(MPa)	T (K)	P(MPa)	T (K)	P(MPa)
285.21	0.91	287.79	1.50	290.90	3.00
286.07	1.10	288.84	1.80	290.98	3.30
		289.68	2.10	291.09	3.60
L _W -L _V -V---->L _W -L _V		290.27	2.40	291.14	3.90
T (K)	P(MPa)	290.77	2.70	291.27	4.55
290.38	2.96			291.27	5.05
291.43	3.00	L _W -L _V -V---->L _W -V		291.32	6.05
292.43	3.05	T (K)	P(MPa)	291.45	7.05
293.43	3.10	286.44	1.08		
294.44	3.16	288.46	1.15	Mole fraction CO ₂ : 0.090	
		292.45	1.13	Mole fraction water: 0.820	
		293.42	1.13	Mole fraction THF: 0.090	
		294.43	1.16		

Table A-22 Experimental data for different equilibrium curves in the system containing CO₂ + THF + water at 18 mol% of CO₂ and 10 mol% THF.

H-L _W -V		H-L _W -L _V		L _W -L _V -V---->L _W -L _V	
T (K)	P(MPa)	T (K)	P(MPa)	T (K)	P(MPa)
284.79	0.90	288.73	2.10	287.44	1.80
285.68	1.05	288.79	2.40	288.49	1.84
286.67	1.20	288.80	3.05	289.44	1.87
287.14	1.35	288.85	4.05	290.43	1.90
287.85	1.50	288.87	5.05	291.43	1.93
288.20	1.65	288.92	6.05	292.48	1.97
288.61	1.80	289.08	7.05		
Mole fraction CO ₂ : 0.180					
Mole fraction water: 0.710					
Mole fraction THF: 0.100					

APPENDIX B

**Measured Equilibrium Data for
Systems CO₂ + water + electrolyte
and CO₂ + THF + water + electrolyte**

Table B-1 Experimental data for different equilibrium curves in the system CO₂ + water + NaCl at 1.5 mol% of NaCl in aqueous solution

H-L _w -V		H-L _w -L _v		L _v -L _w -V---->L _w -L _v	
T (K)	P(MPa)	T (K)	P(MPa)	T (K)	P(MPa)
267.55	0.80	280.69	4.40	277.52	4.04
270.21	1.10	280.80	5.05	278.45	4.14
272.39	1.40	280.87	6.05	279.52	4.26
273.98	1.70	280.93	7.05	280.52	4.36
275.28	2.00			281.52	4.46
276.39	2.30			282.51	4.57
277.34	2.60	Mole fraction CO ₂ : 0.041		283.45	4.67
278.21	2.90	Mole fraction water: 0.943			
279.10	3.20	Mole fraction NaCl: 0.015			
279.69	3.50				
280.09	3.80				
280.52	4.10				

Table B-2 Experimental data for different equilibrium curves in the system CO₂ + water + NaCl at 3.2 mol% of NaCl in aqueous solution

H-L _w -V		H-L _w -L _v		L _v -L _w -V---->L _w -L _v	
T (K)	P(MPa)	T (K)	P(MPa)	T (K)	P(MPa)
270.68	1.50	277.70	3.90	275.51	3.74
272.21	1.80	277.70	4.20	276.53	3.84
273.34	2.10	277.70	5.05	277.46	3.93
274.34	2.40	277.69	6.05	278.45	4.03
275.12	2.70	277.80	7.05		
275.87	3.00			Mole fraction CO ₂ : 0.041	
276.51	3.30			Mole fraction water: 0.927	
277.11	3.60			Mole fraction NaCl: 0.032	

Table B-3 Experimental data for different equilibrium curves in the system CO₂ + THF + water + NaCl at 1 mol% THF and 2 mol% NaCl respectively.

H-L _W -V		H-L _W -L _V -V		H-L _W -L _V	
T (K)	P(MPa)	T (K)	P(MPa)	T (K)	P(MPa)
279.58	0.90	286.86	3.90	286.28	4.50
281.12	1.20	286.50	4.20	286.36	5.05
282.05	1.50			286.44	6.05
283.27	1.80	L _V -L _W -V---->L _W -L _V		286.57	7.05
284.11	2.10	T (K)	P(MPa)		
284.58	2.40	284.52	4.12	L _V -L _W -V---->L _W -V	
285.10	2.70	285.46	4.20	T (K)	P(MPa)
285.69	3.00	286.52	4.30	286.46	3.88
286.16	3.30	287.45	4.38	287.49	4.00
286.57	3.60	288.45	4.47	288.46	4.11
Mole fraction CO ₂ : 0.041 Mole fraction water: 0.93					
Mole fraction THF: 0.01 Mole fraction NaCl: 0.02					

Table B-4 Experimental data for different equilibrium curves in the system CO₂ + THF + water + NaCl at 3 mol% THF and 2 mol% NaCl respectively.

H-L _W -V		H-L _W -L _V -V		H-L _W -L _V	
T (K)	P(MPa)	T (K)	P(MPa)	T (K)	P(MPa)
282.10	0.90	287.57	2.70	288.10	5.05
283.51	1.20	287.92	3.00	288.27	6.05
284.98	1.52	288.04	3.30	288.44	7.05
285.63	1.80	288.08	3.45		
286.44	2.10	288.04	3.60	Mole fraction CO ₂ : 0.04 Mole fraction THF: 0.03 Mole fraction water: 0.91 Mole fraction NaCl: 0.02	
287.16	2.40	288.10	4.05		
L _V -L _W -V---->L _W -L _V		L _V -L _W -V---->L _W -V			
T (K)	P(MPa)	T (K)	P(MPa)		
287.50	4.81	287.51	2.42		
288.44	4.86	289.41	2.43		
289.44	4.91	291.40	2.43		
290.50	4.96				
291.43	5.01				

Table B-5 Experimental data for different equilibrium curves in the system CO₂ + THF + water + NaCl at 5 mol% THF and 2 mol% NaCl respectively.

H-L _w -V		H-L _w -L _v -V		H-L _w -L _v	
T (K)	P(MPa)	T (K)	P(MPa)	T (K)	P(MPa)
282.05	0.90	285.18	1.50	287.49	2.70
283.33	1.05	286.08	1.80	287.58	3.00
284.15	1.20	286.89	2.10	287.58	3.30
		287.35	2.40	287.61	3.55
				287.65	4.55
				287.73	5.55
L _v -L _w -V---->L _w -L _v		L _v -L _w -V---->L _w -V		287.85	6.55
T (K)	P(MPa)	T (K)	P(MPa)		
286.44	2.43	283.49	1.23		
287.50	2.47	285.44	1.30	Mole fraction CO ₂ : 0.04	
288.44	2.51	286.00	1.32	Mole fraction THF: 0.05	
289.45	2.55	287.00	1.36	Mole fraction water: 0.89	
290.38	2.59	288.00	1.39	Mole fraction NaCl: 0.02	
		289.00	1.43		

Table B-6 Experimental data for different equilibrium curves in the system CO₂ + THF + water + NaCl at 7 mol% THF and 2 mol% NaCl respectively.

H-L _w -L _v -V		H-L _w -L _v		L _v -L _w -V---->L _w -L _v	
T (K)	P(MPa)	T (K)	P(MPa)	T (K)	P(MPa)
282.38	0.90	287.67	3.00	286.45	2.89
283.73	1.20	287.78	4.05	287.50	2.94
284.82	1.50	287.90	5.05	288.44	2.99
285.92	1.80	288.08	6.05	289.50	3.04
286.49	2.10	288.14	7.05	290.44	3.09
287.14	2.40				
287.49	2.70	Mole fraction CO ₂ : 0.04		Mole fraction water: 0.87	
		Mole fraction THF: 0.07		Mole fraction NaCl: 0.02	

Table B-7 Experimental data for different equilibrium curves in the system CO₂ + THF + water + NaCl at 5 mol% THF and 5 mol% NaCl respectively.

H-L _w -L _v -V		H-L _w -L _v		L _v -L _w -V---->L _w -L _v	
T (K)	P(MPa)	T (K)	P(MPa)	T (K)	P(MPa)
276.44	0.80	281.79	2.60	281.50	2.45
278.20	1.10	281.79	2.90	282.44	2.49
279.43	1.40	281.97	4.05	283.49	2.54
280.50	1.70	282.09	5.05	284.50	2.59
281.15	2.00	282.14	6.05	285.50	2.64
281.61	2.30	282.20	7.05		
		Mole fraction CO ₂ : 0.04		Mole fraction water: 0.86	
		Mole fraction THF: 0.05		Mole fraction NaCl: 0.05	

Table B-8 Experimental data for different equilibrium curves in the system CO₂ + THF + water + NaCl at 6 mol% THF and 9 mol% NaCl respectively.

H-L _w -L _v -V		H-L _w -L _v		
T (K)	P(MPa)	T (K)	P(MPa)	
279.99	0.90	283.31	3.05	Mole fraction CO ₂ : 0.04
281.51	1.20	283.49	4.05	Mole fraction THF: 0.06
282.68	1.50	283.50	5.05	Mole fraction water: 0.81
283.20	1.80	283.74	6.05	Mole fraction NaCl: 0.09
283.26	2.10	283.88	7.05	
283.38	2.40			

Table B-9 Experimental data for different equilibrium curves in the system CO₂ + THF + water + NaCl at 5 mol% THF and 1 mol% NaCl respectively.

H-L _w -V		H-L _w -L _v -V		H-L _w -L _v	
T (K)	P(MPa)	T (K)	P(MPa)	T (K)	P(MPa)
283.98	0.90	287.29	1.80	289.29	3.60
285.23	1.20	288.05	2.10	289.39	3.90
286.35	1.50	288.56	2.40	289.47	5.05
		288.99	2.70	289.63	6.05
		289.16	3.00	289.82	7.05
		289.22	3.30		
L _v -L _w -V---->L _w -L _v					
T (K)	P(MPa)				
287.44	3.70				
288.41	3.74	Mole fraction CO ₂ : 0.04			
289.48	3.77	Mole fraction THF: 0.05			
290.41	3.82	Mole fraction water: 0.90			
291.46	3.85	Mole fraction NaCl: 0.01			

Table B-10 Experimental data for different equilibrium curves in the system CO₂ + THF + water + NaCl at 5 mol% THF and 3 mol% NaCl respectively.

H-L _w -L _v -V		H-L _w -L _v		L _v -L _w -V---->L _w -L _v	
T (K)	P(MPa)	T (K)	P(MPa)	T (K)	P(MPa)
280.53	0.90	285.75	3.40	285.46	2.42
282.34	1.20	285.75	3.93	286.51	2.47
283.39	1.50	285.87	4.90	287.45	2.51
284.46	1.80	286.04	5.90	288.45	2.55
285.09	2.10	286.10	6.90	289.52	2.60
285.58	2.40			290.46	2.65
285.69	2.90	Mole fraction CO ₂ : 0.04			
		Mole fraction THF: 0.05			
		Mole fraction water: 0.88			
		Mole fraction NaCl: 0.03			

Table B-11 Experimental data for different equilibrium curves in the system CO₂ + THF + water + KBr at 5 mol% THF and 0.5 mol% KBr respectively

H-L _w -V		H-L _w -L _v -V		H-L _w -L _v	
T (K)	P(MPa)	T (K)	P(MPa)	T (K)	P(MPa)
284.66	0.91	288.70	2.10	290.26	3.30
285.97	1.21	289.35	2.40	290.47	3.90
287.07	1.50	289.87	2.70	290.61	5.05
287.97	1.80	290.14	3.00	290.73	6.05
				290.84	7.05
L _v -L _w -V---->L _w -L _v					
T (K)	P(MPa)	Mole fraction CO ₂ : 0.040			
289.42	3.08	Mole fraction THF: 0.050			
292.42	3.22	Mole fraction water: 0.905			
295.43	3.37	Mole fraction KBr: 0.005			
298.41	3.52				
301.46	3.67				
304.44	3.83				

Table B-12 Experimental data for different equilibrium curves in the system CO₂ + THF + water + KBr at 5 mol% THF and 1 mol% KBr respectively.

H-L _w -V		H-L _w -L _v -V		H-L _w -L _v	
T (K)	P(MPa)	T (K)	P(MPa)	T (K)	P(MPa)
283.79	0.91	288.03	2.10	289.45	3.30
285.27	1.20	288.81	2.40	289.44	3.60
286.32	1.50	289.15	2.70	289.57	3.90
287.39	1.80	289.45	3.00	289.63	5.05
				289.75	6.05
				289.85	7.05
L _v -L _w -V---->L _w -L _v					
T (K)	P(MPa)				
288.52	2.97				
291.44	3.11	Mole fraction CO ₂ : 0.04			
294.42	3.24	Mole fraction THF: 0.05			
297.48	3.38	Mole fraction water: 0.91			
300.47	3.53	Mole fraction KBr: 0.01			
303.45	3.67				

Table B-13 Experimental data for different equilibrium curves in the system CO₂ + THF + water + NaBr at 5 mol% THF and 0.5 mol% NaBr respectively.

H-L _w -V		H-L _w -L _v -V		H-L _w -L _v	
T (K)	P(MPa)	T (K)	P(MPa)	T (K)	P(MPa)
284.73	0.91	288.71	2.10	290.34	3.30
286.00	1.20	289.33	2.40	290.36	3.55
286.98	1.50	289.81	2.70	290.50	3.90
287.88	1.80	290.14	3.00	290.61	5.05
				290.72	6.05
				290.80	7.05
L _v -L _w -V---->L _w -L _v					
T (K)	P(MPa)	Mole fraction CO ₂ : 0.040			
3.23	1.61	Mole fraction THF: 0.050			
3.38	1.91	Mole fraction water: 0.905			
3.53	2.20	Mole fraction NaBr: 0.005			
3.69	2.51				
3.86	2.81				
4.02	3.10				

Table B-14 Experimental data for different equilibrium curves in the system CO₂ + THF + water + NaBr at 5 mol% THF and 1 mol% NaBr respectively.

H-L _W -V		H-L _W -L _V -V		H-L _W -L _V	
T (K)	P(MPa)	T (K)	P(MPa)	T (K)	P(MPa)
283.70	0.902814	287.88	2.10	289.31	3.30
285.12	1.200751	288.50	2.40	289.31	3.60
286.01	1.500374	288.93	2.70	289.44	3.90
287.10	1.798539	289.23	3.00	289.52	5.05
				289.60	6.05
				289.70	7.05
L _V -L _W -V---->L _W -L _V					
T (K)	P(MPa)	Mole fraction CO ₂ : 0.040			
288.23	2.96	Mole fraction THF: 0.050			
291.23	3.10	Mole fraction water: 0.90			
294.17	3.23	Mole fraction NaBr: 0.01			
297.24	3.37				
300.19	3.51				
303.19	3.66				

Table B-15 Experimental data for different equilibrium curves in the system CO₂ + THF + water + NaBr at 5 mol% THF and 3 mol% NaBr respectively.

H-L _W -V		H-L _W -L _V -V		H-L _W -L _V	
T (K)	P(MPa)	T (K)	P(MPa)	T (K)	P(MPa)
280.56	0.90	284.66	2.10	286.24	3.30
281.89	1.20	285.13	2.40	286.42	3.60
282.97	1.50	285.56	2.70	286.44	3.90
283.94	1.80	285.95	3.00	286.62	5.05
				286.65	6.05
				286.72	7.05
L _V -L _W -V---->L _W -L _V					
T (K)	P(MPa)	Mole fraction CO ₂ : 0.040			
285.42	3.59	Mole fraction THF: 0.05			
286.42	3.63	Mole fraction water: 0.88			
288.42	3.71	Mole fraction NaBr: 0.03			
291.41	3.83				
294.43	3.96				
297.39	4.09				
300.46	4.22				

Table B-16 Experimental data for different equilibrium curves in the system CO₂ + THF + water + KCl at 5 mol% THF and 0.5 mol% KCl respectively.

H-L _w -V		H-L _w -L _v -V		H-L _w -L _v	
T (K)	P(MPa)	T (K)	P(MPa)	T (K)	P(MPa)
284.67	0.91	288.83	2.10	290.19	3.30
285.95	1.21	289.46	2.40	290.24	3.60
287.07	1.50	289.83	2.70	290.25	3.90
288.06	1.80	290.12	3.00	290.37	5.05
				290.49	6.05
				290.61	7.05
L _v -L _w -V---->L _w -L _v					
T (K)	P(MPa)	Mole fraction CO ₂ : 0.040			
289.42	2.98	Mole fraction THF: 0.050			
291.94	3.08	Mole fraction water: 0.905			
294.41	3.22	Mole fraction KCl: 0.005			
297.47	3.38				
300.39	3.52				
303.44	3.68				

Table B-17 Experimental data for different equilibrium curves in the system CO₂ + THF + water + CaCl₂ at 5 mol% THF and 0.5 mol% CaCl₂ respectively.

H-L _w -V		H-L _w -L _v -V		H-L _w -L _v	
T (K)	P(MPa)	T (K)	P(MPa)	T (K)	P(MPa)
284.24	0.91	288.42	2.10	289.84	3.30
285.71	1.21	289.08	2.40	289.95	3.60
286.84	1.51	289.55	2.70	290.01	3.90
287.66	1.80	289.78	3.00	290.17	5.05
				290.24	6.05
				290.32	7.05
L _v -L _w -V---->L _w -L _v					
T (K)	P(MPa)	Mole fraction CO ₂ : 0.040			
288.43	2.98	Mole fraction THF: 0.050			
291.41	3.13	Mole fraction water: 0.905			
294.41	3.27	Mole fraction CaCl ₂ : 0.005			
297.40	3.41				
300.39	3.56				
303.43	3.72				

Table B-18 Experimental data for different equilibrium curves in the system CO₂ + THF + water + CaCl₂ at 5 mol% THF and 1 mol% CaCl₂ respectively.

H-L _w -V and H-L _w -L _v -V		H-L _w -L _v		L _v -L _w -V---->L _w -L _v	
T (K)	P(MPa)	T (K)	P(MPa)	T (K)	P(MPa)
283.05	0.91	288.40	2.70	288.39	2.90
284.58	1.20	288.58	3.00	290.47	3.00
285.71	1.50	288.64	3.60	292.52	3.10
286.55	1.80	288.82	3.90	294.51	3.20
287.40	2.10	288.87	5.05	296.44	3.29
287.93	2.40	289.00	6.05	298.44	3.39
		289.00	7.05	300.42	3.49
Mole fraction CO ₂ : 0.040				302.48	3.60
Mole fraction THF: 0.050				304.51	3.70
Mole fraction water: 0.90					
Mole fraction CaCl ₂ : 0.01					

Table B-19 Experimental data for different equilibrium curves in the system CO₂ + water + MgCl₂ at 0.2 mol% MgCl₂.

H-L _w -V		H-L _w -L _v		L _v -L _w -V---->L _w -L _v	
T (K)	P(MPa)	T (K)	P(MPa)	T (K)	P(MPa)
277.15	2.50	280.77	4.80	274.21	3.75
275.72	2.10	280.95	6.05	276.25	3.93
274.21	1.70	281.04	7.05	278.28	4.13
271.62	1.30			280.28	4.33
				282.21	4.53
H-L _w -L _v -V					
T (K)	P(MPa)	Mole fraction CO ₂ : 0.040			
280.65	4.20	Mole fraction MgCl ₂ : 0.002			
280.07	3.90	Mole fraction water: 0.958			
279.29	3.40				
278.10	2.90				

Table B-20 Experimental data for different equilibrium curves in the system CO₂ + THF + water + MgCl₂ at 5 mol% THF and 0.5 mol% MgCl₂ respectively.

H-L _W -V		H-L _W -L _V -V		H-L _W -L _V	
T (K)	P(MPa)	T (K)	P(MPa)	T (K)	P(MPa)
284.37	0.91	288.50	2.10	289.84	3.30
285.57	1.20	289.14	2.40	289.90	3.60
286.77	1.50	289.62	2.70	289.94	3.90
287.65	1.80	289.76	3.00	290.02	5.05
				290.14	6.05
				290.24	7.05
L _V -L _W -V---->L _W -L _V					
T (K)	P(MPa)	Mole fraction CO ₂ : 0.040			
289.22	2.95	Mole fraction THF: 0.050			
291.24	3.05	Mole fraction water: 0.905			
294.22	3.19	Mole fraction MgCl ₂ : 0.005			
297.23	3.34				
300.24	3.49				
303.23	3.65				

Table B-21 Experimental data for different equilibrium curves in the system CO₂ + THF + water + MgCl₂ at 5 mol% THF and 1 mol% MgCl₂ respectively.

H-L _W -V and H-L _W -L _V -V		H-L _W -L _V		L _V -L _W -V---->L _W -L _V	
T (K)	P(MPa)	T (K)	P(MPa)	T (K)	P(MPa)
284.52	1.20	288.52	3.00	288.43	3.16
285.53	1.50	288.57	3.30	290.52	3.25
286.59	1.80	288.71	3.90	292.45	3.34
287.29	2.10	288.78	5.05	294.47	3.44
287.88	2.43	288.82	6.05	296.51	3.54
288.34	2.73	289.00	7.05	298.44	3.63
				300.42	3.73
Mole fraction CO ₂ : 0.040				302.48	3.83
Mole fraction THF: 0.050				304.47	3.94
Mole fraction water: 0.90					
Mole fraction MgCl ₂ : 0.01					

Table B-22 Experimental data for different equilibrium curves in the system CO₂ + THF + water + NaF at 5 mol% THF and 0.5 mol% NaF respectively.

H-L _W -V		H-L _W -L _V -V		H-L _W -L _V	
T (K)	P(MPa)	T (K)	P(MPa)	T (K)	P(MPa)
284.98	0.91	288.96	2.10	290.33	3.30
286.22	1.20	289.52	2.40	290.32	3.60
287.22	1.50	290.02	2.72	290.39	3.89
288.19	1.80	290.25	3.00	290.54	5.05
				290.63	6.05
				290.69	7.05
L _V -L _W -V---->L _W -L _V					
T (K)	P(MPa)	Mole fraction CO ₂ : 0.040			
289.17	2.96	Mole fraction THF: 0.050			
291.21	3.05	Mole fraction water: 0.905			
294.24	3.19	Mole fraction NaF: 0.005			
297.17	3.33				
300.20	3.48				
303.20	3.63				

Table B-23 Experimental data for different equilibrium curves in the system CO₂ + THF + water + NaF at 5 mol% THF and 1 mol% NaF respectively.

H-L _W -V and H-L _W -L _V -V		H-L _W -L _V		L _V -L _W -V---->L _W -L _V	
T (K)	P(MPa)	T (K)	P(MPa)	T (K)	P(MPa)
285.80	1.20	289.95	3.00	288.39	2.90
286.86	1.50	289.99	3.30	290.47	3.00
287.86	1.80	290.13	3.60	292.52	3.10
288.63	2.10	290.03	3.90	294.51	3.20
289.21	2.40	290.08	5.05	296.44	3.29
289.81	2.70	290.26	6.05	298.44	3.39
		290.47	7.05	300.42	3.49
Mole fraction CO ₂ : 0.040				302.48	3.60
Mole fraction THF: 0.050				304.51	3.70
Mole fraction water: 0.90					
Mole fraction NaF: 0.01					

SAMENVATTING

Tegen de achtergrond om nieuwe processen te ontwikkelen met koolstofdioxide hydraat heeft deze studie zich bezig gehouden met experimenten om fundamenteel inzicht te verwerven in het fasengedrag en de vormings kinetiek van systemen met koolstofdioxide hydraat. Deze gegevens zijn essentieel bij de ontwikkeling van een procesontwerp van welk proces dan ook waarbij koolstofdioxide hydraat een rol speelt, bijvoorbeeld bij scheidings- en koelprocessen met dit hydraat. Naast experimenten zijn ook rekenmodellen toegepast om het fasengedrag van de systemen te voorspellen. In deze studie is speciaal aandacht geschonken aan de invloed van tetrahydrofuran - een hydraat promoter - en electrolyten op het fasengedrag en de vormingskinetiek van deze systemen alsmede de praktische implicaties ervan.

Het fasengedrag is gemeten met een zogenaamde Cailletet opstelling. In aanwezigheid van tetrahydrofuran zijn significante dalingen in de druk of stijgingen van de temperatuur waargenomen bij vergelijking van de evenwichten in de ternaire systemen met de corresponderende evenwichten in het binaire systeem koolstofdioxide met water. Het optreden van vloeistof-vloeistof ontmenging, welke veelvuldig is waargenomen in het ternaire system, heeft een vierfasenevenwicht $H-L_w-L_v-V$ tot gevolg in het gebied waar hydraatvorming optreedt. Voor dit evenwicht zijn de evenwichtsvoorwaarden onafhankelijk van de tetrahydrofuran- concentratie in het systeem. Voor dit vierfasenevenwicht is veelvuldig pseudo-retrograde gedrag van de hydraatfase waargenomen, waarbij de evenwichtstemperatuur daalt met stijgende druk. De aanwezigheid van een electrolyt in systemen met het gemengde hydraat heeft een reductie van het stabiliteitsgebied van het hydraat tot gevolg, terwijl bovendien een verdere

vergroting van het gebied met vloeistof-vloeistof ontmenging optreedt. Inhibitie van de hydraatvorming door metaalhaliden (elektroliet) neemt toe in de volgorde: $\text{NaF} < \text{KBr} < \text{NaCl} < \text{NaBr} < \text{CaCl}_2 < \text{MgCl}_2$. Van de bestudeerde kationen neemt de inhibitie van de hydraatvorming toe in de volgorde $\text{K}^+ < \text{Na}^+ < \text{Ca}^{2+} < \text{Mg}^{2+}$. Daarnaast daalt de inhibitie van de hydraatvorming door anionen in de volgorde: $\text{Br}^- > \text{Cl}^- > \text{F}^-$. Op grond van deze resultaten kan worden geconcludeerd dat de waarschijnlijkheid van de vorming en de sterkte van de ion-waterstof binding tussen een ion en een watermolecuul alsmede het effect van deze binding op het omringende netwerk van watermoleculen de belangrijkste factoren zijn die bijdragen tot inhibitie van de hydraatvorming door elektrolieten.

Het fasengedrag is gemodelleerd met de combinatie van het van der Waals-Platteeuw model en de Peng-Robinson-Stryjek-Vera toestandsvergelijking (PRSV EoS) met Huron-Vidal-Orbey-Sandler (HVOS) mengregels om respectievelijk de clathraat hydraat fase en de fluïde fasen te beschrijven. Indien elektrolieten aanwezig zijn, is dat effect in rekening gebracht door een Debye-Hückel elektrostatische term. Voor de fluïde fasenevenwichten ($\text{L}_w\text{-L}_v\text{-V} \rightarrow \text{L}_w\text{-L}_v$ en $\text{L}_w\text{-L}_v\text{-V} \rightarrow \text{L}_w\text{-V}$) is uitstekende overeenstemming verkregen tussen de experimentele en de modelberekeningen. Aan de andere kant worden de driefasenevenwichten $\text{H-L}_w\text{-V}$ hydraatevenwichten in de ternaire en quaternaire systemen goed beschreven en is acceptabele overeenstemming gevonden voor de $\text{H-L}_w\text{-L}_v\text{-V}$ en $\text{H-L}_w\text{-L}_v$ evenwichten.

Door gebruik te maken van de gemeten driefasenevenwichten $\text{H-L}_w\text{-V}$ kon de dissociatie-enthalpie van het enkelvoudige en het gemengde hydraat met tetrahydrofuran worden berekend met behulp van de Clausius-Clapeyron vergelijking. Het bleek dat de geschatte waarde significant werd beïnvloed door de compressibiliteitsfactor van de koolstofdioxide in het systeem. Aangetoond is dat deze methode om de dissociatie-enthalpie te

bepalen slechts toegepast kan worden in een beperkt gebied waar de compressibiliteitsfactor ongeveer constant is. Bovendien is ook gevonden dat de dissociatie-enthalpie van het gemengde hydraat beduidend hoger is dan dat van het enkelvoudige koolstofdioxide hydraat. Daarentegen heeft de aanwezigheid van elektrolyet slechts een geringe reductie van de dissociatie-enthalpie van zowel het enkelvoudige als het gemengde hydraat tot gevolg.

De vormingskinetiek van zowel het enkelvoudige koolstofdioxide hydraat als het gemengde hydraat met tetrahydrofuran zijn bestudeerd in een batch reactor volgens de zogenaamde T-cycle methode. De clathraat hydraat vorming kan worden verdeeld in twee gedeelten, namelijk de nucleatie en het groeiproces van het hydraat. Uit de gemeten inductietijd kan worden opgemaakt dat de nucleatie in het gemengde hydraat gemakkelijker verloopt. Gevonden is ook dat de aanwezigheid van natriumchloride in de gemengde hydraatsystemen de inductietijd enigszins vergroot. De activeringsenergie van het gemengde hydraat blijkt significant lager te zijn vergeleken met het enkelvoudige koolstofdioxide hydraat, hetgeen inhoudt dat het gemengde hydraat gemakkelijker groeit. De aanwezigheid van tetrahydrofuran resulteert in een sterk gereduceerde opslagcapaciteit van koolstofdioxide in het gemengde hydraat. Voorts reduceert de aanwezigheid van natriumchloride de opname van koolstofdioxide en wordt de activeringsenergie van de hydraatvorming in het gemengde hydraat vergroot.

De verkregen experimentele resultaten en die verkregen zijn met de rekenmodellen geven een beter inzicht in het fasengedrag en de kinetiek van de hydraatvorming voor zowel het enkelvoudige als het gemengde hydraat met tetrahydrofuran, al dan niet in aanwezigheid van een elektrolyet in de waterfase. Hierdoor is een betere beoordeling mogelijk van eventuele toepassingen van het hydraat in aanwezigheid van tetrahydrofuran. De reductie van de druk van de hydraatevenwichten, de toename van de

dissociatie-enthalpie en de daling van de inductietijd, veroorzaakt door de aanwezigheid van tetrahydrofuran, maakt de toepassing van koolstofdioxide hydraat aantrekkelijk voor praktische toepassingen zoals bijvoorbeeld als koelmedium of als secundaire refrigerant. Echter, de gereduceerde opslagcapaciteit voor koolstofdioxide in het gemengde hydraat maakt de toepassing wellicht minder aantrekkelijk. Daarnaast kan het optreden van het pseudo-retrograde gedrag, waarbij een verschuiving naar lagere temperatuur het stabiliteitsgebied van het hydraat verkleint, tot gevolg hebben dat de toepassing in processen bij omgevingtemperatuur er door belemmerd kunnen worden.

CURRICULUM VITAE

Name: Khalik Bin Mohamad Sabil
Date of birth: December 29, 1974
Place of birth: Kuching, Sarawak, Malaysia

Education

1987 – 1991 Sijil Pelajaran Malaysia (Malaysian Certificate of Education), Kolej Dato' Patinggi Abang Haji Abdillah, Petra Jaya, Kuching, Sarawak, Malaysia.
1991 – 1994 Matriculation Certificate (Science), Matriculation Centre, Universiti Sains Malaysia, 11800 Minden, Pulau Pinang, Malaysia
1994 – 1998 B.Eng. (Honours) in chemical engineering, Universiti Sains Malaysia, Pulau Pinang, Malaysia
1998 – 2001 M.Sc. in chemical engineering, Universiti Sains Malaysia, Pulau Pinang, Malaysia
2005-2009 Ph.D in chemical engineering, Process and Energy, Delft University of Technology, Delft, the Netherlands

Theses

M.Sc. Studies on the Production of Charcoal by Carbonisation using Mangrove Wood in Malaysia
Ph.D. Phase behaviour, thermodynamics and kinetic of clathrate hydrate systems of carbon dioxide in presence of tetrahydrofuran and electrolytes

Employment

1997 Industrial trainee in Sitt Tatt Industrial Gases Sdn. Bhd., Shah Alam Selangor.
1998 Process engineer in Kedah Cement Sdn. Bhd., 07000 Langkawi, Kedah.
2000-2001 Trainee lecturer at Universiti Teknologi Petronas, Bandar Seri Iskandar, 31750 Tronoh, Perak
2001-Present Lecturer at Universiti Teknologi Petronas, Bandar Seri Iskandar, 31750 Tronoh, Perak

PUBLICATIONS

Journals

- Khalik M. Sabil and Cor. J. Peters. Towards CO₂ Sequestration and Applications of CO₂ Hydrates: The Effects of Tetrahydrofuran on The Phase Equilibria of CO₂ hydrates, **Malaysian Journal of Chemical Engineering** 1 (2007), 73-82.
 - Khalik M. Sabil, Geert-Jan Witkamp and Cor. J. Peters. Phase Equilibria of Mixed Carbon Dioxide and Tetrahydrofuran Hydrates in Sodium Chloride Aqueous Solution. Submitted to **Fluid Phase Equilibria**, April 2009.
 - Khalik M. Sabil, Geert-Jan Witkamp and Cor. J. Peters. Estimations of Enthalpies of Dissociation and Hydration Numbers of Single and Mixed Carbon Dioxide Hydrates from Phase Equilibrium Data. Submitted to **Fluid Phase Equilibria**, Special Issue, April 2009.
 - Khalik M. Sabil, Geert-Jan Witkamp and Cor. J. Peters. The Phase Equilibria in Ternary Carbon Dioxide + Tetrahydrofuran + Water System: Effects of Carbon Dioxide Concentration and Pseudo-retrograde Hydrate Behaviour. Submitted to **Journal of Chemical Thermodynamics**, May 2009.
 - Khalik M. Sabil, Vicente R. Román, Geert-Jan Witkamp and Cor. J. Peters. The competing effect of tetrahydrofuran and an electrolyte in carbon dioxide hydrate forming systems and the strength of hydrate inhibition among the metal halides in mixed-CO₂ hydrates. Submitted to **Journal of Chemical Thermodynamics**, May 2009.
 - Khalik M. Sabil, Geert-Jan Witkamp and Cor. J. Peters. The Effects of Tetrahydrofuran Concentration and the Occurrence of Pseudo-retrograde Hydrate Behaviour in the Hydrate Forming Region of Carbon Dioxide + Tetrahydrofuran + Water System. Submitted to **Journal of Physical Chemistry B**, May 2009.
 - Khalik M. Sabil, Geert-Jan Witkamp and Cor. J. Peters. Kinetic of Formation of Mixed Carbon Dioxide and Tetrahydrofuran Hydrates in Water and NaCl Aqueous Solution. Submitted to **Industrial & Engineering Chemistry Research**, June 2009.
-

-
- Khalik M. Sabil, Geert-Jan Witkamp and Cor. J. Peters. Measurement and Modeling of Bubble and Dew Points for Carbon Dioxide systems in Aqueous Tetrahydrofuran Solutions. Submitted to **Journal of Chemical & Engineering Data**, June 2009.

Conference Proceedings/Book of Abstracts

- Khalik M. Sabil and Cor J. Peters. Pseudo-retrograde hydrate phenomena in systems containing carbon dioxide (CO₂) and tetrahydrofuran (THF) in Proceedings of 22nd European Symposium on Applied Thermodynamics (ESAT 2006), 28 June – 1 July 2006, Elsinore, Denmark.
- Khalik M. Sabil and Cor J. Peters. Application of Carbon Dioxide Hydrates in Process Technology: Effect of Tetrahydrofuran on The Phase Behavior of Carbon Dioxide Hydrate in NPS6: Flexible Design, Mission Impossible?, 24-25 October 2006, NH Koningshof, Veldhoven, The Netherlands.
- Khalik M. Sabil and Cor J. Peters. Phase Equilibria in the Ternary System of Carbon Dioxide–Tetrahydrofuran–Water at Gas Hydrate Forming Conditions in AIChE 2006 Annual Meeting, 12-17 November 2006, San Francisco, California, USA.
- Khalik M. Sabil and Cor J. Peters. Sequestration of CO₂ as Hydrates: The Effects of Tetrahydrofuran on the Phase Equilibria of Carbon Dioxide Hydrates in Proceedings of 20th Symposium of Malaysian Chemical Engineers (SOMChE 2006) 19-21 December 2006, Shah Alam, Malaysia.
- Khalik M. Sabil and Cor J. Peters. Clathrate Hydrate Formation in Ternary and Quaternary Systems of Carbon Dioxide, Water, Tetrahydrofuran and Sodium Chloride in Proceedings of Eleventh International Conference on Properties and Phase Equilibria for Product and Process Design (PPEPPD 2007), 20-25 May 2007, Hersonissos, Crete, Greece.
- Khalik M. Sabil and Cor J. Peters. Phase Equilibrium Data of Mixed Carbon Dioxide (CO₂) and Tetrahydrofuran (THF) Clathrate Hydrate in Aqueous Electrolyte Solution in AIChE 2007 Annual Meeting, 4-9 November, 2007, Salt Lake City, Utah, USA.

-
- Khalik M. Sabil, Angel Martin, Geert-Jan Witkamp and Cor J. Peters, Experimental Measurements and Modeling of H-Lw-V Equilibrium Condition for Mixed Hydrate of Carbon Dioxide and Tetrahydrofuran in Aqueous Solution in Proceedings of the 23rd ESAT (European Symposium on Applied Thermodynamics, 29 May – 1 June 2008, Cannes, France.
 - Khalik M. Sabil, Vicente R. Roman, Geert-Jan Witkamp and Cor. J. Peters. Tetrahydrofuran-promoted Clathrate Hydrate Phase Equilibria of CO₂ in Aqueous Electrolyte Solutions in Proceedings of the 6th International Conference on Gas Hydrates (ICGH 2008), 6-10 July 2008, Vancouver, British Columbia, Canada.
 - Khalik M. Sabil, Vicente R. Roman, Geert-Jan Witkamp and Cor. J. Peters Experimental Investigation and Modelling of Bubble and Dew Points in the Ternary System of Carbon Dioxide, Tetrahydrofuran and Water in Proceedings of 20th International Conference on Chemical Thermodynamics (ICCT2008), 2-8 August 2008, Warsaw, Poland.
 - Khalik M. Sabil, Geert-Jan Witkamp and Cor J. Peters. Estimation of Estimations of Enthalpies of Dissociation and Hydration Numbers of Simple and Mixed Carbon Dioxide Hydrates from Phase Equilibrium Data in Proceedings of the 17th Symposium of Thermophysical Properties, 21-26 June 2009, Boulder, USA.
